

---

# Monitoring of greenhouse gases and aerosols at Svalbard and Birkenes in 2021

Annual report

Cathrine Lund Myhre, Tove Svendby, Ove Hermansen, Chris Lunder, Stephen M. Platt, Markus Fiebig, Ann Mari Fjæraa, Georg Hansen, Norbert Schmidbauer and Kerstin Stebel



<b>NILU report 28/2022</b> Norwegian Environment Agency M-2365   2022	ISBN: 978-82-425-3101-8 ISSN: 2464-3327	CLASSIFICATION: A – Unclassified (open report)
DATE 16.11.2022	SIGNATURE OF RESPONSIBLE PERSON Ole-Anders Braathen (sign.) Deputy director	NUMBER OF PAGES 160
TITLE Monitoring of greenhouse gases and aerosols at Svalbard and Birkenes in 2021 Annual report	PROJECT LEADER Wenche Aas	NILU PROJECT NO. O-113007/O-121002
	QUALITY CONTROLLER Kjetil Tørseth	
REPORT PREPARED FOR Norwegian Environment Agency Postboks 5672 Sluppen, 7485 Trondheim	CONTRACT REF. Contract number 17078061	
ABSTRACT This annual report for 2021 summarizes the activities and results of the greenhouse gas monitoring at the Zeppelin Observatory, situated on Svalbard, during the period 2001-2021, and the greenhouse gas monitoring and aerosol observations from Birkenes for 2009-2021.		
NORWEGIAN TITLE Overvåkning av klimagasser og partikler på Svalbard og Birkenes i 2021: Årsrapport.		
KEYWORDS Greenhouse gases/ Drivhusgasser                      Aerosols/ Partikler                                      Climate gases/ Klimagasser                                      Halocarbons/ Halokarboner		
ABSTRACT (in Norwegian) Denne årsrapporten for 2021 presenterer aktiviteter og måleresultater fra klimagassovertvåkingen ved Zeppelinobservatoriet på Svalbard for årene 2001-2021 og klimagassmålinger og klimarelevante partikkelmålinger fra Birkenes for 2009-2021.		
PUBLICATION TYPE: Digital document (pdf)	COVER PICTURE: Source: Kjetil Tørseth, NILU	

© NILU – Norwegian Institute for Air Research

Citation: Myhre, C.L., Svendby, T., Hermansen, O., Lunder, C., Platt, S.M., Fiebig, M., Fjæraa, A.M., Hansen, G., Schmidbauer, N. and Stebel, K. (2022). Monitoring of greenhouse gases and aerosols at Svalbard and Birkenes in 2021. Annual report. (NILU report 28/2022). Kjeller: NILU.

NILU's ISO Certifications: NS-EN ISO 9001 and NS-EN ISO 14001. NILU's Accreditation: NS-EN ISO/IEC 17025.

## Preface

This report presents the 2021 annual results from the national monitoring of greenhouse gas concentrations and climate-relevant particle properties. The observations are done at two atmospheric observatories: one regional background site in southern Norway and one Global background/Arctic site. The observations made are part of the national monitoring programme conducted NILU – Norwegian Institute for Air Research on behalf of The Norwegian Environment Agency. Additionally, the report includes results from aerosol observations at Trollhaugen observatory in Antarctica. These measurements are not a part of the national monitoring programme, but receive direct support from the Norwegian Ministry of Climate and Environment.

The national monitoring programme comprises measurements of 46 greenhouse gases at the Zeppelin Observatory in the Arctic; including a long list of halocarbons, of which most are not only greenhouse gases, but also ozone depleting substances. NILU initiated measurements of methane (CH<sub>4</sub>)-isotope ( $\delta^{13}\text{C}_{\text{CH}_4}$ ) at Zeppelin in 2012 to provide more insight into Arctic sources of CH<sub>4</sub>, and potential changes, as part of a project funded by the Norwegian Research Council. The continuation of these measurements was implemented in the Norwegian Monitoring programme in 2019. NILU upgraded and extended the observational capabilities of the Birkenes Observatory, Agder, and from 2010, the national monitoring programme was extended to include aerosol properties relevant for understanding the effects of aerosols on radiation (particle size, number, scattering and light absorption).

The present report is the third of a series of annual reports in 2022, which cover the national monitoring of atmospheric composition in the Norwegian rural background environment. The other two reports focus on the atmospheric composition and deposition of air pollution of particulate and gas phase of inorganic constituents, particulate carbonaceous matter, ground level ozone and particulate matter (Aas et al., 2022), and the monitoring of the ozone layer and UV (Svendby et al., 2022).

Participation in international programmes is essential for quality assurance and quality control of the Norwegian measurement data and instruments. Data from this report contribute to, and benefit from, the European Research Infrastructure ACTRIS (*Aerosols, Clouds, and Trace gases Research InfraStructure*) and ICOS (*Integrated Carbon Observation System*). Additionally, data and results support and benefit from EMEP (European Monitoring and Evaluation Programme) under CLRTAP (Convention on Long-range Transboundary Air Pollution), and AGAGE (Advanced Global Atmospheric Gases Experiment).

All measurement data presented in the current report are publicly available and can be received by contacting NILU, or they can be downloaded directly from the database: <http://ebas.nilu.no>.

Many people at NILU have contributed to this report, including those responsible for sampling, technical maintenance, chemical analysis and quality control and data management, in particular, Tove Svendby, Ove Hermansen, Chris Lunder, Markus Fiebig, Georg Hanssen, Stephen M. Platt, Kerstin Stebel, Ann Mari Fjæraa and Norbert Schmidbauer.

NILU, Kjeller, 14<sup>th</sup> October 2022  
Cathrine Lund Myhre  
Senior Scientist, Dep. Atmospheric and Climate Research

# Contents

<b>Preface .....</b>	<b>3</b>
<b>Sammendrag.....</b>	<b>6</b>
<b>Summary .....</b>	<b>9</b>
<b>1 Introduction to monitoring of climate gases and aerosols.....</b>	<b>13</b>
1.1 The monitoring programme in 2021.....	13
1.2 The measurements in relation to research and policy agreements .....	13
1.3 The ongoing monitoring programme and the link to networks and research infrastructures .....	15
1.4 Greenhouse gases and aerosols, and their climate effects .....	20
<b>2 Norwegian observations of greenhouse gases.....</b>	<b>23</b>
2.1.1 IPCC AR6 forcing and annual mean value of the main GHG components compared to measurements at Zeppelin Observatory .....	26
2.2 Climate gases with natural and anthropogenic sources.....	28
2.2.1 Carbon dioxide (CO <sub>2</sub> ).....	28
2.2.2 Methane (CH <sub>4</sub> ).....	32
2.2.3 Nitrous Oxide (N <sub>2</sub> O).....	39
2.2.4 Volatile organic compounds (VOC) .....	41
2.2.5 Carbon monoxide (CO).....	46
2.2.6 Chloromethane at the Zeppelin Observatory .....	48
2.2.7 Bromomethane at the Zeppelin Observatory .....	50
2.3 Greenhouse gases with solely anthropogenic sources.....	52
2.3.1 Chlorofluorocarbons (CFCs) at Zeppelin Observatory .....	52
2.3.2 Hydrochlorofluorocarbons (HCFCs) at Zeppelin Observatory .....	55
2.3.3 Hydrofluorocarbons (HFCs) at Zeppelin Observatory .....	57
2.3.4 Halons measured at Zeppelin Observatory.....	61
2.3.5 Other chlorinated hydrocarbons at Zeppelin Observatory.....	63
2.3.6 Perfluorinated compounds at Zeppelin Observatory .....	66
<b>3 Aerosols and climate .....</b>	<b>71</b>
3.1 Analysis of in situ aerosol radiative properties around the world.....	73
3.2 Overview of aerosol observations at Zeppelin, Birkenes and Troll Observatory .....	75
3.3 Observed optical properties of aerosols.....	76
3.3.1 Optical aerosol properties measured at the Birkenes Observatory .....	76
3.3.2 Optical aerosol properties measured at the Zeppelin Observatory .....	80
3.3.3 Optical aerosol properties measured at the Trollhaugen Observatory .....	82
3.4 Measurements of particle number and size .....	84
3.4.1 Physical aerosol properties measured at the Birkenes Observatory.....	84
3.4.2 Physical aerosol properties measured in situ at the Zeppelin Observatory ...	87
3.4.3 Physical aerosol properties measured in situ at the Trollhaugen Observatory	92
3.5 Summary of physical and optical aerosol properties .....	95
3.6 Column optical aerosol properties measured by ground-based remote sensing .....	97
3.6.1 Column optical aerosol properties measured by ground-based remote sensing at Birkenes Observatory.....	97
3.6.2 Column optical aerosol properties measured by ground-based remote sensing at Ny-Ålesund.....	102
3.6.3 Column optical aerosol properties measured by ground-based remote sensing at Troll Station, Antarctica .....	106
3.7 Summary of aerosol column properties .....	109

<b>4</b>	<b>References.....</b>	<b>110</b>
	<b>Appendix I Data Tables .....</b>	<b>119</b>
	<b>Appendix II Description of instruments and methodologies .....</b>	<b>137</b>
	<b>Appendix III Abbreviations.....</b>	<b>157</b>

## Sammendrag

**Alle de viktigste klimagassene CO<sub>2</sub>, CH<sub>4</sub> og N<sub>2</sub>O økte til nye rekordhøye nivåer i 2021, og det er ingen tegn til utflating for noen av disse gassene.**

**CH<sub>4</sub> fortsetter med rekordrask økning, den største vi har registrert siden målingene på Birkenes startet.**

**KFK-gasser fortsetter nedgangen, mens erstatningsgassene øker raskt.**

Denne årsrapporten beskriver aktivitetene og hovedresultatene fra programmet "Overvåkning av klimagasser og aerosoler på Zeppelinobservatoriet på Svalbard og Birkenesobservatoriet i Agder, Norge". Rapporten omfatter målinger av 46 klimagasser på Zeppelinobservatoriet fram til 31. desember 2021 og inkluderer de viktigste naturlig forekommende klimagassene, syntetiske klimagasser, karbonmonoksid (CO), VOCer, og ulike partikkelmålinger som har høy relevans for klimaet. Mange av gassene har også sterk ozonødeleggende effekt. Målingene på Zeppelinobservatoriet gir informasjon om utviklingen av bakgrunnsnivået av klimagasser i Arktis, og alle de 46 gassene i overvåkningsprogrammet blir målt her. Birkenesobservatoriet ligger i et område i Sør-Norge som kan være sterkt påvirket av langtransportert luftforurensning fra Europa, i tillegg til påvirkning fra lokal vegetasjon. På Birkenesobservatoriet gjøres observasjoner av karbondioksid (CO<sub>2</sub>) og metan (CH<sub>4</sub>), samt omfattende målinger av klimarelevante egenskaper til aerosoler (partikler). Aerosoler måles også på Zeppelin og Trollhaugen (Antarktis), men måleprogrammene er ikke like omfattende som på Birkenes.

For klimagassene er utvikling og trender for perioden 2001-2021 rapportert, i tillegg til daglige og årlige gjennomsnittsverdier. Programmet ble utvidet med 16 nye gasser på Zeppelin i 2015. I 2016 ble programmet ytterligere utvidet med seks nye gasser etter modifisering av instrumenteringen ved Zeppelinobservatoriet: tre hydrofluorkarboner (HFC), sulfurylfluorid (SO<sub>2</sub>F<sub>2</sub>), halon H-2402 og nitrogentrifluorid (NF<sub>3</sub>). For de nye komponentene er data innhentet og analysert tilbake til 2010. Resultatene for alle klimagassene er oppsummert i tabell 1 på side 11.

Konsentrasjonene av alle de viktigste klimagassene har økt kraftig siden 2001, bortsett fra ozonødeleggende klorfluorkarboner (KFK-er) og noen få andre halogenererte gasser som er regulert gjennom Montrealprotokollen. De fleste av disse har blitt redusert.

Observasjonene fra 2021 viser nye rekordhøye nivåer for de fleste klimagassene i overvåkningsprogrammet, både på Zeppelin og Birkenes. Årlig midlere CO<sub>2</sub> konsentrasjon i 2021 var 417,4 ppm (parts per million) på Zeppelin og 421,3 ppm på Birkenes. Dette er økninger på henholdsvis 3,2 ppm og 2,5 ppm fra 2020 og ny rekord på begge stasjoner.

Konsentrasjonen av metan var også i 2021 rekordhøy både på Birkenes og på Zeppelin, med årlige middelveier på 1991,7 ppb (parts per billion) på Birkenes og 1981,4 ppb på Zeppelin. I forhold til 2020-nivået er dette en økning på Birkenes på hele 16,4 ppb, den høyeste økningen noen gang registrert på ett år. Også på Zeppelin er økningen betydelig, hele 12,7 ppb. Endringene i løpet av de siste ti årene er store i forhold til utviklingen av metan-nivået i perioden 1998-2005, da endringene var tilnærmet null både på Zeppelin og globalt. Ulike metankilder (for eksempel naturgass og våtmarker) har ulik isotop-signatur (det vil si forhold mellom isotoper). Isotopmålinger av CH<sub>4</sub> på Zeppelin viser en klar nedadgående trend i  $\delta^{13}\text{C}_{\text{CH}_4}$  etter 2012 og frem til ca. 2019. En nedadgående trend i  $\delta^{13}\text{C}_{\text{CH}_4}$ , samtidig med en økning av metankonsentrasjonene, viser at metankildene eller opptaksprosessene har endret seg i løpet av de siste 8 årene. Endringene i  $\delta^{13}\text{C}_{\text{CH}_4}$  på Zeppelin tyder på økte utslipp fra biosfæren (våtmarker) og/eller jordbruk. Data fra 2019 til 2021 indikerer at denne endringen

i kildesammensetning er i ferd med å flate ut, det vil si at balansen mellom kildene ser ut til å ha stabilisert seg. Dette kan også ha sammenheng med utslippsendringer i forbindelse med Covid-19.

Lystgass ( $N_2O$ ) har både naturlige kilder og store menneskeskapte kilder som jordbruk og bergverk.  $N_2O$  nådde også nytt rekordnivå i 2021. Den årlige middelkonsentrasjonen på Zeppelin var 334,5 ppb, en økning på 1,1 ppb siden 2020.

Det er interessant å merke seg at CO målt på Zeppelinobservatoriet har begynt å øke igjen etter en stabil periode. En viktig kilde for CO er skogbranner og det kan virke som de store skogbrannene de siste årene i Sibir, Canada og USA kan forklare økningen vi ser, men det er for tidlig å konkludere. Dette er også i samsvar med episodene vi ser i partikkelmålinger.

De syntetiske, menneskeskapte klimagassene som inngår i overvåkningsprogrammet på Zeppelin er fire klorfluorkarboner (KFK-er), tre hydroklorfluorkarboner (HKFK-er), og 11 hydrofluorkarboner (HFK-er). De to sistnevnte gruppene er KFK-erstatninger. I tillegg inngår tre haloner, en gruppe med åtte andre halogenerte klimagasser, samt fire perfluorerte karboner (PFK-er) med svært høyt globalt oppvarmingspotensial (GWP). Videre rapporteres sulfurylfluorid, svovelhexafluorid, og nitrogentrifluorid, hvorav de to siste er meget sterke klimagasser.

Generelt avtar konsentrasjonen av KFK-gasser, mens de øvrige gassene øker da disse ofte er erstatningsgasser for KFK-ene. For et par år siden ble det oppdaget ukjente og urapporterte utslipp av KFK-11 i Asia, noe som bremsset den markante nedadgående trenden i de globale målingene av KFK-11. Utviklingen i KFK-gassene gir likevel grunn til optimisme, fordi konsentrasjonen for de fleste av disse gassene er synkende. KFK-115 er et unntak, her ser vi en liten økning fra 2019-2021. Samtidig økte konsentrasjonene av KFK-erstatningsstoffene, HKFK-er og HFK-er, i perioden 2001-2021. For HKFK-er har det riktignok vært mindre økning de siste årene, og for HKFK-142b er det observert en nedadgående trend som startet i 2017. For HKFK-141b har årsmiddelet på Zeppelin vært nokså stabilt siden 2016. Konsentrasjonen av HFK-gassene har økt kraftig siden 2001, og med få unntak (HFK-152a og HFC-365mfc) ser den økende trenden ut til å fortsette. Konsentrasjonene av disse menneskeskapte HFK-ene er fortsatt svært lave, noe som betyr at bidraget til den globale oppvarmingen per i dag er lite, men gitt den ekstremt sterke økningen og bruken av disse gassene, er det viktig å følge utviklingen nøye i fremtiden.

Konsentrasjonene av PFK-er og svovelfluorider ( $SF_6$  og  $SO_2F_2$ ) er også lave. PFK-14 er høyest, med en årlig middelværdi på 88,0 ppt (parts per trillion) i 2021, en økning på 1.0 ppt fra 2020. Konsentrasjonen av  $SF_6$  bør også følges nøye, ettersom denne forbindelsen har en atmosfærisk levetid på 3 200 år og et GWP på hele 25 200. Denne forbindelsen har økt med hele 111% siden målingene startet på Zeppelin i 2001.

Aerosoler består av små partikler i atmosfæren som både kan ha avkjølende og oppvarmende effekter. Partiklenes klimapåvirkning avhenger av mengden partikler og absorpsjonsegenskapene til enkeltpartiklene. Konsentrasjonen av partikler på Birkenes bestemmes i hovedsak av den langtransporterte luftforurensningen fra det kontinentale Europa, i tillegg til regionale og lokale vegetasjonskilder (biogene kilder).

Transportepisodene som ble observert i 2021 på Birkenes stasjon har ofte opphav i Sentral- og Sørøst-Europa. Luftmasser transporteres over land over en lengre periode. Noen ganger overlappes disse hendelsene med utslipp fra skogbranner i Sørøst-Europa. Etter oppstart av fysiske og optiske aerosolobservasjoner på Birkenes i 2010, har vi ikke sett noen signifikante trender i aerosolegenskaper (partikkelantall, aerosol optisk tykkelse (AOD), Ångstrøm koeffisient) noe som også er i samsvar med nyere trendstudier av aerosolegenskaper som dekker hele kloden.

På Zeppelin er situasjonen litt annerledes. Ved å sammenstille våre aerosolmålinger med resultater fra andre samarbeidspartnere, finner vi en nedadgående trend i aerosol-absorpsjonen, noe som viser at konsentrasjonen av sot eller såkalt svart karbon går ned. Observasjoner av den totale kolonnen av aerosoler over Ny-Ålesund (aerosol optisk dybde, AOD) viser økte konsentrasjoner om våren sammenlignet med resten av året. Dette fenomenet, som kalles arktisk dis (*Arctic haze*), skyldes

transport av forurensning fra lavere breddegrader i løpet av vinteren/våren, hovedsakelig fra Europa og Russland. I 2021 ser vi transportepisoder av aerosol fra industrielle utslipp i det russiske Arktis (Kola/Yamal/Kanin-halvøya). Unntaket er transporthendelsen tidlig i august 2021, sannsynligvis forårsaket av en skogbrann i Sverige.

Partiklene på Trollhaugen i Antarktis er preget av naturlige storskalaprosesser med en veldig konstant årssyklus. Episoder observert vinteren 2021 skyldes luftmasser påvirket av utslipp fra en nabostasjon 360 km til øst.



## Summary

**All the most important greenhouse gases CO<sub>2</sub>, CH<sub>4</sub> and N<sub>2</sub>O increased to new record levels in 2021, and there are no signs of leveling off for any of these gases.**

**CH<sub>4</sub> continues with a record strong increase, the largest we have registered since the measurements at Birkenes started.**

**CFC-gases continue to decline, while their replacement gases increase rapidly.**

This annual report describes the activities and main results of the programme “*Monitoring of greenhouse gases and aerosols at the Zeppelin Observatory, Svalbard, and Birkenes Observatory, Agder, Norway*”. The report presents the measurements of 46 climate gases at the Zeppelin Observatory up to 31<sup>st</sup> December 2021, including the most important naturally occurring well-mixed greenhouse gases, synthetic greenhouse gases, reactive short lived gases as volatile organic compounds (VOCs), and CO in addition to various particle properties with high relevance to climate. The measurements at Zeppelin Observatory provide the trends in background level concentrations of climate gases in the Arctic, and all the 46 climate gases in the programme are monitored at this site.

At the Birkenes Observatory in Southern Norway, carbon dioxide (CO<sub>2</sub>) and methane (CH<sub>4</sub>) measurements are undertaken in addition to a comprehensive aerosol measurement programme. Birkenes is highly influenced by long-range transport of pollutants from the European continent as well as local vegetation/terrestrial interactions. Aerosol measurements are also performed at Zeppelin and Trollhaugen (Antarctica), although less extensively than at Birkenes.

Many of the gases in this report also have strong ozone depleting effects. The development and trends in the measured constituents for the period 2001-2021 are reported, in addition to daily and annual means. In 2015, the programme at Zeppelin was extended to include 16 new climate gases, all with measurements starting in 2010. In 2016, the programme was further extended to include six more species after instrumentation modification at the Zeppelin Observatory: three hydrofluorocarbons (HFCs), sulphuryl fluoride (SO<sub>2</sub>F<sub>2</sub>), halon H-2402 and nitrogen trifluoride (NF<sub>3</sub>). The main results for 2021 for all climate gases are summarized in Table 1. The concentrations of all main greenhouse gases measured at both Zeppelin and Birkenes have been increasing since 2001, except for the ozone-depleting chlorofluorocarbons (CFCs) and a few halogenated gases regulated through the successful Montreal Protocol.

The observations from 2021 show new record high levels for most climate gases measured. The annual average CO<sub>2</sub>-concentration in 2021 was 417.4 ppm at Zeppelin and 421.3 ppm at Birkenes. The increases from 2020 are 3.2 ppm 2.5 ppm, respectively.

The concentration of CH<sub>4</sub> also reached new record highs in 2021 at Birkenes and Zeppelin, with annual mean concentrations of 1991.7 ppb at Birkenes and 1981.4 ppb at Zeppelin. The level at Birkenes gives a new record annual increase of 16.4 ppb. At Zeppelin, the increase was 12.7 ppb. For the isotopic signature of CH<sub>4</sub>, a clear trend in  $\delta^{13}\text{C}_{\text{CH}_4}$  is evident after 2012. The observed negative shifts in ambient  $\delta^{13}\text{C}_{\text{CH}_4}$  and increases in the CH<sub>4</sub> ambient mixing ratio (the relative abundance of one atmospheric gas compared to all the others) at the same time, imply changes in the balance of sources and potentially sinks. The developments in  $\delta^{13}\text{C}_{\text{CH}_4}$  observed at Zeppelin suggest increase in biosphere and/or agriculture (wetland or ruminant) emissions. For 2019 to 2021 the data indicate that the recent shift in the source/sink balance may have stabilised. This might be related to emission changes during the Covid-19 lockdown.

The mean N<sub>2</sub>O-concentration at Zeppelin was also record high in 2021. The annual mean concentration was 334.5 ppb, an increase of 1.1 ppb since 2020.

It is interesting to note that CO measured on Zeppelin Observatory has started to increase again, after a stable period. An important source of CO is forest fires, and it may seem that the major forest fires in recent years in Siberia, Canada and the United States explain the increase we are seeing, but it is too early to conclude. This is consistent with the episodes we see in particle measurements as well.

The synthetic manmade greenhouse gases included in the monitoring programme at Zeppelin are 4 chlorofluorocarbons (CFCs), 3 hydrochlorofluorocarbons (HCFCs), and 11 HFCs – the last two being CFC substitutes. In addition, three halons, a group of 8 halogenated gases, and 4 perfluorinated carbons (PFCs) with very high global warming potentials, are included. Furthermore, SF<sub>6</sub>, NF<sub>3</sub> and SO<sub>2</sub>F<sub>2</sub> were reported for the first time in 2016. SF<sub>6</sub> and NF<sub>3</sub> are extremely strong greenhouse gases.

In general, the concentration of CFC-gases has decreased, while their replacements have increased. Recently, new and previously unreported CFC-11 emission sources were discovered in Asia, which slowed down the rate of CFC-11 decrease globally. Still, the development of the CFC-gases measured at Zeppelin is very encouraging as the concentrations of the dominating species are declining. CFC-115 is an exception and we see an increase in the concentration of this compound. Contrary to the CFCs, the CFC substitutes HCFCs and HFCs have increased over the period 2001-2021. For the HCFCs, a relaxation in the upward trend has been observed in recent years, and HCFC-142b shows a small decrease over last four years. However, for HFCs a strong increase has been observed since 2001, and the increasing trend is continuing except for HFC-152a, which has been relatively stable the last ten years. The contribution from these manmade gases to global warming is small today, as the concentrations of HFCs are still very low. However, given the extremely rapid increase in the use of these gases and their high global warming potentials (GWP, determined relative to CO<sub>2</sub>), it is crucial to follow their development.

Atmospheric concentrations of PFCs, SO<sub>2</sub>F<sub>2</sub> and SF<sub>6</sub> are also low. PFC-14 is amongst the highest, with a mixing ratio of 88.0 ppt in 2021, an increase of 1.0 ppt since 2020. SF<sub>6</sub> should also be followed closely, as this compound has an atmospheric life-time of 3 200 years and an extremely high GWP of 25 200. This compound has increased by 111% since 2001.

Aerosols consist of small particles in the atmosphere. They can have warming or cooling effects on climate, depending on the particle loading, their properties, and where they are located. Aerosol loads and properties at Birkenes are mainly influenced by long-range transport of air pollution from continental Europe, combined with regional sources like biogenic particle formation. Episodes visible in 2021 originate often in Central and South-East Europe. Air masses are being transported over land over an extended period. Occasionally, these events are superimposed by emissions from wildfires in South-Eastern Europe.

At Zeppelin, the situation is different. By comparing aerosol absorption data collected at Zeppelin with data from collaborating institutes, a decreasing trend is observed, indicating a decrease of black carbon (BC, mostly soot) at Zeppelin. Observations of the total amount of aerosol particles in the atmosphere above Ny-Ålesund (aerosol optical depth) show high concentrations during springtime compared to the rest of the year. This phenomenon, called Arctic haze, is due to transport of pollution from lower latitudes accumulating in the Arctic atmosphere during winter/spring. In 2021, most of the investigated episodes at the Zeppelin station originate from industrial emissions in the Russian Arctic (Kola/Yamal/Kanin peninsula). The exception is the transport event in early August 2021, likely caused by a forest fire in Sweden.

The aerosol at Trollhaugen, Antarctica, is characterised by natural, hemispheric scale processes with a very constant annual cycle. Episodes observed in Winter 2021 can be connected to emissions from a neighbouring stations 360 km east of Troll and on the Antarctic peninsula.

Table 1: Key findings; Greenhouse gases measured at Zeppelin, Ny-Ålesund; lifetimes in years<sup>1</sup>, global warming potential (GWP over 100 years, when available<sup>1</sup>), annual mean concentrations for 2021 and their long term trends per year over the measurement period. CO<sub>2</sub> and CH<sub>4</sub> are also measured at Birkenes. Concentrations are in ppm (parts per million) for CO<sub>2</sub>, ppb (part per billion) for CH<sub>4</sub>, CO, and N<sub>2</sub>O, and ppt (parts per trillion) for the other gases. The trend method is described in appendix II.

Component		Lifetime	GWP	Annual mean 2021	Absolute change last year	Trend/yr
Carbon dioxide - Zeppelin	CO <sub>2</sub>	**	1	417.4	3.2	2.5
Carbon dioxide - Birkenes				421.3	2.5	2.5
Methane - Zeppelin	CH <sub>4</sub>	11.8	28	1981.4	12.7	6.7
Methane - Birkenes				1991.7	16.4	9.0
Carbon monoxide	CO	few months	-	128.0	10.3	-0.8
Nitrous oxide	N <sub>2</sub> O	109	273	334.5	1.08	1.01
<b>Chlorofluorocarbons</b>						
CFC-11	CCl <sub>3</sub> F	52	5 560	222.6	-2.44	-1.77
CFC-12	CF <sub>2</sub> Cl <sub>2</sub>	102	11 200	498.0	-3.67	-2.64
CFC-113	CF <sub>2</sub> ClCFCl <sub>2</sub>	93	6 520	69.1	-0.41	-0.63
CFC-115	CF <sub>3</sub> CF <sub>2</sub> Cl	540	9 600	8.8	0.05	0.03
<b>Hydrochlorofluorocarbons</b>						
HCFC-22	CHClF <sub>2</sub>	11.9	1 960	258.6	1.06	5.42
HCFC-141b	C <sub>2</sub> H <sub>3</sub> FCl <sub>2</sub>	9.4	860	26.2	0.11	0.49
HCFC-142b	CH <sub>3</sub> CF <sub>2</sub> Cl	18	2 300	22.6	-0.23	0.46
<b>Hydrofluorocarbons</b>						
HFC-125	CHF <sub>2</sub> CF <sub>3</sub>	30	3 740	39.4	3.77	1.83
HFC-134a	CH <sub>2</sub> FCF <sub>3</sub>	14	1 530	126.0	5.90	5.24
HFC-152a	CH <sub>3</sub> CHF <sub>2</sub>	1.6	164	10.6	0.14	0.38
HFC-23	CHF <sub>3</sub>	228	14 600	35.6	1.14	1.08
HFC-365mfc	CH <sub>3</sub> CF <sub>2</sub> CH <sub>2</sub> CF <sub>3</sub>	8.9	914	1.34	0.01	0.06
HFC-227ea	CF <sub>3</sub> CHFCF <sub>3</sub>	36	3 600	2.07	0.17	0.12
HFC-236fa	CF <sub>3</sub> CH <sub>2</sub> CF <sub>3</sub>	213	8 690	0.22	0.01	0.01
HFC-245fa	CHF <sub>2</sub> CH <sub>2</sub> CF <sub>3</sub>	7.7	858	3.83	0.13	0.21
HFC-32	CH <sub>2</sub> F <sub>2</sub>	5.4	771	32.7	4.04	2.46
HFC-4310mee	C <sub>5</sub> H <sub>2</sub> F <sub>10</sub>	17	1 600	0.32	0.01	0.01
HFC-143a	CH <sub>3</sub> CF <sub>3</sub>	51	5 810	28.8	1.69	1.55
<b>Perfluorinated compounds</b>						
PFC-14	CF <sub>4</sub>	50 000	7 380	87.98	1.03	0.94
PFC-116	C <sub>2</sub> F <sub>6</sub>	10 000	12 400	5.10	0.10	0.09

\* The measurements of these components have higher uncertainty. See Appendix I for more details.

<sup>1</sup> From Scientific Assessment of Ozone Depletion: 2010 (WMO, 2011b) and the 6<sup>th</sup> Assessment Report of the IPCC 2021

\*\* Carbon dioxide does not have a specific lifetime because it is continuously cycled between the atmosphere, oceans and land biosphere and its net removal from the atmosphere involves a range of processes with different time scales.

Component		Lifetime	GWP	Annual mean 2021	Absolute change last year	Trend/yr
PFC-218	C <sub>3</sub> F <sub>8</sub>	2600	9 290	0.73	0.02	0.02
PFC-318	c-C <sub>4</sub> F <sub>8</sub>	3200	10 200	1.95	0.09	0.06
Sulphurhexafluoride	SF <sub>6</sub>	3 200	25 200	10.84	0.40	0.30
Nitrogen trifluoride	NF <sub>3</sub>	569	17 400	2.78	0.30	0.23
Sulphuryl fluoride	SO <sub>2</sub> F <sub>2</sub>	36	4 630	2.87	0.13	0.10
<b>Halons</b>						
H-1211	CBrClF <sub>2</sub>	16	1 930	3.18	-0.091	-0.07
H-1301	CBrF <sub>3</sub>	72	7 200	3.39	0.004	0.02
H-2402	CBrF <sub>2</sub> CBrF <sub>2</sub>	28	2 170	0.40	-0.002	-0.01
<b>Halogenated compounds</b>						
Chloromethane	CH <sub>3</sub> Cl	0.9	5.5	511.04	2.56	-0.48
Bromomethane	CH <sub>3</sub> Br	0.8	2.4	6.76	0.07	-0.14
Dichloromethane	CH <sub>2</sub> Cl <sub>2</sub>	0.49	11.2	68.77	5.75	1.97
Trichloromethane	CHCl <sub>3</sub>	0.5	20.6	12.71	-0.38	0.20
Carbon tetrachloride	CCl <sub>4</sub>	32	2200	76.16	-1.01	-0.93
Trichloroethane	CH <sub>3</sub> CCl <sub>3</sub>	5	161	1.36	-0.17	-1.60
Trichloroethene	CHClCCl <sub>2</sub>	0.02	0.04	0.31	0.01	-0.01
Tetrachloroethene	CCl <sub>2</sub> CCl <sub>2</sub>	0.30	6.3	2.14	0.02	-0.10
<b>Volatile Organic Compounds (VOC)</b>						
Ethane	C <sub>2</sub> H <sub>6</sub>	Ca 78 days*		1541.37	18.94	-
Propane	C <sub>3</sub> H <sub>8</sub>	Ca 18 days*		352.12	11.87	-
Butane	C <sub>4</sub> H <sub>10</sub>	Ca 8 days*		115.85	-3.62	-
Pentane	C <sub>5</sub> H <sub>12</sub>	Ca 5 days*		41.88	0.42	-
Benzene	C <sub>6</sub> H <sub>6</sub>	Ca 17 days*		69.30	Not available 2018-2021	
Toluene	C <sub>6</sub> H <sub>5</sub> CH <sub>3</sub>	Ca 2 days*		20.51		

\*The lifetimes of VOCs are strongly dependent on season, sunlight, other components etc. The estimates are global averages given in C. Nicholas Hewitt (ed.): *Reactive Hydrocarbons in the Atmosphere*, Academic Press, 1999, p. 313. The times series for these are short and the trend is very uncertain.

## Monitoring of greenhouse gases and aerosols at Svalbard and Birkenes in 2021

### Annual report

## 1 Introduction to monitoring of climate gases and aerosols

### 1.1 The monitoring programme in 2021

The atmospheric monitoring programme presented in this report focuses on the concentrations of greenhouse gases and on selected particle physical and optical properties relevant for the understanding of climate change. Sampling sites are at Svalbard in the Norwegian Arctic (Zeppelin Observatory), where observations are considered to be representative for well-mixed background concentration levels, and a second site in southern Norway (Birkenes Observatory), where observations are more influenced by regional and local sources (Figure 1). A third site is in the Antarctic (Trollhaugen station).

The main objectives are to quantify the levels of the main greenhouse gases including ozone depleting substances, describe the relevant optical and physical properties of aerosols, and document their development over time. Measurements of the greenhouse gas concentrations and aerosol properties are core data for studies and assessments of climate change, and also crucial in order to evaluate mitigation strategies and their effectiveness. The Norwegian monitoring sites are located in areas where the influence of local sources is minimal, hence the sites are representative for a wider region allowing detection of long-term

*The purpose of the monitoring programme is to study the long-term development of climate gases and aerosols (particles). Measurements are performed at three sites and the results are Norwegian contributions to European and global observation networks. changes in atmospheric composition.*



*Figure 1: Location of NILU's atmospheric supersites measuring greenhouse gases and aerosol properties. Trollhaugen in Antarctica is not shown.*

### 1.2 The measurements in relation to research and policy agreements

The Norwegian greenhouse gas and aerosol monitoring programme is set up to meet national and international obligations and needs for greenhouse gas and aerosol measurement data, both for the scientific community, national environmental authorities and global policy making.

**Greenhouse gases:** The Paris Agreement was negotiated and adopted by consensus at the 21<sup>st</sup> Conference of the Parties of the UNFCCC in Paris on 12<sup>th</sup> December 2015. The Paris Agreement entered into force on 4<sup>th</sup> November 2016. As of September 2022, as many as 194 of the 198 Parties to the Convention, have ratified the Protocol<sup>2</sup>. The crucial aim of the Paris agreement is to keep the increase

<sup>2</sup> <https://unfccc.int/process/the-paris-agreement/status-of-ratification>

in the global average temperature to well below 2°C compared to pre-industrial levels and to pursue efforts to limit the temperature increase to 1.5°C. The EU Heads of State and Governments agreed in October 2014 on the headline targets and the architecture for the EU framework on climate and energy for 2030. As part of the European Green Deal, the Commission decided in July 2021 to raise the 2030 greenhouse gas emission reduction target, including emissions and removals, to at least 55% compared to 1990, and to be total zero in 2050. In the Norwegian “*Klimaloven*”<sup>3</sup> targets include a cut in greenhouse gas emissions by at least 50% and up to 55% by 2030 compared to 1990 levels<sup>4</sup>.

The ‘global methane pledge’ was launched at COP 26 in November 2021 in Glasgow<sup>5</sup>. The over 100 parties to the pledge, including the EU, US, and Norway agree to take voluntary actions to contribute to a collective effort to reduce global methane emissions at least 30 percent from 2020 levels by 2030. Participants also commit to moving towards using the highest tier IPCC good practice inventory methodologies, as well as working to continuously improve the accuracy, transparency, consistency, comparability, and completeness of national greenhouse gas inventory reporting under the UNFCCC and Paris Agreement, and to provide greater transparency in key sectors.

**Ozone depleting substances and their replacement gases:** In 1987 the Montreal Protocol was signed and entered into force in 1989 in order to reduce the production, use and eventually emission of the ozone-depleting substances (ODS). The amount of most ODS in the troposphere is now declining slowly and is expected to be back to pre-1980 levels around year 2050. It is central to follow the development of the concentration of these ozone depleting substances in order to verify that the Montreal Protocol and its amendments work as expected. The development of the ozone layer above Norway is monitored closely, and the results of the national monitoring of ozone and UV is presented in “*Monitoring of the atmospheric ozone layer and natural ultraviolet radiation: Annual report 2021*” (Svendby et al. 2022). The ozone depleting gases and their replacement gases are also strong greenhouse gases making it even more important to follow the development of their concentrations.

To control the new replacement gases, a historical agreement was signed on 15<sup>th</sup> October 2016 when negotiators from 197 countries agreed to reduce the production and consumption of hydrofluorocarbons (HFCs). The agreement was finalized at the United Nations (UN) meeting in Kigali, Rwanda, aiming to reduce the use of HFCs by more than 80% over the course of the twenty-first century. The agreement in Kigali represents an amendment of the 1987 Montreal Protocol. The HFCs can be up to 10 000 times as effective at trapping heat compared to carbon dioxide. Today HFCs account for a small fraction of the greenhouse gas emissions, have low concentrations and have had limited influence on the global warming up to now. However, the use of HFCs is growing rapidly and the projected HFC emissions could contribute up to 0.5°C of global warming by the end of this century if not regulated (Xu et al., 2013). The agreement in Kigali entered into force in January 2019 and is now legally binding for the countries that have ratified the amendment.

<sup>3</sup> <https://lovdata.no/dokument/NL/lov/2017-06-16-60>

<sup>4</sup> Details here: <http://ec.europa.eu/clima/policies/strategies/2030/> and here [http://www.consilium.europa.eu/uedocs/cms\\_data/docs/pressdata/en/ec/145397.pdf](http://www.consilium.europa.eu/uedocs/cms_data/docs/pressdata/en/ec/145397.pdf)

<sup>5</sup> <https://www.globalmethanepledge.org/>

<sup>6</sup> Norwegian Environment Agency monitoring reports

### 1.3 The ongoing monitoring programme and the link to networks and research infrastructures

In response to the need to monitor greenhouse gases and ozone depleting substances, the *Norwegian Environment Agency* and *NILU – Norwegian Institute for Air Research (NILU)* first signed a contract commissioning NILU to run a programme for monitoring greenhouse gases at the Zeppelin Observatory, close to Ny-Ålesund in Svalbard in 1999. This national programme now includes monitoring of 46 greenhouse gases and trace gases at the Zeppelin Observatory in the Arctic, many of them also ozone depleting substances. In 2009, NILU upgraded and extended the observational activity at the Birkenes Observatory in Aust-Agder. From 2010, the Norwegian Environment Agency/NILU monitoring programme was extended to also include the new observations from Birkenes of the greenhouse gases CO<sub>2</sub> and CH<sub>4</sub> and selected aerosol observations particularly relevant for the understanding of climate change. Relevant components are also reported in “*Monitoring of long-range transported air pollutants in Norway, annual report 2021*”<sup>6</sup> (Aas et al., 2021), this includes particulate and gaseous inorganic constituents, particulate carbonaceous matter, ground level ozone and particulate matter for 2021.

The locations of both sites are shown in Figure 1, and pictures of the sites are shown in Figure 3. The Zeppelin Observatory (78.90° N, 11.88° E) is located on the Zeppelin Mountain at 472 m above sea level on Spitsbergen. The unique location of the Zeppelin Observatory at Svalbard, together with the infrastructure of the scientific research community in Ny-Ålesund, makes it ideal for monitoring the global changes of concentrations of greenhouse gases and aerosols in the atmosphere. There are few local sources of emissions that can influence the observations, and the Arctic location is also important as the Arctic is a particularly vulnerable region. In relation to the 30 year anniversary of Zeppelin Observatory, NILU has written a very comprehensive paper where we detail the establishment of the Zeppelin Observatory including historical measurements of atmospheric composition in the European Arctic (Platt et al., 2022) (Figure 2). The paper presents a history of the measurements at the observatory and review the current state of the European Arctic atmosphere, including results from trends in greenhouse gases, chlorofluorocarbons (CFCs) and hydrochlorofluorocarbons (HCFCs), other traces gases, persistent organic pollutants (POPs) and heavy metals, aerosols and Arctic haze, and atmospheric transport phenomena.

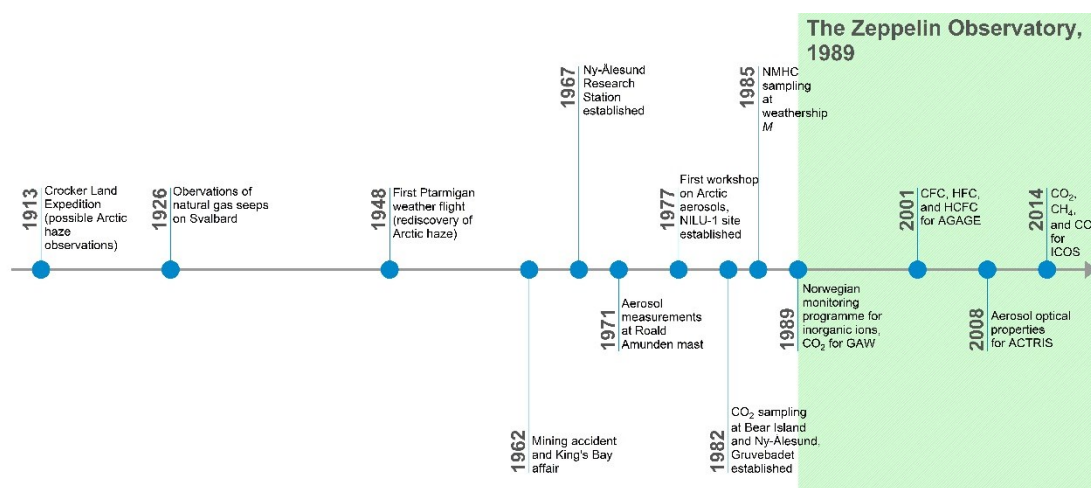


Figure 2: Timeline of various Arctic atmospheric observations, measurement sites, and later measurement programmes, see Platt et al. (2022)

The observations at the Birkenes Observatory complement the Arctic site. Birkenes Observatory is located in a forest area with few local sources. However, the Observatory often receives long-range

transported pollution from Europe and the site is ideal to analyse the contribution of long range transported greenhouse gases and aerosol properties.



*Figure 3: The two atmospheric observatories included in this programme, Zeppelin above and Birkenes to the left. A 75 m tall mast was installed at Birkenes in 2020.*

Data and results from the national monitoring programme are also included in various international programmes. Both sites contribute to EMEP ([European Monitoring and Evaluation Programme](http://www.emep.org)) under the CLRTAP (Convention on Long-range Transboundary Air Pollution). Data from the sites are also reported to CAMP (Comprehensive Atmospheric Monitoring Programme) under OSPAR (the Convention for the Protection of the marine Environment of the North-East Atlantic, <http://www.ospar.org>), AMAP (Arctic Monitoring and Assessment Programme <http://www.amap.no>), WMO/GAW (The World Meteorological Organization, Global Atmosphere Watch programme, <http://www.wmo.int>) and AGAGE (Advanced Global Atmospheric Gases Experiment).



Zeppelin and Birkenes are both included in two central European environmental research infrastructures (RI) focusing on climate forcers and air quality. International collaboration and harmonisation of these types of observations are crucial for improved processes understanding and satisfactory quality of data to assess trends. The two central RIs are ICOS (Integrated Carbon Observation System, <https://www.icos-ri.eu>) focusing on the understanding of carbon cycle, and ACTRIS (Aerosols, Clouds, and Trace gases Research InfraStructure, [www.actris.eu](http://www.actris.eu)) focusing on short-lived aerosol climate forcers and related reactive gases, and clouds. For the latter RI project, ACTRIS-Norway has been funded by the Norwegian Research Council from 2022 to support and improve the ACTRIS Data Centre. The participation in these RIs ensure required quality of the data with harmonised methods and measurements across Europe and also a global link to have comparable data and results on global scale. This is essential to reduce the uncertainty in trends and in the observed levels of the wide range of climate forcers. Overall, the networks EMEP and AGAGE, and the research infrastructures ACTRIS and ICOS are crucial for quality assurance and quality control of the Norwegian measurement data and instruments. All measurements included in this report follow the protocols, methodology and recommendations of these frameworks. This is a prerequisite for harmonised and comparable data on both European and global scale, see Table 2 at page 18. (Additionally, the implementation of Norwegian measurements in ICOS through the ICOS-Norway<sup>7</sup> project is described in the Appendix II.)

NILU hosts the data centres of the European Monitoring and Evaluation Programme (EMEP), ACTRIS and the WMO Global Atmosphere Watch (GAW) World Data Centre for Aerosol (WDCA) and GAW-World Data Centre for Reactive Gases (WDCRG), and numerous other projects and programs (e.g. AMAP, HELCOM). Data reported from these frameworks are accessible and can be downloaded directly from the EBAS data base: <http://ebas.nilu.no>. All data from the national monitoring programme and from these frameworks are reported to this database, and through this accessible for all types of users. It is important to highlight that NILU's work in ACTRIS and also hosting the WMO GAW World Data Centres for Aerosols and reactive trace gases, among many other synergy effects, ensures efficient dissemination of data on atmospheric aerosol properties collected within the Norwegian climate monitoring programme, to the scientific community. Among others, ACTRIS develops a primary standard for calibrating instruments measuring aerosol absorption, one of the properties of atmospheric black carbon, and developing quality standards for measuring the aerosol particle size distribution in order to further improve assessments of aerosol climate forcing. Another project relevant in this context is *ENVironmental Research Infrastructures building Fair services Accessible for society, Innovation and Research* (ENVRI-FAIR)<sup>8</sup> project. ENVRI-FAIR is an umbrella project for all environmental research infrastructures funded or supported by the EU under H2020. The objective is to make data FAIR, which means "*FAIR—Findable, Accessible, Interoperable, Reusable*" (Wilkinson et al., 2016). One of its goals is to put data from the atmospheric, marine, tectonic, and biosphere domains into a common context by making the data interoperable, i.e. visible in common services. The efforts started with achieving this goal first within the atmospheric domain, and NILU is leading the implementation of FAIRness within the atmospheric domain, across all European Research Infrastructures.

Compiled key information on the national monitoring programme is listed in Table 2. From 2015 the programme was extended with 16 new greenhouse gases and reactive trace gases, mainly HFCs and non-methane hydrocarbons. For some of those, quality assured measurements were possible to retrieve from the start in 2010 (many parameters from this period were initially measured and recorded, but only processed after being added to the monitoring programme). From 2016 NF<sub>3</sub> and 4 PFCs and SO<sub>2</sub>F<sub>2</sub> were also added. More detailed information on the monitoring programme and measurement frequencies are provided in Appendix II. For the measurements of aerosol properties, more details are presented in chapter 3.

---

<sup>7</sup> <https://no.icos-cp.eu>

<sup>8</sup> <http://envri.eu/envri-fair/>

Table 2: Summary of the measurement programme, run by NILU, at Birkenes and Zeppelin Observatory. The blue colour indicates the extension and components added to the program in 2015.

Component	Birkenes Start	Zeppelin Start	International network, QA programme in bold	Comment
<b>Trace gases</b>				
CO <sub>2</sub>	2009	2012	<b>ICOS</b>	Measured at Zeppelin since 1988 by Univ. Stockholm. By NILU at Zeppelin since 2012, now included in the programme. Qualified as ICOS class 1 site since 2017 and ICOS class 2 site since 2020 for Birkenes
CH <sub>4</sub>	2009	2001	<b>ICOS</b>	ICOS labelling and implementation in 2017 for Zeppelin, 2020 for Birkenes
N <sub>2</sub> O	-	2009	<b>ICOS</b>	ICOS labelling and implementation in 2017
CO	●	2001	<b>ICOS</b>	ICOS labelling and implementation in 2017
<b>CFCs</b>				*The measurements marked "*": these components are not within the required precision of AGAGE, but a part of the AGAGE quality assurance programme. This is related to the measurements in the period 2001-2010, before the installation of the Medusa instrument. After 2010, the measurements are with the same precision as the rest of the measurements in the AGAGE network.
CFC-11*				
CFC-12*				
CFC-113*				
CFC-115*				
<b>HCFCs</b>		2001/2010 and later		
HCFC-22				
HCFC-141b				
HCFC-142b				
<b>HFCs</b>				
HFC-125				
HFC-134a				
HFC-152a				
HFC-23				
HFC-227ea				
HFC-236fa				
HFC-245fa				
HFC-365mfc				
HFC-32				
HFC-4310mee				
HFC-143a				
<b>PFCs</b>				
PFC-14				
PFC-116				
PFC-218				
PFC-318				
<b>Halons</b>				
H-1211				
H-1301				
H-2402				
<b>Other chlorinated</b>				
CH <sub>3</sub> Cl				
CH <sub>3</sub> Br				
CH <sub>2</sub> Cl <sub>2</sub>				
CHCl <sub>3</sub>				
CCl <sub>4</sub>				
CH <sub>3</sub> CCl <sub>3</sub>				
CHClCCl <sub>2</sub> *				
CCl <sub>2</sub> CCl <sub>2</sub> *				
<b>Other fluorinated</b>				
SF <sub>6</sub>		2001		
NF <sub>3</sub>		2016		
SO <sub>2</sub> F <sub>2</sub>		2010		
<b>VOCs</b>		2010		
C <sub>2</sub> H <sub>6</sub> – ethane			<b>ACTRIS, EMEP</b>	

Component	Birkenes Start	Zeppelin Start	International network, QA programme in bold	Comment
<b>Trace gases</b>				
C <sub>3</sub> H <sub>8</sub> – propane				VOCs were included in the national monitoring programme from 2015, but the measurements are harmonised back to 2010.
C <sub>4</sub> H <sub>10</sub> – butane				
C <sub>5</sub> H <sub>12</sub> – pentane				
C <sub>6</sub> H <sub>6</sub> – benzene				
C <sub>6</sub> H <sub>5</sub> CH <sub>3</sub> – toluene				
<b>Aerosol measurements</b>				
Absorption properties	2009	2015	<b>ACTRIS</b> , EMEP	Measured by Univ. of Stockholm at Zeppelin, New from late 2015
Scattering properties	2009	-	<b>ACTRIS</b> , EMEP	Measured by Univ. of Stockholm at Zeppelin
Number Size Distribution	2009	2010	<b>ACTRIS</b> , EMEP	Reported in Aas et al., 2022
Cloud Condensation Nuclei	2012	-	<b>ACTRIS</b>	Zeppelin: In collaboration with Korean Polar Research Institute
Aerosol Optical depth	2010	2007	<b>AERONET</b> , <b>GAW-PFR</b>	Birkenes: AERONET, Ny-Ålesund: GAW-PFR
PM <sub>10</sub>	2001		<b>EMEP</b>	Reported in Aas et al., 2022
PM <sub>2.5</sub>	2001		<b>EMEP</b>	
Chemical composition -inorganic	1978	1979	<b>EMEP</b>	
Chemical composition - carbonaceous matter	2001		<b>EMEP</b>	

## 1.4 Greenhouse gases and aerosols, and their climate effects

The Intergovernmental Panel on Climate Change (IPCC) is the UN body for assessing the science related to climate change. IPCC's Sixth Assessment Report (IPCC AR6) and the contribution from Working Group I "*Climate Change 2021: The Physical Science Basis*" was published in August 2021. This substantial climate assessment report presents most up-to-date physical understanding of the climate system and climate change, bringing together the latest advances in climate science, and combining evidence from paleoclimate, observations, process understanding, and global and regional climate simulations. Their conclusions are based on a variety of independent indicators, some of them are observations of atmospheric compositional change.

The first main statement in the "Summary for Policymakers" (SPM) is even clearer than in the AR5 report from 2013, and leaves no doubt about the substantial climate change and associated impact on the earth system

***It is unequivocal that human influence has warmed the atmosphere, ocean and land. Widespread and rapid changes in the atmosphere, ocean, cryosphere and biosphere have occurred.***

From IPCC AR6 – 2021 and the summary for policy makers

The overall conclusion with respect to the development of the concentrations of the main greenhouse gases is:

***Observed increases in well-mixed greenhouse gas (GHG) concentrations since around 1750 are unequivocally caused by human activities. Since 2011 (measurements reported in AR5), concentrations have continued to increase in the atmosphere, reaching annual averages of 410 ppm for carbon dioxide (CO<sub>2</sub>), 1866 ppb for methane (CH<sub>4</sub>), and 332 ppb for nitrous oxide (N<sub>2</sub>O). Land and ocean have taken up a near-constant proportion (globally about 56% per year) of CO<sub>2</sub> emissions from human activities over the past six decades, with regional differences (high confidence)***

From IPCC AR6 – 2021 and the summary for policy makers

Human influence has warmed the climate at a rate that is unprecedented in at least the last 2000 years. Observed changes in global mean temperature since 1850-1900 period is slightly higher than 1 degree (IPCC, 2021b, Figure 2.3). A detailed explanation of the new estimates of global warming to date is included in the Cross-Chapter Box 2.3 in IPCC (2021).

The observed warming is driven by emissions from human activities, with greenhouse gas warming partly masked by aerosol cooling. There is a new interesting illustrative figure showing the contribution from the changes in the various atmospheric components to the warming on the period 2010-2019, relative to the temperature in 1850-1900, see Figure 4.

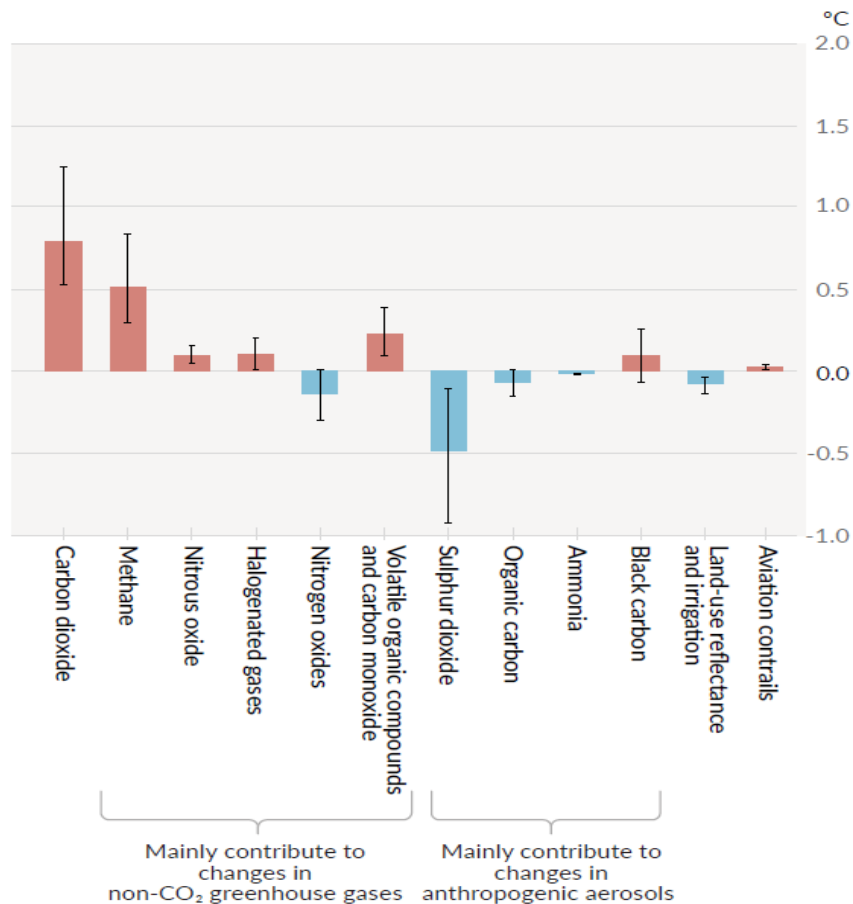


Figure 4: Contributions to 2010–2019 warming relative to 1850–1900, assessed from radiative forcing studies. Figure from IPCC AR6, SPM – panel c of SPM.2 (IPCC, 2021b). The figure shows temperature changes from individual components of human influence, including emissions of greenhouse gases, aerosols and their precursors; land-use changes (land-use reflectance and irrigation); and aviation contrails. Whiskers show very likely ranges. Estimates account for both direct emissions into the atmosphere and their effect, if any, on other climate drivers. For aerosols, both direct (through radiation) and indirect (through interactions with clouds) effects are considered

The left part of Figure 4 shows the contribution from GHG gases, and the right part the impact from anthropogenic changes in aerosol components where e.g., sulphur dioxide and organic carbon is important for the cooling effect. The basic metric to compare the effect of the various climate change drivers is radiative forcing (RF). RF is the net change in the energy balance of the Earth system due to some imposed change. RF provides a quantitative basis for comparing potential climate response to different changes and the values in Figure 4 are assessed from radiative forcing studies. Forcing is often presented as the radiative change from one time-period to another, such as pre-industrial to present-day. For many forcing agents the RF is an appropriate way to compare the relative importance of their potential climate effect. However, rapid adjustments in the troposphere can either enhance or reduce the perturbations, leading to large differences in the forcing driving long-term climate change. In the AR5 IPCC report it was also introduced a new concept, the effective radiative forcing (ERF): the energy imbalance after allowing for atmospheric temperatures, water vapor, and clouds to adjust to the forcing agent, while keeping surface conditions (specifically temperature) unchanged. Figure 5 shows the ERF of the main components referring to a change in the atmospheric level since 1750, pre-industrial time.

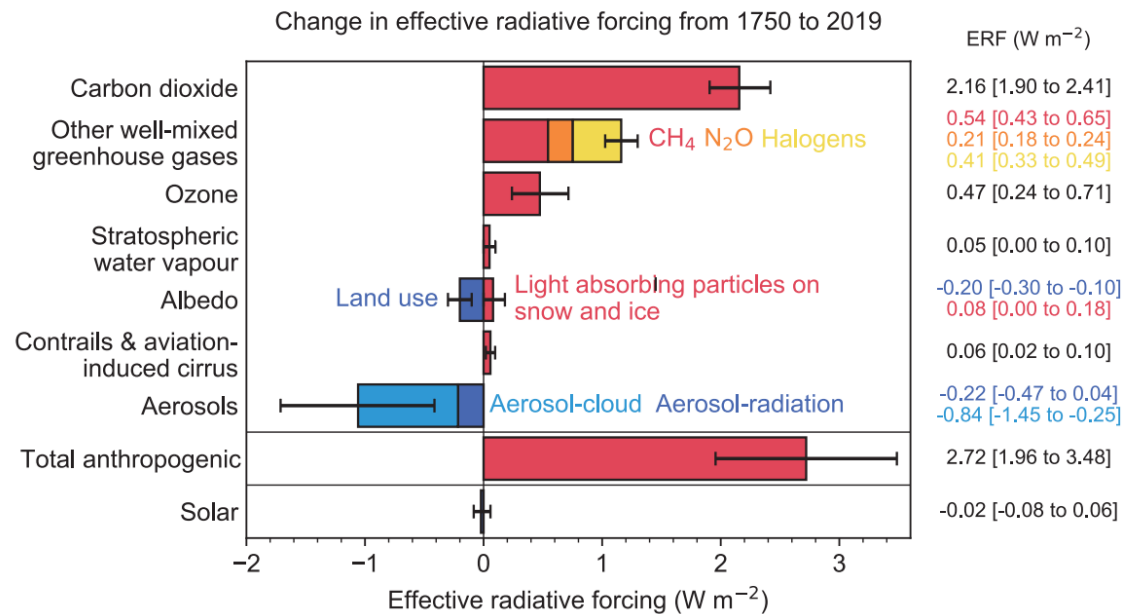


Figure 5: Change in effective radiative forcing (ERF) from 1750 to 2019 by contributing forcing agents (carbon dioxide, other well-mixed greenhouse gases (WMGHGs), ozone, stratospheric water vapour, surface albedo, contrails and aviation-induced cirrus, aerosols, anthropogenic total, and solar). Solid bars represent best estimates, and very likely (5–95%) ranges are given by error bars. Non-CO<sub>2</sub> WMGHGs are further broken down into contributions from methane (CH<sub>4</sub>), nitrous oxide (N<sub>2</sub>O) and halogenated compounds. Surface albedo is broken down into land-use changes and light-absorbing particles on snow and ice. Aerosols are broken down into contributions from aerosol–cloud interactions (ERF<sub>aci</sub>) and aerosol–radiation interactions (ERF<sub>ari</sub>). (Taken from IPCC, 2021 Figure 7.6.)

Chapter 2, “Changing state of the climate system”, presents all types of atmospheric and surface observations, including observations of greenhouse gases since the start of the observations in mid-1950s and changes in aerosols since the 1980s. This monitoring programme measures all relevant GHGs and optical and physical particle properties. Through the link and contribution to the international programmes EMEP, and AGAGE, the research infrastructures ACTRIS, ICOS the national program contribute to the trends and global mean data included in AR6 (see also section 2.1.1 at page 26 for details about the GHGs and in section 3.1 at page 73 for aerosols).

## 2 Norwegian observations of greenhouse gases

NILU measures 46 climate gases at the Zeppelin Observatory at Svalbard and 2 at Birkenes, in addition to surface ozone reported in Aas et al., 2022. The results and analyses of the climate gas measurements are presented in this chapter. Furthermore, observations of CO<sub>2</sub> for the time period 1988-2012 at Zeppelin performed by the Stockholm University - Department of Environmental Science and Analytical Chemistry (ACES), are included in this report.

Table 3 summarises the main results for 2021 and the trends over the period 2001-2021. The table also includes 2021 global annual mean values given in Bulletin of the American Meteorological Society (BAMS) (Lan et al., 2022).

*Table 3: Greenhouse gases measured at Zeppelin and Birkenes; lifetimes in years, global warming potential (GWP) for 100 year horizon and annual mean for 2021, change last year, and trends per year over the measurement period. Red is increasing and blue is decreasing trends. Global means for 2021 taken from Bulletin of the American Meteorological Society (Lan et al., 2022) are included for comparison. All concentrations are mixing ratios in ppt, except for methane, nitrous oxide and carbon monoxide (ppb) and carbon dioxide (ppm).*

Component		Life-time	GWP	Global mean BAMS 2021	Annual mean 2021	Absolute change last year	Trend/yr
Carbon dioxide - Zeppelin	CO <sub>2</sub>	-	1	-	417.4	3.2	2.5
Carbon dioxide - Birkenes					421.3	2.5	2.5
Methane - Zeppelin	CH <sub>4</sub>	11.8	28	-	1981.4	12.7	6.7
Methane - Birkenes					1991.7	16.4	9.0
Carbon monoxide	CO	few months	-	-	128.0	10.3	-0.8
Nitrous oxide	N <sub>2</sub> O	109	273	-	334.5	1.08	1.01
<b>Chlorofluorocarbons</b>							
CFC-11	CCl <sub>3</sub> F	52	5 560	222.2	222.6	-2.44	-1.77
CFC-12	CF <sub>2</sub> Cl <sub>2</sub>	102	11 200	493.9	498.0	-3.67	-2.64
CFC-113	CF <sub>2</sub> ClCFCl <sub>2</sub>	93	6 520	68.5	69.1	-0.41	-0.63
CFC-115	CF <sub>3</sub> CF <sub>2</sub> Cl	540	9 600	-	8.8	0.05	0.03
<b>Hydrochlorofluorocarbons</b>							
HCFC-22	CHClF <sub>2</sub>	11.9	1 960	248.9	258.6	1.06	5.42
HCFC-141b	C <sub>2</sub> H <sub>3</sub> FCl <sub>2</sub>	9.4	860	24.6	26.2	0.11	0.49
HCFC-142b	CH <sub>3</sub> CF <sub>2</sub> Cl	18	2 300	21.5	22.6	-0.23	0.46
<b>Hydrofluorocarbons</b>							
HFC-125	CHF <sub>2</sub> CF <sub>3</sub>	30	3 740	34.7	39.4	3.77	1.83
HFC-134a	CH <sub>2</sub> FCF <sub>3</sub>	14	1 530	118.9	126.0	5.90	5.24
HFC-152a	CH <sub>3</sub> CHF <sub>2</sub>	1.6	164	7.2	10.6	0.14	0.38
HFC-23	CHF <sub>3</sub>	228	14 600	34.9	35.6	1.14	1.08
HFC-365mfc	CH <sub>3</sub> CF <sub>2</sub> CH <sub>2</sub> CF <sub>3</sub>	8.9	914	1.05	1.34	0.01	0.06
HFC-227ea	CF <sub>3</sub> CHFCF <sub>3</sub>	36	3 600	1.87	2.07	0.17	0.12
HFC-236fa	CF <sub>3</sub> CH <sub>2</sub> CF <sub>3</sub>	213	8 690	-	0.22	0.01	0.01
HFC-245fa	CHF <sub>2</sub> CH <sub>2</sub> CF <sub>3</sub>	7.7	858	-	3.83	0.13	0.21
HFC-32	CH <sub>2</sub> F <sub>2</sub>	5.4	771	23.6	32.7	4.04	2.46

Component		Life-time	GWP	Global mean BAMS 2021	Annual mean 2021	Absolute change last year	Trend/yr
HFC-4310mee	C <sub>5</sub> H <sub>2</sub> F <sub>10</sub>	17	1 600	-	0.32	0.01	0.01
HFC-143a	CH <sub>3</sub> CF <sub>3</sub>	51	5 810	26.5	28.8	1.69	1.55
<b>Perfluorinated compounds</b>							
PFC-14	CF <sub>4</sub>	50 000	7 380	87.4	87.98	1.03	0.94
PFC-116	C <sub>2</sub> F <sub>6</sub>	10 000	12 400	5.03	5.10	0.10	0.09
PFC-218	C <sub>3</sub> F <sub>8</sub>	2600	9 290	0.721	0.73	0.02	0.02
PFC-318	c-C <sub>4</sub> F <sub>8</sub>	3200	10 200	1.9	1.95	0.09	0.06
Sulphurhexafluoride	SF <sub>6</sub>	3 200	25 200	10.63	10.84	0.40	0.30
Nitrogen trifluoride	NF <sub>3</sub>	569	17 400	-	2.78	0.30	0.23
Sulphuryl fluoride	SO <sub>2</sub> F <sub>2</sub>	36	4 630	-	2.87	0.13	0.10
<b>Halons</b>							
H-1211	CBrClF <sub>2</sub>	16	1 930	3.03	3.18	-0.09	-0.07
H-1301	CBrF <sub>3</sub>	72	7 200	3.31	3.39	0.004	0.02
H-2402	CBrF <sub>2</sub> CBrF <sub>2</sub>	28	2 170	0.396	0.40	-0.002	-0.01
<b>Halogenated compounds</b>							
Chloromethane	CH <sub>3</sub> Cl	0.9	5.5	547.2	511.04	2.56	-0.48
Bromomethane	CH <sub>3</sub> Br	0.8	2.4	6.61	6.76	0.07	-0.14
Dichloromethane	CH <sub>2</sub> Cl <sub>2</sub>	0.49	11.2	-	68.77	5.75	1.97
Trichloromethane	CHCl <sub>3</sub>	0.5	20.6	-	12.71	-0.38	0.20
Carbon tetrachloride	CCl <sub>4</sub>	32	2200	76.2	76.16	-1.01	-0.93
Trichloroethane	CH <sub>3</sub> CCl <sub>3</sub>	5	161	1.2	1.36	-0.17	-1.60
Trichloroethene	CHClCCl <sub>2</sub>	0.02	0.04	-	0.31	0.01	-0.01
Tetrachloroethene	CCl <sub>2</sub> CCl <sub>2</sub>	0.30	6.3	-	2.14	0.02	-0.10
<b>Volatile Organic Compounds (VOC)</b>							
Ethane	C <sub>2</sub> H <sub>6</sub>	Ca 78 days*		-	1541.37	18.94	2.77
Propane	C <sub>3</sub> H <sub>8</sub>	Ca 18 days*		-	352.12	11.87	-15.72
Butane	C <sub>4</sub> H <sub>10</sub>	Ca 8 days*		-	115.85	-3.62	-7.42
Pentane	C <sub>5</sub> H <sub>12</sub>	Ca 5 days*		-	41.88	0.42	-2.49
Benzene	C <sub>6</sub> H <sub>6</sub>	Ca 17 days*		-	69.30	-	-
Toluene	C <sub>6</sub> H <sub>5</sub> CH <sub>3</sub>	Ca 2 days*		-	20.51	-	-

\*The lifetimes of VOCs are strongly dependent on season, sunlight, other components etc. The estimates are global averages given in C. Nicholas Hewitt (ed.): *Reactive Hydrocarbons in the Atmosphere*, Academic Press, 1999, p. 313. The times series for these are short and the trend is very uncertain.



Most greenhouse gases and other climate gases have numerous sources, both anthropogenic and natural. Trends and future changes in concentrations are determined by their sources and sinks, and in section 2.2 observations and trends of the monitored greenhouse gases with both natural and anthropogenic sources are presented in more detail. In Section 2.3 the detailed results of the ozone depleting substances with purely anthropogenic sources are presented.

For annual trend calculations we have used the method described in Appendix II. In order to estimate uncertainties, we have applied an updated method taking auto-correlated errors in the fitted model residuals into account. Appendix II also includes a description of the measurements at the Zeppelin and Birkenes Observatories in more detail. Generally, Zeppelin Observatory is a unique site for observations of changes in the background level of atmospheric components. All peak concentrations of the measured gases are significantly lower here than at other sites at the Northern hemisphere, due to the station's remote location. Birkenes is closer to the main source areas. Further, the regional vegetation is important for regulating the carbon cycle, resulting in much larger variability in the concentration level compared to the Arctic region.

### 2.1.1 IPCC AR6 forcing and annual mean value of the main GHG components compared to measurements at Zeppelin Observatory

This section relates the annual mean value of the main GHG components at Zeppelin to the values reported in AR6 IPCC published August 2021. The values used in AR6 refers to the 2019 year, and relates this to development since pre-industrial times, the previous report (AR5), and the year 2011. Comparison with measurements from Zeppelin Observatory is of particular interest. Zeppelin Observatory is monitoring the northern hemisphere but also global changes of concentrations of greenhouse gases and aerosols in the atmosphere.

In 2019, concentrations of CO<sub>2</sub>, CH<sub>4</sub> and N<sub>2</sub>O reached global mean levels of 410 ppm, 1866 ppb, and 332 ppb, respectively (IPCC, 2021). The atmospheric concentration of these gases has increased from the pre-industrial time (1750) to 2019 by 47.3%, 157.8%, and 23.0%, respectively. These changes are larger than those between glacial and interglacial periods over the last 800,000 years, and illustrated for CO<sub>2</sub> in Figure 6.

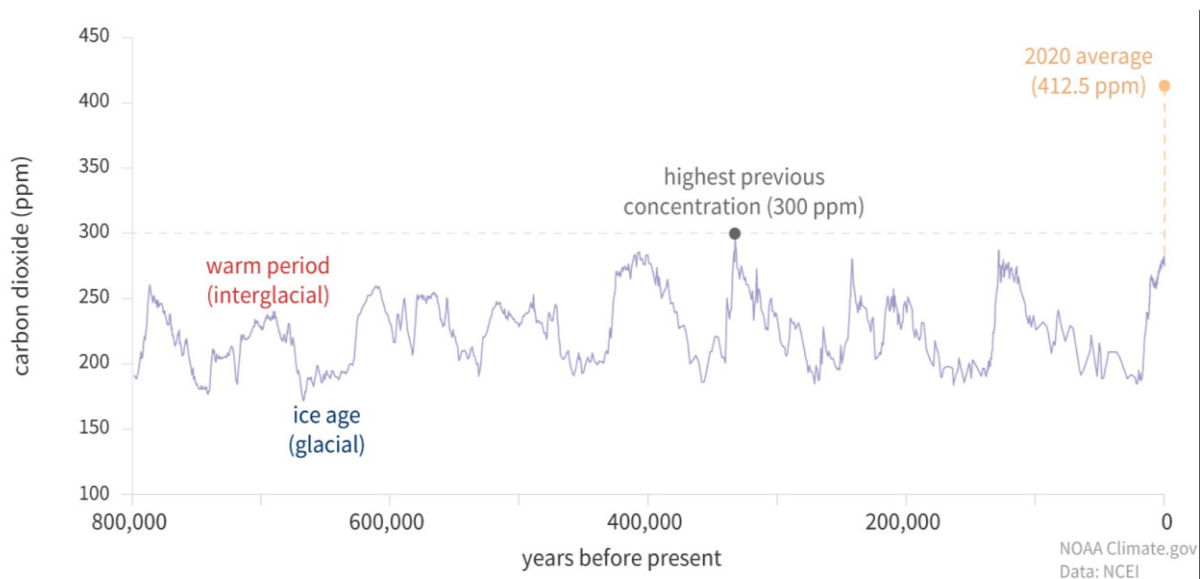


Figure 6: Global atmospheric CO<sub>2</sub> in parts per million (ppm) for the past 800,000 years. Graph by NOAA Climate.gov (<https://www.climate.gov/news-features/understanding-climate/climate-change-atmospheric-carbon-dioxide>)

The average annual CO<sub>2</sub> increase from 2000 through 2011 was 2.0 ppm/yr. From 2011 through 2019 it was 2.4 ppm/yr, which is higher than that of any comparable time periods since global measurements began (IPCC, 2021).

The change in the GHG concentrations results in increase of the direct radiative forcing. The best estimate of the total radiative forcing from CO<sub>2</sub>, CH<sub>4</sub>, and N<sub>2</sub>O in 2019 relative to 1750 is 2.9 W m<sup>-2</sup>, an increase of 12.5% from 2011 (IPCC, 2021). For CO<sub>2</sub>, the forcing since 1750 is now 2.16 Wm<sup>-2</sup> since 1750 (compared to 1.88 Wm<sup>-2</sup> in AR5) and the CH<sub>4</sub> forcing has increased to 0.54 Wm<sup>-2</sup> since 1750 (from 0.48 Wm<sup>-2</sup> in AR5). Radiative forcing from halogenated components in 2019 was 0.4 Wm<sup>-2</sup>, an increase of 3.5% since 2011. Table 4 summarizes the changes in the concentration of CO<sub>2</sub>, CH<sub>4</sub>, and N<sub>2</sub>O between 2011 and 2019 as included in AR6 (IPCC 2021), considering measurements from the global NOAA and AGAGE networks, and from the Zeppelin Observatory.

*Table 4: Comparison of atmospheric mixing ratios observed in 2011 and 2019, and relative change since 2011, estimated from the NOAA and AGAGE global networks presented in AR6 (IPCC, 2021) and observations at the Zeppelin Observatory. Units are in ppm for CO<sub>2</sub> and ppb for CH<sub>4</sub> and N<sub>2</sub>O.*

Species	Network/station	2011	2019	Change (%)
CO <sub>2</sub>	NOAA - <i>global mean</i>	390.5	409.9	5.0
	AGAGE - <i>global mean</i>	390.9	410.5	5.0
	Zeppelin	392.5	411.9	4.9
CH <sub>4</sub>	NOAA - <i>global mean</i>	1803.1	1866.6	3.5
	AGAGE - <i>global mean</i>	1813	1877	3.5
	Zeppelin	1880	1953	3.9
N <sub>2</sub> O	NOAA - <i>global mean</i>	324.2	331.9	2.4
	AGAGE - <i>global mean</i>	324.3	332.0	2.4
	Zeppelin	324.2	332.1	2.4

For CO<sub>2</sub> and CH<sub>4</sub> the annual mean values at Zeppelin are higher than the global means reported in AR6. This is due to the fact the Zeppelin is at the Northern Hemisphere, where the main emissions are. However, the percentage changes are at the same level. Methane has a larger variation than CO<sub>2</sub> since it has a shorter lifetime, hence the local/hemispheric influence is larger. For CO<sub>2</sub>, the data from NOAA and AGAGE show an increase of 5.0% from 2011 to 2019, whereas the measured change at Zeppelin is 4.9%. The CH<sub>4</sub> increase at Zeppelin (3.9%) is slightly higher than the global mean increases from NOAA and AGAGE (3.5%). For N<sub>2</sub>O the measured increase from 2011 through 2019 from NOAA, AGAGE and Zeppelin are all 2.4%.

For the CFCs and other halogenated compounds there is also consistency between percentage changes measured at Zeppelin and data from AGAGE. For CFC-11, CFC-12, and CFC-113 the percentage 2011-2019 changes from AGAGE are -4.8%, -4.7%, and 6.3%, respectively. The corresponding changes at Zeppelin are -4.5%, -4.9%, and -6.2%. HFC-32 is the halogenated compound where the atmospheric concentration is growing fastest: from 2011 through 2019 AGAGE and Zeppelin reported increases of 304% and 284%, respectively. The concentration of HFC-125 has also increased dramatically from 2011 to 2019: changes of 186% and 174% are estimated from the AGAGE and Zeppelin data, respectively.

## 2.2 Climate gases with natural and anthropogenic sources

The annual mean concentrations for all gases included in the programme for all years are given in Appendix I, Table A 1 at page 120. All the trends, uncertainties and regression coefficients are found in Table A 2 at page 123. Section 2.2 focuses on the measured greenhouse gases that have both natural and anthropogenic sources.

### 2.2.1 Carbon dioxide (CO<sub>2</sub>)

**Key findings for CO<sub>2</sub>:** *CO<sub>2</sub> concentrations have increased in all years, in accordance with accumulation of gas in the atmosphere and the global development and increase in anthropogenic emissions. The annual CO<sub>2</sub> means in 2021 reached new record levels: 417.4 ppm at Zeppelin and 421.3 ppm at Birkenes. The increases from 2020 to 2021 are 3.2 ppm and 2.5 ppm, respectively. The annual atmospheric CO<sub>2</sub> increase continues to be high, with no sign of a reduced increase, including no sign of an effect of COVID-19 related lockdowns, neither at the Zeppelin nor Birkenes Observatories.*

Carbon dioxide (CO<sub>2</sub>) is the most important anthropogenic greenhouse gas, with a radiative forcing of 2.16 Wm<sup>-2</sup> since the year 1750 (IPCC, 2021). This strong forcing is due to the large increase in concentration over the years. CO<sub>2</sub> is the end-product of the atmospheric oxidation of all main VOCs, and levels have increased by more than 50 % since preindustrial times. This is mainly due to emissions from fossil fuel combustion and land-use change.

#### *On Emissions of CO<sub>2</sub>*

The Global Carbon Project<sup>9</sup> <http://www.globalcarbonproject.org> provides yearly updates on estimated emissions. CO<sub>2</sub> emissions are from fossil fuel burning (including oil, gas, coal and flaring) and cement production. Global fossil CO<sub>2</sub> emissions were 36.7 ± 2 GtCO<sub>2</sub> in 2019, a 61% increase compared to 1990 levels. Comparing the various periods, CO<sub>2</sub> emissions increased by 0.9 % per year from 1990 – 2000. Then for the next 10 years, the increase was 3.0% per year from 2000-2010, and 0.9% from 2010-2018. The global growth is driven by the underlying changes at the country level, in particular the total emissions in China and India are increasing. From 2019 to 2020 it was a record decrease in CO<sub>2</sub> emissions (-5.4%) related to COVID-19. However, the global fossil CO<sub>2</sub> emissions in 2021 were almost back to the pre-COVID levels, around 36.4 GtCO<sub>2</sub>.

The global carbon project provides an estimate of the overall impact of COVID-19 on regional emissions. While China's emissions declined strongly during February 2020, the maximum emission decline in the rest of the world was reached in April 2020. Global emissions from transport, especially road transport, were especially affected by the restrictions aimed at reducing infection rates. Except from a few years with international crises, the global fossil CO<sub>2</sub> emissions have risen steadily over the last decades.

#### *The measurements*

NILU started CO<sub>2</sub> measurements at the Zeppelin Observatory in 2012 and the results are presented in Figure 7, together with the time series provided by ITM, University of Stockholm, back to 1988. After upgrading Birkenes in 2009, there are continuous measurements of CO<sub>2</sub> and CH<sub>4</sub> from mid May 2009 also at this site.

---

<sup>9</sup> Used with permission of the Global Carbon Project under the Creative Commons Attribution 4.0 International license

The atmospheric daily mean CO<sub>2</sub> concentration measured at the Zeppelin Observatory for the period mid 1988-2021 is presented in Figure 7 (upper panel), together with the 2009-2021 time series for Birkenes in the lower panel.

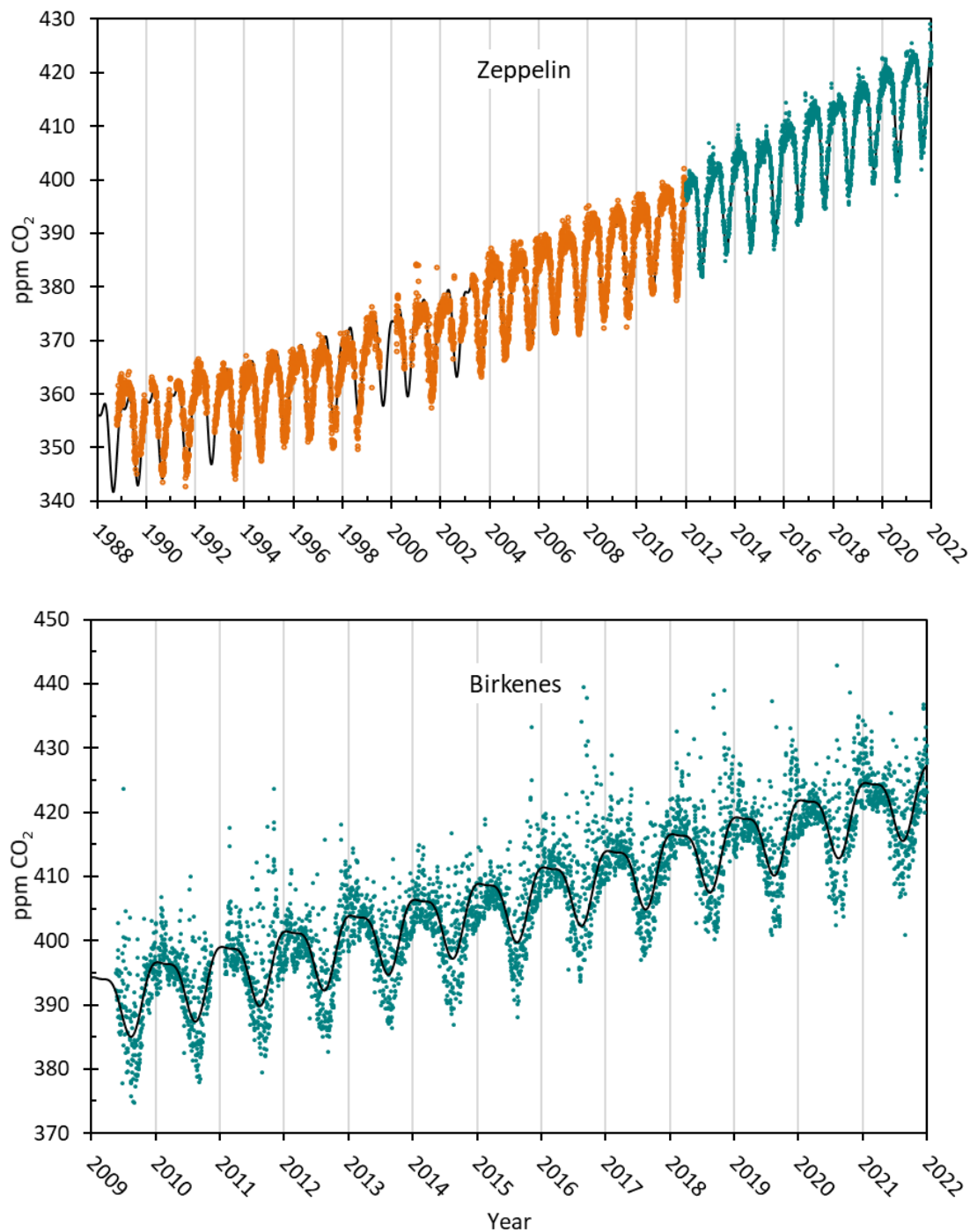


Figure 7: The atmospheric daily mean CO<sub>2</sub> concentrations measured at the Zeppelin Observatory for the period mid 1988-2021 are presented in the upper panel. Prior to 2012, ITM University of Stockholm provided all data, shown in orange. The green dots represent measurements from the Picarro instrument installed by NILU in 2012. CO<sub>2</sub> measurements at Birkenes are shown in the lower panel, the green dots are daily mean concentrations. The black solid line is empirical fitted CO<sub>2</sub> mixing ratio.

The results show continuous increase since the start of the observations at both sites, and as can be seen there is larger CO<sub>2</sub> variability at Birkenes than Zeppelin. At Zeppelin the largest variability is during winter/spring, whereas Birkenes has large variability all year around. In summer there is also a clear diurnal variation with high values during the night and lower values during daytime (not shown). This is mainly due to changes between plant photosynthesis and respiration, but also the general larger meteorological variability and diurnal change in planetary boundary layer, particularly during summer, contributes to larger variations in the concentrations. In 2020, NILU installed a 75 m mast, to also measure above the canopy (see the appendix and Figure 59 included there at page 146) to limit these influences.

In addition to the diurnal variations, there are also episodes with higher CO<sub>2</sub> levels at both sites due to long range transport of pollution. In general, there are high levels when the meteorological situation results in transport from Central Europe or United Kingdom at Birkenes, and from central Europe or Russia at Zeppelin.

The maximum daily mean CO<sub>2</sub> value in 2021 at Zeppelin was 429.2 ppm, measured on 17<sup>th</sup> December. During this period the wind direction and atmospheric circulation pattern indicate that air was transported from Eastern Europe and Russia. At Birkenes the highest daily mean value in 2021 was as high as 436.7 ppm, measured 12<sup>th</sup> December. This day the air at Birkenes had mainly been transported from Central Europe and Russia, shifting to the UK and Atlantic sector in the afternoon.

Figure 8 shows the development of the annual mean concentrations of CO<sub>2</sub> measured at Zeppelin for the period 1988-2021 (in orange) together with the values from Birkenes (in green) for the period 2009-2021. The global annual mean values as given by WMO (WMO, 2021) are in black. The yearly annual changes at Zeppelin and Birkenes are shown in the lower panel.

The annual mean CO<sub>2</sub> values at Birkenes and Zeppelin are higher than the global annual mean value as there are more anthropogenic sources and pollution at the Northern hemisphere. The mixing of air between the two hemispheres takes about 2-3 years' time. The CO<sub>2</sub> annual mean in 2021, shown in Figure 8 (upper panel), was 421.3 ppm and 417.4 ppm at Birkenes and Zeppelin, respectively. The annual CO<sub>2</sub> changes illustrated in Figure 8, lower panel, shows an increase of 3.2 ppm at Zeppelin from 2020 to 2021. At Birkenes the CO<sub>2</sub> increase from 2020 to 2021 was 2.5 ppm. The global mean annual CO<sub>2</sub> increase from 2020 to 2021 is not yet published.

Trend analyses based on method described in Appendix II show that CO<sub>2</sub> at Birkenes and Zeppelin both increase by 2.5 ppm/yr, in line with the average annual increase published in AR6 IPCC, 2021. This corresponds to an annual increase of ~0.64 %/yr. These trend analyses are based on data from Picarro instruments, only (which were installed by NILU in 2012). If we use the entire Zeppelin time series back to 1988, the trend is less pronounced (~0.55%/yr), indicating that the CO<sub>2</sub> increase has intensified over the last decade.

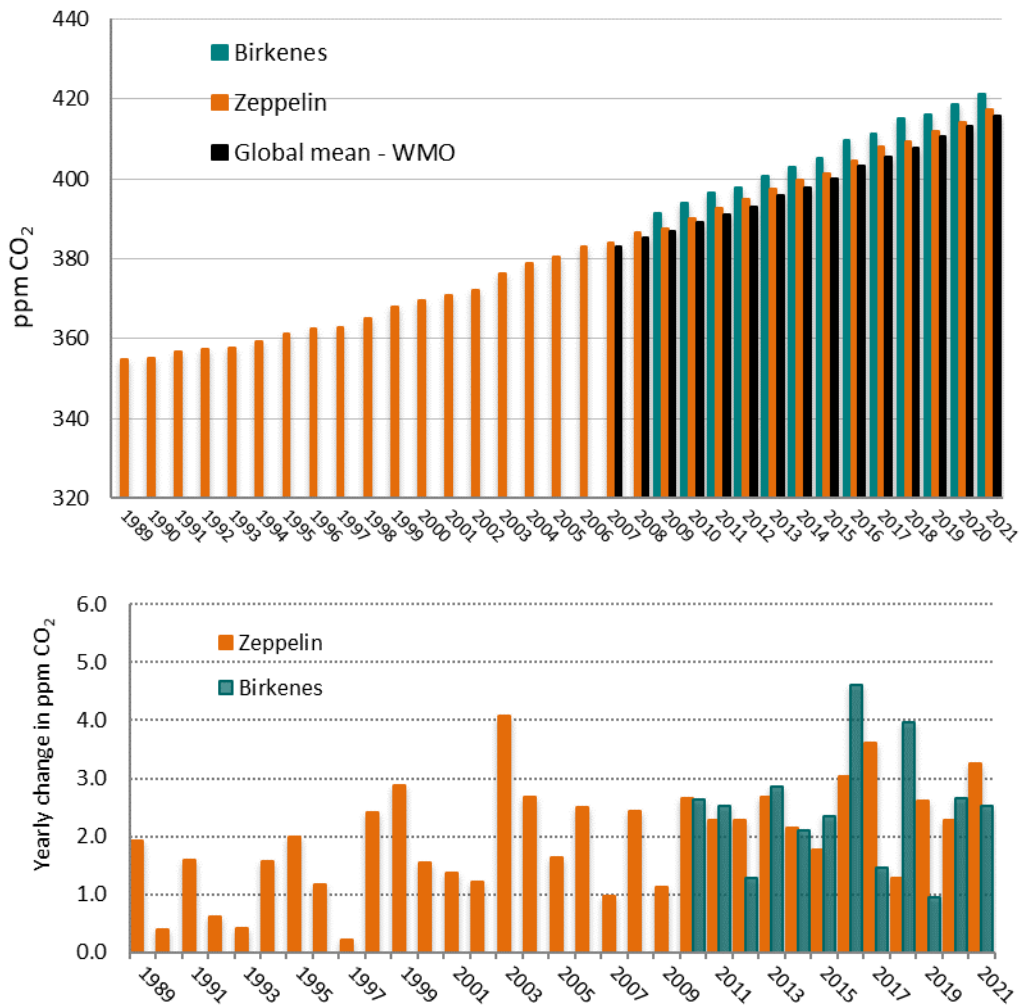


Figure 8: Upper panel: the annual mean concentrations of CO<sub>2</sub> measured at Zeppelin Observatory for the period 1989-2021 shown in orange. Prior to 2012, ITM University of Stockholm provides all data. The annual mean values from Birkenes are shown as green bars. The global mean values as given by WMO (2008-2021) are included in black. The yearly annual increases are shown in the lower panel, orange for Zeppelin, green for Birkenes.

It is interesting to note that in 2018, Europe experienced one of the worst droughts of the last 20 years. The extensive heatwave and drought in 2018 had a negative impact on vegetation across Western and Northern Europe. An exceptionally long period of high temperatures and little precipitation resulted in an unprecedented browning of vegetation. It also meant that Europe's vegetation took up limited CO<sub>2</sub> from the atmosphere (Thompson et al., 2020, Ramonet et al 2020). We can also see signs of this at Birkenes (in Figure 8), as 2018 was one of the years with highest annual change in CO<sub>2</sub>.

## 2.2.2 Methane (CH<sub>4</sub>)

**Key findings for Methane:** In 2021, the annual average methane concentration at Zeppelin increased by 12.7 ppb from previous year and reached a record level of 1981.4 ppb. At Birkenes the annual mean value in 2021 was 1991.7 ppb, 16.4 ppb higher than previous year. This is the highest increase that is registered at this station. These strong increase in methane concentrations are of great concern as the processes behind it are not well constrained and can be due to climate feedback emission processes.

Methane (CH<sub>4</sub>) is the second most important greenhouse gas from human activity after CO<sub>2</sub>. The IPCC has reported a radiative forcing of 0.54 W m<sup>-2</sup> since 1750 and up to 2019 (IPCC, 2021). Etminan et al. (2016) presented revised forcing estimates for all main greenhouse gases, and for CH<sub>4</sub> this resulted in 25% stronger forcing than given in the IPCC Fifth Assessment Report, and the updates are taken into account in AR6 (IPCC 2021).

In addition to being a dominant greenhouse gas, methane also plays central role in atmospheric chemistry. The atmospheric lifetime<sup>10</sup> of methane is 11.8 years (IPCC 2021), when indirect effects are included, as explained in Section 1.4. Excluding indirect effects, the lifetime is ca 9-10 years.

The average CH<sub>4</sub> concentration in the atmosphere is determined by a balance between emission from the various sources and reaction and removal by free hydroxyl radicals (OH) to eventually produce water and CO<sub>2</sub>. A small fraction is also removed by surface deposition and reaction with Cl. Since the reaction with OH also represents a significant loss path for the OH itself, additional CH<sub>4</sub> emission will consume additional OH and thereby increasing its own lifetime, implying further increases in atmospheric CH<sub>4</sub> concentrations (and in those of all other compounds significantly removed by OH, i.e. most VOCs) (Isaksen and Hov, 1987; Prather et al., 2001), i.e. a positive feedback.

The concentration of CH<sub>4</sub> was, after a strong increase during the 20<sup>th</sup> century, relatively stable over the period 1998-2006 (Dalsøren et al., 2016). The global average change was close to zero for this period, also at Zeppelin. Since 2005 a strong increase in the CH<sub>4</sub> levels is evident from our observations both at Zeppelin and Birkenes as well as observations at other sites, and in the global mean (WMO, 2021).

### On Emissions of CH<sub>4</sub>

The Global Carbon Project <http://www.globalcarbonproject.org> rereleased new and updated emission estimates and global methane budget 15<sup>th</sup> July 2020. No updates are released after this. The emission estimates are for 2017, and they are compared to mean emissions for the period 2000-2006. According to the Global Carbon Project and the underlying peer-reviewed papers (Saunio et al., 2020 and Jackson et al. 2020) the distribution between natural and anthropogenic sources of CH<sub>4</sub> is approximately 40% natural sources, and 60% of the sources are direct result of anthropogenic emissions. The main anthropogenic sources include emissions from agriculture (e.g., rice paddies, ruminant animals), waste and extraction and combustion of fossil fuels (oil, gas and coal). CH<sub>4</sub> is the principal component of natural gas and leakage from pipelines and off- and on-shore installations are a known source of atmospheric CH<sub>4</sub>. The main natural sources are tropical, boreal and Arctic wetlands, freshwater systems (lakes and rivers), and geological sources such as terrestrial and marine seeps and volcanoes. Of natural sources there is a large unknown potential methane source under the ocean floor, so called methane hydrates and seeps.

Global Carbon Project report (Saunio et al., 2020) that the increasing anthropogenic methane emissions arise approximately equally from agricultural and fossil fuel sources. According to the estimate from this project, anthropogenic emissions dominate in the northern mid-latitudes, with the highest contribution from agriculture and waste emissions (42 % of total emissions), closely followed by fossil fuel emissions (31 % of total emissions). Boreal regions are largely dominated by wetland

---

<sup>10</sup> Time taken to decay to 1/e, 1/2.7, of original levels



emissions (60 % of total emissions). The situation is different in the polar regions and southern hemisphere (see also section 2.2.2.2.). Despite rapidly warming air temperatures (World Meteorological Organization, 2019), methane emissions from northern high-latitude systems (>60°N) were virtually unchanged in 2017 relative to the average value for 2000–2006. Other regions contributed the most to greater methane emissions in 2017 compared with 2000–2006: Africa and the Middle East, China, and South Asia and Oceania. Here, agriculture and waste contributed 60% of this increase and fossil fuels the remaining 40%, with a slight decrease estimated for biomass and biofuel burning. It is worth noting that Europe is the only region with a slight decrease in CH<sub>4</sub> emissions in 2017 compared to the period 2000-2006.

More broadly, wetlands and freshwater systems are the largest source of methane but also the greatest source of uncertainty in the current global methane budget. Furthermore, a large unknown for the future arises due to a possible feedback via thawing permafrost. Permafrost contains CH<sub>4</sub>, which may be directly released to the atmosphere. Furthermore, melting permafrost can create water logged soils and release carbon stores, creating new high latitude wetlands also linked with CH<sub>4</sub> emissions (a secondary effect). The balance between the release of CO<sub>2</sub> and CH<sub>4</sub> from thawing permafrost, will thus also depend on the precipitation and changes in moisture.

### *The measurements*

Figure 9 shows daily mean observations of CH<sub>4</sub> at Zeppelin since the start in 2001 (upper panel) and Birkenes since start in 2009 (lower panel). As can be seen from the figures there has been an increase in the concentrations of CH<sub>4</sub> at both sites the last years, and in general the concentrations are higher at Birkenes than at Zeppelin. The highest ambient CH<sub>4</sub> concentration ever detected at Zeppelin, 2043 ppb, was measured on the 17<sup>th</sup> December 2021. The transport pattern on this day indicates a strong influence from Eastern Europe and Russia. Fugitive emissions from Russian gas installations are normally the source of such high CH<sub>4</sub> values. The maximum CH<sub>4</sub> daily mean value recorded at Birkenes in 2021 was 2111 ppb, measured 29<sup>th</sup> November.

For both Zeppelin and Birkenes, the seasonal variations are clearly visible, although stronger at Birkenes than Zeppelin. This is due to longer distance to the sources at Zeppelin, and thus the sink through reaction with OH dominates the variation. The larger variations at Birkenes are explained by both the regional sources in Norway, as well as a stronger impact of pollution transported from central Europe or UK.

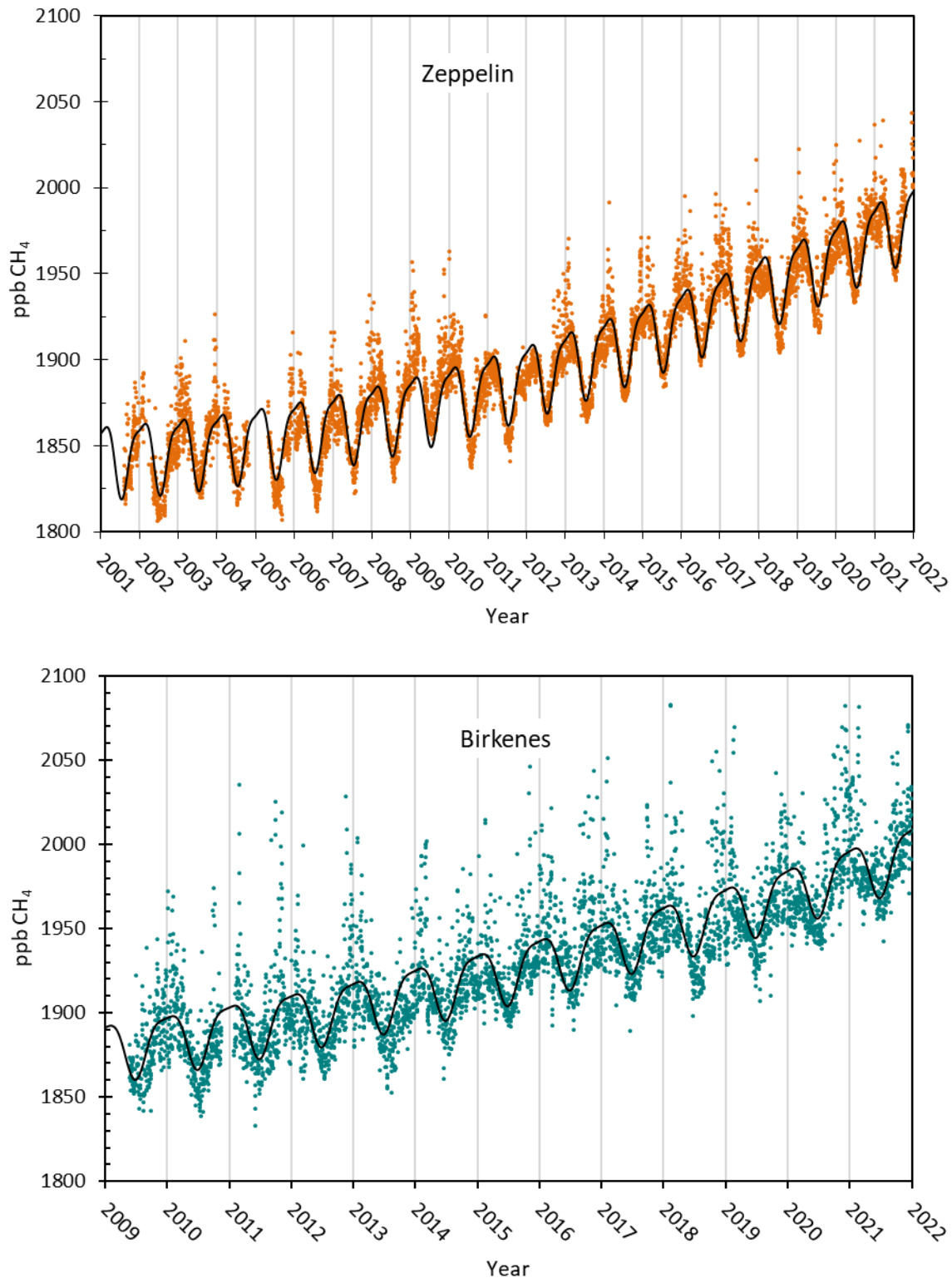


Figure 9: The upper panel shows observations of daily averaged methane mixing ratio for the period 2001-2021 at the Zeppelin Observatory. The black solid line is empirical fitted methane mixing ratio. The lower panel shows the daily mean observations for Birkenes (green dots).

At Zeppelin there are now 21 years of data for which the trend has been calculated. To retrieve the annual trend in methane for the entire period the observations have been fitted by an empirical

equation, shown as the black solid line in Figure 9. This corresponds to a trend of 6.7 ppb/yr or 0.37%/yr. For Birkenes, shown in Figure 9 lower panel, the time series is shorter and the trend analysis is less accurate. The trend calculations demonstrate a CH<sub>4</sub> increase of 9.0 ppb/yr (0.49%/yr) for the period 2009-2021.

The annual methane increases over the last years is visualised in Figure 10, showing the CH<sub>4</sub> annual mean concentration at Zeppelin for the period 2001-2021 (orange) and Birkenes for the period 2009-2021 (green). The global mean values given by WMO from 2005-2020 (WMO, 2021) are included for comparison. The big difference between global mean, and the observations at Zeppelin and Birkenes is due to the fact that most emissions are in the Northern hemisphere.

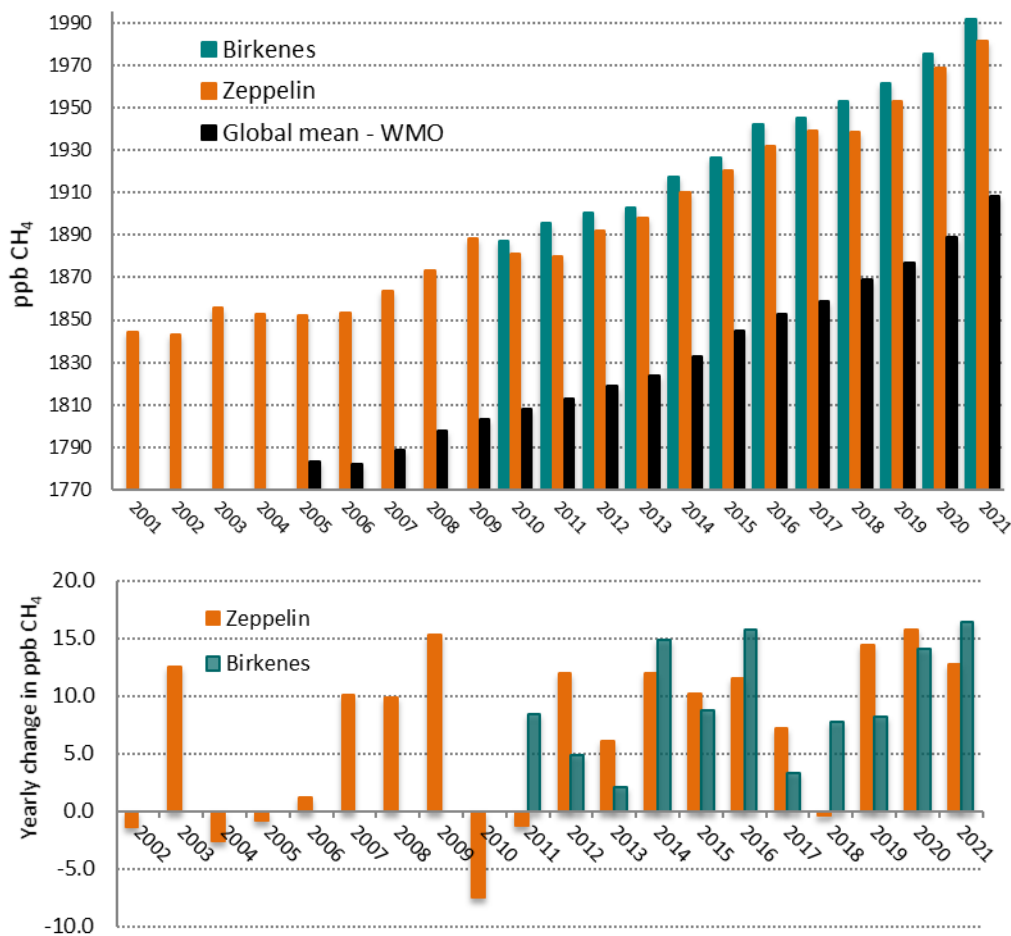


Figure 10: Top: Development of the annual mean mixing ratio of methane in ppb measured at the Zeppelin Observatory (orange bars) for the period 2001-2021, Birkenes for the period 2010-2021 in green bars, compared to global mean provided by WMO as black bars (WMO, 2006-2021). The yearly annual increases are shown in the lower panel, orange for Zeppelin, green for Birkenes.

The annual means are based on the measured methane values, however, model fitted values are used to fill in gaps if measurements are missing. Figure 10 demonstrates a gradual increase in the concentrations of methane at both Zeppelin and Birkenes the last decade. The annual mean concentrations in 2021 were 1991.7 and 181.4 at Birkenes and Zeppelin, respectively. For Zeppelin, there is an increase of 12.7 ppb from 2020 to 2021. For Birkenes, the increase is as high as 16.4 ppb

from 2020 to 2021. This is the highest annual increase detected at Birkenes, leading to a record in both concentration and change from last year.

### 2.2.2.1 Observations of the atmospheric $\delta^{13}\text{C}_{\text{CH}_4}$ and discussion of potential change in $\text{CH}_4$ sources

The isotopic signature of  $\text{CH}_4$  (expressed as  $\delta^{13}\text{C}_{\text{CH}_4}$ ) varies by emission source (France et al., 2016, see Figure 11) and measurements of the isotopic signature provides very valuable information for the understanding of the development of  $\text{CH}_4$  sources, complementing other measurements (e.g.  $\text{CH}_4$ ,  $\text{CO}$  and ethane). As can be seen from Figure 11 the isotopic signatures of  $\text{CH}_4$  from e.g. biomass burning is different from natural gas. Leaks from gas installations, world-wide, both onshore and offshore might be an increasing source. Hence, it is essential to find out if the increase since 2005

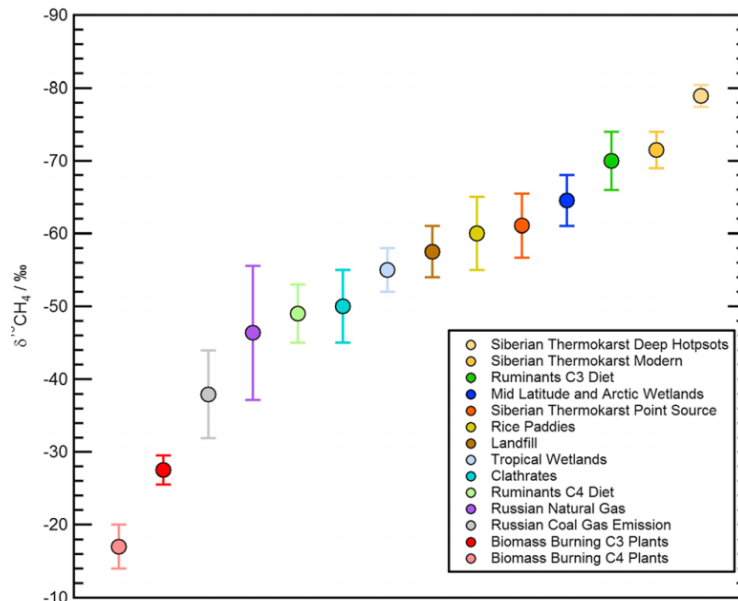


Figure 11: Isotopic ranges of  $\delta^{13}\text{C}_{\text{CH}_4}$  for a variety of  $\text{CH}_4$  sources as given in France et al., 2016.

is due to high emissions from point sources, or if it is caused by newly initiated processes releasing methane to the atmosphere e.g. the thawing of the permafrost layer or processes in the ocean, both related to permafrost and others. As a part of a research project under Norwegian Research Council (2011-2013<sup>11</sup>) NILU initiated measurements of  $\delta^{13}\text{C}_{\text{CH}_4}$  at Zeppelin in the year 2012 to provide more insight into Arctic sources of  $\text{CH}_4$ , and potential changes. The continuation of these measurements was implemented into the Norwegian Monitoring programme in 2017. Figure 12 shows the full time series of  $\delta^{13}\text{C}_{\text{CH}_4}$  since May 2012 (red dots) to the end of 2020, together with ambient  $\text{CH}_4$  concentrations (blue line) measured at the Zeppelin Observatory. The observations are mainly 2 times per week, performed in the morning. (For details about the measurements, see Appendix II).

A clear reduction (shift towards more negative values) in  $\delta^{13}\text{C}_{\text{CH}_4}$  is evident after 2012, parallel to the increase in the ambient concentration. Back in the 1980's,  $\delta^{13}\text{C}_{\text{CH}_4}$  shifted to more positive values, indicative of gas leaks and coal emissions (as  $\delta^{13}\text{C}_{\text{CH}_4}$  of fossil fuels is slightly higher than the ambient average), but it seems that increases in  $\text{CH}_4$  concentrations since 2005 have been accompanied by a negative shift in  $\delta^{13}\text{C}_{\text{CH}_4}$ , as illustrated in Figure 12 until the start of 2019. However, since 2019, this seems to have stopped, and the development is more stable now. The reason for this is not yet clear, highlighting the ongoing potential for surprises. A possible influence of the COVID 19 related lockdowns is currently being investigated.

These recent negative shifts in ambient  $\delta^{13}\text{C}_{\text{CH}_4}$ , and increases in the  $\text{CH}_4$  mixing ratio imply changes in the balance of sources and sinks, i.e., since changes in total fossil fuel emissions cannot account for a negative shift they also cannot entirely account for increases in the mixing ratio. Hence the development in  $\delta^{13}\text{C}_{\text{CH}_4}$  observed at Zeppelin suggests a role for biosphere and/or agriculture (wetland or ruminant) emissions, since these do have strongly negative  $\delta^{13}\text{C}_{\text{CH}_4}$  compared to ambient values and

<sup>11</sup> <https://www.forskningsradet.no/prosjektbanken/#/project/NFR/207587>

fossil sources. Changes in the sink (reaction with hydroxyl radicals, OH) is also a possibility. It is worth noting that as the major sink for almost all atmospheric Volatile Organic Compounds (VOCs), changes in OH would have profound implications for the whole atmosphere.

Ethane and methane are emitted together from fossil oil and gas sources. If fossil oil and gas is the main cause of the increase, both components would show an increase. Accordingly, the global decrease in ethane supports the hypothesis that wetland changes is a large contributor to the change in CH<sub>4</sub> (also assuming no large scale increases in ruminant livestock farming).

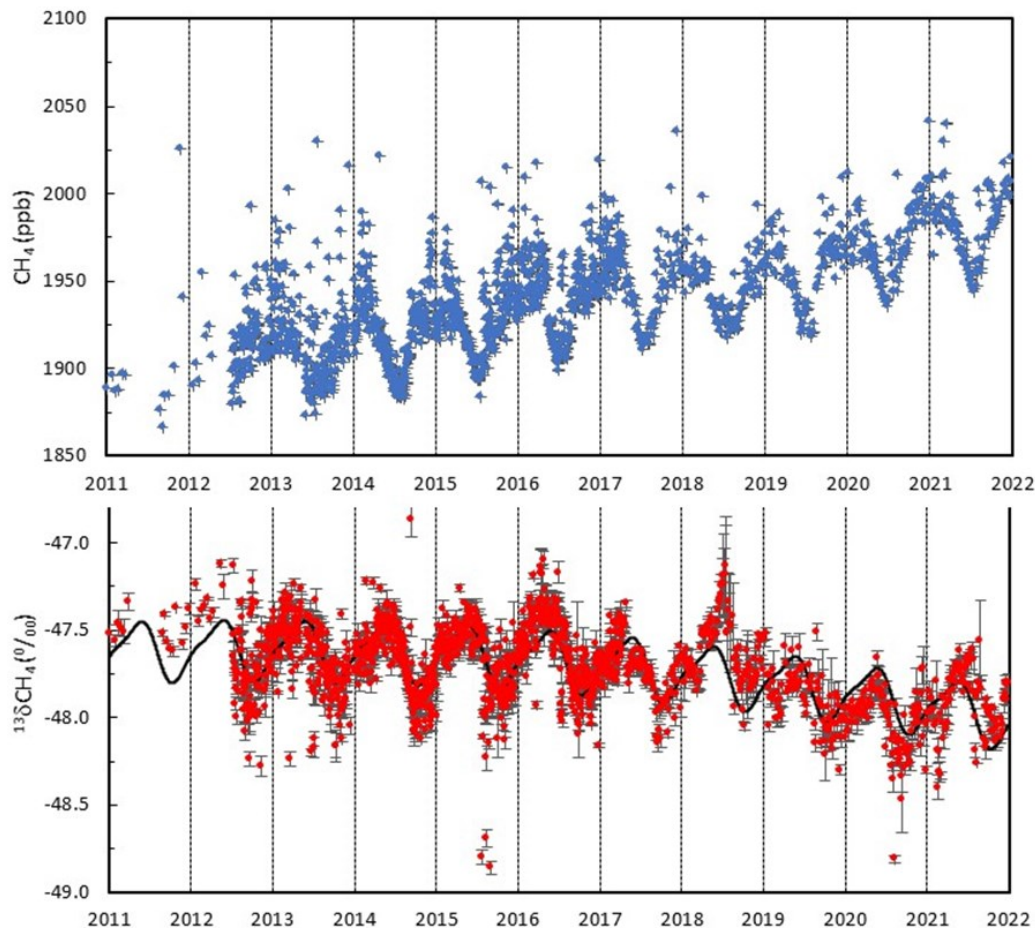


Figure 12: Long term measurements of methane concentration (CH<sub>4</sub>, blue) and the <sup>13</sup>C isotopic signature of CH<sub>4</sub> ( $\delta^{13}\text{C}-\text{CH}_4$ , red) at the Zeppelin Observatory, Svalbard 78°N.

Additionally, recent and ongoing scientific discussions point in the direction of increased emissions from wetlands located both in the tropical region and in the Arctic region. Thawing of permafrost, both in terrestrial regions and in marine region, might introduce new possible methane emission sources initiated by the temperature increase the last years in the Arctic region, but the new revised methane budget does not support this.

Gas hydrates at the sea floor are widespread in thick sediments in this area between Spitsbergen and Greenland. These gas hydrates can decompose if temperatures increase or pressure decreases. Hence, if the sea bottom warms or sea level decreases (e.g. due to raising of the sea bed as the Greenland Ice sheet melts), this might initiate further emissions from this source. This was the core of the large polar research project *MOCA - Methane Emissions from the Arctic Ocean to the Atmosphere: Present and*

*Future Climate Effects*<sup>12</sup>, which started at NILU in October 2013, and was finalized spring 2017. NILU started a new project in 2021 to further explore the global and Arctic methane budget, see section 2.2.2.2 for more information about ReGAME.

To summarise, isotopic signatures provide very valuable data for understanding the development of the source of CH<sub>4</sub>, but careful interpretation of observational data and emission inventories is required before assigning observed shifts to a particular source. The observations in 2019 and 2020 indicate that a relative change among sources have stopped, at least for this period. This further demonstrates the need for observational data on emission fluxes from the large natural reservoirs. There is most likely a combination of causes explaining the increase in methane the last years, and the dominating reason is not clear. A possible explanation is increased methane emissions from wetlands and agriculture, both in the tropics as well as in the Arctic region, in addition to increases in emission from the fossil fuel industry in some areas, but this alone cannot explain the development in the isotopic signature of CH<sub>4</sub> at Zeppelin.

### 2.2.2.2 Reliable global methane emissions estimates in a changing world-REGAME

Increases in atmospheric methane (CH<sub>4</sub>) since 2007 decrease the effectiveness of current measures undertaken to meet the Paris Agreement goal of holding the increase in the global average temperature to well below 2°C above pre-industrial levels and pursuing efforts to limit the temperature increase to 1.5°C. This urgently needs better assessment. Furthermore, uncertainties in sources of CH<sub>4</sub> under climate change limit our knowledge of future needed abatement measures. The NFR-funded ReGAMEproject is a large-scale interdisciplinary project (from 2021-2025) with the aim of providing a reliable assessment of the global atmospheric methane budget.

To better constrain the global methane budget, we will include isotopic time series, and for the first time, satellite data fields from Sentinel 5P in inversion models (in collaboration with the University of Vienna). To investigate the effects of changing atmospheric chemistry on methane sources, and particularly the main methane sink, the OH radical, we collaborate with CICERO and will use the OsloCTM model, again incorporating isotopic time series. Furthermore, according to the latest IPCC report, the Arctic is warming at more than twice the global rate. Increases in extreme heat events, fire regimes, and permafrost thaw have accompanied this warming, all of which can contribute to increased methane (CH<sub>4</sub>) emissions. Sub-sea CH<sub>4</sub> seepage (see box) is also anticipated to increase in a warmer world, while the Arctic is projected to reach practically ice-free conditions in summer at least once before 2050, with unclear effects on ocean emissions and weather patterns. Hence, following up on the successful MOCA project, in ReGAME we will also investigate the role of polar regions and potential tipping points (e.g., thawing permafrost and subsea gas hydrates, see box) with a dedicated high-resolution, regional Arctic inversion model, informed by oceanographic observations to elucidate the location of subsea-seeps and other potential emissions sources as well as their temporal variability, in collaboration with the center for Arctic gas hydrates (CAGE). Assessment of the role of changing ice cover will be done during the ReGAME project (by

#### What are gas hydrates?

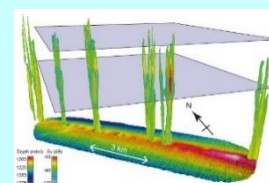
Large amounts of natural gas, mainly methane, are stored in the form of hydrates in continental margins worldwide, particularly, in the Arctic. Gas hydrate consists of ice-like crystalline solids of water molecules encaging gas molecules, and is often referred to as 'the ice that burns'.



#### What are seeps?

Cold seeps are locations where hydrocarbons are emitted from sub-seabed gas reservoirs into the ocean. This can be both from petroleum reservoirs and methane hydrates.

The illustration is gas bubbles rising 800 m up from Vestnesa Ridge, offshore Svalbard (Smith et al. 2014).



<http://cage.uit.no>

<sup>12</sup> <http://moca.nilu.no/>

including a new atmospheric laboratory on the ice-breaking vessel RV Kronprins Haakon (including online monitoring of methane and flask sampling, as currently performed on the RV Helmer Hanssen).

The outcomes of this project will be summarized in a report for policy makers, enabling society to evaluate our current climate change strategies and provide knowledge essential to future stewardship of the Earth's climate.

<p>The <b>primary objective</b> of <i>REGAME</i> is to constrain the global CH<sub>4</sub> budget</p> <p><b>Secondary objectives</b> are to:</p> <ol style="list-style-type: none"> <li>1. Assess the status of CH<sub>4</sub> reservoirs such as wetlands and ocean</li> <li>2. Survey ocean CH<sub>4</sub> seeps in the Arctic and assess temporal variability and dynamics of seep fluxes</li> <li>3. Incorporate isotopic tracers in models (FLEXPART/OsloCTM)</li> <li>4. Develop the use of the Ensemble Kalman Filter method to use S5P CH<sub>4</sub> in inversions with FLEXPART</li> <li>5. Investigate the added value of satellite data in inversions</li> <li>6. Determine implications of improved CH<sub>4</sub> budget and state of CH<sub>4</sub> reservoirs for the Paris Agreement and produce a report for policy makers</li> </ol>
---------------------------------------------------------------------------------------------------------------------------------------------------------------------------------------------------------------------------------------------------------------------------------------------------------------------------------------------------------------------------------------------------------------------------------------------------------------------------------------------------------------------------------------------------------------------------------------------------------------------------------------------------------------------------------------------------------------------------------------------------------------------------------------------------------------------------------------------------------

### 2.2.3 Nitrous Oxide (N<sub>2</sub>O)

**Key findings Nitrous Oxide:** *N<sub>2</sub>O is a strong greenhouse gas and contributes ~6% to the total forcing of well-mixed greenhouse gases since 1750. N<sub>2</sub>O is also the major source of the ozone-depleting NO and NO<sub>2</sub>, thus the component influences the stratospheric ozone layer. The global mean level of N<sub>2</sub>O has increased from around 270 ppb prior to industrialization to an annual mean of 334.5 ppb at Zeppelin in 2021.*

Nitrous Oxide (N<sub>2</sub>O) is a greenhouse gas with both natural and anthropogenic sources. The sources include oceans, tropical forests, soil, biomass burning, cultivated soil, animal manure, use of particular synthetic fertilizers, and various industrial processes. There are high uncertainties in the major soil, agricultural, combustion and oceanic sources of N<sub>2</sub>O. Anthropogenic sources contribute approximately to 45% of total global N<sub>2</sub>O emission according to Global Carbon Project.

Also, frozen peat soils in Arctic tundra is reported as a potential source (Repo et al., 2009), but studies identify tropical and sub-tropical regions as the largest source regions (Thompson et al., 2013). N<sub>2</sub>O is an important greenhouse gas with a radiative forcing of 0.21 W m<sup>-2</sup> since 1750 (IPCC, 2021). N<sub>2</sub>O is also the major source of the ozone-depleting nitric oxide (NO) and nitrogen dioxide (NO<sub>2</sub>) in the stratosphere, thus the component is also influencing the stratospheric ozone layer (WMO, 2018).

N<sub>2</sub>O has increased from around 270 ppb prior to industrialization and up to an average global mean of 333.2 ppb in 2020 (WMO, 2021). In 2009, NILU installed a new instrument at Zeppelin measuring N<sub>2</sub>O with high time resolution of 15 minutes. The instrument was in full operation in April 2010 and has later been upgraded to comply with ICOS. The results for 2010-2021 are presented in Figure 13. As seen from Figure 13 there has been a gradual increase in N<sub>2</sub>O at Zeppelin since the measurements started in 2010. For the period 2010-2021 the overall trend is 1.0 ppb/yr, an increase of 0.3%/yr.

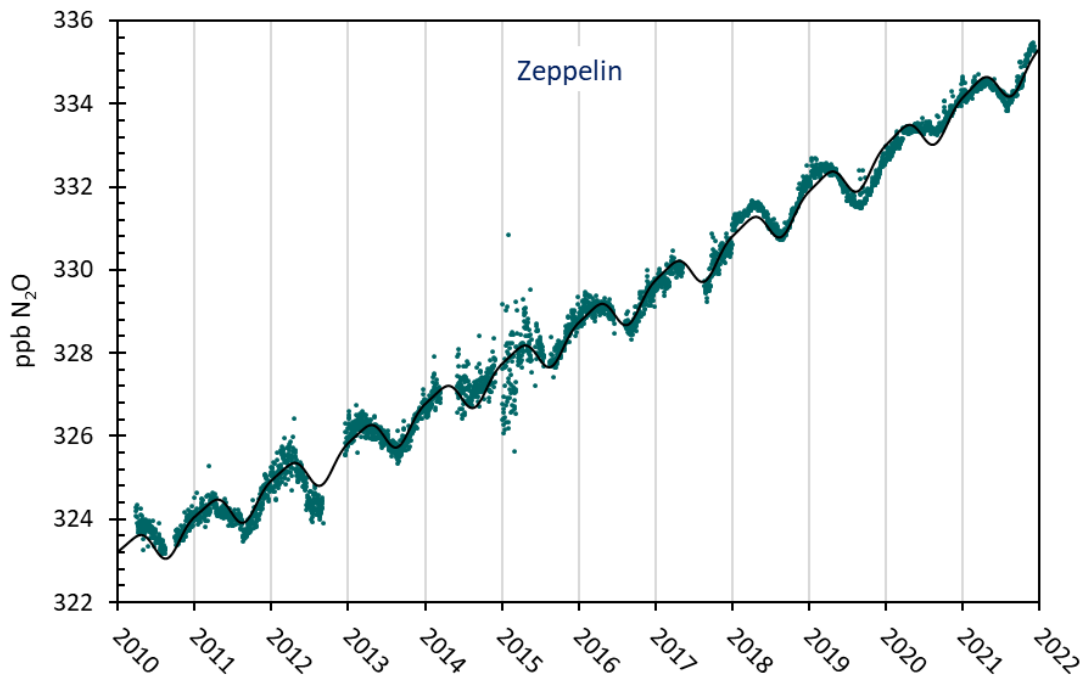


Figure 13: Measurements of N<sub>2</sub>O at the Zeppelin Observatory for 2010-2021. The black line is empirical modelled N<sub>2</sub>O mixing ratio.

Figure 14 shows annual average concentrations of N<sub>2</sub>O measured at Zeppelin for the periods 2010-2021. The global annual means of N<sub>2</sub>O (WMO, 2021) are included as black bars for comparison. The concentrations at Zeppelin are slightly higher than the global means. The annual mean N<sub>2</sub>O value at Zeppelin was 334.5 ppb in 2021, an increase of 1.1 ppb from the 2020 annual mean value.

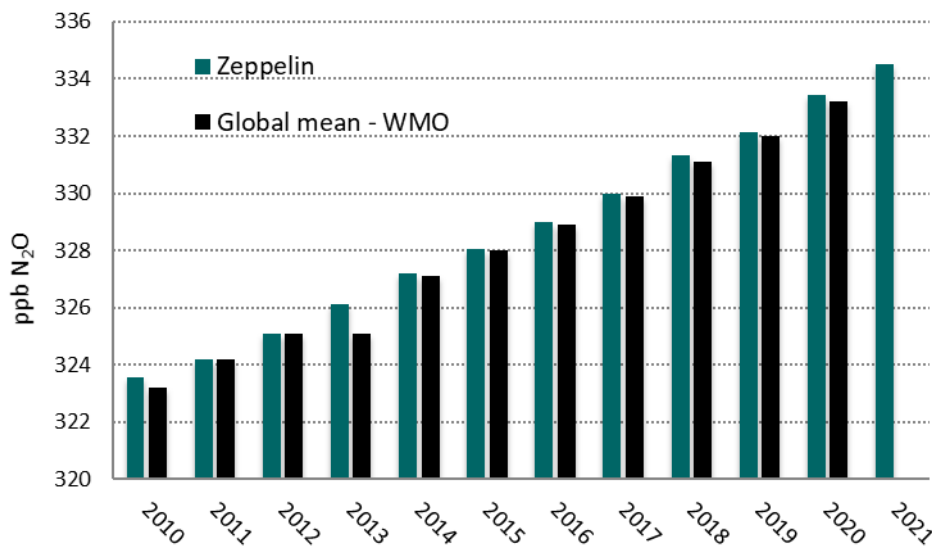


Figure 14: Annual mean concentration of N<sub>2</sub>O at the Zeppelin Observatory for 2010-2021.



## 2.2.4 Volatile organic compounds (VOC)

**Key findings – VOCs:** *The VOCs are short lived greenhouse gases with low direct greenhouse gas effects. However, they have an indirect climate effect as they influence the levels of e.g., aerosols, ozone, and CO. Furthermore, they are important for surface ozone. Six different VOCs have been measured at Zeppelin since September 2010. The annual mean concentrations vary from one year to another and for most compounds it is not possible to draw any conclusions about developments and trends at this early stage.*

Volatile Organic Compounds (VOCs) represent a large group of carbon-based compounds that have a high vapour pressure and easily evaporate at room temperature. VOC oxidation contributes to the production of tropospheric ozone and influences photochemical processes, both impacting climate and air quality. Sources of VOCs (here ethane, propane, butane, pentane, benzene and toluene) are both natural (mostly geological but also from wildfires) and anthropogenic (fossil fuels). CH<sub>4</sub> and VOCs are co-emitted from oil and natural gas sources, for CH<sub>4</sub> to ethane the mass ratio varies from 7 to 14 (Helmig et al., 2016). The atmospheric ethane budget is not fully understood, and state-of-the-art atmospheric models underestimate ethane-mixing ratios, implying that current emission inventories require additional sources to balance the global atmospheric ethane budget.

Helmig *et al.* (2016) showed, from long-term observations of ethane from a global network that concentrations were increasing (since circa 2010), and that there was a strong latitudinal gradient, with the highest abundances observed in the Arctic, and a steep decline towards the south. They concluded that emissions from North American oil and natural gas development was the primary cause of the increasing concentrations. However, observations at Zeppelin indicate that the ethane concentrations have started to decline after 2015. Another study by Nicewonger et al. (2016) used analysis of polar ice cores to estimate the pre-industrial emissions and concluded that natural ethane emissions from geologic seeps contributed significantly to the preindustrial ethane budget, and Etiope and Ciccioli (2009) suggested that a substantial part of the missing ethane source can be attributed to gas seepage (classified as geologic seeps), but they did not include the Arctic in their study.

A study in Nature Geoscience performed under the MOCA project unveils a need of revising previous ethane and propane emissions studies, as these emissions have been underestimated by more than 50%. Such a revision could in turn improve our understanding of the forceful and related methane emissions (Dalsøren et al., 2018).

There has been large progress recently in the access to quality assured measurements of VOC under ACTRIS, with high time resolution. In a study by Dalsøren et al. (2018) atmospheric measurement data from a number of sites were compared to simulations from an atmospheric chemistry transport model. It was found that a substantial increase of the emissions is needed to match the model predictions. Dalsøren et al (2018) showed that substantial geologic emissions are necessary to reproduce observations of preindustrial ethane concentrations. This provides an important constraint on both preindustrial and current natural emission budgets, reducing the relative contribution of fossil sources.

In 2010 a Medusa-GCMS instrument was installed at Zeppelin, which made it possible to perform online VOC measurements. Figure 15 shows the daily mean observations of the four non-methane hydrocarbons included in the programme in 2010: ethane, propane, butane, and pentane.

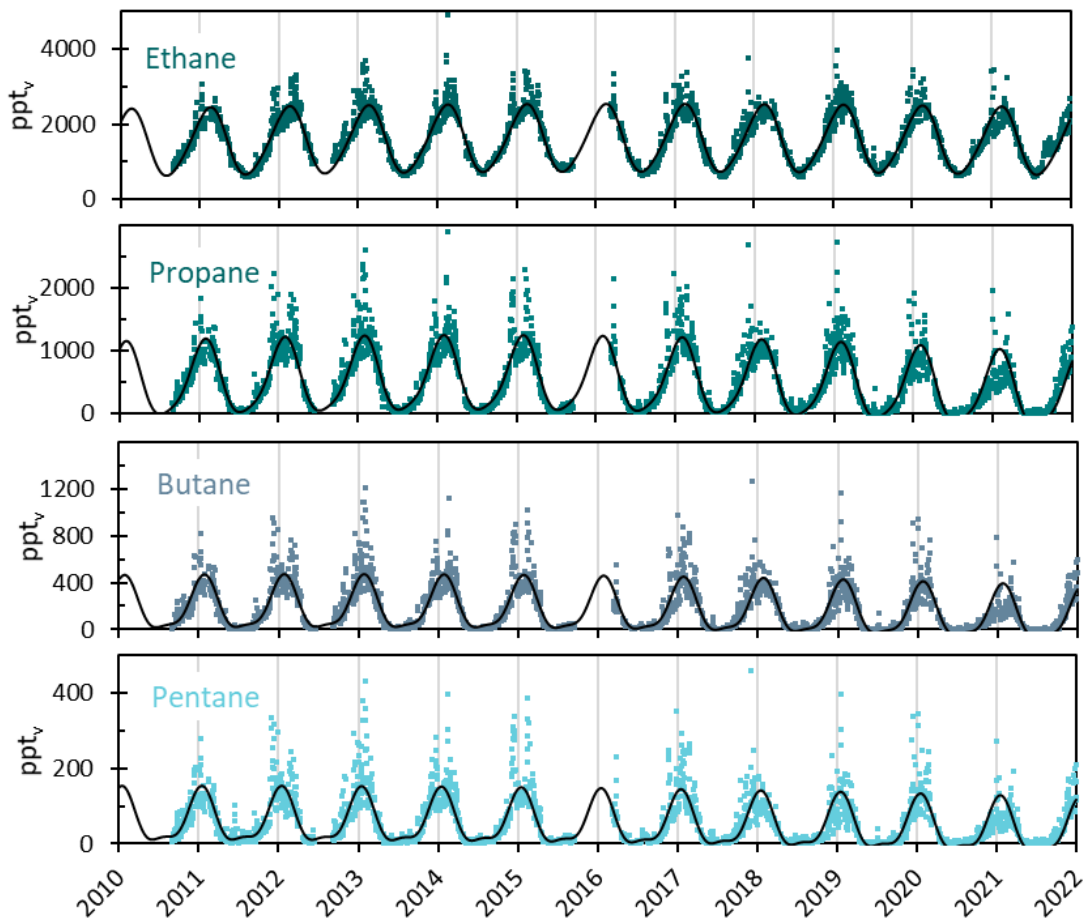


Figure 15: Observations of daily averaged mixing ratios of ethane, propane, butane, and pentane for the period September 2010 – 2021 at the Zeppelin Observatory. The black line is empirical modelled mixing ratio.

Due to the short lifetimes, ranging from a few days for pentane to 2-3 months for ethane, the annual cycles are very strong and are regulated by OH reactions. The annual mean from 2011 to 2021 are shown in Figure 16.

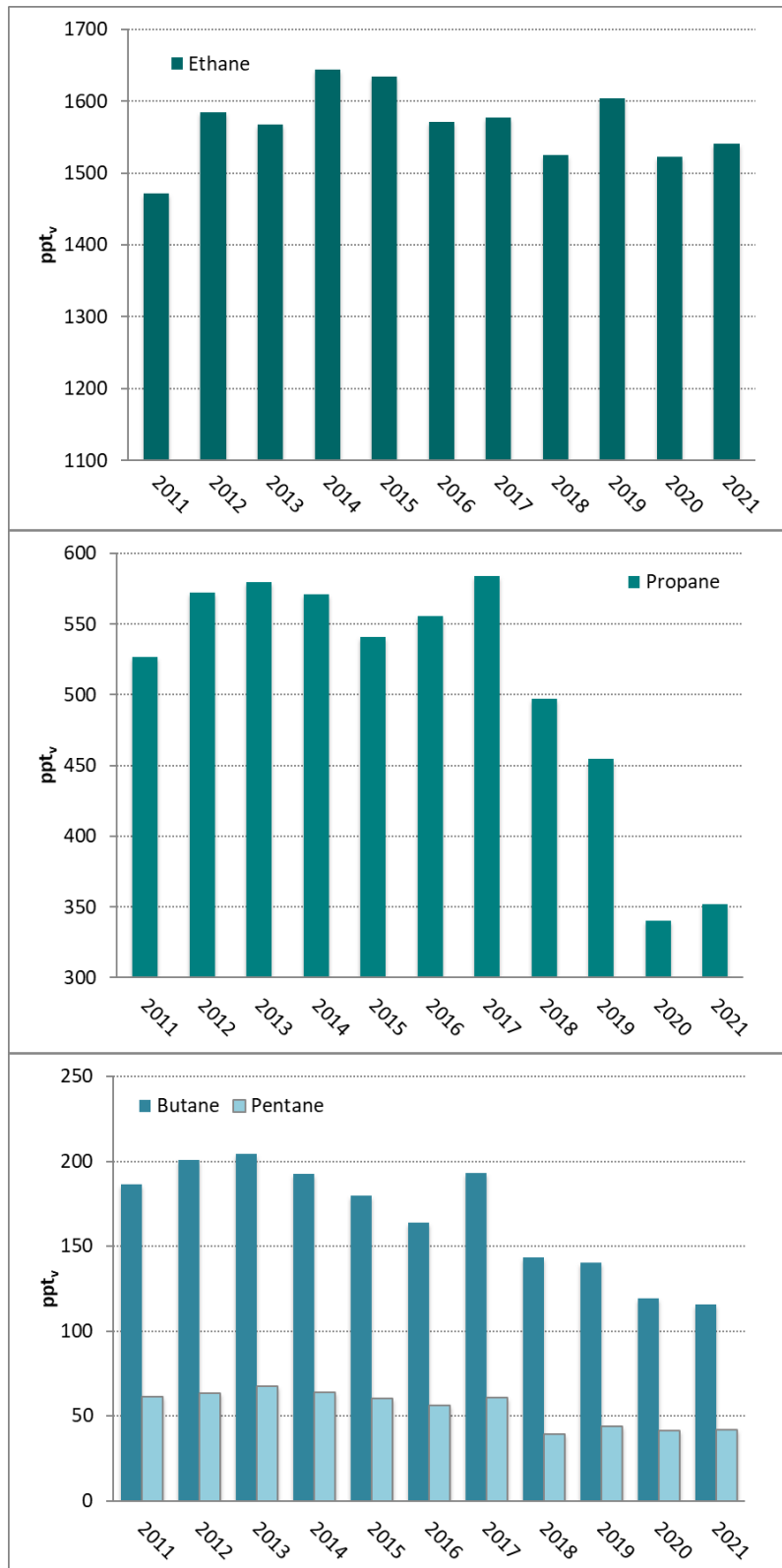


Figure 16: Development of the annual means of the measured non-methane hydrocarbons at the Zeppelin Observatory for the period 2011-2021. Upper panel in dark green: ethane, mid-panel propane, and lower panel butane and pentane. All values are in ppt.

As seen from the figure the annual mean concentrations vary from one year to another and for most compounds it is not possible to draw any definite conclusions about development and trend. However, for propane, butane, and pentane it has been a gradual decrease in the annual mean value the last 6-7 year (except for 2017). For ethane, the development is more uncertain.

At Zeppelin we aim to measure two other aromatic VOCs, benzene and toluene, which belong to a group of VOCs found in petroleum hydrocarbons, such as gasoline. These compounds have attracted much attention since they are considered carcinogens, but they are also relevant for climate. The VOCs have relatively short atmospheric lifetimes and small direct impact on radiative forcing. However, anthropogenic secondary organic aerosols (SOA) are formed from photo oxidation of benzene and toluene (Ng et al., 2007), which indirectly impacts the climate (negative forcing). The SOA formation from these VOCs is most effective under low-NO<sub>x</sub> conditions and when ambient concentration of organic aerosols is high. Thus, benzene and toluene influence climate through their production of secondary organic aerosols and their involvement in photochemistry, i.e., production of O<sub>3</sub> in the presence of light.

Figure 17 shows the daily mean observations of benzene and toluene at Zeppelin for the period 2010-2021. After an upgrade of the Medusa-GCMS in fall 2017, the benzene and toluene values became unrealistically low. The upgrade was required to measure the low concentrations of the halogenated gases. Thus, the measurements performed in 2018 to 2020 are mainly flagged as “missing”.

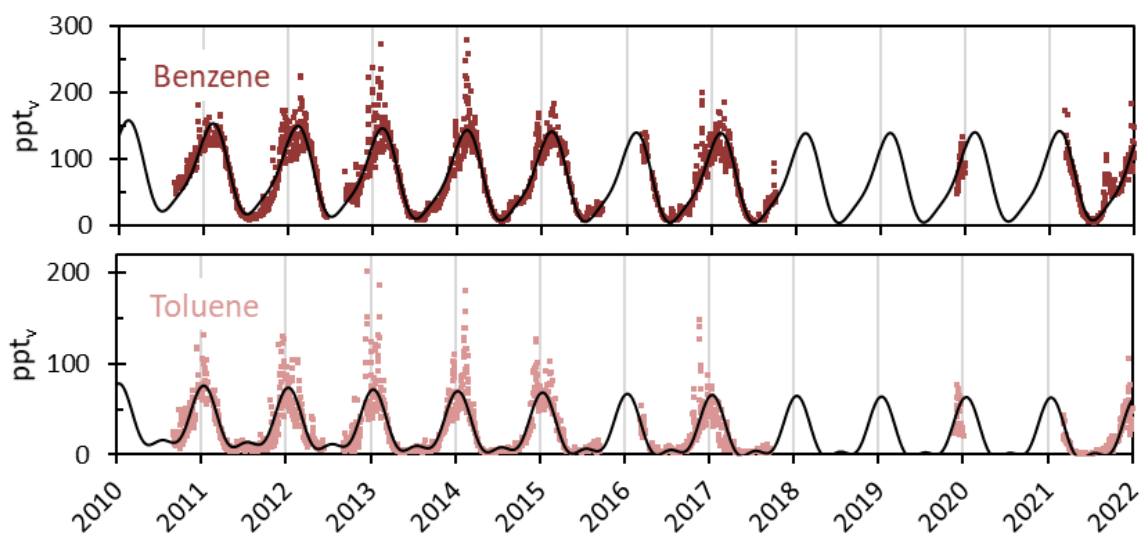


Figure 17: Observations of daily averaged mixing ratio of benzene (upper panel) and toluene (lower panel) for the period September 2010 – 2021 at the Zeppelin Observatory. The black line is empirical modelled mixing ratio.

As can be seen from the figure there are strong annual variations, mainly explained by the reactions induced by sunlight. The annual means of benzene and toluene for the period 2011-2021 are presented in Figure 18. The figure shows a declining tendency for both compounds from 2011 to 2017, however, in 2021 the benzene average was higher than previous years. As explained above annual mean values were not calculated from the measurements in 2018 to 2020, which makes the trend estimates very uncertain. The shaded/patterned bars in Figure 18 implies that the annual means 2018-2020 primarily are based on model values (i.e. the black curve in Figure 17).

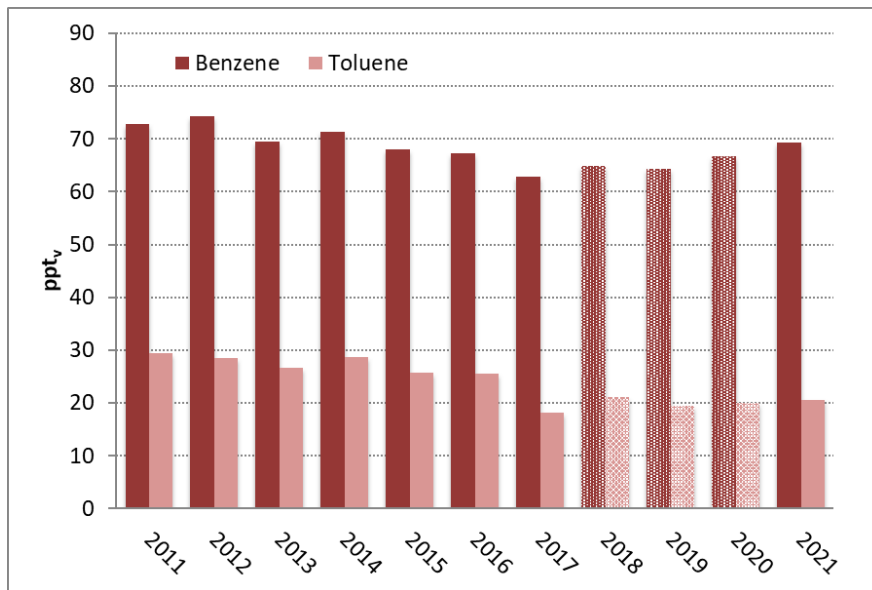


Figure 18: Development of the annual means of benzene (brown) and toluene (light red) for the period 2011 – 2021 at the Zeppelin Observatory. All concentrations are in ppt. Note that benzene and toluene in 2018-2020 mainly are based on model data.

### 2.2.5 Carbon monoxide (CO)

**Key findings CO:** CO is not a greenhouse gas but considered as a climate relevant gas as it affects the levels of methane and ozone. CO is also an excellent tracer for long-range transport of smoke from fires. CO has been measured at Zeppelin since 2001. For the period 2001-2021 a decreasing trend of -0.83 ppb/yr is recorded. In 2021 there were strong CO transport episodes registered at Zeppelin traced back to fires in Siberia, at the same time we also see an annual mean increase in the CO level at Zeppelin, due to an increase in the late summer maximum. In 2021 the annual average CO concentration at Zeppelin was 128 ppb.

Atmospheric carbon monoxide (CO) has both natural and anthropogenic sources. CO is produced when various organic gases are oxidized, such as methane, VOCs emitted from fossil fuel, and gases from biomass burning. Additionally, emissions from plants and ocean are important sources. CO is not considered as a direct greenhouse gas, as it does not absorb terrestrial thermal IR energy strongly enough. However, CO modulates the level of methane and production of tropospheric ozone, which are both very important greenhouse gases. Hence, CO is considered as a climate gas although not a greenhouse gas. CO also plays a key role in the control of OH radicals.

CO at Zeppelin is included in the current monitoring programme and for ICOS and the observed CO mixing ratios for the period September 2001-2021 are shown in Figure 19.

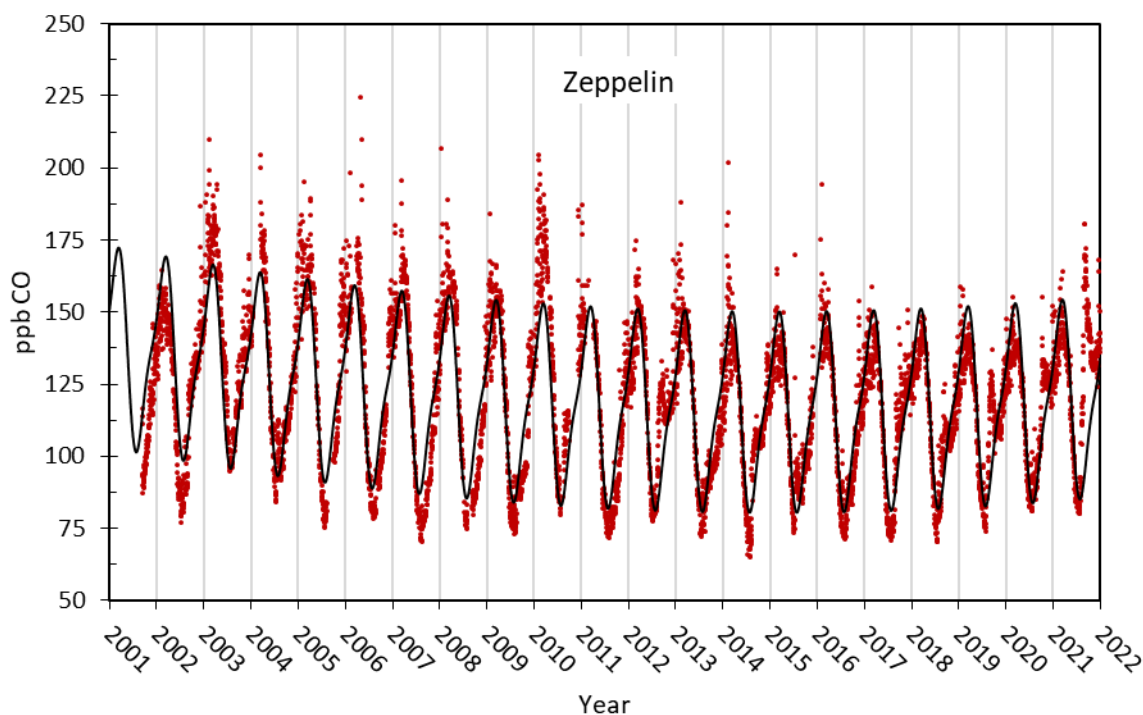


Figure 19: Observations of carbon monoxide (CO) from September 2001 to 2021 at the Zeppelin observatory. Red dots: daily averaged observed mixing ratios. The solid line is the empirical fitted mixing ratio.

The concentrations of CO show characteristic seasonal variations with a clear annual cycle with a late winter (February/March) maximum and a late summer (August) minimum. This seasonal cycle is driven by variations in OH concentration as a sink, emission by industries and biomass burning, and transport of air on a large scale. As seen from the figure there are also peak values which are due to long-range transport of polluted air to Zeppelin and the Arctic. The highest mixing ratio of CO ever observed at

Zeppelin is 225 ppb, measured on the 2<sup>nd</sup> of May 2006. This peak value was due to agricultural fires in Eastern Europe. In general, CO is an excellent tracer for transport of smoke from fires (biomass burning, agricultural- or forest fires). Notable the seasonal variations are getting smaller the last five years and the annual mean is increasing (Figure 20). However, for the period 2001-2021 a trend of -0.83 ppb/yr is calculated.

The development of the annual CO means at Zeppelin for the period 2001-2021 is presented in Figure 20. Overall, the CO concentration at Zeppelin shows a decrease during the period 2003 to 2009, and stable levels the last years with a small peak in 2010. The last 3-5 years there has been an increase in the annual average CO concentration, especially in 2021. Wildfires is the most probable explanation of the record high CO summer values measured at Zeppelin in 2021. A daily maximum value is of 180.0 ppb was measured 2. September 2021, which is almost twice the value normally measured this time of the year (see Figure 21, left panel). Enhanced concentrations of benzene (Figure 21, right panel) strengthen the hypotheses that the air is influenced by smoke from forest fires.

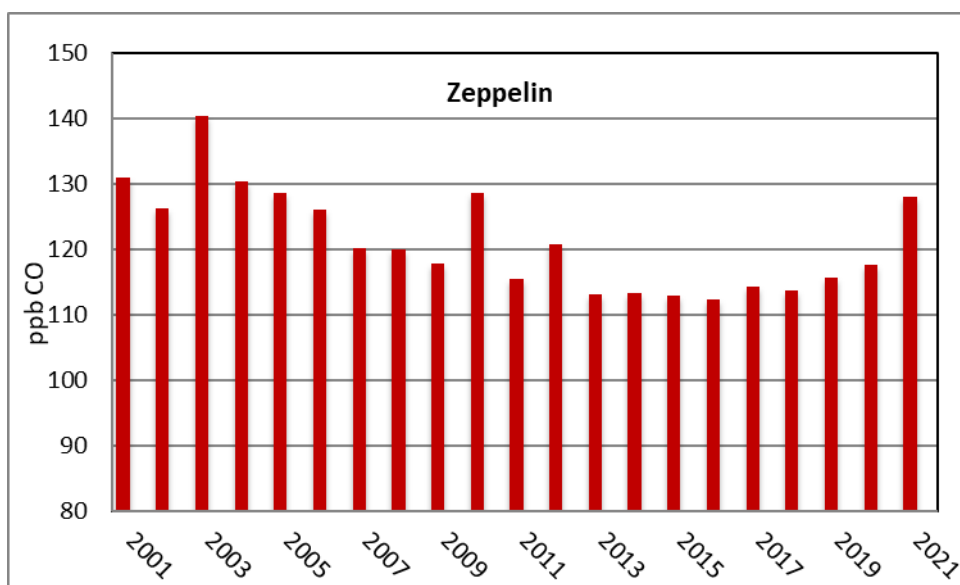
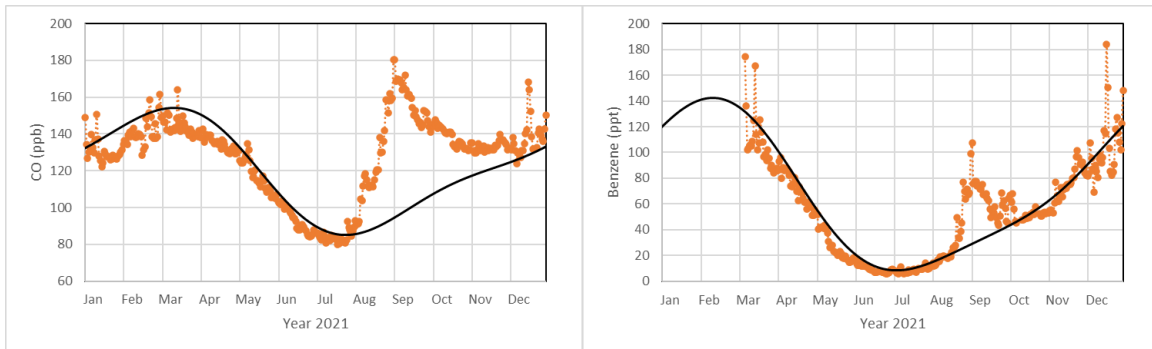


Figure 20: Development of the annual means of CO measured at the Zeppelin Observatory for the period 2001-2021. The values are in ppb.

An unprecedented amount of wildfires have been raging in various regions of the Arctic, including Siberia, Greenland and Alaska the last 3 years. They have been caused by record-breaking temperatures and lightning, fuelled by strong winds. These fires emit significant smoke and toxic gases into the atmosphere, which make their way across the ocean. There were extreme CO episodes in the year 2019 and 2021 as there were heavy fires in Siberia, in particular.



*Figure 21: An unprecedented amount of wildfires have been raging in various regions of the Arctic, including Greenland, Alaska and Siberia the last 3 years. The Figure to the left shows enhanced CO levels at Zeppelin in August and September 2021, whereas the right Figure shows enhanced levels of benzene during the same period. The high concentrations of CO and benzene are probably related to the massive wildfires in Siberia, Russia, during the summer 2021.*

### 2.2.6 Chloromethane at the Zeppelin Observatory

**Key findings - Chloromethane:** The atmospheric concentration of chloromethane is relatively stable. The gas has a dominating natural origin and is not regulated through the Kyoto or Montreal protocols. The annual mean  $\text{CH}_3\text{Cl}$  concentration at Zeppelin has decreased by  $\sim 1.9\%$  over the last 20 years.

Chloromethane (also called methyl chloride,  $\text{CH}_3\text{Cl}$ ) is the most abundant chlorine containing organic gas in the atmosphere. It contributes approximately 16% to the total chlorine from the well-mixed gases in the troposphere (WMO, 2014b), and through this a strong contributor to ozone depletion. The main sources of chloromethane are natural, and the dominating sources include ocean, biomass burning, fungi, wetlands, rice paddies, and tropical forests. Due to the dominating natural sources, this compound is not regulated through the Montreal or the Kyoto protocols. To reach the stratosphere, the lifetime in general needs to be above the order of 2-4 years, but this is also dependent on the source strength and the regional distribution of the gas. Chloromethane has a relatively high mixing ratio and contributes to the stratospheric chlorine burden.

The result of the measurements of this gas for the period 2001-2021 is shown in Figure 22. The lifetime of chloromethane is only one year, resulting in large seasonal fluctuations due to rapid changes in emission, as shown in Figure 22.



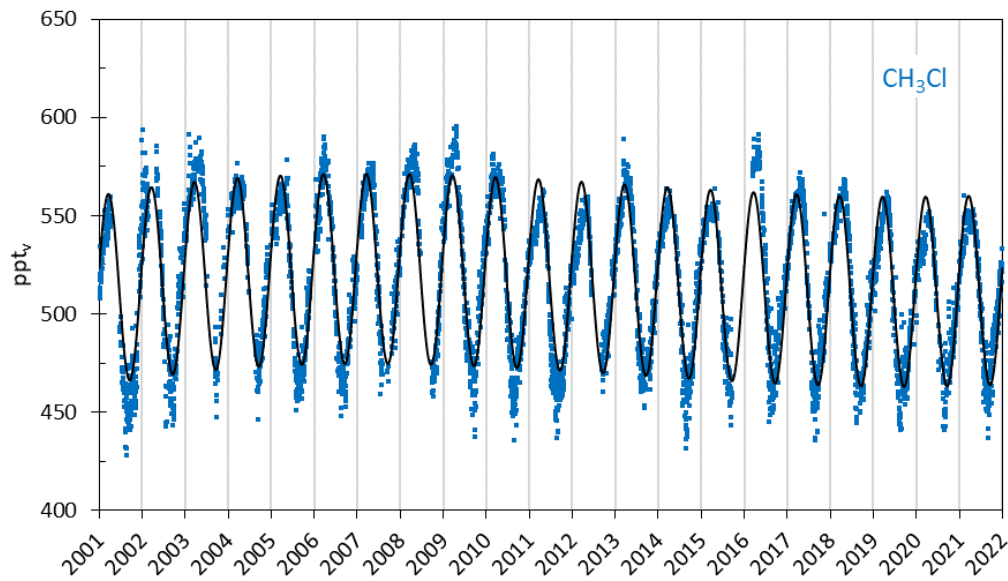


Figure 22: Observations of chloromethane,  $\text{CH}_3\text{Cl}$ , for the period 2001-2021 at the Zeppelin Observatory. Blue dots: daily averaged concentrations from the observations. Solid line: empirical fitted mixing ratios.

The annual means of chloromethane for the period 2001-2021 are shown in Figure 23. Days with missing observations are filled with empirical fitted data. Only small changes have been observed since the measurements started in 2001. The trend for the period 2001-2021 is  $-0.48$  ppt/yr ( $-1.9\%$  for the entire period). From 2002 to 2009 the annual mean chloromethane concentrations were relatively stable at a level around 520 ppt, but since 2009 there has been larger variability and a decreasing tendency, except from 2016 where the annual mean value was 10 ppt higher than previous year. The black bars in Figure 23 show that the global annual means, published by BAMS in “State of Climate” 2016-2021 (Last report: Lan et al., 2022), are 30-40 ppt (6-7%) higher than the annual mean values at the Zeppelin Observatory. This is likely explained by strong emission sources in the tropics, resulting in increased  $\text{CH}_3\text{Cl}$  mixing ratios towards lower latitudes (Umezawa et al., 2014). Zeppelin is less affected by this, due to the short lifetime.

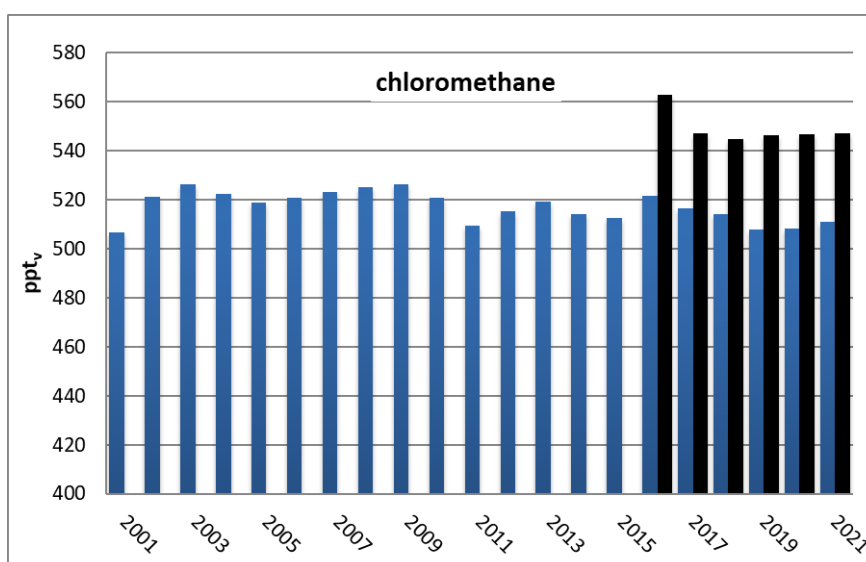


Figure 23: Development of Chloromethane annual means measured at the Zeppelin Observatory for the period 2001-2021. Global annual means for 2016-2021 are included as black bars. All units are in pptv.

### 2.2.7 Bromomethane at the Zeppelin Observatory

**Key findings - Bromomethane:** The atmospheric concentration of  $\text{CH}_3\text{Br}$  at Zeppelin has decreased by ~26% since the observations started in 2001. The decrease is a result of the implementation of the Montreal Protocol. However,  $\text{CH}_3\text{Br}$  has many natural sources with uncontrolled fluctuations from one year to another. The annual mean mixing ratio in 2021 was 6.8 pptv.

Bromomethane (also called Methyl bromide,  $\text{CH}_3\text{Br}$ ) is an important reservoir for atmospheric bromine, which reacts with ozone to deplete the ozone layer.  $\text{CH}_3\text{Br}$  has both natural and anthropogenic sources. The natural sources such as the ocean, plants, and soil, can also be a sink for this gas. The primary anthropogenic source of bromomethane has been from its use as a fumigant, e.g. for pest control and pesticide in the control of weeds. Other anthropogenic sources of  $\text{CH}_3\text{Br}$  include the combustion of leaded gasoline, biomass burning, and emissions from certain crop species. Even though bromomethane is a natural substance, the additional contribution from anthropogenic sources contributes to the man-made depletion of the ozone layer. Total organic bromine from halons and bromomethane peaked in the mid-1990s, but the tropospheric concentration has decreased by ~25% over the past 20 years. Also, the stratospheric abundance of bromide has started to decrease (WMO, 2018).

The result of the daily averaged observations of bromomethane for the period 2001-2021 is shown in Figure 24. Bromomethane is a greenhouse gas which is twice as strong as  $\text{CO}_2$  and has a lifetime of 0.8 years (Myhre et al., 2013b). The short lifetime explains the strong annual and seasonal variations of this compound.

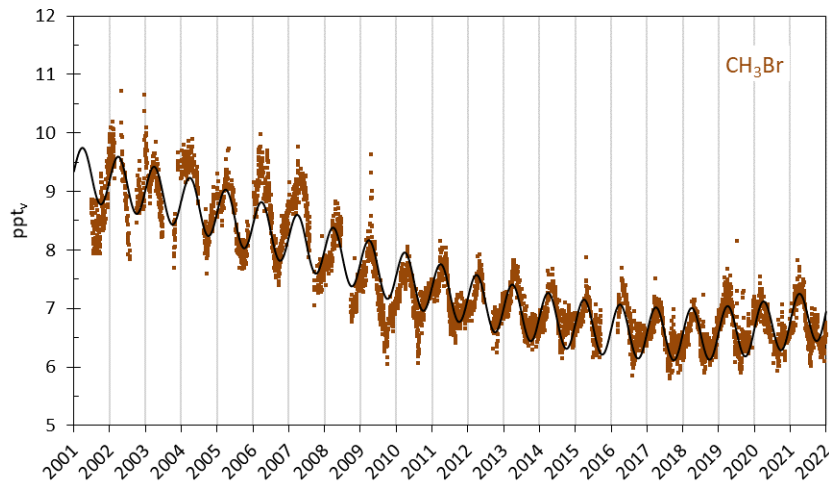


Figure 24: Observations of Bromomethane,  $\text{CH}_3\text{Br}$ , for the period 2001-2021 at the Zeppelin Observatory. Brown dots: daily averages mixing ratios from the observations. Solid line: empirical fitted mixing ratios.

The development of the annual means for the period 2001-2021 is presented in Figure 25. For this period there is a trend in the mixing ratio of  $-0.14$  ppt/yr. The overall observed change since 2001 is  $-2.4$  ppt, i.e.  $-26\%$ . In 2021 the annual mean  $\text{CH}_3\text{Br}$  concentration was  $6.8$  ppt, which is close to the mean values from the previous two years. In general, the decline in bromomethane is explained by considerable reduction in emissions; The use of  $\text{CH}_3\text{Br}$  has decreased steadily as a result of the implementation of the Montreal Protocol. Total reported anthropogenic emissions have declined by about  $85\%$  from the peak value, and atmospheric  $\text{CH}_3\text{Br}$  abundance is now near the expected natural background (WMO, 2018).

The global mean mixing ratios published by BAMS in “State of the Climate” (Last report: Lan et al., 2022), presented by the black bars in Figure 25, were  $6.6$  to  $6.7$  ppt during the period 2016-2021. This is close to the annual mean values observed at the Zeppelin Observatory.

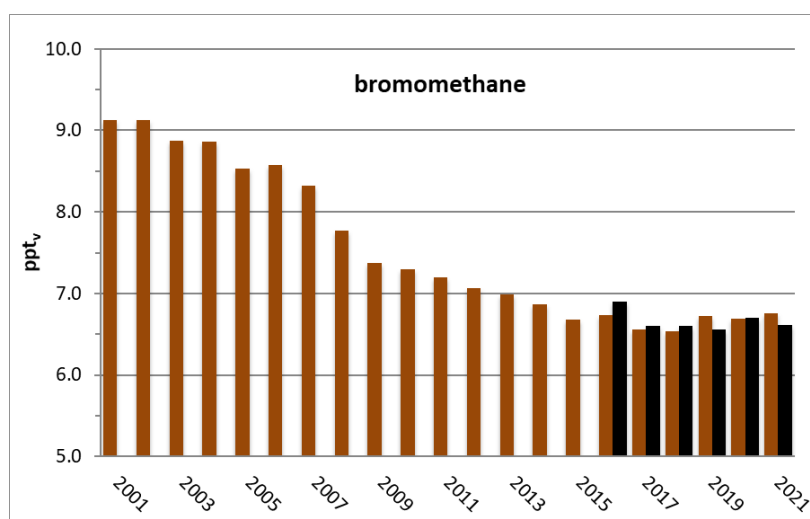


Figure 25: Development of the annual means of bromomethane measured at the Zeppelin Observatory for the period 2001-2021. The global annual mean for 2016-2021 are included as black bars.

## 2.3 Greenhouse gases with solely anthropogenic sources

The gases presented in this chapter have solely anthropogenic sources. These man-made greenhouse gases include CFCs, HCFCs, HFCs, SF<sub>6</sub>, NF<sub>3</sub>, SO<sub>2</sub>F<sub>2</sub> and halons, and most of these gases did not exist in the atmosphere before the 20<sup>th</sup> century. Although the gases have much lower concentration levels than most of the natural gases mentioned in the previous section, they are strong infrared absorbers, many of them with extremely long atmospheric lifetimes resulting in high global warming potentials (see Table 3). As a group, the gases contribute to around 12% to the overall global radiative forcing since 1750 (Myhre et al., 2013b). The annual mean concentrations for all years and all gases included in the monitoring programme are given in Appendix I (Table A 1, page 120), whereas trends, uncertainties and regression coefficients are found in Table A 2.

Some of these gases are ozone depleting, and consequently regulated through the Montreal protocol. Especially chlorine and bromine from CFCs, HCFCs and halons contribute to the depletion of the ozone layer, allowing increased UV radiation to reach the earth's surface, with potential impact not only on human health and the environment, but on agricultural crops as well. In 1987 the Montreal Protocol was signed in order to reduce the production and use of these ozone-depleting substances (ODSs) and the amount of ODSs in the troposphere reached a maximum around 1995. The amount of most ODSs in the troposphere is now declining slowly and the concentrations are expected to be back to pre-1980 levels around year 2050. In the stratosphere the peak ODS level was reached around year 2000. According to WMO (2018) the amount of Equivalent Effective Stratospheric Chlorine (EESC) declined by about 9% in the Polar regions and 13-17% in Mid-latitude regions from mid 1990s to 2016.

There are two generations of substitutes for the CFCs. The first generation is included in the Montreal protocol as they also deplete the ozone layer. This comprises the HCFCs listed in Table 2. The second-generation substitutes, the HFCs, are included in the Kyoto protocol and in the amendment to the Montreal Protocol agreed in Kigali in 2016. The general situation now is that the CFCs are declining, while their substitutes are increasing, and some of them are increasing rapidly.

### 2.3.1 Chlorofluorocarbons (CFCs) at Zeppelin Observatory

**Key findings - CFCs:** *The development of the CFC levels at Zeppelin is promising and in good accordance with the compliance of the Montreal protocol. The concentrations of CFC-11, CFC-12 and CFC-113 are all declining, and the mixing ratios of these gases are reduced with approximately 14.1%, 9.0% and 15.1% since 2001, respectively. Studies have shown that the rate of decline in CFC-11 slowed down by ~50% after 2012, both globally and at Zeppelin due to unreported emissions in China. However, the Chinese emission has been back to a pre-2013 level after 2019. Also, CFC-115 has increased by 7.2% since 2001 and the increase intensified after 2013. This might be related to Chinese emissions.*

In total, four chlorofluorocarbons (CFCs) are measured and analysed at the Zeppelin observatory: CFC-11, CFC-12, CFC-113, and CFC-115. These are the main ozone depleting gases. The anthropogenic emissions started around the 1930s, and all these compounds were restricted in the Montreal protocol from 1987. The main sources of these compounds were foam blowing, aerosol propellant, temperature control (refrigerators), solvents, and the electronics industry. The highest production of the CFCs took place around 1985, with maximum emissions around 1987. The lifetimes of these compounds are long, from 45 to over one thousand years (see Table 3), and combined with strong infrared absorption properties their GWPs are high.

Figure 26 shows the daily averaged observed mixing ratios of the four CFCs. Before 2010/2011 the instrumentation for measurements of CFCs at Zeppelin was not in accordance with recommendations and criteria of AGAGE, and consequently there are relatively high uncertainties in the observations of these compounds, see also Appendix I. From September 2010, new and improved instrumentation was installed at Zeppelin, providing more accurate observations of CFCs. The higher precision is clearly

visualised in Figure 26, but due to several severe instrumental problems in 2013/14, 2015/16 and 2019 there are some periods without CFC measurements<sup>13</sup>.

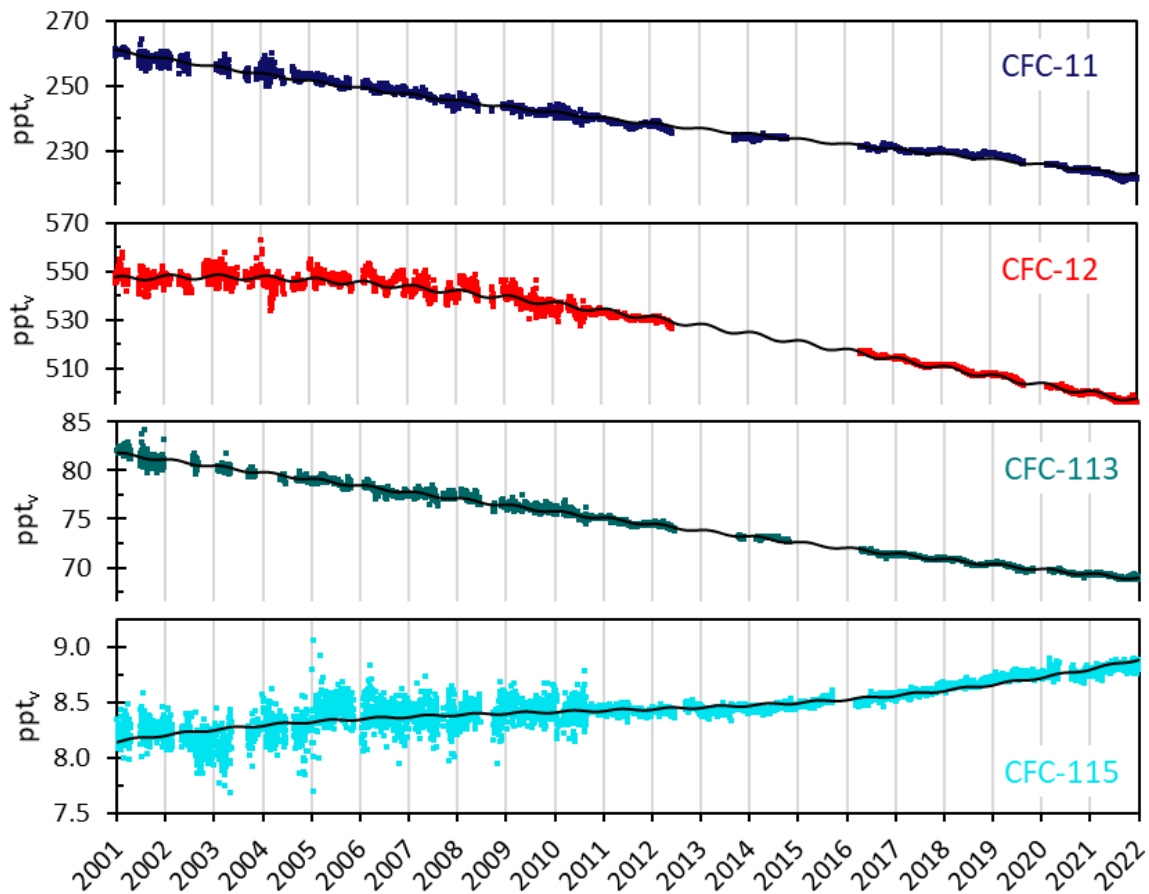


Figure 26: Daily averaged mixing ratios of the monitored CFCs at the Zeppelin observatory for the period 2001-2021: CFC-11 (dark blue), CFC-12 (red), CFC-113 (green) and CFC-115 (light blue). The solid lines are empirical fitted mixing ratios.

The trends per year for CFC-11, CFC-12 and CFC-113, given in Table 2, are all negative. The decreases are -1.8, -2.6, and -0.6 ppt/yr for CFC-11, CFC-12 and CFC-113, respectively. For the compound CFC-115 the trend is still slightly positive, +0.026 ppt/yr, and there has also been a small increase the last few years, after a stable period. It should be noted that the ambient concentration of CFC-115 is relatively low compared to CFC-11 and CFC-12, but it has a very long lifetime of 540 years, which limits our ability to reduce the abundance in the atmosphere. In total, the development of the CFC levels at the global background site Zeppelin is promising and in accordance with the compliance of the Montreal protocol.

Studies from Rigby et al. (2019) showed that the rate of decline of atmospheric CFC-11 concentrations slowed down by about 50% after 2012, caused by new production and unreported CFC-11 emissions in China, strongly inconsistent with the Montreal Protocol agreement. Also, studies from Vollmer et al. (2018) conclude that a large fraction of the current global emissions of CFC-115 originate from the

<sup>13</sup> The instrumentation is not in accordance with recommendations and criteria of AGAGE for measurements of the CFCs and there are larger uncertainties in the observations of this compound, see also Appendix I. This is also why these compounds are particularly sensitive to instrumental problems.

Chinese mainland. However, a publication from Park et al. (2021) indicates that the CFC-11 emissions in eastern China returned to pre-2013 levels in 2019. This demonstrates the importance of maintaining good monitoring networks, both to detect possible changes in ODSs, but also to detect possible effects of climate change on the ozone layer.

The 2001-2021 annual means for all the observed CFCs at Zeppelin are shown in Figure 27. Also, the global annual means in 2016 – 2021 as reported in “State of the Climate”, BAMS (Dlugokencky et al., 2018 and 2019; Hall et al., 2017 and 2020; Lan et al., 2021 and 2022) are included as black bars for comparison. As can be seen, the observed concentrations at Zeppelin are close to the global mean for these compounds, as the lifetimes are long and there are hardly any present-day emissions.

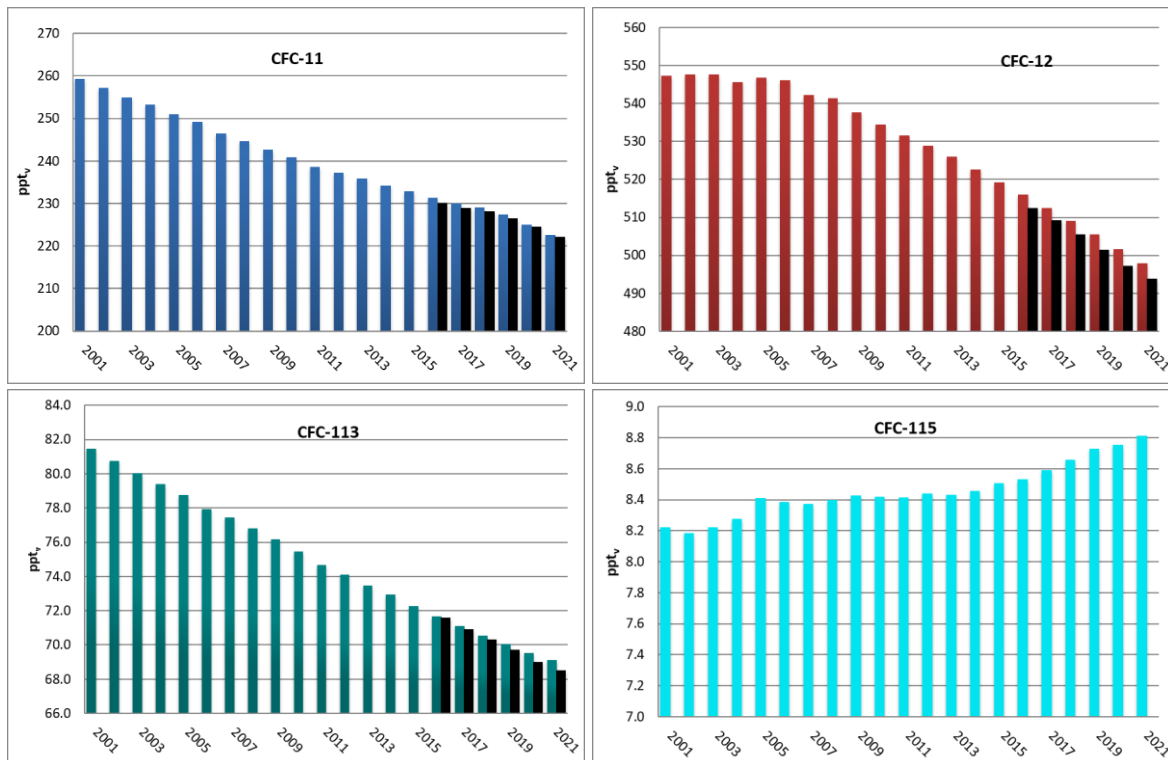


Figure 27: Development of CFC annual means at the Zeppelin Observatory for the period 2001-2021. Upper left panel: CFC-11, upper right panel: CFC-12, lower left panel: CFC-113, lower right panel: CFC-115. See Appendix I for data quality and uncertainty. The global annual means for 2016-2021 are included as black bars. All units are in ppt.

According to WMO (2018) the global mean mixing ratio of CFC-11 (from the AGAGE network) decreased with approximately 1.3 ppt/yr from 2015 to 2016. This is in accordance with the measurements at Zeppelin. As mentioned above, the rate of atmospheric CFC-11 decline slowed down after 2012. At Zeppelin, the average rate was -2.1 ppt/yr prior to 2012 and -1.6 ppt/yr after 2012. CFC-12 (the red diagram) has a very high GWP, 11 200, and it is also the most abundant CFC. This makes CFC-12 a very potent greenhouse gas. The global mean estimates from the AGAGE network, show that the atmospheric mixing ratio of CFC-12 decreased at a rate of -0.7%/yr from 2015 to 2016 (WMO, 2018). This fits well with our observations at Zeppelin the last years. CFC-12 had a maximum around 2003-2005, but there has been a clear reduction over the last years: 49 ppt since 2005.

### 2.3.2 Hydrochlorofluorocarbons (HCFCs) at Zeppelin Observatory

**Key findings - HCFCs:** The CFC substitutes HCFC-22, HCFC-141b and HCFC-142b have increased significantly since the measurements started at Zeppelin in 2001. HCFC-22 has a growth rate of 5.4 ppt/yr, whereas HCFC-141b and HCFC-142b have average growth rates of 0.5 ppt/yr. From 2001 to 2021 HCFC-22, HCFC-141b and HCFC-142b increased by 63%, 56% and 58%, respectively. HCFC-22 is still increasing, but the rate has slowed down. The situation is even more encouraging for HCFC-141b and HCFC-1412b, where concentrations have stabilized or declined the last five years.

Hydrochlorofluorocarbons, HCFCs, represent the first generation of replacement gases for CFCs. Their lifetimes are rather long, see Table 3, and although not as stable and persistent in the atmosphere as CFCs, they can still reach the stratosphere where they can destroy the ozone layer. Consequently, these gases are regulated through the Montreal protocol. The Norwegian monitoring programme includes three HCFC species: HCFC-22 (removed from AGAGE since 2019), HCFC-141b and HCFC-142b. These compounds are mainly used as refrigerants, foam blowing agents and solvents. The use of the gases worldwide is now frozen, but they are yet not completely phased out. All these gases potentially have a strong warming effect due to their high GWPs, e.g. (see Table 3) HCFC-142b has the highest GWP, with a warming potential 2 300 times stronger than CO<sub>2</sub>, per kg gas emitted.

The daily averaged observations of the three HCFCs are shown in Figure 28 for the period 2001-2021.

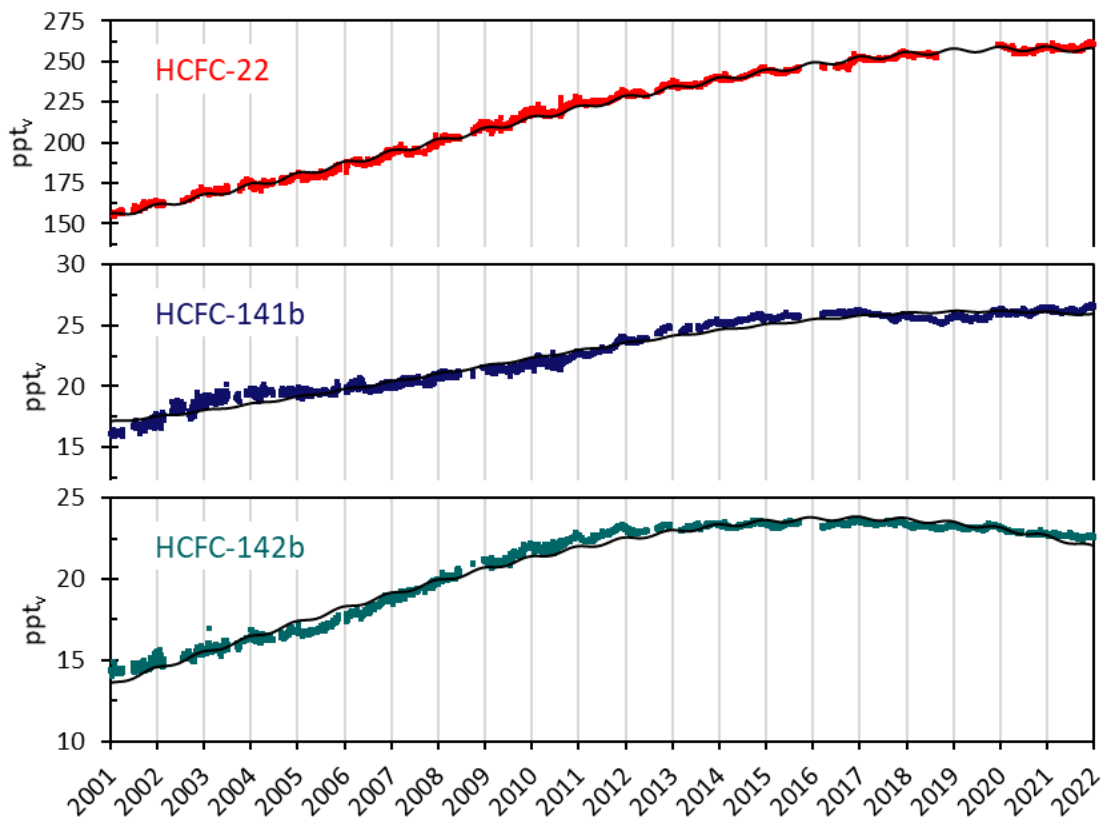


Figure 28: Daily averaged mixing ratios of the monitored HCFCs for the period 2001-2021 at the Zeppelin observatory: HCFC-22 (red), HCFC-141b (dark blue), and HCFC-142b (green). The solid lines are empirical fitted mixing ratios. All units are in ppt.

HCFC-22, HCFC-141b and HCFC-142b have all increased over the period 2001-2021. HCFC-22 is the most abundant HCFC species and has been increasing at a rate of 5.4 ppt/yr over the period 2001-2021. The concentration of the two other compounds, HCFC-141b and HCFC-142b, are a factor of ten lower than HCFC-22, and the increase in absolute annual means are also a factor of ten lower; HCFC-

141b and HCFC-142b both increased by 0.5 ppt/yr over the period 2001-2021. However, the development is encouraging for HCFC-141b and HCFC-142b, which have stabilized or even decreased after 2017. This is best illustrated in Figure 27, which shows the annual means for the full period. The rate of increase for HCFC-22 has also slowed down the last 5-6 years. Ten years ago, HCFC-22 increased by 7-8 ppt/yr. From 2020 to 2021 the increase was reduced to 1.1 ppt. With lifetimes in the order of 10-20 years, it is important to continue monitoring the development of the HCFCs for many years to come, as they have a significant influence on the ozone layer and are also strong greenhouse gases. The global annual means for 2016-2021 are included in Figure 27 as black bars (Hall et al. 2017 and 2020; Dlugokencky et al. 2018 and 2019; Lan et al., 2021 and 2022). The observed concentrations at Zeppelin are 4-6% higher than the global means, due to location in the northern Hemisphere, closer to emission sources.

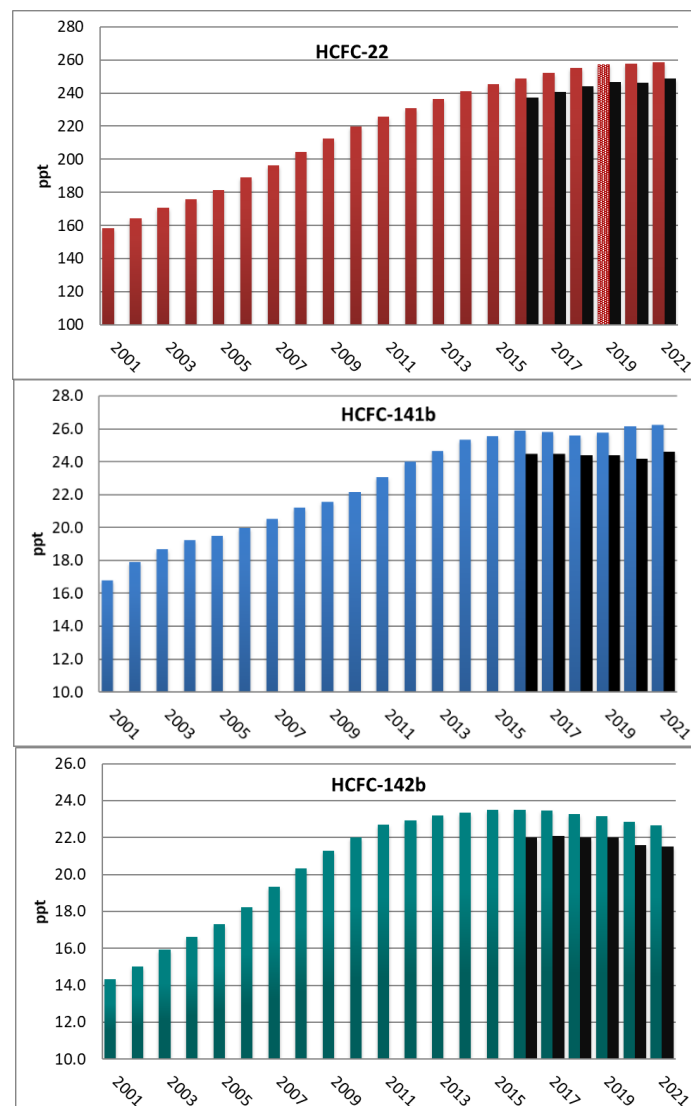


Figure 29: Development of the annual means of observed HCFCs at the Zeppelin Observatory for the period 2001-2021. HCFC-22 (red), HCFC-141b (blue), and HCFC-142b (green). The global annual means in 2016 to 2021 are included as black bars. All units are in ppt.



### 2.3.3 Hydrofluorocarbons (HFCs) at Zeppelin Observatory

**Key findings - HFCs:** *The hydrofluorocarbons (HFCs) were introduced as replacements for the ozone depleting CFCs and HCFCs. They are not harmful to the ozone layer since they do not contain chlorine, but they are strong greenhouse gases. The mixing ratios of HFC-125, HFC-134a, and HFC-152a have been measured at the Zeppelin observatory since 2001, and over the period 2001-2021 the concentrations have increased by 1685%, 497% and 313%, respectively. Eight new HFCs were introduced to the monitoring programme in 2015 and 2016: HFC-23, HFC-365mfc, HFC-227ea, HFC-236fa, HFC-245fa, HFC-32, HFC-143a, and HFC-4310mee. The mixing ratios of these gases are analysed back to 2010, showing an average increase of 4-10%/yr, except for HFC-32 which increases by as much as 17%/yr. HFC-152a is the only HFC which has levelled off and stabilized the last years, but for HFC-365mfc the growth rate has also declined the last 4-5 years. For the other HFCs the steep increase continued in 2021. The contribution from the HFCs to the global warming is still relatively small but given the rapid atmospheric increase it is crucial to follow the development of these gases. The phase-down of HFCs under the Montreal Protocol, agreed in Kigali in 2016, is important in curbing the growth in these gases.*

HFCs are the so-called second-generation replacements of CFCs, which means that they are considered as better alternatives to the CFCs with respect to the ozone layer than HCFCs, as they do not contain chlorine or bromine. However, many of these compounds are strong greenhouse gases. 1 kg of HFC-23 is as much as 12 400 times more powerful greenhouse gas than CO<sub>2</sub> (see Table 3). The phase-out of HFCs under the Montreal Protocol was under negotiation for many years and the successful agreement in Kigali, October 2016, represented an important progress. Presently, the contribution to global warming posed by HFCs is very limited. However, most of the compounds are increasing rapidly. The compounds are strong infrared absorbers with high GWP hence it is crucial to reduce future emissions.

For the period 2001-2021 three compounds have been measured at the Zeppelin Observatory: HFC-125, HFC-134a, and HFC-152a. HFC-125 is mainly used as a refrigerant and fire suppression agent. HFC-134a is used as a temperature control for domestic refrigeration and automobile air conditioners, whereas HFC-152a is used as a refrigerant and propellant for aerosol sprays and in gas duster products. Since 1990, when HFC-134a was almost undetectable in the atmosphere, the concentration of this gas has risen massively, and HFC-134a is currently the HFC with highest atmospheric concentration.

In 2015 five new HFCs were included in the Norwegian monitoring programme: HFC-23, HFC-365mfc, HFC-227ea, HFC-236fa, and HFC-245fa. In 2016 three additional HFCs were introduced to the programme: HFC-32, HFC-143a, and HFC-4310mee. All these species have been measured at Zeppelin since 2010, but they have not been analysed or reported to an international data base until 2016. The development of HFC-23 should be followed carefully since this gas has a relatively high concentration and an extremely high GWP. HFC-23 is a by-product of the production of HCFC-22 and is also used in the semiconductor industry. In addition, it is a useful refrigerant and fire suppressant.

Generally, the new HFCs are used for refrigeration and air conditioning, foam blowing, and fire extinguishing. Both HFC-245fa and HFC-365mfc are substitutes for HCFC-141b in foam blowing applications. HFC-236fa is also a foaming agent, in addition to a fire suppression agent and a refrigerant. HFC-227ea is mainly used to suppress fire in data equipment and telecommunication facilities, and in protection of flammable liquids and gases. HFC-227ea is also used as an aerosol propellant in pharmaceutical dose inhalers for e.g. asthma medication.

The three new HFCs introduced to the monitoring programme in 2016, are mainly used for refrigeration (HFC-32 and HFC-143a). In addition, HFC-143a is applied as propellant in canned air products for cleaning electronic equipment. HFC-4310mee is mainly used as a cleaning solvent in the electronics industry.

The seasonal cycles in HFC mixing ratios are closely linked to the lifetimes and variations in the incoming solar radiation. HFC-152a has the shortest lifetime (1.6 year), and as seen in Figure 30 HFC-152a has the most distinct seasonal cycle. The gas is mainly destroyed in the lowest part of the atmosphere by photolysis and reactions with OH.

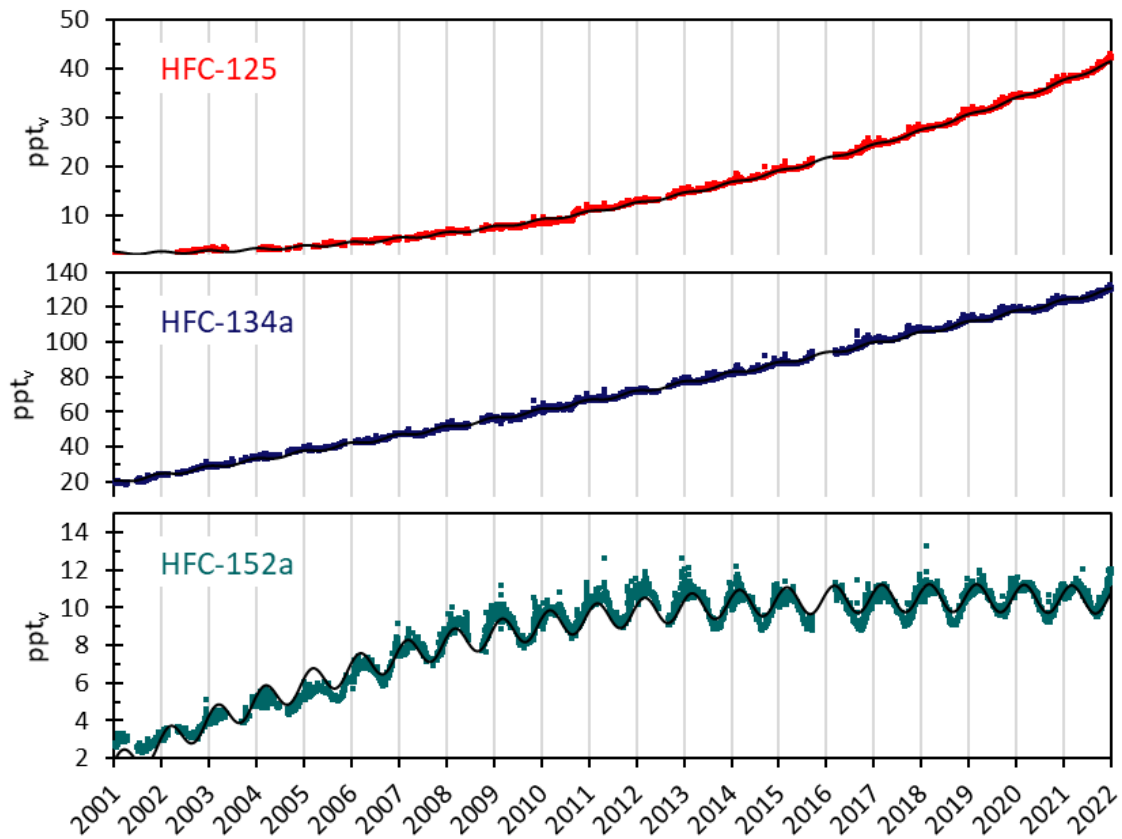


Figure 30: Daily averaged concentrations of the monitored HFCs for the period 2001-2021 at the Zeppelin observatory: HFC-125 (red), HFC-134a (dark blue), and HFC-152a (green). The solid lines are empirical fitted mixing ratios.

For the period 2001-2021 all HFCs shown in Figure 30 have increased significantly. HFC-134a has an increasing trend of 5.2 ppt/yr, which leaves this compound as the one with highest change per year of all the halocarbons measured at Zeppelin the last decade. The mixing ratios of HFC-125, HFC-134a and HFC-152a have increased by as much as 1685%, 497% and 313% since 2001, respectively. For HFC-125 we can even see an accelerating trend. HFC-152a, however, is the only HFC where the rapid increase has levelled off and stabilized after 2012. This is partly due to the shorter lifetime and rapid response to emission changes. This is clearly illustrated in Figure 30 and Figure 32. For HFC-365mfc the growth rate has also declined the last 4-5 years.

The eight new HFCs included in the programme in 2015 and 2016 are shown in Figure 31, which clearly demonstrates that the concentrations of all HFCs have increased steadily since 2010. The compounds generally increase by 4-10%/yr, except from HFC-32 which has an average increase of 17%/yr.

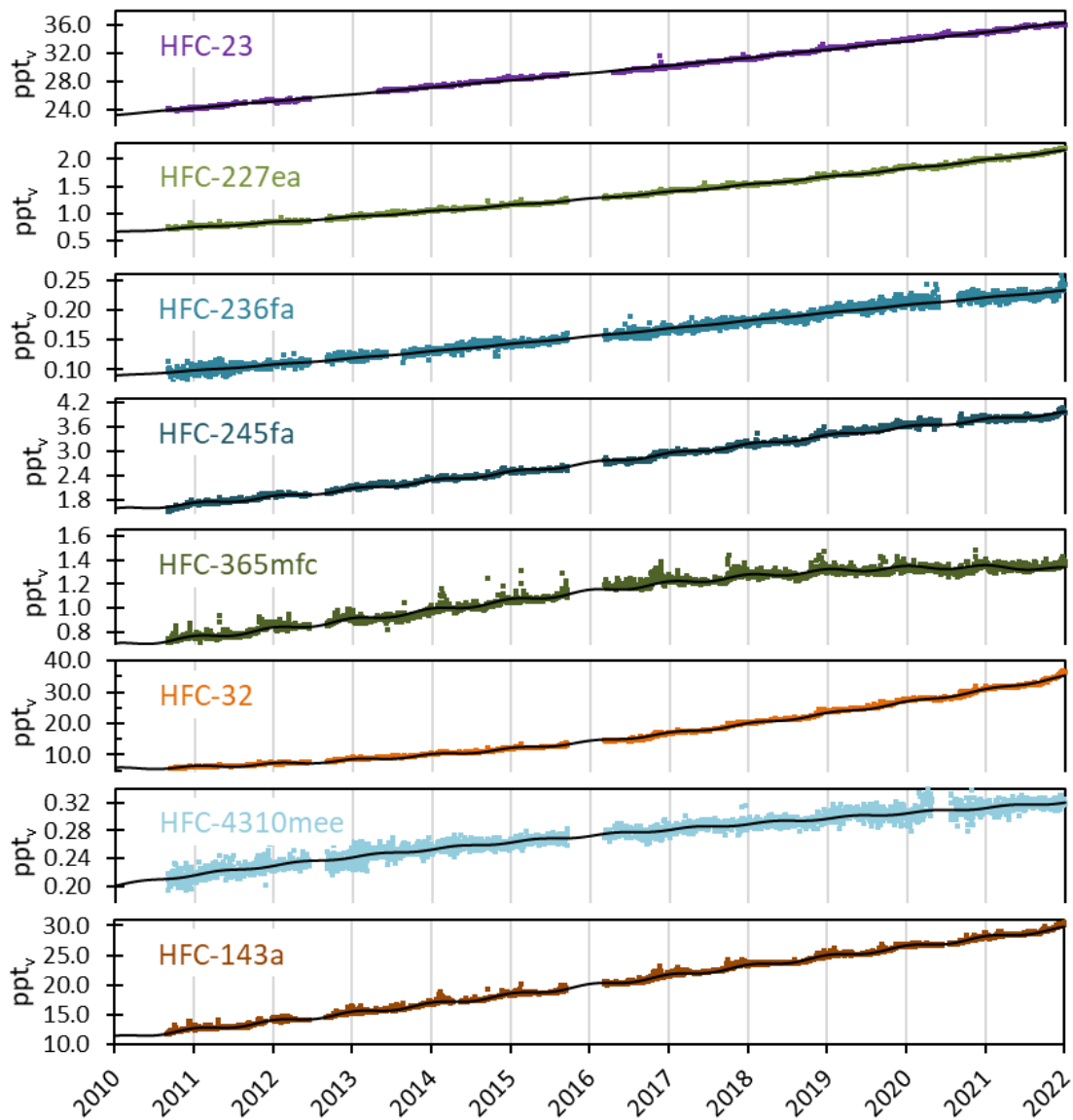


Figure 31: Daily averaged concentrations of monitored HFCs at the Zeppelin observatory for the period 2010-2021: HFC-23 (violet), HFC-227ea (light green), HFC-236fa (blue), HFC-245fa (dark blue), HFC-365mfc (dark green), HFC-32 (orange), HFC-4310mee (light blue), and HFC-143a (brown). The solid lines are empirical fitted mixing ratios.

The development of annual means of all reported HFCs are shown in Figure 32. The global annual means of 2016 - 2021 as given in Hall et al. (2017; 2020), Dlugokencky et al. (2018; 2019), and Lan et al. (2021; 2022) are included as black bars for comparison. As for HCFCs the concentrations at Zeppelin are higher than the global means. Also, the increasing tendency for most HFCs is clear, even if the concentrations are still very low, particularly for the new HFC-365mfc, HFC-245fa, HFC-236fa, HFC-227ea, and HFC-4310mee, with 3.8 ppt as maximum for HFC-245fa.

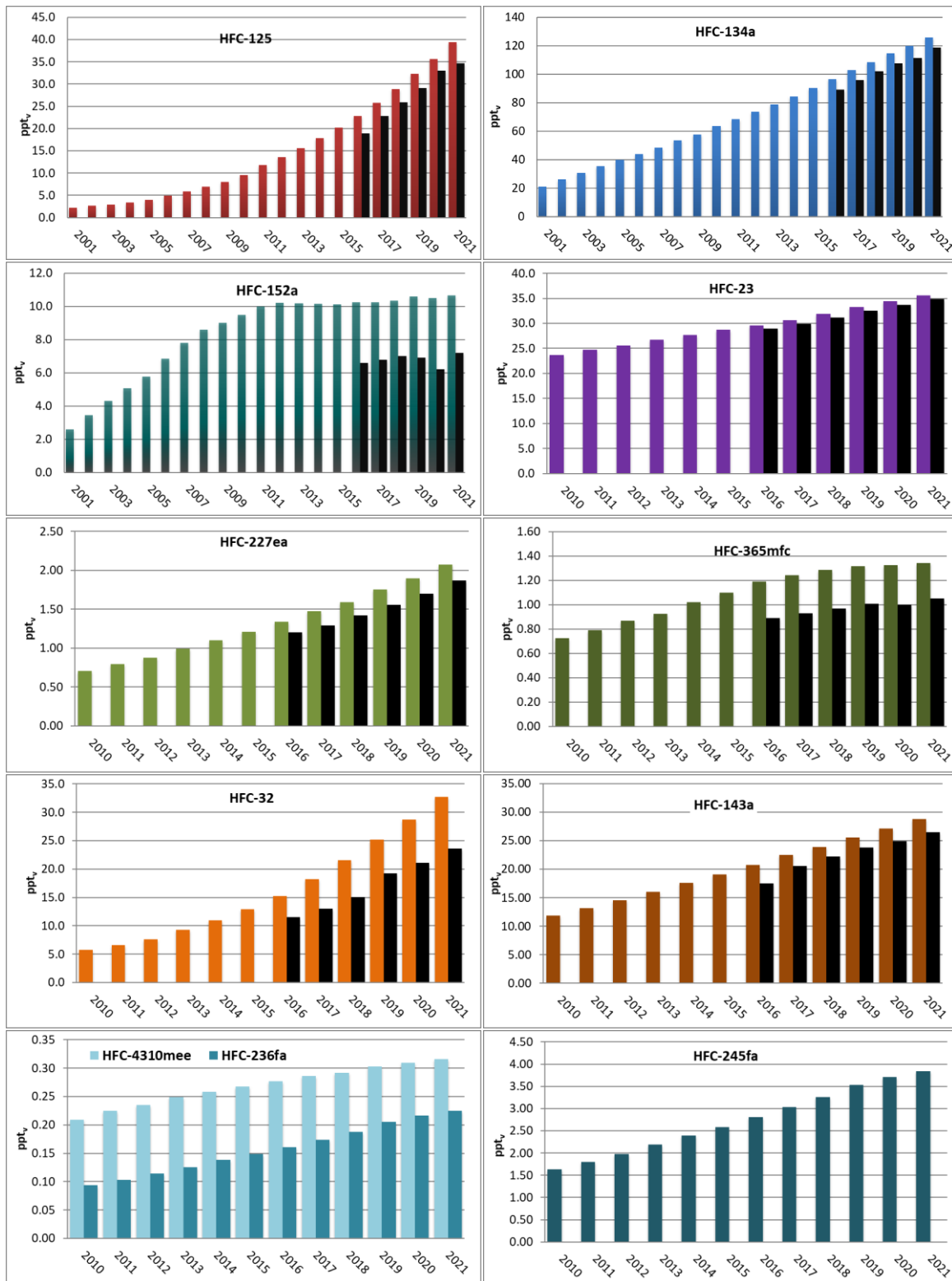


Figure 32: Development of the annual means of observed HFCs at the Zeppelin Observatory. For the period 2001-2021: HFC-125 (red), HFC-134a (blue), and HFC-152a (dark green). For the period 2010-2021: HFC-23 (violet), HFC-227ea (light green), HFC-365mfc (dark green), HFC-32 (orange), HFC-143 (brown), and light to dark blue: HFC-4310mee, HFC-236fa, and HFC-245fa. The global annual means in 2016-2021 are included as black bars, when available.

### 2.3.4 Halons measured at Zeppelin Observatory

**Key findings - Halons:** Halons are bromine containing halocarbons that contribute both to the depletion of the ozone layer and to global warming. Three halons are measured at Zeppelin: H-1211, H-1301, and H-2402. For H-1211 a maximum was observed in 2004, followed by a gradual decline. The concentration of H-1211 is ~27% lower today than when the measurements started in 2001. H-2402 has decreased by ~15% since 2010. H-1301, however, has increased by ~13% from 2001 to 2021, but no increase has been measured the last 5-6 years. According to the last Ozone Assessment (WMO, 2018) the stratospheric bromine concentration has now started to decrease.

Halons are greenhouse gases containing bromine. Thus, regulations of halons are also important to protect the ozone layer. If bromine reaches the stratosphere (high atmosphere), it is even more effective in destroying ozone than chlorine. The halons are regulated through the Montreal protocol and the concentration of most of these substances are decreasing. The main source of halons has been fire extinguishers.

From 2001 to 2015 two halons were measured and analysed at the Zeppelin observatory: H-1301 and H-1211. In 2016 H-2402 was also included in the monitoring programme, where data were analysed back to 2010. H-2402 was used primarily in the former USSR and was the main halon fire suppressant in that region.

The ambient concentrations of the three halons are fairly low,- below 4 ppt. Figure 33 shows the daily average concentrations of the monitored halons at Zeppelin. The halon trend analyses, listed in Table 2 and visualized in Figure 33, show an increase for H-1301 during the period 2001-2021 and a decrease for H-1211. The concentration of H-1211 is ~27% lower today than when the measurements started in 2001, whereas H-1301 has increased by ~13%. However, the concentration of H-1301 has stabilized and no increase has been measured the last 5-6 years. The new compound, H-2402, shows a relaxation of ~15% from 2010 to 2021. The development of the annual means for all three compounds are shown in Figure 34.

The annual means have not changed dramatically over the measured period, which is explained by low emissions and relatively long lifetimes (16 years for H-1211, 72 years for H-1301, and 28 years for H-2402). However, clear declines are evident for H-1211 and H-2402, which have the shortest lifetimes. According to the last Ozone Assessment report (WMO, 2018) the total stratospheric bromine concentration decreased by ~0.15 ppt/yr from 2012 to 2016.

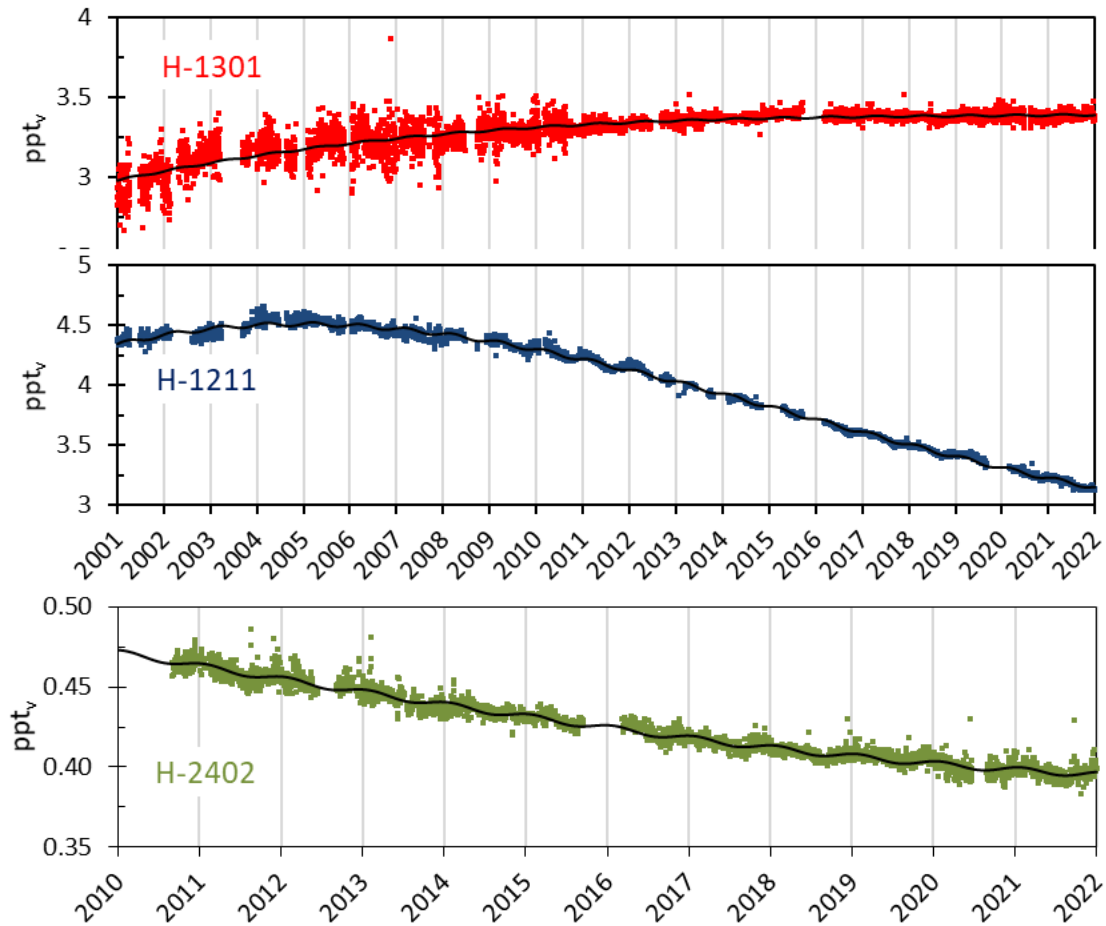


Figure 33: Daily averaged concentrations of the monitored halons at the Zeppelin Observatory. For the period 2001-2021: H-1301 (red) and H-1211 (blue). For the period 2010-2021: H-2402 (green). The solid lines are empirical fitted mixing ratios.

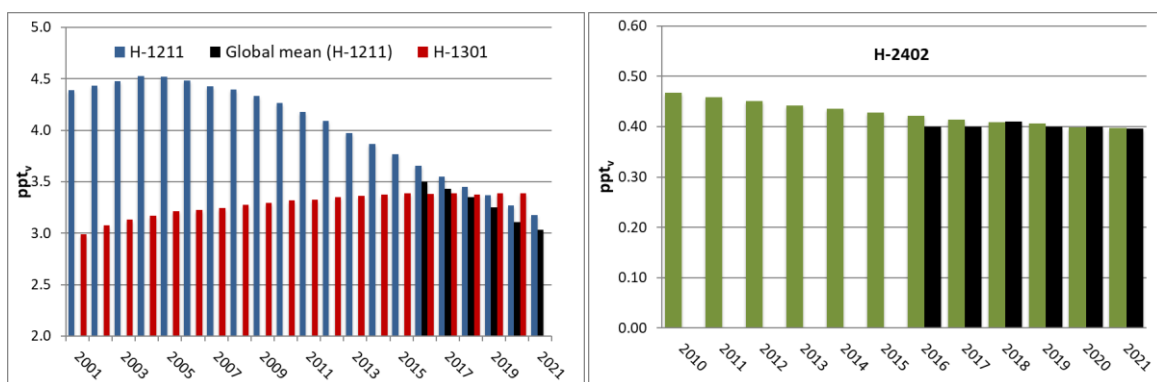


Figure 34: Development of the annual means of the observed halons at the Zeppelin Observatory. Red: H-1301, blue: H-1211, and green: H-2402. The global annual means in 2016 to 2021 are included as black bars. All units are in ppt.

### 2.3.5 Other chlorinated hydrocarbons at Zeppelin Observatory

**Key findings - Other chlorinated greenhouse gases.** In addition to chloromethane and bromomethane described in section 2.2.6 and 2.2.7, the following six chlorinated gases are measured at the Zeppelin Observatory: Trichloroethane ( $\text{CH}_3\text{CCl}_3$ ), dichloromethane ( $\text{CH}_2\text{Cl}_2$ ), trichloromethane ( $\text{CHCl}_3$ ), trichloroethene ( $\text{CHClCCl}_2$ ), tetrachloroethene ( $\text{CCl}_2\text{CCl}_2$ ), and carbon tetrachloride ( $\text{CCl}_4$ ). The concentration of most of these gases are decreasing. Possible exceptions are trichloromethane and dichloromethane, which increased significantly from 2007 to 2017. However, the last 3-4 years the annual mean concentrations of trichloromethane at Zeppelin has decreased. Dichloromethane also seemed to decrease from 2017 to 2019, but from 2020 to 2021 an increase of 9% was measured.

This section describes the following components measured at the Zeppelin Observatory: Trichloroethane (also called methyl chloroform,  $\text{CH}_3\text{CCl}_3$ ), dichloromethane ( $\text{CH}_2\text{Cl}_2$ ), trichloromethane (also called chloroform,  $\text{CHCl}_3$ ), trichloroethene (TCE,  $\text{CHClCCl}_2$ ), and tetrachloroethene (PCE,  $\text{CCl}_2\text{CCl}_2$ ). The daily average concentrations are shown in Figure 36. Additionally, carbon tetrachloride ( $\text{CCl}_4$ ) was included in the monitoring programme in 2015. The main sources of all these substances are solvents.

The global fraction of trichloroethane ( $\text{CH}_3\text{CCl}_3$ ), which is controlled under the Montreal Protocol, has been declining steadily since the peak values in the early 1990s. In 2016 the global amount of  $\text{CH}_3\text{CCl}_3$  reaching the stratosphere was reduced by 98% of its maximum value (WMO, 2018). The measurements at Zeppelin show that the concentration has decreased to 1.4 ppt in 2021, a reduction of 96% since the measurements started in 2001. Today trichloroethane contributes negligible to the atmospheric chlorine burden.

It is worth noting the strong increase in dichloromethane (violet) and trichloromethane (light blue) from 2007 to 2017, seen in Figure 35 and Figure 36. Dichloromethane has a lifetime of less than 6 months and responds rapidly to emissions changes, where about 90% has industrial origin. Its main applications are from paint strippers, degreasers, and solvents, in foam production and blowing applications or as an agricultural fumigant (WMO, 2011). The natural sources of dichloromethane, which account for ~10% of the total emissions, is mainly from biomass burning and marine sources. At Zeppelin dichloromethane has increased by ~119% since 2001. The growth rate seemed to stabilize after 2017, but from 2020 to 2021 an increase of as much as 9% has been measured.

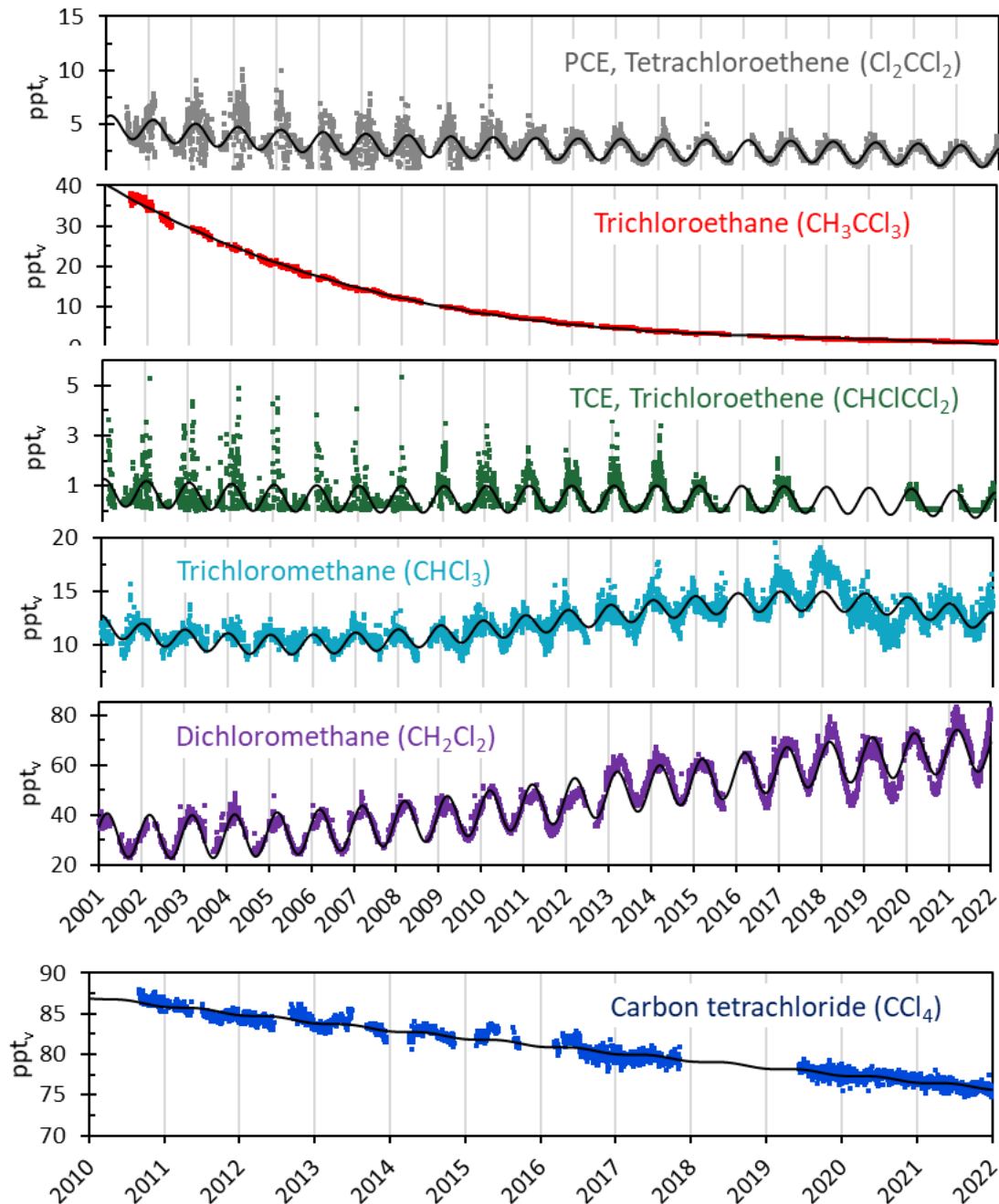


Figure 35: Daily averaged concentrations of chlorinated hydrocarbons at the Zeppelin observatory: For the period 2001-2021: Tetrachloroethene (grey), trichloroethane (red), trichloroethene (green), trichloromethane (light blue), and dichloromethane (violet). For the period 2010-2021: carbon tetrachloride (dark blue). Solid lines are empirical fitted mixing ratios.

Trichloromethane (light blue) has a lifetime of  $\sim 0.5$  year, thus the response to emission changes is also relatively rapid. The annual mean value of trichloromethane at Zeppelin increased by 37% from 2001 to 2017 and similar increases were observed at other sites (e.g. Mauna Loa at Hawaii and Barrow in Alaska). However, there has been a clear decrease in trichloromethane at Zeppelin the last four years, and the annual mean concentration in 2021 was 2.6 ppt below the 2017 peak value. The reason for these rapid changes is not yet clear, but they might be explained by natural sources.



Even if trichloromethane and dichloromethane have relatively short lifetimes, modelling studies imply that chlorine from these compounds can reach the lower stratosphere and potentially destroy stratospheric ozone (Hossaini et al., 2017). Thus, sustained growth in these compounds might offset some of the gains achieved by the Montreal Protocol, further delaying recovery of Earth's ozone layer.

The atmospheric concentrations of trichloroethene (TCE; green) and tetrachloroethene (PCE; grey) are low, and the measured annual variabilities are quite high, especially before 2011 due to instrumental limitations (see appendix 2). This makes it difficult to draw conclusions about trends and development of these species. In 2021 the annual average concentration of PCE was 2.1 ppt, the same value as previous year.

The concentration of carbon tetrachloride ( $\text{CCl}_4$ ) has been measured at Zeppelin since 2010. This compound was once a popular solvent in organic chemistry, but because of its adverse health effects it is rarely used any more. Today  $\text{CCl}_4$  is sometimes applied as a solvent for infrared spectroscopy. For the period 2010-2021 the annual mean values have decreased by 1.1%/yr, i.e. from 86.6 ppt in 2010 to 76.2 ppt in 2021.

It should be noted that no annual mean values of TCE were calculated from the measurements in 2018 to 2020. This is related to the upgrade of the Medusa-GCMS in 2017 (see Appendix II), which caused problems for this compound. Thus, most of the TCE measured performed in 2018 and 2019 are flagged as "absent".

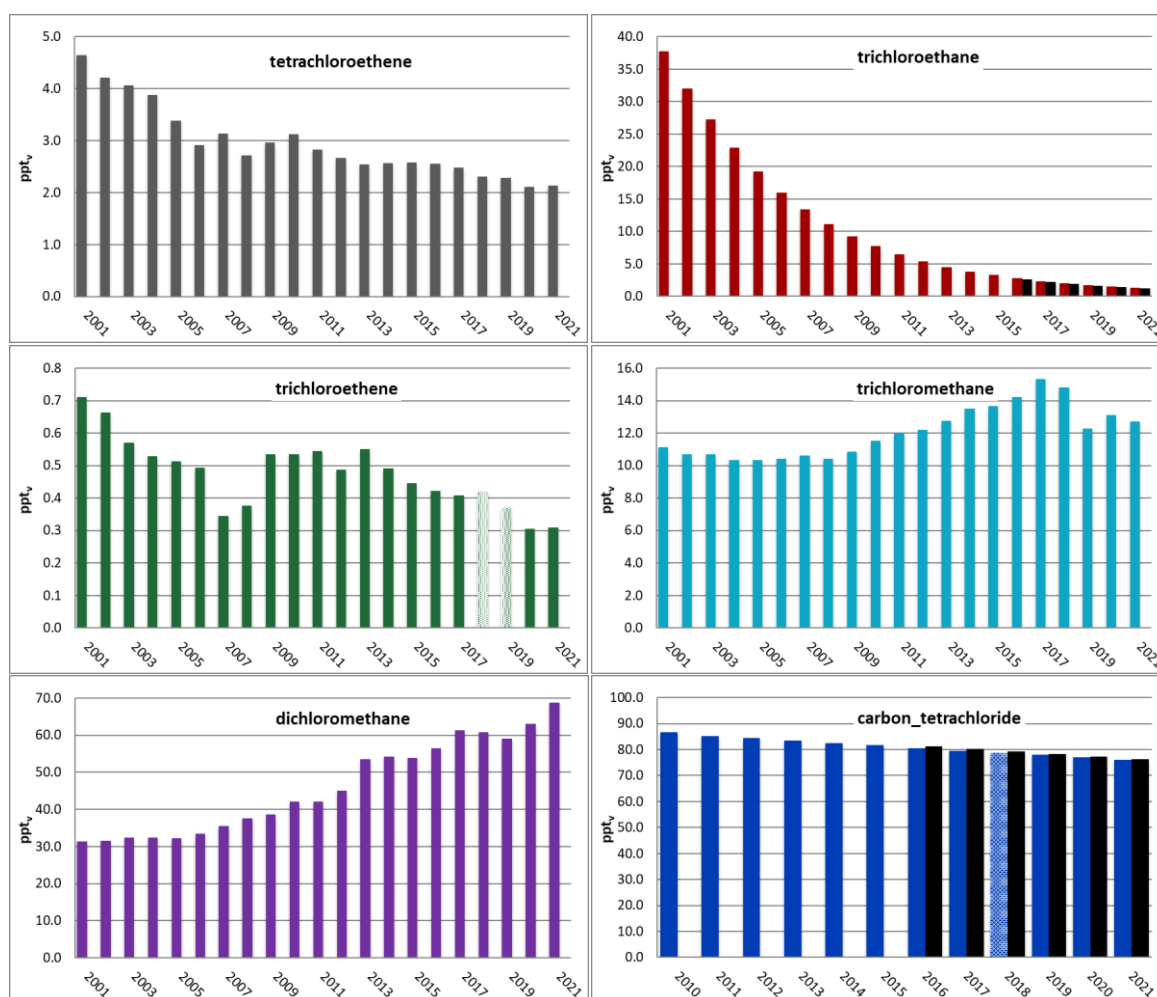


Figure 36: Annual means of the chlorinated hydrocarbons. Upper panel: tetrachloroethane (grey) and trichloroethane (red). Mid panel: trichloroethene (TCE, green) and trichloromethane (light blue). Lower panel: dichloromethane (violet) and carbon tetrachloride (CCl<sub>4</sub>, dark blue). The global annual means for CH<sub>3</sub>CCl<sub>3</sub> and CCl<sub>4</sub> in 2016-2021 are included as black bars, when available. All units are in ppt. Note that TCE data from 2018 and 2019 mainly are based on model data.

### 2.3.6 Perfluorinated compounds at Zeppelin Observatory

**Key findings – Perfluorinated compounds.** This group of compounds include SF<sub>6</sub>, SO<sub>2</sub>F<sub>2</sub>, NF<sub>3</sub>, PFC-14, PFC-116, PFC-218, and PFC-318. Generally, these compounds are extremely potent greenhouse gases, but their concentrations are still low. An exception is PFC-14, which had a mixing ratio of 88.0 ppt in 2021, an increase of 1.0 ppt since 2020. SF<sub>6</sub> should also be followed closely, as this compound has an atmospheric lifetime of 3 200 years and an extremely high GWP of 25 200. This compound has increased by 119% since 2001.

Perfluorinated compounds belong to a group of long-lived greenhouse gases, and their contribution to the Earth's radiative forcing has increased over the past several decades. The impact of these highly fluorinated compounds on climate change is a concern because of their exceptionally long atmospheric lifetimes, as well as their strong absorption in the infrared "window" region (Baasandorj et al., 2012).

Up to 2015, the Norwegian national monitoring programme only included measurements of one perfluorinated compound, SF<sub>6</sub>. However, other perfluorinated compounds are also very powerful

greenhouse gases with atmospheric lifetimes up to 50 000 years (See Table 3) and with increasing concentrations in the atmosphere. From 2010 NILU extended the monitoring of perfluorinated compounds at Zeppelin, after new and improved instrumentation was installed. Several of these compounds, so-called perfluorocarbons (PFCs), were included in the current monitoring programme in 2015, with analysis back in time to September 2010. Two additional compounds were included in the 2016 monitoring programme: Nitrogen trifluoride (NF<sub>3</sub>) and Sulphuryl fluoride (SO<sub>2</sub>F<sub>2</sub>). For the latter compound data was analysed back to 2010. The instrument at Zeppelin was re-built and optimised in 2015 and 2016, which made it possible to measure NF<sub>3</sub>. Thus, NF<sub>3</sub> data are only available from 2016 and onwards.

### **2.3.6.1 Sulfurhexafluoride (SF<sub>6</sub>), Sulphuryl fluoride (SO<sub>2</sub>F<sub>2</sub>), Nitrogen trifluoride (NF<sub>3</sub>)**

Sulfurhexafluoride, SF<sub>6</sub>, is an extremely strong greenhouse gas emitted to the atmosphere mainly from the production of magnesium and in the electrical industry for high-voltage circuit breakers, switch gears and other electrical equipment. This component has been a part of the monitoring programme since 2001. The atmospheric lifetime of this compound is 3 200 years, and the global warming potential is 25 200, which means that the emission of 1 kg of SF<sub>6</sub> has a warming potential which is 25 200 times stronger than 1 kg emitted CO<sub>2</sub>.

Sulphuryl fluoride, SO<sub>2</sub>F<sub>2</sub>, has a lifetime of 36 years and a GWP of 4 630. SO<sub>2</sub>F<sub>2</sub> is normally used as a pesticide fumigant for dried fruits, nuts, and other agricultural commodities that must be kept pest-free during storage. It is one of the most common replacements for bromomethane, an ozone-depleting substance whose use is being phased out.

Nitrogen trifluoride, NF<sub>3</sub>, has a lifetime of 569 years and a GWP as high as 17 400, meaning that it also is an extremely strong greenhouse gas. NF<sub>3</sub> is used in the manufacturing of new generation solar panels, flat-screen televisions, touch-sensitive screens, and electronic processors. The use of NF<sub>3</sub> has widely increased in the past because of the rising demand in flat-screen televisions and microelectronics.

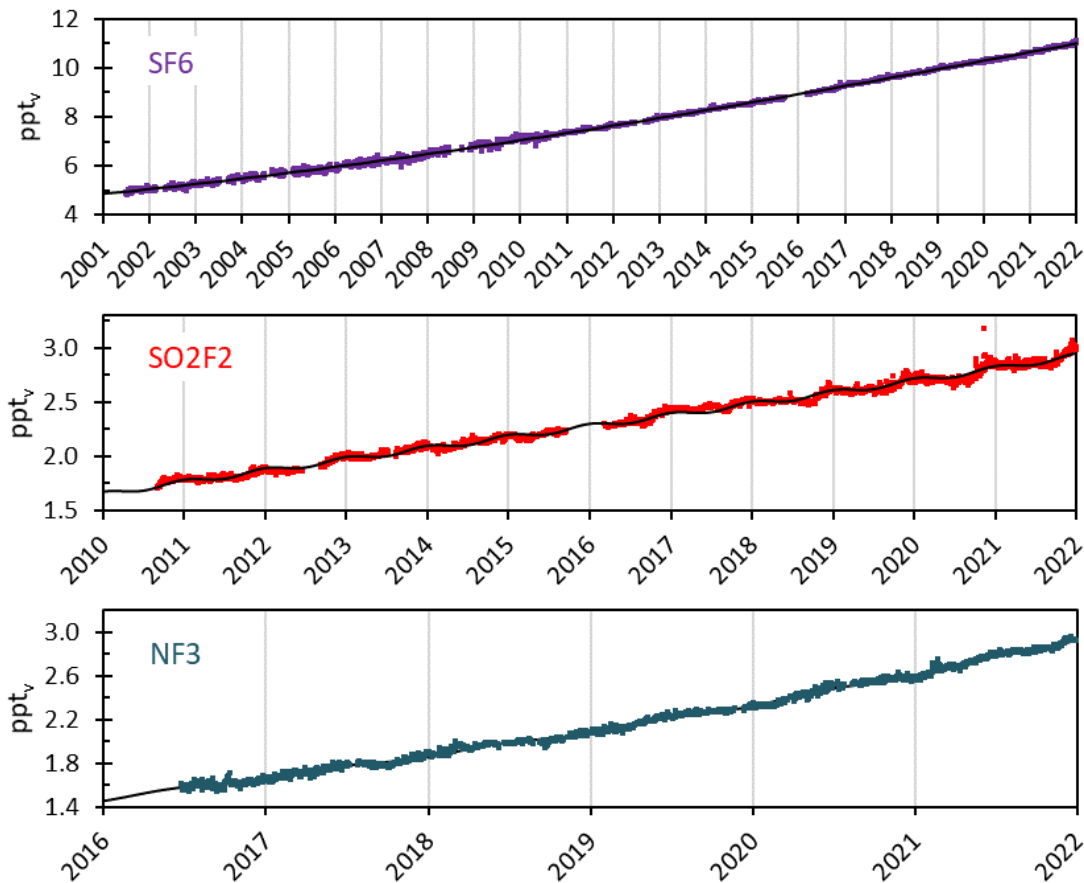


Figure 37: Daily averaged concentrations at the Zeppelin Observatory. Upper panel:  $\text{SF}_6$  for the period 2001-2021. Middle panel:  $\text{SO}_2\text{F}_2$  for the period 2010-2021. Lower panel:  $\text{NF}_3$  from mid 2016 to 2021. Solid lines are statistical fitted mixing ratios.

The daily averaged concentrations of  $\text{SF}_6$ ,  $\text{SO}_2\text{F}_2$  and  $\text{NF}_3$  are presented in Figure 37.  $\text{SF}_6$  is increasing with a rate of 0.30 ppt/yr and has increased as much as 119% since the start of our measurements in 2001. The instrumentation before 2010 was not optimal for measurements of  $\text{SF}_6$ , thus there are higher uncertainties for this compound's mixing ratios than for most of the other compounds reported from 2001 to 2010 (see Appendix I).

The concentration of  $\text{SO}_2\text{F}_2$  has also increased significantly the last years (see Figure 37). The total increase for the period 2010-2021 is 1.16 ppt (68%). Daily average observations of  $\text{NF}_3$  are visualized in Figure 37, lower panel, and the figure clearly demonstrates a continued increase since the measurements started in June 2016. The annual average  $\text{NF}_3$  concentration in 2021 was 2.78 ppt, an increase of 1.16 ppt (72%) from 2017.

Figure 38 shows annual average concentrations of  $\text{SF}_6$  (left panel) and  $\text{SO}_2\text{F}_2$  (right panel) measured at Zeppelin for the periods 2001-2021 and 2010-2021, respectively. The global annual means of  $\text{SF}_6$  in 2016 - 2021 (Hall et al., 2017 and 2020; Dlugokencky et al., 2018 and 2019; Lan et al., 2021 and 2022) are included as black bars for comparison. Again, the concentrations at Zeppelin are slightly higher than the global means.

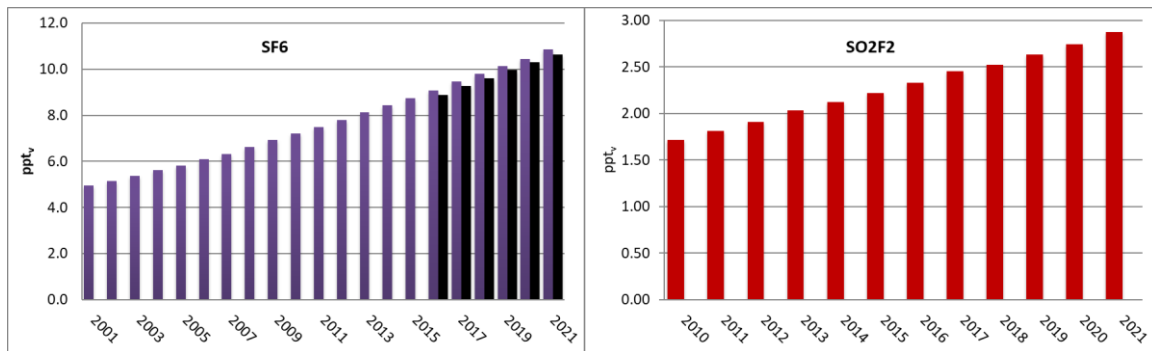


Figure 38: Annual means of SF<sub>6</sub> for the period 2001-2021 (left) and SO<sub>2</sub>F<sub>2</sub> for the period 2010-2021 (right) at the Zeppelin observatory. The global annual means for SF<sub>6</sub> in 2016 to 2021 are included as black bars.

### 2.3.6.2 Perfluorocarbons or PFC's: PFC-14, PFC-116, PFC-218, PFC-318

Perfluorocarbons or PFCs are compounds that contain only carbon and fluorine. Four of these compounds are currently measured and reported at Zeppelin: PFC-14, PFC-116, PFC-218, and PFC-318. PFC-14, also called tetrafluoromethane or CF<sub>4</sub>, is the most persistent PFC greenhouse gas with an atmospheric lifetime of 50 000 years and a greenhouse warming potential of 7 380. It is used as a low temperature refrigerant, in electronics microfabrication, and in neutron detectors. Another potent greenhouse gas is hexafluoroethane, PFC-116, which has an atmospheric lifetime of 10 000 years and a GWP of 12 400. The gas is used as an etchant in e.g. semiconductor manufacturing, and aluminium and semiconductor manufacturing industries are the major emitters of PFC-116. Fraser et al. (2013) showed that the release of PFC-14 at Hydro's aluminium plant in Australia was 10 times greater than the release of PFC-116. Octafluoropropane, PFC-218, which has an atmospheric lifetime of 2 600 years and a GWP of 9 290, is also used in the electronics industry as a plasma etching material. In medicine, PFC-218 microbubbles reflect sound waves well and is used to improve the ultrasound signal backscatter. Octafluorocyclobutane, PFC-318, with an atmospheric lifetime of 3 200 years and a GWP of 10 200, is the third most abundant PFC in the atmosphere (Oram et al., 2012). Although a number of potential sources of PFC-318 have been reported, including electronic and semi-conductor industries, there remains a large discrepancy in the atmospheric budget. A study from Mühle et al. (2019) suggests that production of Teflon and other fluorochemicals in China, India, and Russia is a likely source of PFC-318, as pyrolysis of HCFC-22 produces PFC-318 as a by-product

The daily averaged concentrations of the PFCs measured at Zeppelin are shown in Figure 39. For the period 2010-2021 PFC-116, PFC-218 and PFC-318 increased by 24%, 31%, and 52%, respectively. For PFC-14 no data exist until October 2014, but the measurements in 2015 to 2021 indicate that the concentration of PFC-14 increases by ~1.1%/yr.

The development of the annual means of the PFCs are shown in Figure 40. For PFC-116 the global annual mean in 2016 to 2021 (Hall et al., 2017 and 2020; Dlugokencky et al., 2018 and 2019; Lan et al., 2021 and 2022) are shown as black bars for comparison. The concentrations of most PFCs are relatively low. However, PFC-14 is an exception. With an annual mean concentration of 88.0 ppt in 2021, a lifetime of 50 000 years and GWP of 7 380, this is an important greenhouse gas that should be followed carefully.

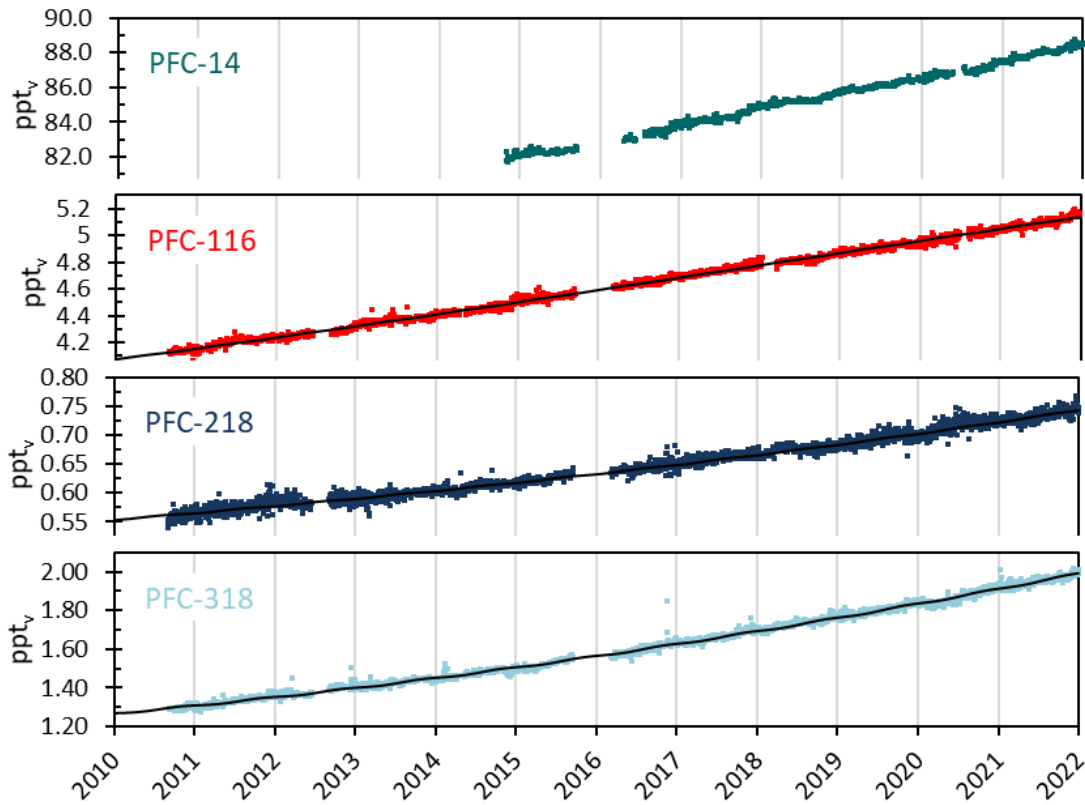


Figure 39: Daily averaged concentrations of perfluorocarbons at the Zeppelin observatory for the period 2010-2021: PFC-14 (green), PFC-116 (red), PFC-218 (dark blue), and PFC-316 (light blue). PFC-14 is only ranging back to autumn 2014. The solid lines are statistical fitted mixing ratios.

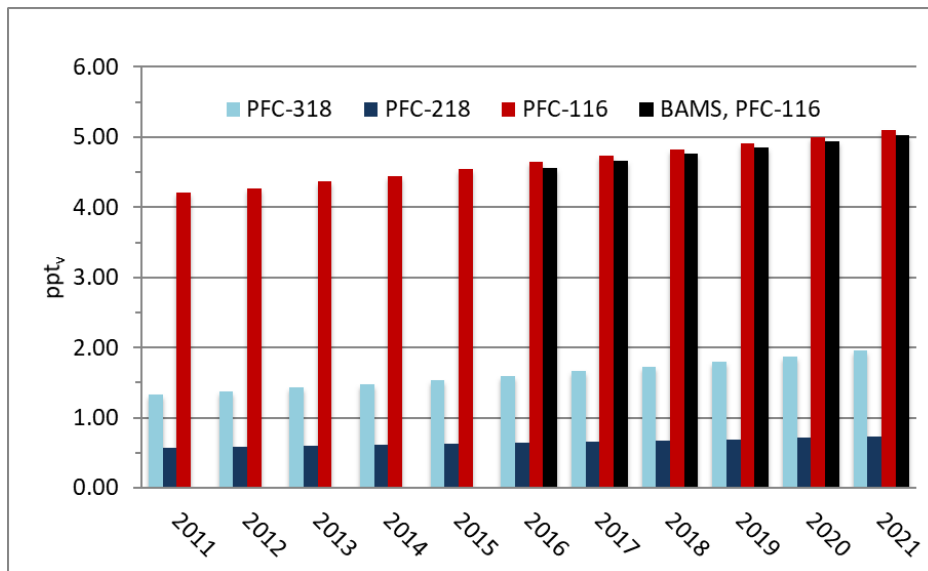


Figure 40: Annual mean concentrations of perfluorocarbons for the period 2010-2021 at the Zeppelin observatory: PFC-116 (red), PFC-218 (dark blue), and PFC-318 (light blue). The global annual means for PFC-116 in 2016 to 2021 are included as black bars.

### 3 Aerosols and climate

Atmospheric aerosol influences climate by scattering incoming solar radiation back into space or absorbing the radiation. This so-called direct aerosol climate forcing results mostly in cooling, but can be moderated if the aerosol itself absorbs solar radiation, e.g. if it consists partly of light absorbing carbon or light absorbing minerals. In this case, the aerosol warms the surrounding atmosphere. Atmospheric aerosol influences climate as outlined in section 1.4. Atmospheric aerosol particles also affect the reflectivity and lifetime of clouds, which is termed the indirect aerosol climate effect. The effect can be cooling as well as warming for climate, but in most cases, the cloud reflectivity and lifetime are increased, leading again to a cooling effect (see Figure 5). Figure 41 gives an overview of the main natural and anthropogenic sources of atmospheric aerosols, also described in detail the annual report of Aas et al. (2022) on long range transport of air pollution.

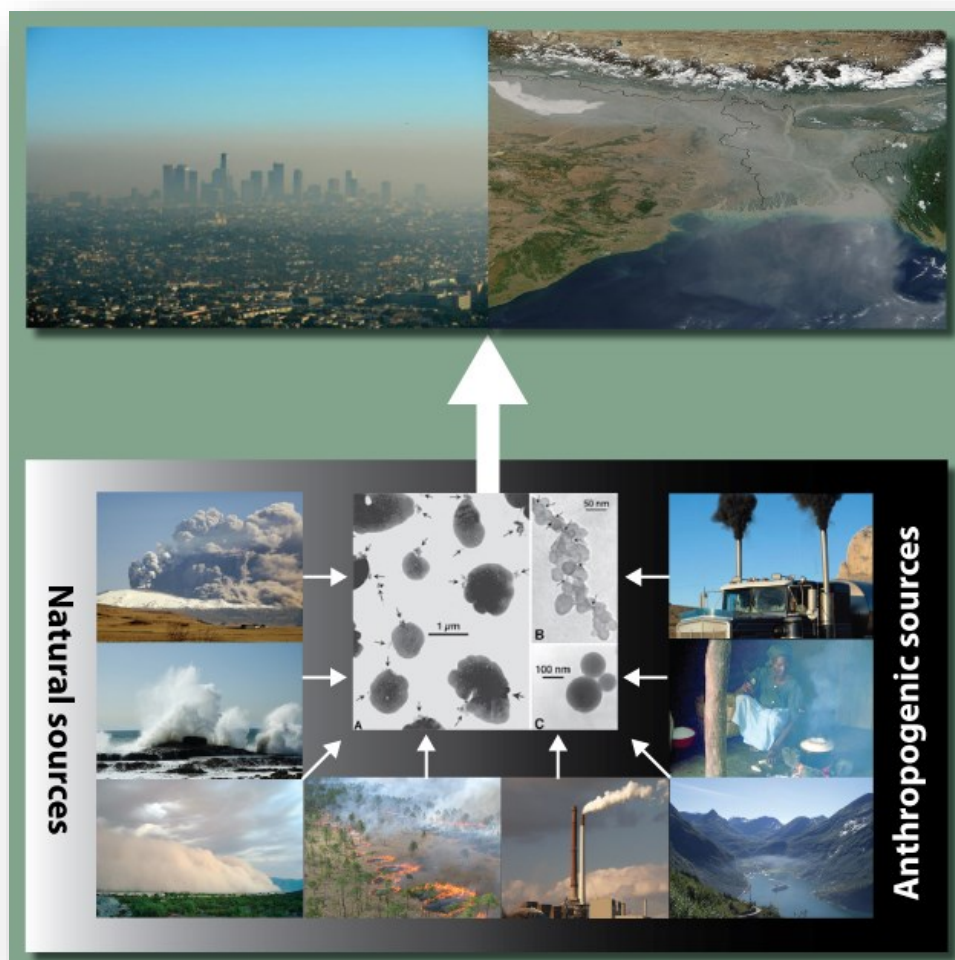


Figure 41: Illustration of the main natural and anthropogenic sources of atmospheric aerosols taken from Myhre et al (2013b). Top: local and large-scale air pollution. Sources include (bottom, counter clockwise) volcanic eruptions (producing volcanic ash and sulphate), sea spray (sea salt and sulphate aerosols), desert storms (mineral dust), savannah biomass burning (BC and OC), coal power plants (fossil fuel BC and OC, sulphate, nitrate), ships (BC, OC, sulphates, nitrate), cooking (domestic BC and OC), road transport (sulphate, BC, VOCs yielding OC). Additionally, Biogenic VOC to SOA and primary biological (e.g. pollen) from vegetation is crucial. Center: Electron microscope images of (A) sulfates, (B) soot, (C) fly ash, a product of coal combustion (Posfai et al., 1999).

With respect to monitoring climate change and the atmospheric constituents exerting an effect on climate, this year marks the publication of the 6<sup>th</sup> IPCC assessment report (AR6) of WG1 (IPCC 2021). Putting the data on atmospheric aerosol properties documented in this report into the context of AR6, a few relevant findings of AR6 are summarised below:

- Aerosol loadings across Northern Hemisphere mid-latitudes increased between 1700 and the late 20<sup>th</sup> century before declining after 2000 due to air quality measures, while increases over South Asia and East Africa are still ongoing due to industrialisation (Gulev et al., 2021).
- Atmospheric aerosol led to a negative radiative forcing throughout the industrial period, ERF =  $-1.3$  [ $-2.0$  to  $-0.6$ ]  $\text{W m}^{-2}$ . To this, aerosol-cloud interactions (indirect aerosol climate effect) contributed  $-1.0$  [ $-1.7$  to  $-0.3$ ]  $\text{W m}^{-2}$ , whereas direct aerosol-radiation interaction (direct aerosol climate effect) contributed  $-0.3$  [ $-0.6$  to  $0.0$ ]  $\text{W m}^{-2}$  (IPCC 2021, Forster et al., 2021).
- The negative aerosol ERF offset a significant part of the positive (warming) ERF due to greenhouse gases (IPCC 2021, Chap7)
- The cooling aerosol climate effect (negative ERF) also increased between 1750- late 20<sup>th</sup> century before declining after 2000.
- It is now less important compared to other climate forcing agents, e.g. well-mixed greenhouse gases. This recent decrease of negative aerosol radiative forcing has thus led to a positive ERF (warming) last years.
- Due to the decreasing relative contribution of aerosol climate forcing, the induced uncertainty on climate projections is decreasing as well. Nevertheless, the aerosol effect remains the largest uncertainty in ERF between 1750- 2019.
- Smaller absolute and relative negative aerosol climate forcings, resulting in a net warming climate effect, projected to continue into the future (IPCC 2021, Gulev et al., 2021).
- Carbonaceous aerosol loads have decreased over several regions of the Northern Hemisphere (IPCC 2021, Chap6).
- COVID-19 lockdowns led to a discernible temporary improvement of air quality in most regions, but changes to global and regional climate are undetectable above internal variability (IPCC 2021, Naik et al., 2021).
- AR6 states it as virtually certain that hot extremes and heatwaves are more frequent and more intense across most land regions since the 1950s, with high confidence that human-induced climate change is the main driver of these changes (IPCC 2021b). Heatwaves in the Arctic are strongly linked with increased atmospheric transport/exchange at high latitudes. Increased high latitude air mass exchange also implies increased poleward transport of aerosol pollution. This should be carefully monitored due to the potential for rapid, large-scale changes in relative pollution levels considering the clean starting conditions, alongside the potential for feedbacks.



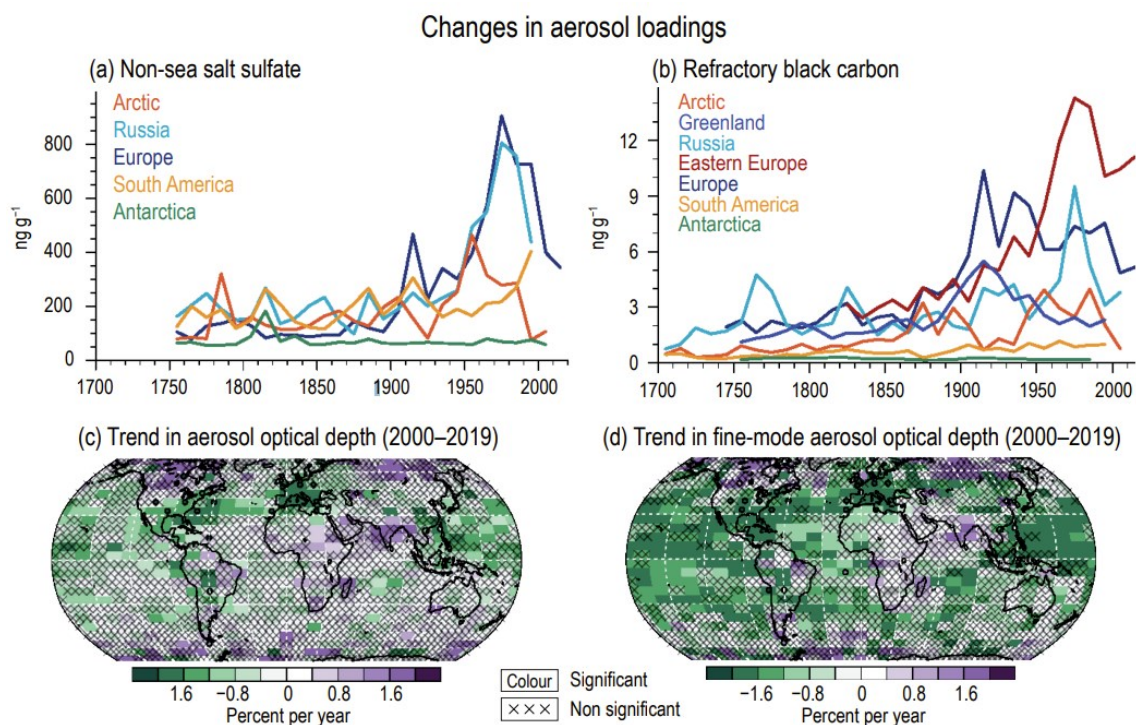


Figure 42: The temporal and regional development of atmospheric loads of relevant aerosol component loadings or properties (Figure 2.9 in Gulev et al., 2021): a) concentration of particulate non-sea salt sulphate in regions of the globe; b) concentration of particulate refractory black carbon in regions of the globe; c) regional trend of aerosol optical depth for the years 2000–2019; d) regional trend of fine-mode aerosol optical depth for the years 2000–2019. The trends illustrate the increase of aerosol loading throughout the industrialised period until the late 20<sup>th</sup> century, and the decrease since then due to measures for improving air quality.

### 3.1 Analysis of in situ aerosol radiative properties around the world

In preparation of IPCC AR6, several studies have presented the global status and trends in aerosol properties using, among others, data and results from the Norwegian national monitoring programme. Among these articles are several initiated by the WMO Global Atmosphere Watch (GAW) programme and ACTRIS, in which the observations of aerosol properties at Zeppelin, Birkenes, and Trollhaugen are used directly or indirectly in AR6:

1. Laj et al. 2020, entitled “A global analysis of climate-relevant aerosol properties retrieved from the network of Global Atmosphere Watch (GAW) near-surface observatories”. This article gives an overview over the GAW station network measuring climate relevant aerosol particle properties at surface stations, with link to ACTRIS as quality assurance and quality control framework (see section 1.3 on page 15). The properties observed comprise particle light scattering and absorption coefficient, particle number concentration and size distribution.
2. Collaud Coen et al. (2020), entitled “Multidecadal trend analysis of in situ aerosol radiative properties around the world”. A subset of Laj et al., data from 52 stations worldwide is used in Collaud Coen et al., to provide a robust analysis of the long-term (>10 yr) trends of aerosol optical properties. This study contains a detailed discussion of trends in climate relevant

optical aerosol properties, namely particle scattering, backscattering, and absorption coefficient, but also the derived properties single scattering albedo, scattering and absorption Ångström coefficient (see section 3.3 for a definition of these terms). Also, the evolution of trends and their causes are evaluated.

3. Gliß et al. (2020), entitled “*Multi-model evaluation of aerosol optical properties in the AeroCom phase III Control experiment, using ground and space based columnar observations from AERONET, MODIS, AATSR and a merged satellite product as well as surface in-situ observations from GAW sites*”. The authors use synthetic observations generated by those climate models feeding into IPCC AR6, and compare them to corresponding real-world observations. Comparisons include aerosol optical depth by space and surface based remote sensing, as well as observations of aerosol optical properties from the GAW network.
4. Mortier et al. (2020), entitled “*Evaluation of climate model aerosol trends with ground-based observations over the last two decades - an AeroCom and CMIP6 analysis*”. The authors take the trends discovered in atmospheric aerosol observations (aerosol optical depth from surface remote sensing, aerosol optical properties and mass of particulate matter from surface in situ stations), and investigate whether climate models can reproduce these. Since observations aren’t representative for the whole globe, they use the climate models to extrapolate the trends in the observations to the global level.
5. Pandolfi et al. (2018), entitled “*A European aerosol phenomenology – 6: scattering properties of atmospheric aerosol particles from 28 ACTRIS sites*”. Looks at the spatial distribution of the aerosol particle scattering coefficient  $\sigma_{sp}$  across Europe, as well as diurnal and annual patterns. Find a gradient of increasing values from northern/western stations towards the centre of Europe.
6. Zanatta et al. (2016), entitled “*A European aerosol phenomenology-5: Climatology of black carbon optical properties at 9 regional background sites across Europe*”. Major findings: 1) Both  $\sigma_{ap}$  and mEC in southern Scandinavia and Central Europe have a distinct seasonality with maxima during the cold season and minima during summer, opposite trend at Mediterranean sites; 2) mass absorption cross-section of black carbon is homogeneous over Europe; 3) presence of non-absorbing matter induces an enhancement of black carbon absorption.
7. Putaud et al. (2010), entitled “*A European aerosol phenomenology – 3: Physical and chemical characteristics of particulate matter from 60 rural, urban, and kerbside sites across Europe*”. Synthesizes data on aerosol (particulate matter, PM) physical and chemical characteristics (PM<sub>10</sub> and/or PM<sub>2.5</sub> mass, aerosol particle number concentrations, PM chemistry), which were obtained over the past decade in aerosol research and monitoring activities at more than 60 natural background, rural, near-city, urban, and kerbside sites across Europe. Find, among others: 1) organic matter, sulfate and nitrate as main constituents of both PM10 and PM2.5; 2) total carbon/PM10 ratio increases from rural to kerbside sites.

This series of publications demonstrates how time series of high-quality observations of atmospheric aerosol properties can feed into IPCCs Assessment Reports, contributing to improved understanding of ongoing climate change, and predictions. The value chain leads from data management and quality control by network participation, via trend assessment at the network level, to validation and improvement of model produced climate predictions.

These studies provide an in-depth analysis of trends in surface in situ observations of atmospheric aerosol properties, to which the observations covered by this report contribute. They also investigate how well these trends are captured by climate models feeding into IPCC AR6. While such in-depth studies usually coincide with these assessment reports, there now exist services which quantify such

trends in observations, as well as the agreement with climate models, on a continuous basis. One such is operated by the Norwegian Meteorological Institute as part of the ACTRIS research infrastructure.<sup>14</sup>

### 3.2 Overview of aerosol observations at Zeppelin, Birkenes and Troll Observatory

This monitoring programme includes measurements of aerosol properties relevant for quantifying the direct and indirect aerosol climate effect from three NILU operated/partly operated observatories : 1) Zeppelin Observatory (in collaboration with the Norwegian Polar Institute and Stockholm University); 2) Birkenes Atmospheric Observatory, Aust-Agder, Southern Norway; 3) Trollhaugen Atmospheric Observatory, Antarctica (observatory operated by NILU, main station operated by Norwegian Polar Institute). The observations cover the particle concentration as a function of particle size (physical aerosol property), as well as particle light scattering and absorption as a function of wavelength (optical aerosol properties), See Table 5 for details.

*Table 5: Aerosol observations at Zeppelin, Birkenes and Troll Observatory. Observations contributing to ACTRIS follow ACTRIS recommendations. Parameters in green are funded by the Norwegian Environment Agency and Ministry of Climate and Environment. The rest is funded by NILU and other institutes. Parameters included in this report, are printed in green.*

	Zeppelin	Birkenes	Trollhaugen
<b>Particle Number Size Distribution (PNSD) (fundamental to all aerosol processes)</b>	fine and coarse mode (0.01 $\mu\text{m} < D_p < 10 \mu\text{m}$ ), coarse mode since autumn 2020, NILU	fine and coarse mode (0.01 $\mu\text{m} < D_p < 10 \mu\text{m}$ )	fine mode (0.01 $\mu\text{m} < D_p < 0.8 \mu\text{m}$ )
<b>Number Size Distribution of Refractory Particles (proxy for BC PNSD)</b>	fine mode (0.01 $\mu\text{m} < D_p < 0.8 \mu\text{m}$ ), NILU	---	---
<b>Aerosol Scattering Coefficient (addressing direct climate effect)</b>	spectral at 450, 550, 700 nm, in collaboration with Stockholm University	spectral at 450, 550, 700 nm	spectral at 450, 550, 700 nm
<b>Aerosol Absorption Coefficient (addressing direct climate effect)</b>	single wavelength at 525 nm, (Stockholm University); single wavelength at 670 nm (Stockholm University); 7-wavelength (Demokritos Athens); 7-wavelength (NILU)	spectral at 470, 522, 660 nm; 7-wavelength (NILU)	spectral at 470, 522, 660 nm; 7-wavelength installed 2020
<b>Aerosol Optical Depth (addressing direct climate effect)</b>	spectral at 368, 412, 500, 862 nm in collaboration with WORCC (in Ny-Ålesund)	spectral at 340, 380, 440, 500, 675, 870, 1020, 1640 nm, in collaboration with Univ. Valladolid	spectral at 368, 412, 500, 862 nm
<b>Aerosol Chemical Composition (addressing direct + indirect climate effect)</b>	inorganic ions (ion chromatography), heavy metals (inductively-coupled-plasma mass-spectrometry)	main components (daily resolution, offline filter-based, ion chromatography), heavy metals (inductively-coupled-plasma mass-spectrometry)	inorganic ions and POPs (ion chromatography), discontinued from 2011 due to local contamination.
<b>Aerosol Chemical Speciation (direct + indirect climate effect, source attribution, transport)</b>	Particle main chemical species (hourly resolution, online mass spectrometry)	Particle main chemical species (hourly resolution, online mass spectrometry)	---

<sup>14</sup> <https://actris.nilu.no/Content/trends>

	Zeppelin	Birkenes	Trollhaugen
<b>Particle Mass Concentration</b>	---	PM <sub>2.5</sub> , PM <sub>10</sub>	PM <sub>10</sub>
<b>Cloud Condensation Nuclei (addressing indirect climate effect)</b>	size integrated number concentration at variable supersaturation in collaboration with Korean Polar Research Institute	---	---

### 3.3 Observed optical properties of aerosols

Aerosol particle absorption and scattering are decisive for the cooling or warming effect of aerosol in climate. All types of particles are scattering solar radiation, but the higher the fraction of particle absorption, the more warming the aerosol becomes. The absorption depends on the particle composition; black carbon (e.g., soot) and some minerals absorb radiation.

In the following sections, the aerosol optical properties measured at the Birkenes, Zeppelin and Trollhaugen observatories are presented. Time series of aerosol scattering coefficients, aerosol absorption coefficients, derived Ångström coefficients for both, and single scattering albedo are shown. All properties are measured for particles with aerodynamic diameter  $D_{p,aero} < 10 \mu\text{m}$  and at relative humidity  $< 40\%$ , thus avoiding water uptake by particles. This protocol follows the recommendations provided by ACTRIS. This is crucial to have comparable data at Zeppelin, Trollhaugen and Birkenes, and with other sites on European and global scale. For more details concerning measurement principles and quality assurance routines, please see Appendix II and Laj et al (2020).

For optical aerosol properties, information is contained both in the absolute level and in the values at different wavelengths relative to each other. In order to make this spectral information accessible, the Ångström coefficient ( $\text{\AA}$ ) has been defined. It can be calculated for optical aerosol properties, both for scattering and for absorption, and it describes the wavelength dependence of the respective property. Higher values of the scattering Ångström coefficient  $\hat{a}_{sp}$  correlate with higher concentration ratios of particles in the fine size range ( $D_p < 1 \mu\text{m}$ ) as compared to the coarse size range ( $D_p > 1 \mu\text{m}$ ). Moreover, the relative size of particles determining an optical aerosol property decreases with wavelength, i.e., smaller wavelengths “see” smaller particles in relative terms, larger wavelengths “see” larger particles. Already with these simple qualitative rules, many features exhibited by spectral aerosol optical property data in general and Ångström coefficient data in particular can be interpreted meaningfully.

The single scattering albedo  $\nu_0$  quantifies the fraction of light scattered by the particles rather than being absorbed. It is defined as the ratio of scattering efficiency to total extinction efficiency (the sum of scattering and absorption). It thus quantifies how absorbing the average aerosol particle is, with  $\nu_0$  values decreasing with increasing absorption of the average particle. For a purely scattering aerosol,  $\nu_0$  is 1, and decreases with increasing fraction of light absorbing components in the aerosol particle phase.

#### 3.3.1 Optical aerosol properties measured at the Birkenes Observatory

**Key findings aerosol optical properties Birkenes:** *There are no statistically significant trends in aerosol optical properties observed at Birkenes, agreeing with findings at other European stations and recent trend analyses (e.g., Collaud Coen et al., 2020). Aerosol scattering shows a stronger presence of smaller particles in summer than in winter. The reason for these seasonal differences lies in summer aerosol*

*being influenced by biogenic emissions which tends to give large amounts of newly formed small particles. In contrast, aerosol absorption shows a higher contribution of smaller (newer) particles in winter than in summer, reflecting the winter contribution of wood burning for domestic heating. In 2021, the transport episodes originate often in Central and South-East Europe. Occasionally, these events are superimposed by emissions from wildfires in South-Eastern Europe.*

A comprehensive suite of instruments observing in situ optical aerosol properties relevant to direct climate effects has been in operation at Birkenes since 2010, hereunder including the scattering coefficient  $\sigma_{sp}$  and the absorption coefficient  $\sigma_{ap}$  at various wavelengths. Figure 43 summarises these observations for 2010 – 2021 in time series of the observations themselves and relevant directly derived parameters. The data gap in 2019 is caused by a failure of the integrating nephelometer, measuring the particle scattering coefficient  $\sigma_{sp}$ , which also affected the particle absorption measurements since these depend on the nephelometer for bias corrections.

Panel a) of Figure 43 displays the time series of the scattering coefficient  $\sigma_{sp}$  at 450, 550, and 700 nm. Thin lines represent daily average values for the respective wavelength, whereas the heavy green line represents the running 55-day median for easier visibility of seasonal averages (green wavelength at 550 nm only for clarity). The  $\sigma_{sp}$  time series exhibits significant variability on the time scale of days, illustrating that particle load in an air mass varies with air mass type and thus air mass origin, i.e. with the regional weather situation on a time scale of 1 – 3 days. When focussing on the graph of the running median, a weak seasonal variation can be detected, with values higher in summer than winter.

Panel b) of Figure 43 shows the time series of the scattering Ångström coefficient  $\hat{\alpha}_{sp}$ . It was calculated from the multi-wavelength observations of the scattering coefficient  $\sigma_{sp}(\lambda)$ , again as daily averages (thin line) and running 55-day median (heavy line). As for  $\sigma_{sp}$ , the strongest variability is associated to a time scale of 1-3 days, indicative of changes associated with air mass type, origin, and synoptic weather situation. Looking at the running median however, the seasonal cycle is more pronounced for  $\hat{\alpha}_{sp}$  than for  $\sigma_{sp}$ , with  $\hat{\alpha}_{sp}$  values around 1.1 in winter and 1.8 in summer. This indicates a stronger contribution of smaller particles (i.e., particles with  $D_p$  smaller than about 120 nm) to  $\sigma_{sp}$  in summer than in winter. This is consistent with number concentrations of particles in this size range exhibiting a similar seasonal cycle, as will be discussed below. The time series of  $\sigma_{sp}$  and  $\hat{\alpha}_{sp}$  don't show any trend, which is consistent with the findings for other European continental background stations at Jungfrauoch (Switzerland, mountain top), Hohenpeissenberg (Southern Germany, elevated boundary layer), and Pallas (Northern Finland, boreal background) (Collaud Coen et al., 2013, 2020). Also, the range of  $\sigma_{sp}$  values encountered, 3 - 50  $\text{Mm}^{-1}$  with an annual average of about 11.4  $\text{Mm}^{-1}$ , is consistent with findings at comparable stations (Delene & Ogren, 2002).

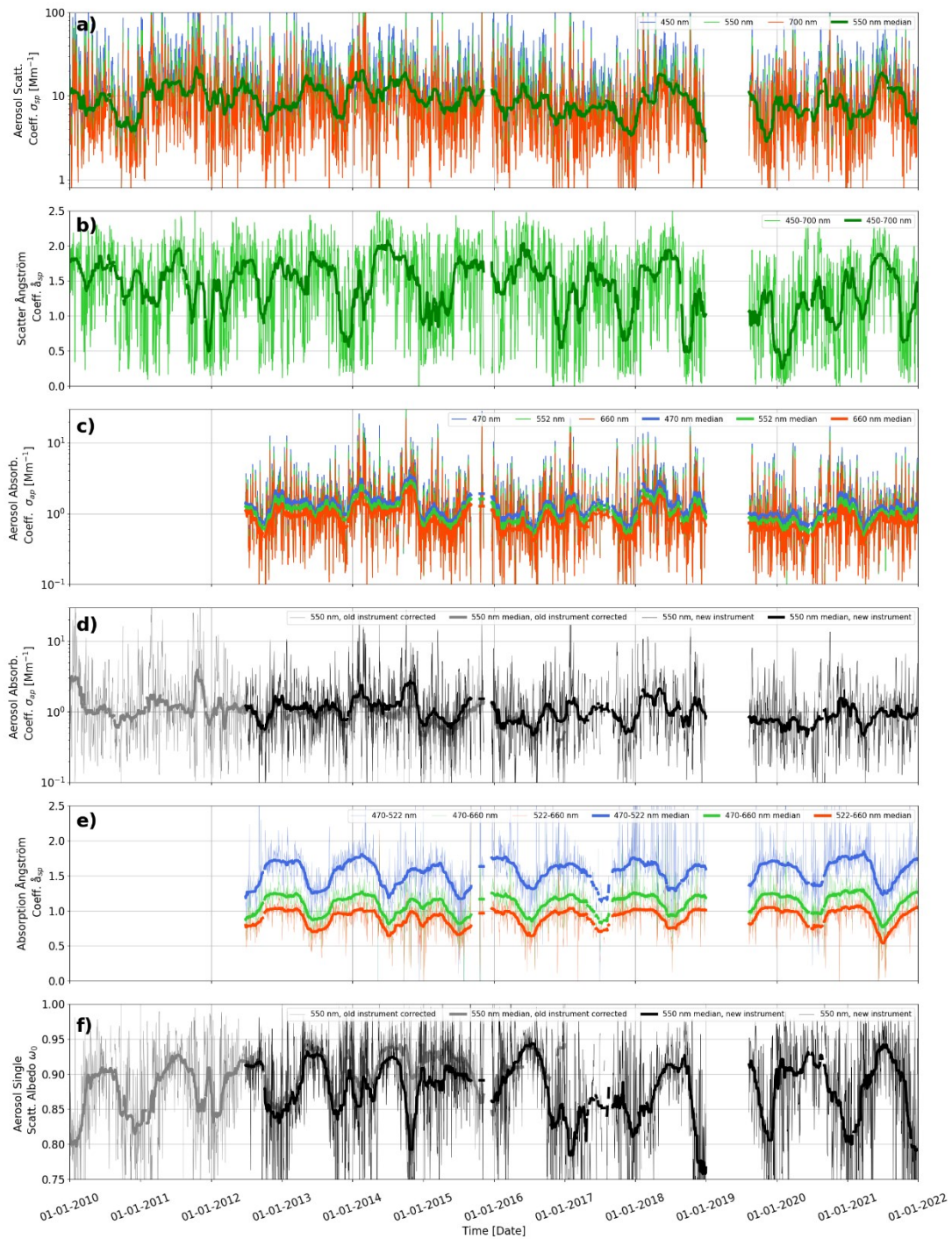


Figure 43: Time series of aerosol particle optical property daily means measured for 2010 - 2021 at Birkenes. Panel a) shows the aerosol scattering coefficient  $\sigma_{sp}$  at 450, 550, and 700 nm wavelength measured by integrating nephelometer. Panel c) the aerosol absorption coefficient  $\sigma_{ap}$  at 470, 522, and 660 nm wavelength measured by the newer filter absorption photometer, Panel d) the aerosol absorption coefficient  $\sigma_{ap}$  at 550 nm of the older filter absorption photometer, shifted from the instrument wavelength at 525 nm for consistent comparison assuming an absorption Ångström coefficient of 1. Panels b) and e) show the derived properties scattering and absorption Ångström coefficient  $\ddot{\alpha}_{sp}$  and  $\ddot{\alpha}_{ap}$ , respectively, while Panel f) depicts the single scattering albedo  $\omega_0$ . All plots also depict the running 55-day medians of the respective properties as heavy lines to visualize seasonal variations. To demonstrate consistency between old and new filter absorption photometer, respective comparison lines are displayed.

The observations of the particle absorption coefficient  $\sigma_{ap}$  at Birkenes were upgraded in 2012 and in November 2017. All 3 concerned instruments use the same physical principle, tracking the change of attenuation of light that passes through a filter while the filter is loaded with sampled particles. The 2012 instrument measures  $\sigma_{ap}$  at 3 wavelengths (470, 522, 660 nm) with considerably less electronic noise and significantly better long-term stability than the previous instrument of 2010 with one wavelength (522 nm). The 2017 instrument extends the spectral range to 7 wavelengths (370, 470, 525, 590, 660, 880, 950 nm). Panel c) of Figure 43 displays the  $\sigma_{ap}$  time series of the 2012, 3-wavelength filter absorption photometer, Panel d) the data of the 2010 one wavelength instrument. For the 2010 instrument, the wavelength has been recalculated to the same green wavelength as observed by the nephelometer (550 nm) assuming an absorption Ångström coefficient of 1. Both panels use thin lines for daily averages, heavy lines for the running 55-day medians. The data of the 2017 instrument have been evaluated for consistency with the 2012 instrument over a whole year (see Appendix II). The data of the two instruments show a correlation coefficient  $R^2$  of 0.97, i.e., 97% of the variation in one instrument is explained by the variation in the other instrument. This ensures that the 2017 instrument will continue the  $\sigma_{ap}$  time series consistently. The data of the 2017 instrument are displayed separately in Figure 44 below to prevent excessive information density in Figure 43.

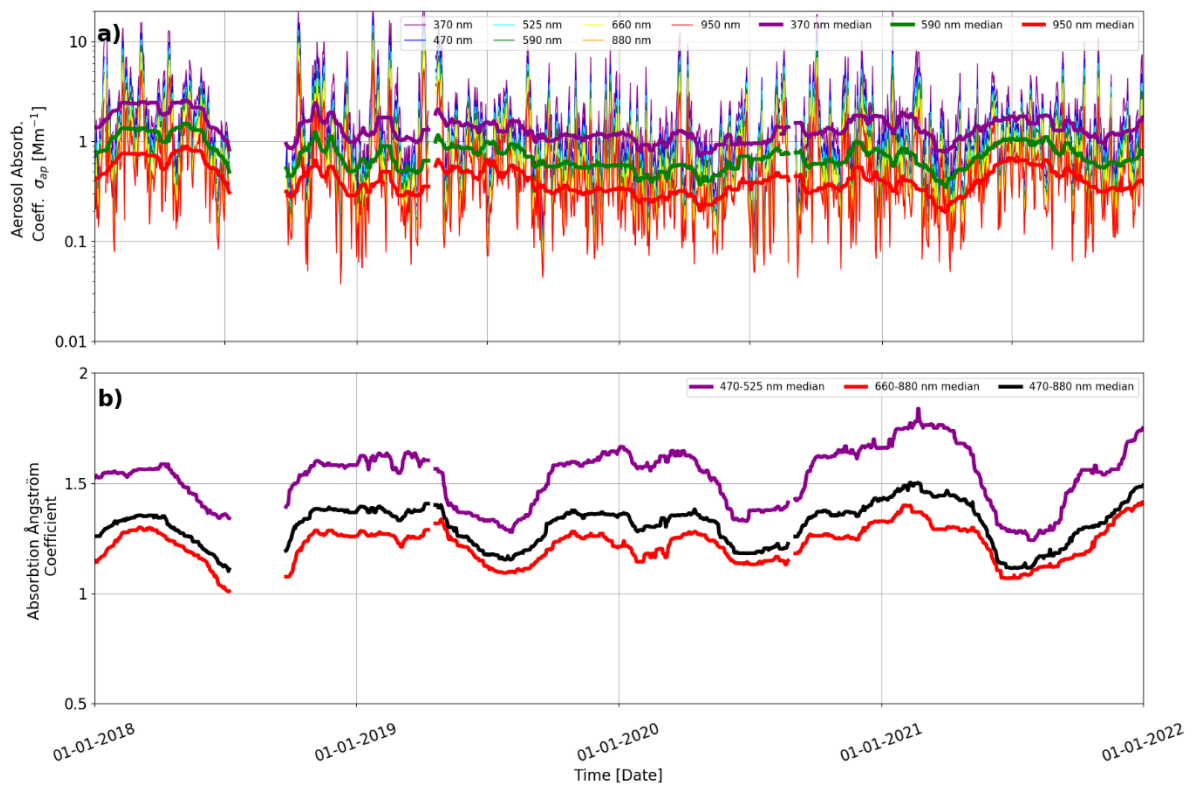


Figure 44: Time series of aerosol particle absorption coefficient  $\sigma_{ap}$  (top) and the absorption Ångström coefficient  $\hat{\alpha}_{ap}$  (bottom), both daily means, measured by the filter absorption photometer deployed at Birkenes in November 2017. The time series covers the years 2018 - 2021.

Turning back to Figure 43, Panel d) also displays the  $\sigma_{ap}$  running median time series of the 2012 filter absorption photometer (also recalculated to 550 nm wavelength) together with the data of the 2010 instrument as an indicator for the goodness of overlap between the two instruments measuring the same property (see Appendix II for more details).

Apart from the variation with synoptic transport and air mass origin,  $\sigma_{ap}$  does not seem to exhibit significant seasonal variation. The values of  $\sigma_{ap}$  are in the range of  $0.3 - 4 \text{ Mm}^{-1}$  with annual means around  $1 \text{ Mm}^{-1}$ .

In order to cover the largest possible time period, panel f) of Figure 43 shows the time series of the aerosol particle single scattering albedo  $\omega_0$  based on the time series of the older filter absorption photometer (grey lines), again daily averages (thin line) and 55-day running median (heavy line), together with the respective time series of the new instrument (black lines). The most prominent feature in the  $\omega_0$  time series is the pronounced annual cycle, varying between  $0.86 - 0.96$ , with lower  $\omega_0$  values and higher particle absorption in winter. The annual cycle in  $\omega_0$  has been discussed in previous reports of the Birkenes aerosol dataset and has been connected to the combustion of biomass in wood stoves for domestic heating in the winter season.

Panel e) of Figure 43 is based on data of the 2012 filter absorption photometer, measuring  $\sigma_{ap}$  at three wavelengths, as opposed to one wavelength with the 2010 instrument. Panel e) depicts the time series of the absorption Ångström coefficient  $\hat{a}_{ap}$  for all three wavelength pairs provided by the new instrument. Similar, Figure 44 (bottom) shows  $\hat{a}_{ap}$  for three wavelength pairs of the newest instrument. For  $\hat{a}_{ap}$ , the information on relative particle size concerns not the overall aerosol particle phase, but the fraction of absorbing particles. Thus, considering  $\hat{a}_{ap}$  data allows to investigate changes in source and transport of the absorbing particle fraction in the aerosol. When looking at the  $\hat{a}_{ap}$  data, an annual cycle is apparent that is opposite of the annual cycles seen in scattering Ångström coefficient  $\hat{a}_{sp}$  and single scattering albedo  $\omega_0$ . Both  $\hat{a}_{sp}$  and  $\omega_0$  increase in summer as compared to winter,  $\hat{a}_{sp}$  because of a summer increase in small particles due to particle formation from biogenic precursors,  $\omega_0$  because of fewer combustion emissions in summer than in winter. For  $\hat{a}_{ap}$ , values increase in winter as compared to summer, indicating, in relative terms, higher abundance of smaller absorbing particles in winter than in summer. This observation is consistent with assuming emissions from domestic heating by wood stoves to contribute to the Birkenes winter aerosol, which is the explanation for the decreased winter values of  $\omega_0$ . The size of the absorbing aerosol particles increases with aerosol age. Consequently, a smaller size of the absorbing particles indicates a younger combustion aerosol and a closer combustion source, which is consistent with a scattered distribution of houses using wood stoves for heating, i.e. typical for Southern Norway. The previous instrument upgrade of aerosol absorption measurements in Birkenes has thus provided another indication for the contribution of wood stove emissions to the Birkenes winter aerosol.

### 3.3.2 Optical aerosol properties measured at the Zeppelin Observatory

**Key findings aerosol optical properties Zeppelin:** *The aerosol absorption measurements at Zeppelin station are conducted in collaboration with the Greek Demokritos-Athens research institute, and continue a time series that has been started 2001. The decreasing trend in aerosol absorption observed since 2001 by Eleftheriadis et al. (2009) has continued, and fits with the trend observed at other surface in situ stations in the Arctic (Coen et al., 2013; Collaud Coen et al., 2020). The spectral dependence of particle light absorption at Zeppelin indicates a contribution of absorbing components with spectral dependence due to chemical composition, e.g., brown carbon or mineral dust. Most of the investigated episodes at the Zeppelin station originate from industrial emissions in the Russian Arctic (Kola/Yamal/Kanin peninsula). The exception is the transport event in early August 2021, likely caused by a forest fire in Sweden.*

The in situ optical properties of the particles at Zeppelin Observatory covered in this report are more limited as compared to Birkenes and Trollhaugen. NILU operates only one filter absorption photometer, an AE33 aethalometer, at Zeppelin measuring the absorption coefficient  $\sigma_{ap}(\lambda)$  between



370-950 nm wavelength. A nephelometer providing the spectral scattering coefficient  $\sigma_{sp}(\lambda)$  is also deployed at Zeppelin, but operated by Stockholm University, and data are therefore not available for this report. This excludes calculation and discussion of the particle single scattering albedo.

Figure 45 summarises the 2015 – 2021 time series, i.e., 6.5 years of spectral aerosol particle absorption coefficient  $\sigma_{ap}(\lambda)$  data collected at Zeppelin Observatory since deployment of the aethalometer in June 2015. The top panel displays daily averaged  $\sigma_{ap}(\lambda)$  data for all seven wavelengths (thin lines), as well as running 55-day medians (bold lines), here only for three wavelengths to improve readability of the graph. The bottom panel shows graphs of the absorption Ångström coefficient  $\tilde{a}_{ap}$  for three wavelength pairs representing short wave end, long wave end, and full range of the measured wavelength spectrum. The  $\tilde{a}_{ap}$  data are plotted as 55-day median only, since daily averages are too noisy due to the low particle load commonly observed at Zeppelin.

The time series of  $\sigma_{ap}$  (top panel of Figure 45) exhibits the same annual cycle as described already in the data of the other aethalometer instrument at Zeppelin collected in earlier years (Eleftheriadis et al., 2009), with lower values in summer and higher ones in winter. These variations have been attributed to changes in combustion aerosol sources caused by emissions from domestic heating in the relevant source regions, e.g., Northern and Central Russia (Law & Stohl, 2007). This pattern is moderated by incidents of emissions from large forest fires reaching the Arctic, which can increase aerosol particle absorption in episodes also in summer (e.g., Stohl et al., 2007). Absolute values of  $\sigma_{ap}$  vary in the range of 0.02 – 2  $\text{Mm}^{-1}$  at Arctic Zeppelin station, with median values roughly a factor of 5 lower than at boreal Birkenes, but a factor of 4 larger than at Antarctic Trollhaugen station.

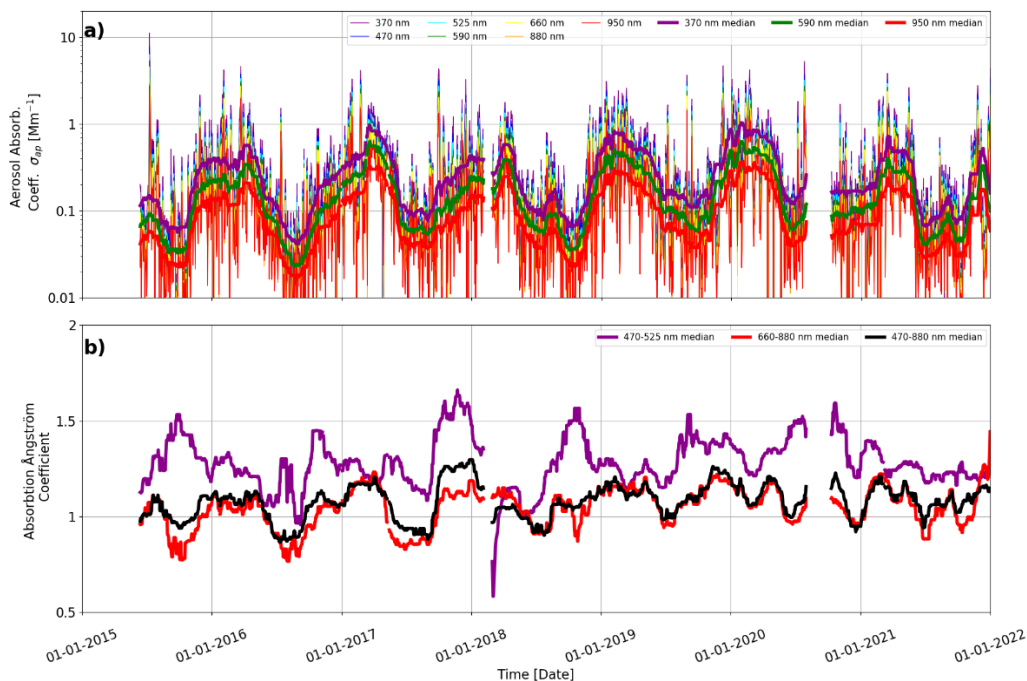


Figure 45: 2015 – 2021 time series graphs of data collected by the filter absorption photometer at Zeppelin Observatory since deployment in June 2015. Top: daily means of absorption coefficient at all seven measured wavelengths (thin lines), and 55-day running medians for top, middle and bottom of observed spectral range (heavy lines). Bottom: 55-day running medians of absorption Ångström coefficient, top, bottom, and whole observed spectral range.

Also interesting in the data provided by the filter absorption photometer is the aerosol absorption Ångström coefficient  $\hat{a}_{ap}$ . The  $\hat{a}_{ap}$  values exhibit a distinct spectral dependence on wavelength, with  $\hat{a}_{ap}$  for shorter wavelengths deviating to higher values as compared to  $\hat{a}_{ap}$  at larger wavelengths for periods of lower aerosol absorption, i.e., in summer. Such a behaviour can be caused by absorbing aerosol components that exhibit a spectral dependence in absorption, e.g., brown carbon or dust. For black carbon in contrast,  $\hat{a}_{ap}$  at shorter and larger wavelength agree at values around 1.

### 3.3.3 Optical aerosol properties measured at the Trollhaugen Observatory

**Key findings aerosol optical properties Trollhaugen:** *The length of the time series of data on optical aerosol properties at Trollhaugen is still too short for drawing conclusions on trends. The annual cycle of the aerosol optical properties at Trollhaugen has been studied in detail, and is associated with a natural, hemispheric-scale atmospheric pattern. The same annual cycle with higher particle loads and larger particles in summer is observed also at other stations on the central Antarctic continent.*

This section covers the aerosol optical properties collected at the station after the relocation in January 2014 from the Troll main base to Trollhaugen located above and upwind of the previous location. At the location of the old station, up to 80% of the collected data were contaminated by diffuse (unavoidable) emissions from the main buildings, making the scientific value and interpretation of the data from the old location difficult.

At Trollhaugen station, the same comprehensive set of instruments for observing optical aerosol properties as used in Birkenes is deployed. These cover the spectral scattering coefficient  $\sigma_{sp}(\lambda)$ , the spectral absorption coefficient  $\sigma_{ap}(\lambda)$ , as well as the derived properties scattering and absorption Ångström coefficient  $\hat{a}_{sp}$  and  $\hat{a}_{ap}$ , parameterising the wavelength dependence of  $\sigma_{sp}$  and  $\sigma_{ap}$ , as well as the single scattering albedo  $\omega_0$ . Figure 46 summarises the corresponding data collected at Trollhaugen for the years 2014 – 2021.

Starting with the time series of  $\sigma_{sp}(\lambda)$  in panel a) of Figure 46, a slight annual cycle can be observed, with superimposed peaks throughout the year. The peaks are associated with intrusions of marine air during storm episodes, while the annual cycle is caused by an annual cycle of the particle number size distribution (PNSD) in Antarctic background air, with higher particle loads and larger particles in summer. The same annual cycle in the PNSD also explains the annual cycle in the scattering Ångström coefficient  $\hat{a}_{sp}$  plotted in panel b).

An annual cycle can also be detected in the  $\sigma_{ap}(\lambda)$  time series depicted in panel c) of Figure 46, even though the filter absorption photometer operates constantly around the detection limit. The minimum in the cycle occurs in Southern hemisphere winter when the Antarctic vortex decreases transport from lower latitudes through the lower and mid-troposphere. In the absorption Ångström coefficient  $\hat{a}_{ap}$  time series shown in panel d), the annual cycle is rather weakly pronounced, with the lowest values also occurring in winter.

The time series of the single scattering albedo  $\omega_0$  (panel e) of Figure 46) shows the highest values close to 1, i.e., almost no particle absorption at all, in Antarctic winter, coincident and consistent with the minimum in particle absorption. Lower  $\omega_0$  values, i.e., higher average particle absorption, occur towards summer when the Antarctic continent is subject to stronger transport from mid-latitude sources through the lower part of the troposphere.

Optical aerosol properties are tightly connected to the physical aerosol properties, which is why they are ideally interpreted together. The annual cycle in the optical aerosol properties observed at Trollhaugen is caused by a corresponding annual cycle in the physical properties, which will be discussed in section 3.4.3.

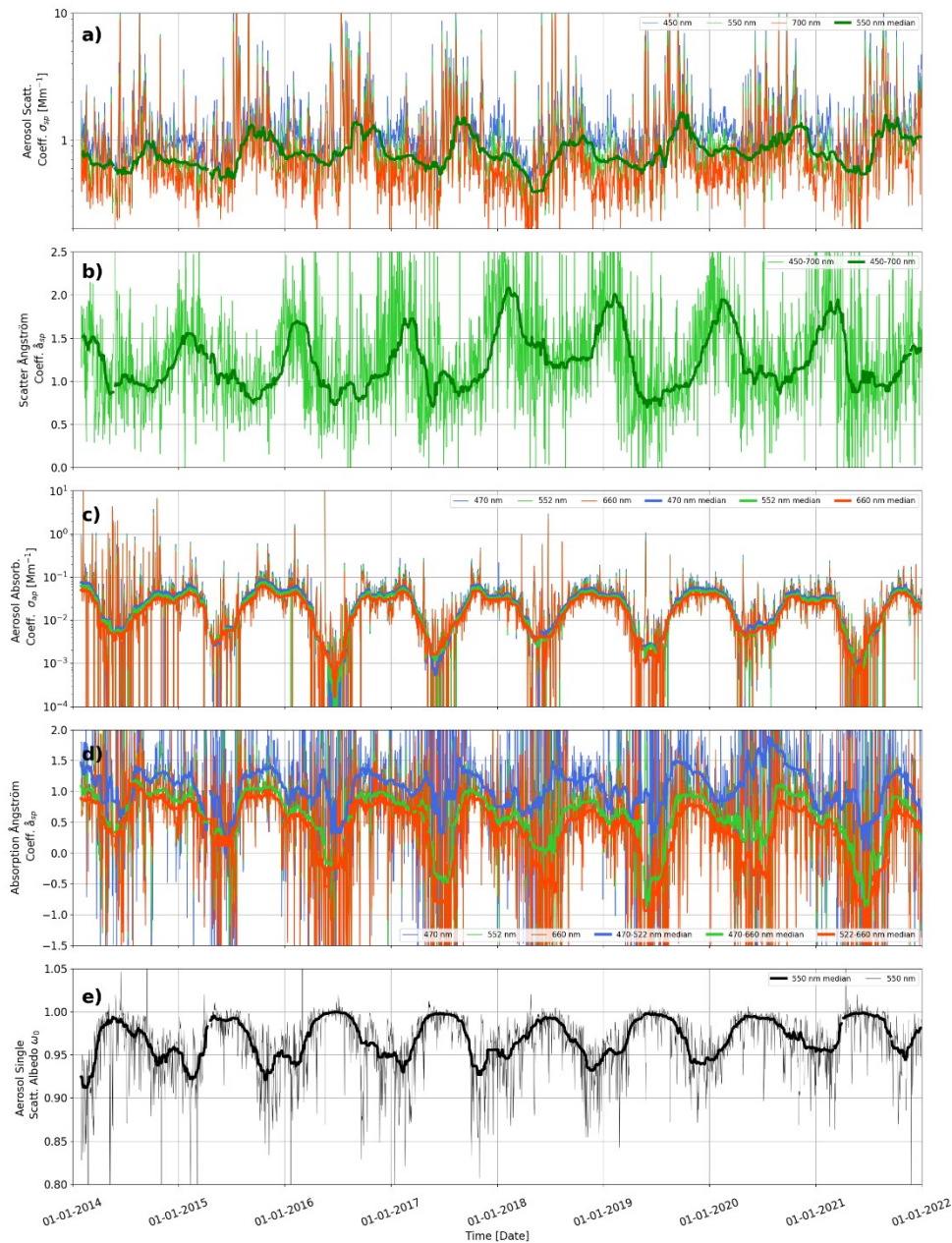


Figure 46: Time series of aerosol particle optical property daily means measured for 2014 - 2021 at Trollhaugen station. Panel a) shows the aerosol scattering coefficient  $\sigma_{sp}$  at 450, 550, and 700 nm wavelength measured by integrating nephelometer. Panel c) the aerosol absorption coefficient  $\sigma_{ap}$  at 470, 522, and 660 nm wavelength measured by filter absorption photometer. Panels b) and d) show the derived properties scattering and absorption Ångström coefficient  $\hat{a}_{sp}$  and  $\hat{a}_{ap}$ , respectively, while Panel e) depicts the single scattering albedo  $\omega_0$ . All plots also depict the running 55-day medians of the respective properties as heavy lines to visualize seasonal variations.

### 3.4 Measurements of particle number and size

#### 3.4.1 Physical aerosol properties measured at the Birkenes Observatory

**Key findings aerosol physical properties Birkenes:** Size segregated aerosol particle concentrations at Birkenes do not exhibit any obvious trend. This corresponds to findings obtained at other Nordic stations within ACTRIS and EMEP. The particle size distribution at Birkenes is governed by 5 major sources: 1) clean Arctic background aerosol; 2) Central and Eastern European aerosol; 3) Arctic haze; 4) fine fraction biogenic aerosol; 5) wood combustion aerosol from domestic heating. A major transport episode observed in early October 2021 can be traced to sources of dust in central Asia, combined with forest fire emissions from Ukraine. Other observed episodes concern Central European winter pollution, and boreal forest summer emissions.

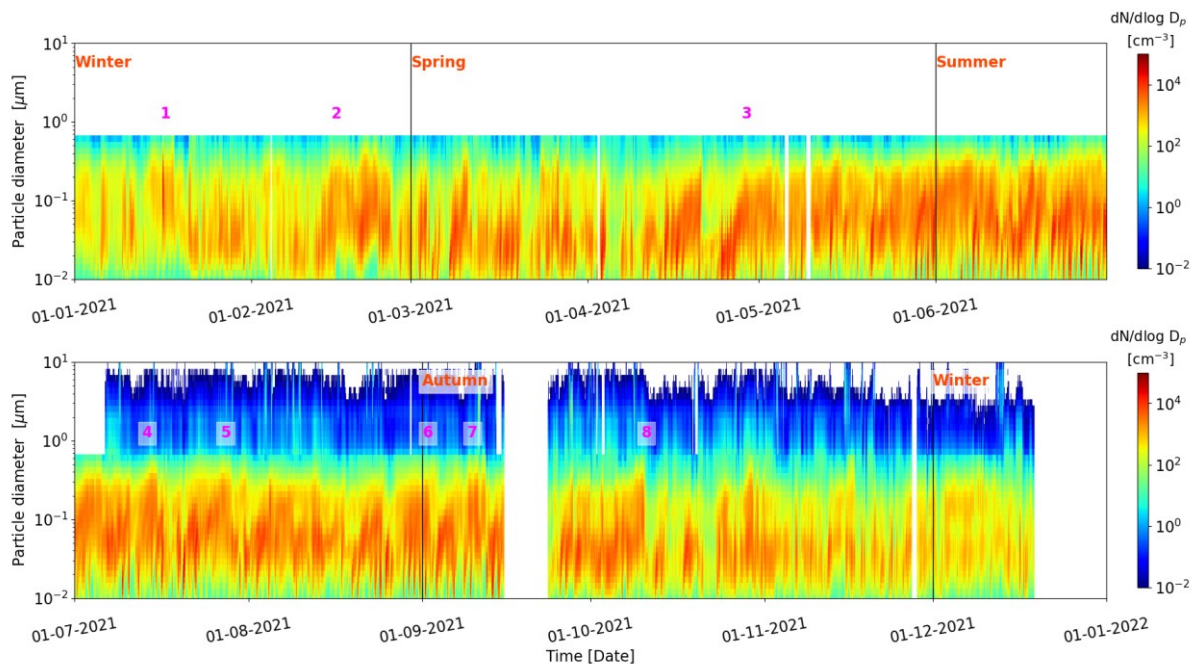


Figure 47: 2021 time series of particle number size distribution at Birkenes. Episodes are marked by magenta numbers, with episode numbers referring to Table 6.

Figure 47 shows the time series of the particle number size distribution (PNSD) measured at Birkenes in 2021. In this plot type, the x-axis shows the time of the observation, whereas the y-axis shows the particle diameter  $D_p$  on a logarithmic scale. The logarithmic colour scale is the particle concentration, normalised to the logarithmic size interval,  $dN/d\log D_p$ . The use of logarithmic axis is common when displaying particle size information since both, particle diameter and particle concentration, tend to span several orders of magnitude while containing relevant information over the whole scale. In this report, the PNSD reported for Birkenes is intended to cover the whole size range between 0.01 – 10  $\mu\text{m}$  by combining the information of two instruments, one each focussing on the fine ( $D_p < 1 \mu\text{m}$ ) and coarse ( $D_p > 1 \mu\text{m}$ ) size ranges, into a common PNSD product (see Appendix II for details). For the common PNSD product, both instruments need to agree in their overlap size range. At observation times when this criterion isn't met, the resulting PNSD is rejected, which can lead to gaps in the PNSD time series. This normally occurs predominantly in winter when the aerosol particles are absorbing, which affects the instrument covering the coarse size range, an Optical Particle Size Spectrometer (OPSS). Existing operating procedures and quality standards defined by the European research infrastructure ACTRIS have been used (Wiedensohler et al., 2012), but cover only the fine particle size range.

The OPSS follows a schedule of manufacturer calibrations, which is traceable only to a master unit, but not to an independent SI standard. This limits options for in-the-field QA and calibration measures using portable SI standards. In 2019, the OPSS experienced calibration issues, which were addressed by a major manufacturer overhaul. After repair, the instrument did not operate normally, which first in 2021 could be traced to a faulty firmware installed during the 2019 overhaul. Today, the instrument is back in normal operation, but a replacement is still pursued. These incidents highlight the need for manufacturer independent, SI traceable calibration options and operation procedures. In this context, the role of station networks such as ACTRIS and WMO GAW cannot be overstated.

Table 6: Selected transport events observed at Birkenes in 2021, together with characteristics and air mass origin determined by trajectory analysis.

#	Time Begin	Time End	Comment	Air mass origin (backwards order)	Air mass type
1	2021-01-16 11:00	2021-01-16 18:00	Pronounced accumulation mode <sup>1</sup> centred at Dp = 130 nm	Southern Norway	domestic heating
2	2021-02-15 12:00	2021-02-25 12:00	Period of long-processed aerosol, Dp centre just below 100 nm	France, Benelux, Germany, Poland, Denmark	continental winter pollution
3	2021-04-28 00:00	2021-05-03 12:00	Particle formation growing over several days into a stable Aitken mode <sup>2</sup> around Dp = 80 nm	Southern Norway, Southern-Sweden, Norwegian Sea	Regional particle formation event over boreal forest
4	2021-07-13 12:00	2021-07-15 15:00	Elevated accumulation mode fraction, paired with increased particle absorption	Northern Norway, Northern Sweden, North Sea, Latvia, Lithuania, Belarus, Ukraine	Possibly wildfires in Ukraine
5	2021-07-27 00:00	2021-07-29 00:00	Elevated accumulation mode	UK, North Sea, South-Sweden, Poland, Slovakia, Hungary, West Ukraine	Possibly wildfires in Poland
6	2021-09-01 00:00	2021-09-02 12:00	Particle formation growing over several days into a stable Aitken mode around Dp = 80 nm	Southern Norway, Norwegian Sea	Regional particle formation event over boreal forest
7	2021-09-09 03:00	2021-09-12 06:00	Pronounced accumulation mode at Dp = 150 nm	South-UK, North Atlantic Ocean, France, Benelux states, Germany, Czechia	Processing over continent, possibly mixed with biomass burning from SE Europe.
8	2021-10-10 00:00	2021-10-10 15:00	Pronounced accumulation mode at Dp = 120 nm	North Sea, Northern Germany, Poland, Ukraine, Russia	Possibly wildfires in Ukraine

<sup>1</sup>Accumulation mode: particles of size >100 to <1000 nm formed when various atmospheric gasses condense to form new aerosol mass.

<sup>2</sup>Aitken mode: particles of size <100 nm formed when various atmospheric gasses condense to form new aerosol mass.

There doesn't exist any unique connection between the PNSD and air mass type, but the PNSD still is rather characteristic for the air mass, and can serve, together with the single scattering albedo  $\omega_0$ , and the scattering Ångström coefficient  $\hat{a}_{sp}$ , as valuable indication of air mass origin, which at Birkenes shifts with the synoptic weather situation. Consequently, the information content of a PNSD time series plot is too high to be discussed in detail in this overview-type annual report. The PNSD and  $\omega_0$  observations reconfirm findings from earlier years on the dominant air mass types at Birkenes, which consist of: 1) clean Arctic background aerosol; 2) Central and Eastern European aerosol; 3) biogenic aerosol, i.e. vegetation emitted precursor gases condensing to the particle phase by photooxidation; 4) wood combustion aerosol from domestic heating. Selected transport events observed at Birkenes are listed in Table 6 together with characteristics and air mass origin determined by trajectory analysis.

Transport episodes observed in 2021 originate often in Central and South-East Europe. Air masses are being transported over land over an extended period, where they pick up biogenic precursor gases which are photochemically oxidised. The condensing vapours form particle volume in the accumulation mode size range around 100 nm particle diameter or even larger. Occasionally, these events are superimposed by emissions from wildfires in South-Eastern Europe. In a changing climate, heatwaves are projected to increase in frequency and intensity (IPCC, 2021b, SPM), where heatwaves are associated with strong poleward transport. It needs to be observed further whether these heatwaves are associated with the observed type of long-range, surface-level transport of dust and biomass burning pollution that influences air quality over large areas.

In order to condense the information in the PNSD time series, Figure 48 shows the time series of selected PNSD integrals, i.e., the concentration of particles falling into selected size intervals. The size intervals are chosen to represent characteristic processes governing the atmospheric aerosol (see Appendix II for more details): 1) the Aitken-mode size range, 0.02 – 0.1  $\mu\text{m}$ ; 2) the accumulation mode size range, 0.1 – 1  $\mu\text{m}$ ; 3) the coarse mode size range, 1 – 10  $\mu\text{m}$ . The time series in Figure 48 represent daily averages over these PNSD integrals for the whole period since the Birkenes station upgrade in 2010, as well as the corresponding running 55-day medians to highlight seasonal variations. The respective size range integral particle concentrations are denoted  $N_{\text{ait}}$  for the Aitken mode,  $N_{\text{acc}}$  for the accumulation mode, and  $N_{\text{coa}}$  for the coarse mode.

As to be expected, the particle concentration in the Birkenes aerosol in absolute terms is dominated by the Aitken mode particles, followed by the accumulation mode. Also, the most prominent feature in Figure 48 is exhibited by the particle concentrations in these two modes, a clear annual cycle caused by the same underlying physical process. In summer, the vegetation emits gaseous aerosol precursors, which are photo-oxidised and condense onto Aitken-mode particles or form those directly. These particles coagulate, increasing the concentration of accumulation mode particles. These same processes increasing  $N_{\text{ait}}$  and  $N_{\text{acc}}$  in summer are also responsible for increasing the scattering Ångström coefficient  $\hat{a}_{sp}$  in summer. The processes controlling  $N_{\text{coa}}$  are decoupled from those controlling  $N_{\text{ait}}$  and  $N_{\text{acc}}$ . Coarse mode particles are formed from bulk material, their concentration is affected by wind speed (levitating dust, spores, pollen), snow cover, and rain (both inhibiting dust levitation).

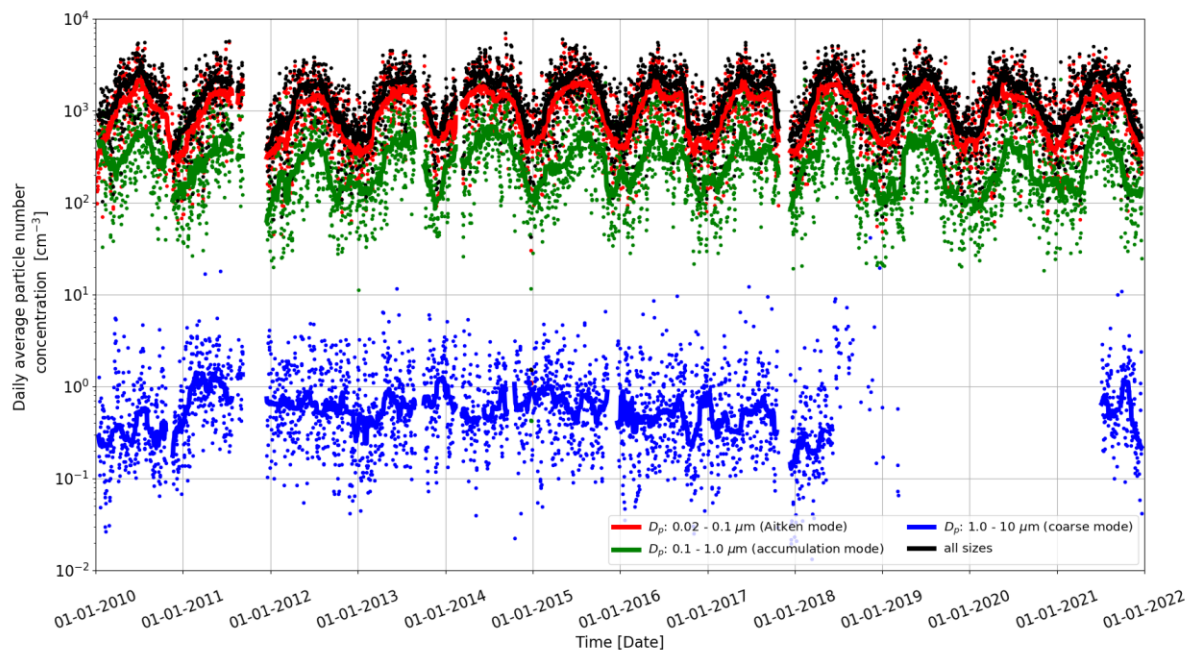


Figure 48: Birkenes 2010-2021 time series of particle number concentration integrated over selected size ranges representing the different physical processes governing the atmospheric aerosol. The dotted graphs represent daily averages of the respective size range, the lines the 55-day running median.

### 3.4.2 Physical aerosol properties measured in situ at the Zeppelin Observatory

**Key findings aerosol physical properties Zeppelin:** Zeppelin particle size distribution data exhibit the well-known Arctic haze pattern. Trends in this pattern cannot be studied yet due to too short the time series. Observations of the particle size distribution in the refractory particle fraction can serve as indicator of aerosol processing time.

A Differential Mobility Particle Sizer (DMPS) instrument, measuring the particle number size distribution, was installed at Zeppelin in 2016 primarily to calibrate the ACSM instrument, but included continuous monitoring as an additional benefit. The same instrument type, operated in a different mode, is used to *measure* the particle number size distribution (PNSD) in the particle diameter range 0.01  $\mu\text{m}$  – 0.8  $\mu\text{m}$  at Birkenes and Trollhaugen stations. It was therefore decided to deploy the Zeppelin DMPS in the same way when not needed for calibrating the ACSM instrument.

As an additional feature, the Zeppelin DMPS has been upgraded late 2017 to also provide the PNSD of refractory (non-volatile) particles. The refractory particle fraction is often used as a proxy for the absorbing aerosol particle fraction, which will allow to study changes in particle absorption on a microphysical basis in the Arctic environment routinely. The corresponding data [are available in real-time](#) with only 1 hour delay.

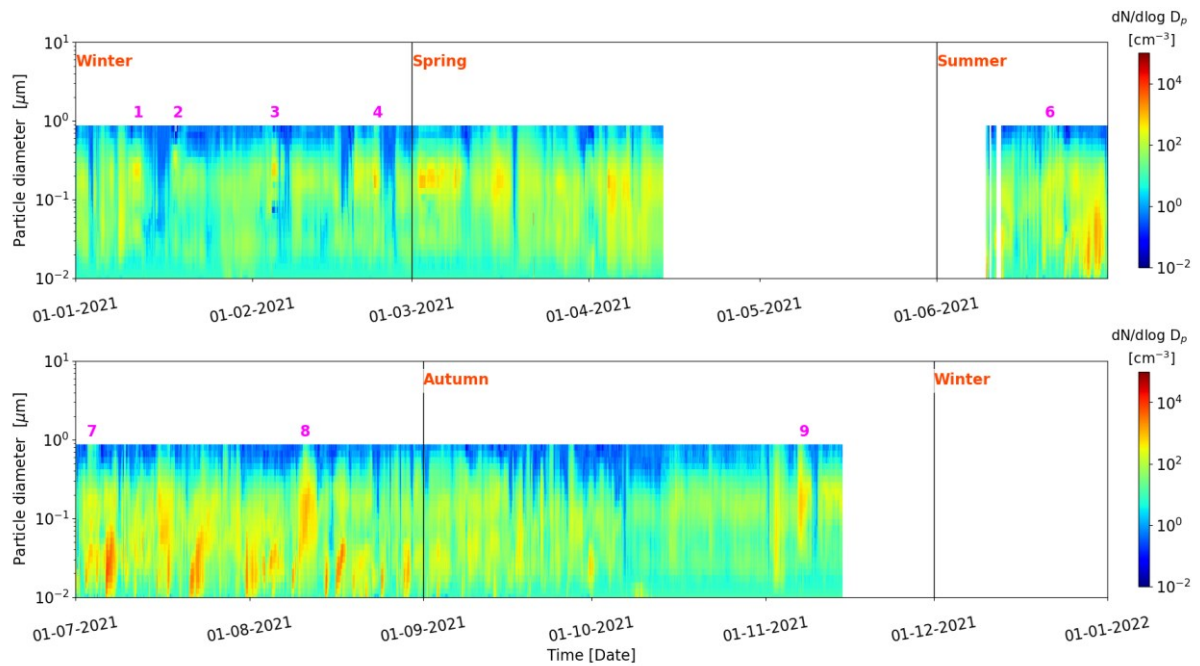


Figure 49: 2021 time series of particle number size distribution from the DMPS at Zeppelin. Episodes are marked by magenta numbers, with episode numbers referring to Table 7.

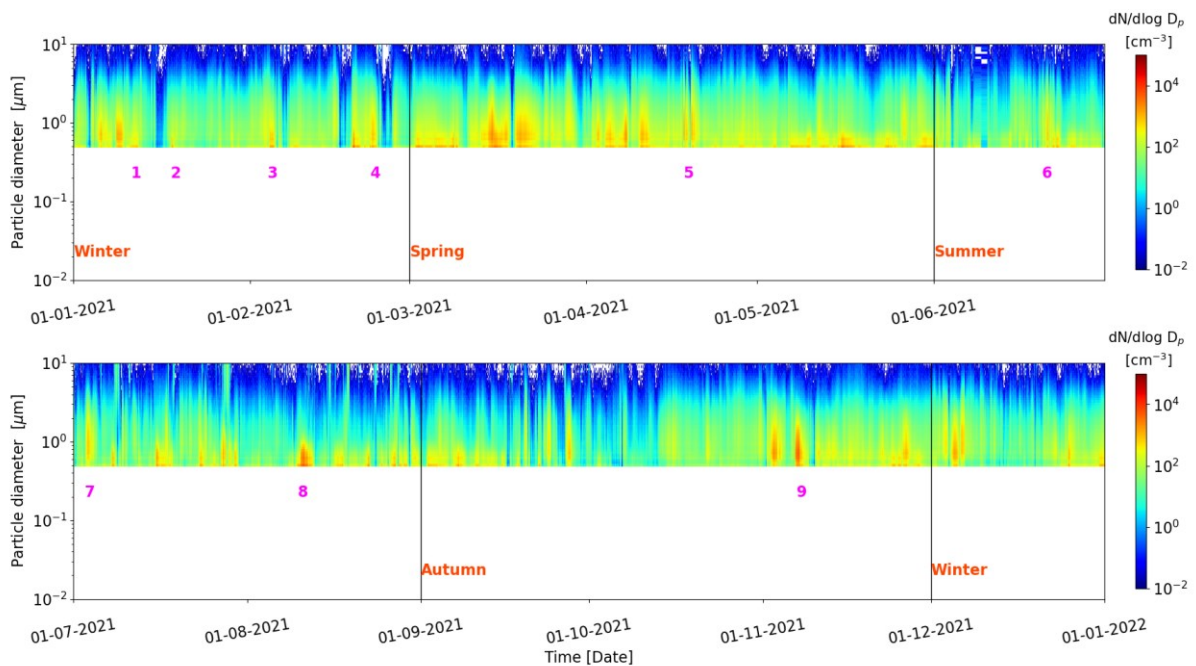


Figure 50: 2021 time series of particle number size distribution from the APS at Zeppelin. Episodes are marked by magenta numbers, with episode numbers referring to Table 7

At Zeppelin, the DMPS has recently been combined with an instrument covering the coarse particle size range larger  $1 \mu\text{m}$ . The Aerodynamic Particle Sizer (APS) measures the PNSD up to  $10 \mu\text{m}$  particle diameter using acceleration of particles in an air stream. Figure 49 presents the Zeppelin PNSD data



available for this report for 2021 in the same way as for Birkenes and Trollhaugen, with one PNSD time series panel per season. The new APS data are shown in Figure 50.

In contrast to mid-latitudes, air masses don't shift quite as rapidly at polar latitudes due to a smaller influence of frontal systems, making weather patterns more persistent at least in parts of the year. This allows to interpret the information on air mass types contained in PNSD data in more detail. Focussing in on Panel a) of Figure 49 displaying the PNSD data of winter 2021, periods with a uni-modal size distribution are visible. This means the PNSD is dominated by a single mode, in this case the accumulation mode with a peak around 0.25  $\mu\text{m}$  particle diameter. Such a PNSD is typical of early-phase Arctic haze (Heintzenberg, 1980), which is also detectable in late autumn and early spring, Figure 49. Arctic haze is formed chemical reactions in aerosol particles trapped under the winter Arctic vortex while the particle mass increases from industrial emissions under the vortex (e.g., Law & Stohl, 2007).

*Table 7: Selected transport events observed at Zeppelin in 2021, together with characteristics and air mass origin determined by trajectory analysis.*

#	Time Begin	Time End	Comment	Air mass origin (backwards order)	Air mass type
1	2021-01-11 12:00	2021-01-12 03:00	Pronounced accumulation mode, $D_p > 200$ nm	Kola peninsula	Domestic heating
2	2021-01-18 03:00	2021-01-18 18:00	Pronounced accumulation mode, $D_p > 300$ nm	Novaya Zemlya, North Central Siberia	Flaring
3	2021-02-04 12:00	2021-02-05 00:00	Pronounced accumulation mode, $D_p > 200$ nm	Arctic sea, North Central Siberia	Probably domestic heating
4	2021-02-22 09:00	2021-02-23 00:00	Pronounced accumulation mode, $D_p \sim 150$ nm	Murmansk region	Domestic heating
5	2021-04-18 00:00	2021-04-20 00:00	coarse particles in size distribution	Greenland Sea, Greenland, Iceland Norwegian Sea, UK	Sea spray
6	2021-06-20 18:00	2021-06-21 06:00	coarse particles in size distribution	Greenland Sea, Arctic Ocean	Sea spray
7	2021-07-03 12:00	2021-07-04 00:00	coarse particles in size distribution	Greenland Sea, Greenland, Canada	Sea spray
8	2021-08-10 12:00	2021-08-11 18:00	Pronounced accumulation mode, $D_p \sim 150$ nm, increased particle absorption	Greenland Sea, Greenland Norwegian Sea, South Central Sweden, UK, Canada	Possibly forest fires in Central Sweden
9	2021-11-07 00:00	2021-11-07 18:00		Arctic Ocean, Canada, Siberia	Flaring

The late spring and summer PNSD at Zeppelin (Figure 49) is somewhat more variable than in winter due to less stable atmospheric conditions. Particle formation events can be observed, with peak in the PNSD at particle diameters between 0.01–0.02  $\mu\text{m}$ . These are triggered by photo-chemical production of chemical species that condense into the particle phase, and don't find enough existing particle surface to condense on, thus forming new particles.

There are several transport events visible in the 2021 PNSD data, where a selection has been marked and numbered in Figure 49. The same events are listed in Table 7 summarising the time, the characteristics, air mass origin determined by trajectories, and air mass type. The transport events are characterised by dominant modes in the accumulation mode size range, occasionally accompanied by a detached Aitken-mode. Most of the investigated events originate from industrial emissions in the Russian Arctic (Kola/Yamal/Kanin peninsula). The exception is the transport event in early August 2021, likely caused by a forest fire in Sweden. It needs to be monitored whether climate change will affect transport patterns, frequency and magnitude of such long-range transport events from lower to high latitudes, including possible effects for surface air quality under transport. Such a connection is thinkable since the amplitude of mid-latitude circulation patterns ("Rossby-waves") is projected to increase in a warming climate due to a decreasing temperature difference between polar and subtropical latitudes. This in turn leads to increased meridional transport. This type of transport has been investigated on a cases basis (e.g., Groot Zwaafink et al., 2022) or for certain pollutants (Hansen et al., 2015), but a dedicated study focussing on Norway seems to be lacking.

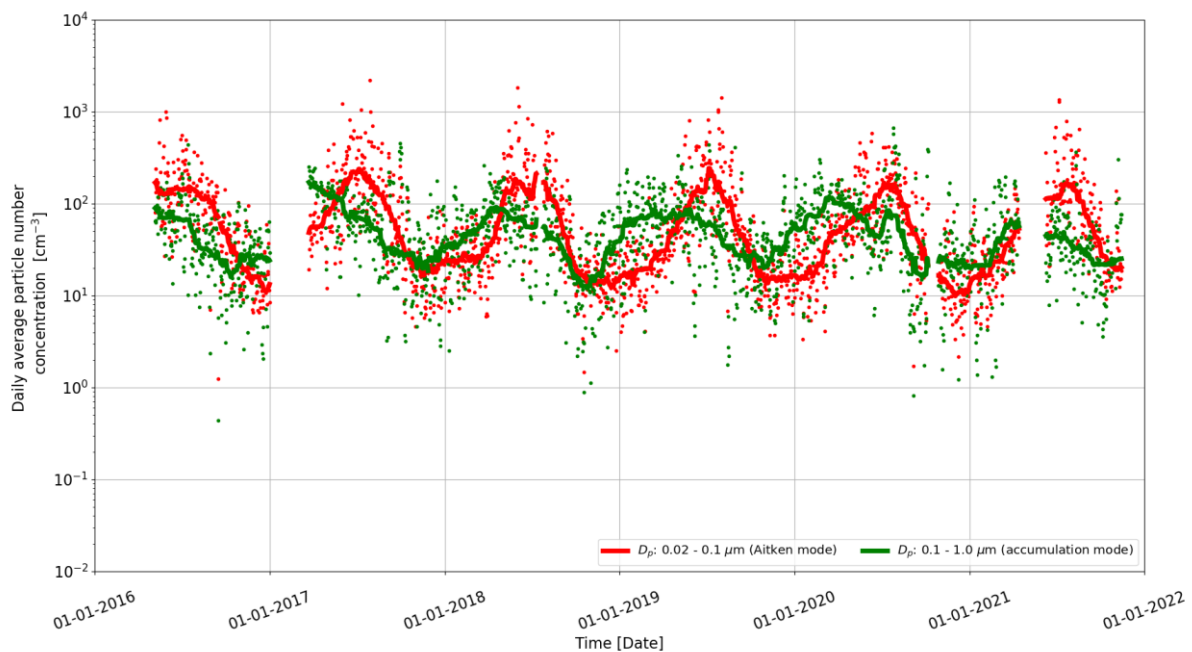


*Figure 51: Zeppelin 2016-2021 time series of particle number concentration integrated over selected size ranges representing the different physical processes governing the atmospheric aerosol. The dotted graphs represent daily averages of the respective size range, the lines the 55-day running median.*

Figure 51 summarises the 2016-2021 Zeppelin PNSD data by displaying time series of the PNSD size integrals for the Aitken mode  $N_{\text{ait}}$  ( $0.02 \mu\text{m} < D_p < 0.1 \mu\text{m}$ ) and  $N_{\text{acc}}$  ( $0.1 \mu\text{m} < D_p < 1 \mu\text{m}$ ). Apart from particle concentrations an order of magnitude lower than at boreal Birkenes, the most prominent feature of the graph is the point in early November where the  $N_{\text{acc}}$  running median becomes consistently larger than  $N_{\text{ait}}$  running median. This behaviour is typical for auto-processed aerosols and occurs normally only for shorter events. At Zeppelin, this point marks the onset of the Arctic haze period. The data gap in 2021 was caused by a valve failure of the thermodenuder system, inducing a

vacuum in the system and resulting in further damage. A larger maintenance operation became necessary.

Figure 52 displays the annual time series of the PNSD measured at Zeppelin in the non-volatile (refractory) particle fraction in 2021, again with one panel per season. The refractory particle fraction is measured by heating the aerosol sample to 250°C prior to measuring the PNSD. It can be considered as proxy for the BC particle fraction but contains also mineral dust and condensed species which become non-volatile by charring or oligomerisation while the sample is heated.

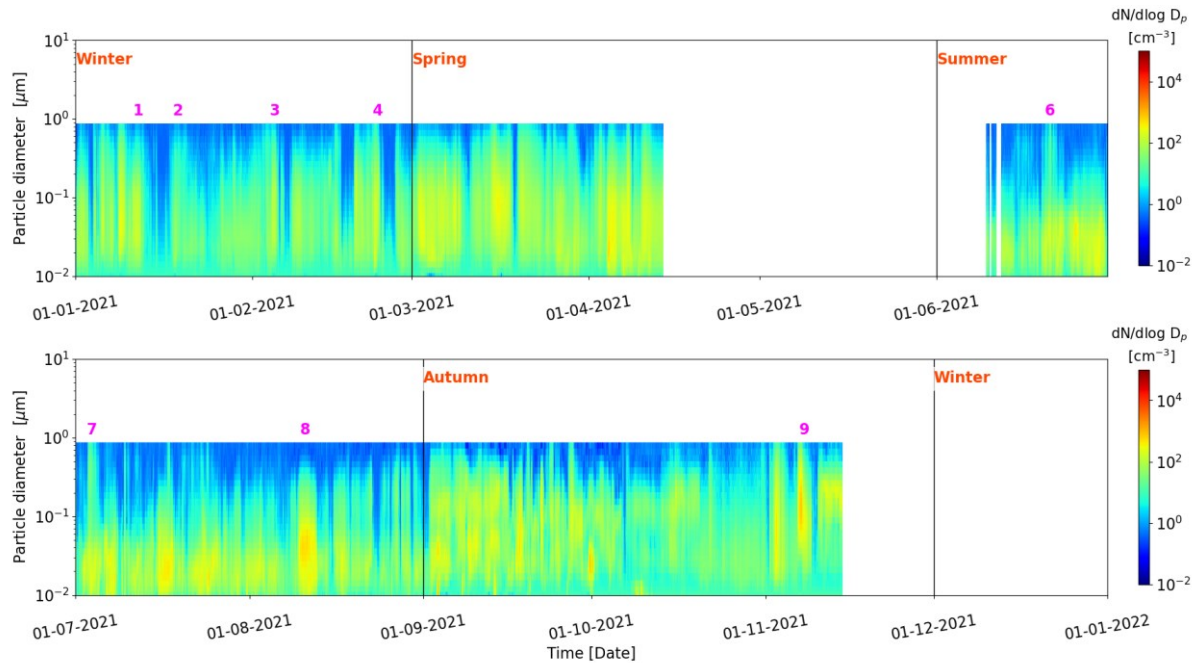


Figure 52: 2021 time series of particle number size distribution of the non-volatile particle fraction at Zeppelin. Episodes are marked by numbered red bars, with episode numbers referring to Table 7.

As most obvious distinction between the PNSD of the ambient aerosol (Figure 49) and the PNSD of the non-volatile aerosol fraction (Figure 52), the particle number concentration levels are around half-a-magnitude lower in the non-volatile as compared to the ambient aerosol. The PNSD is almost exclusively mono-modal, with the single mode peaking in the Aitken-size range between 0.25-0.5  $\mu\text{m}$  particle diameter. The peak diameter increases with the auto-processing and lifetime of the aerosol. The refractory particle component increases in size due to coagulation, and not modulated by volatile particle components.

Similar as before, Figure 53 summarises the 2018-2021 Zeppelin PNSD data for the refractory particle fraction by displaying time series of the PNSD size integrals for the Aitken mode  $N_{\text{ait}}$  ( $0.02 \mu\text{m} < D_p < 0.1 \mu\text{m}$ ) and accumulation mode  $N_{\text{acc}}$  ( $0.1 \mu\text{m} < D_p < 1 \mu\text{m}$ ). As mentioned before, the overall level of  $N_{\text{ait}}$  and  $N_{\text{acc}}$  for the refractory particle fraction is roughly half an order of magnitude lower than for the respective counterparts in the ambient aerosol. An annual cycle might be visible, now confirmed by four years of data.

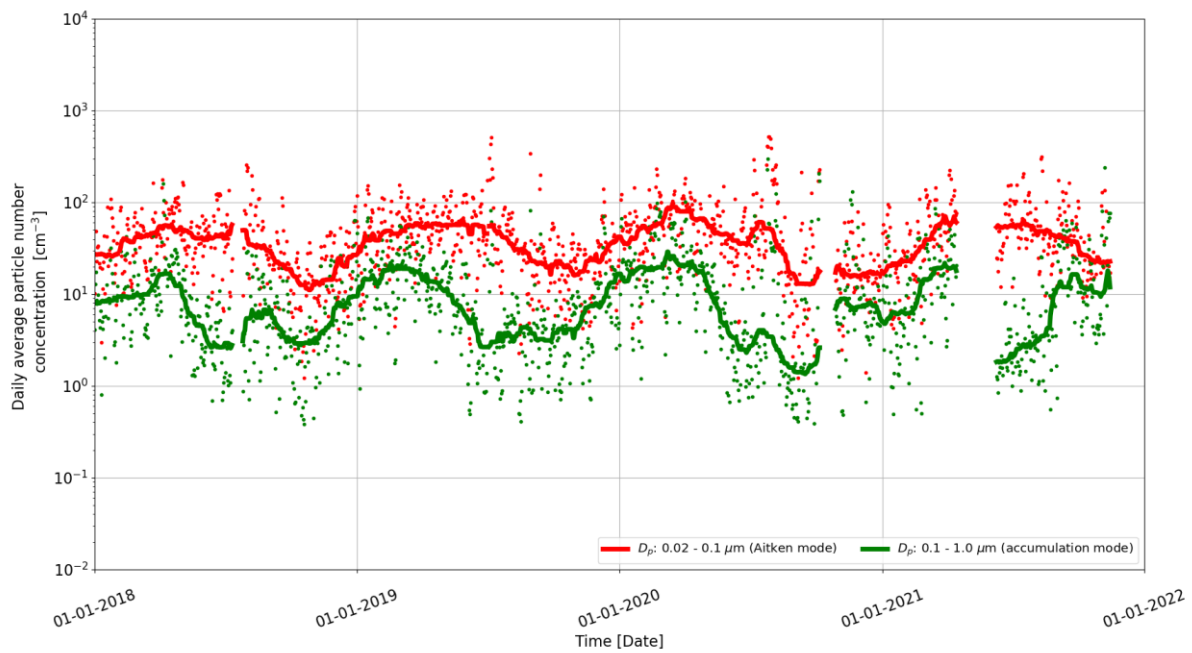


Figure 53: Zeppelin 2018-2021 time series of number concentration in the refractory particle fraction integrated over selected size ranges representing the different physical processes governing the atmospheric aerosol. The dotted graphs represent daily averages of the respective size range, the lines the 55-day running median.

### 3.4.3 Physical aerosol properties measured in situ at the Trollhaugen Observatory

**Key findings aerosol physical properties Trollhaugen:** The length of the time series of reliable data on the aerosol particle number size distribution at Trollhaugen is too short for drawing conclusions on trends. The annual cycle of the PNSD at Trollhaugen has been studied in detail, and is associated to a natural, hemispheric-scale atmospheric pattern. Antarctic background air descends over the Central continent from the upper troposphere/lower stratosphere. At that altitude, it has been transported to the pole after being uplifted (and cleaned by wet removal) at mid- or tropical latitudes. Episodes of mono-modal aerosol intrusions during winter can be connected to emissions from research stations 360 km east of Trollhaugen.

In contrast to mid-latitudes, polar latitudes exhibit more stable atmospheric conditions with less influence of frontal systems. This is especially true for the Antarctic continent due to colder inland temperatures and the absence of land masses in the mid- to high-latitude Southern hemisphere that could disturb the atmospheric air flow, as compared to the Northern hemisphere. This makes air masses well-defined in these regions, and their associated aerosol properties easier to interpret than under shifting Northern mid-latitude conditions.

This section only covers data collected at the station after the relocation in January 2014 from the Troll main base to Trollhaugen located above and upwind of the previous location. At the old station location, up to 80% of the collected data were locally contaminated by diffuse (unavoidable) emissions from the main station buildings, making a statistically meaningful interpretation of the data from the old location difficult.

The DMPS system measuring the PNSD at Trollhaugen station has been re-built on-site during the station maintenance visit of January/February 2016, causing a gap in the PNSD time series in January 2016. After the re-build, the system conforms to the quality standards of the ACTRIS research

infrastructure, and the observed size range has been extended from 0.03 – 0.8  $\mu\text{m}$  to 0.01 – 0.8  $\mu\text{m}$ , making it now suitable to study formation of new particles. As a consequence, absolute particle concentrations measured by the system before and after remodelling are not directly comparable. This disadvantage has been accepted in favour of a wider range of applications for the DMPS system.

Figure 54 plots the 2021 Trollhaugen PNSD data in the same way as for Birkenes. Due to the rather well-defined atmospheric conditions over the Antarctic continent, 2021 is again rather representative also for previous years. Please observe that the times for the panels are the same as for the Northern hemisphere stations, but that seasons in the Southern hemisphere are shifted by 6 months.

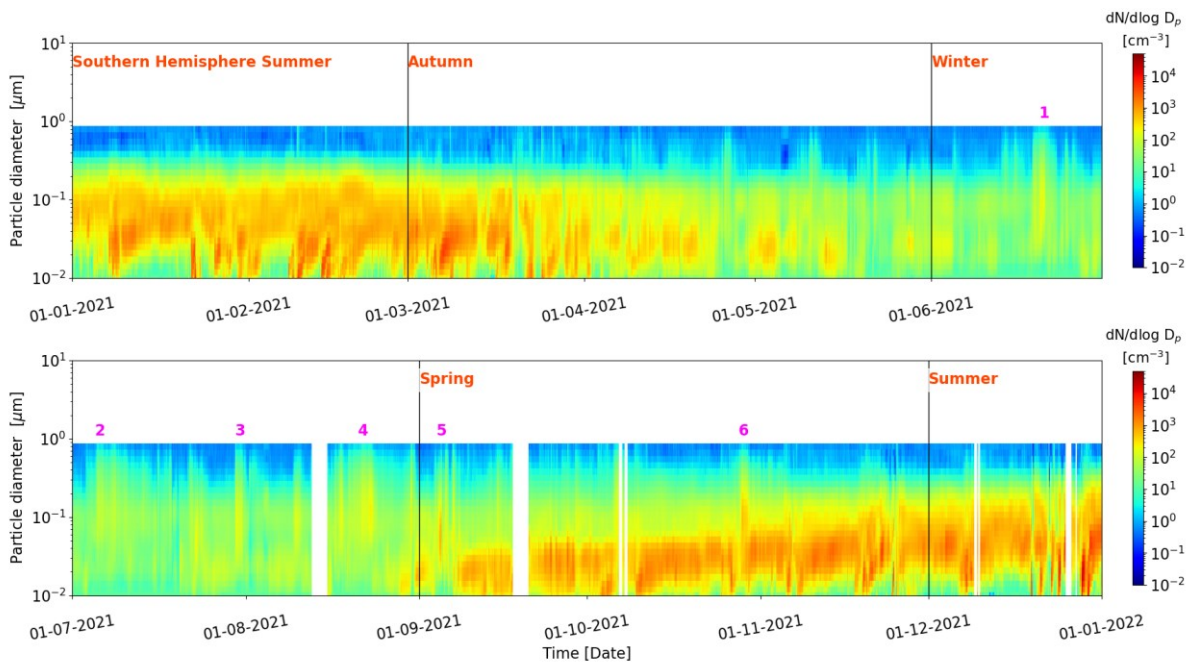


Figure 54: 2021 time series of particle number size distribution at Trollhaugen. Episodes are marked by magenta numbers, with episode numbers referring to Table 8.

Even though the Antarctic continent is among the most pristine regions on the globe, new particle formation events triggered by photo-chemical oxidation of precursor substances can be observed in Antarctic summer. Formation of new particles is not a function of available condensable vapour alone, but also of the available particle surface. If the available particle surface becomes too small to accept the condensing vapour, new particles occur. This ratio doesn't depend on the absolute amount of aerosol particles. Thus, formation of new particles can occur anywhere on the globe.

A year-round feature observed at Trollhaugen is the intrusion of marine air associated with marine storms. These have been observed even at South Pole and are visible in the PNSD when the particle concentration at the upper end of the particle size range increases.

The probably most prominent feature in the Trollhaugen annual PNSD time series data is the annual cycle visible in the background aerosol. Particle concentrations are low in winter over the whole observed PNSD size range, and nucleation events lacking. In spring, particle concentrations in the diameter range 0.01 – 0.03  $\mu\text{m}$  increase, and the central particle diameter of this peak increases throughout spring until reaching values around 0.09  $\mu\text{m}$  in summer. Towards autumn and winter, the cycle reverses.

Table 8: Selected transport events observed at Trollhaugen in 2021, together with characteristics and air mass origin determined by Lagrangian backward plume analysis.

#	Time Begin	Time End	Comment	Air mass origin (backwards order)	Air mass type
1	2021-06-20 00:00	2021-06-21 00:00	Single accumulation mode, concentration increased relative to background	Antarctic coast east of Troll station, Southern Atlantic Ocean.	Likely emissions from neighbouring station.
2	2021-07-05 12:00	2021-07-06 12:00	Single accumulation mode, concentration increased relative to background	Mostly Antarctic coast east of Troll station, small contribution of Southern Indian Ocean	Likely emissions from neighbouring station.
3	2021-07-30 06:00	2021-07-31 12:00	Single accumulation mode, concentration increased relative to background	Antarctic coast east of Troll station, Southern Atlantic Ocean.	Likely emissions from neighbouring station.
4	2021-08-21 18:00	2021-08-23 18:00	Single accumulation mode, concentration increased relative to background	Mostly Antarctic coast east of Troll station, small contribution of Southern Indian Ocean	Likely emissions from neighbouring station.
5	2021-09-04 15:00	2021-09-05 00:00	Single Aitken mode in particle number size distribution	Air masses straight from East, ocean South of Africa	Very likely fresh emissions from neighbouring station.
6	2021-10-28 18:00	2021-10-29 00:00	Single accumulation mode, concentration increased relative to background	Mostly Antarctic coast east of Troll station, small contribution of Southern Indian Ocean	Likely emissions from neighbouring station.

Despite the uniform character of the air mass cycle at Trollhaugen, transport episodes occur also here, some of which are marked in Figure 54 and explained in Table 8. In Antarctica, transport episodes remain visible also for very long transport times due to pristine background particle concentrations. These long transport time require use of Lagrangian backward plume modelling in order to determine air mass origin instead of “simple” trajectory modelling. In 2021, episodes observed at Trollhaugen were mostly caused by emissions of the neighbouring station in the East.

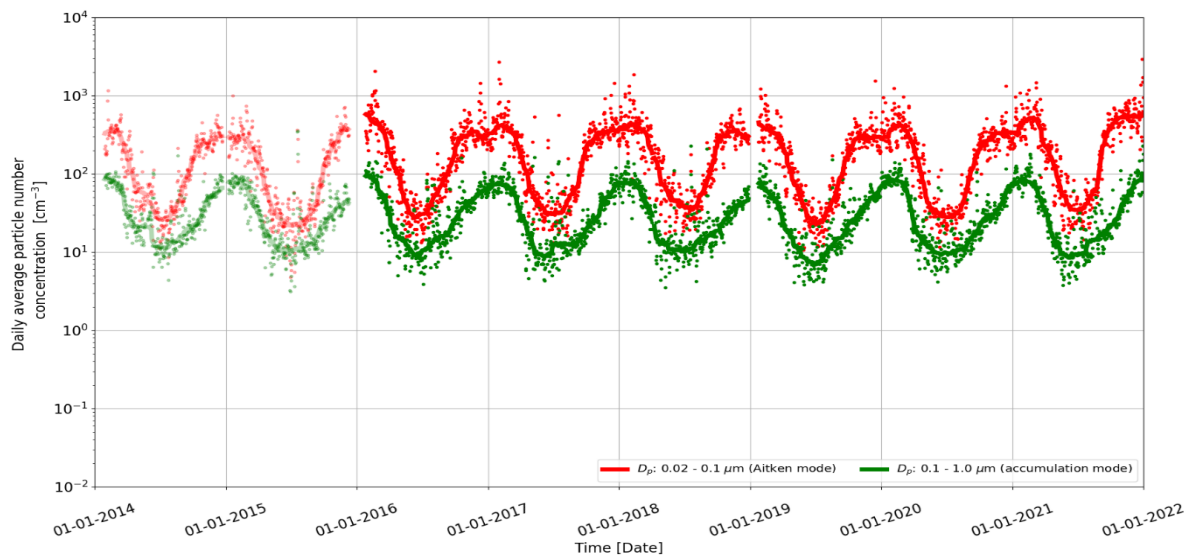


*Figure 55: 2014-2021 time series of particle number concentration integrated over selected size ranges representing the different physical processes governing the atmospheric aerosol. The dotted graphs represent daily averages of the respective size range, the lines the 55-day running median. Data of the DMPS instrument prior to its upgrade are plotted in lighter colour as reminder that data before and after remodelling aren't directly comparable due to extension of the particle size range observed by the instrument.*

The annual cycle in the Antarctic background PNSD is reflected by the PNSD size integrals for the Aitken mode  $N_{ait}$  ( $0.02 \mu\text{m} < D_p < 0.1 \mu\text{m}$ ) and  $N_{acc}$  ( $0.1 \mu\text{m} < D_p < 1 \mu\text{m}$ ) plotted in Figure 55, with higher particle concentrations in summer than in winter. A study based on data collected at Troll (Fiebig et al., 2014) connects the annual cycle to transport patterns seen by Antarctic background air. Antarctic background air descends over the central continent from the upper troposphere/lower stratosphere region, where it has been transported from mid-latitudes or even the tropics at the same altitude. At these lower latitudes, it had been uplifted by frontal conveyers (mid-latitudes) or tropical anvil clouds. The uplift process, associated with extensive wet removal of particles in the frontal or anvil cloud system, explains the cleanliness of the air.

Fiebig et al. (2014) raise the hypothesis that the annual cycle of the Antarctic background aerosol is caused by the annual variation of solar insolation seen by the air during this transport pattern. The hard UV radiation in the upper troposphere would oxidise water-insoluble vapours that survived wet removal during uplift of the air. The oxidation products would subsequently condense into the particle phase, causing the observed annual cycle in the Antarctic background PNSD.

### 3.5 Summary of physical and optical aerosol properties

Aerosol particle absorption and scattering are decisive for the cooling or warming effect of aerosols on climate. All types of aerosols are scattering solar radiation, but the higher fraction of aerosol absorption, the more warming is the aerosol. The absorption depends on the composition; black carbon (e.g., soot), certain organic compounds (brown carbon), and some minerals absorb radiation. The number size distribution of the aerosol particles also determines the scattering properties. In order to summarise the measurements of physical and optical aerosol properties observed at Birkenes,

Trollhaugen, and Zeppelin stations, annual and seasonal means of the main parameters are collected in Table A 3 for the physical parameters, and in Table A 4 for the optical parameters (see Appendix I) Focussing first on the columns for Birkenes, Aitken-mode particle concentrations  $N_{ait}$  for the summer and winter show surprisingly little variation over the years. Relative to previous years, particle concentrations in 2021 for winter are close to the multi-year range, which applies also to summer concentrations. Similarly, spring  $N_{ait}$  concentrations are close to those for many previous years, whereas those for autumn are lower, but all still within the range seen in previous years. Variations of this kind are not unusual and depend on the actual transition from winter to summer weather and vice versa. Late onset of summer weather in spring and early onset of winter weather in autumn will decrease the  $N_{ait}$  particle concentrations for these seasons. Also, for the accumulation mode seasonal average particle concentrations  $N_{acc}$ , spring values are in the middle of the variability range, autumn values at the lower end, whereas summer and winter values don't show exceptional deviations.

At Birkenes,  $N_{ait}$  values for winter are typically around 33% of their summer values due to lack of biogenic particle production from the gas-phase. They depend on emissions from domestic heating, with higher values for colder winters. With spring and autumn as transition periods between the winter and summer extreme values, the variability of  $N_{ait}$  in these seasons depends on the pace of transition between summer and winter. The same tendencies apply to the accumulation mode particle concentration  $N_{acc}$ .

Coarse mode particle concentrations at Birkenes have a tendency to be up to a factor of 2 smaller in winter than in summer due to less crustal particle production with a snow-covered ground. Particle concentrations at Birkenes don't exhibit any obvious trend over time.

Aitken and accumulation mode particle concentrations at Trollhaugen are an order of magnitude lower than at Birkenes, reflecting the pristine conditions in Antarctica. Their pronounced annual cycle and its cause has been discussed in section 3.4.3. Both concentrations show little variability over the years, reflecting the fact that atmospheric composition in Antarctica is still mostly governed by natural processes whose large-scale pattern changes slowly.

Zeppelin particle size distribution data exhibit the well-known Arctic haze pattern. Trends in this pattern cannot be studied in this context due to the short time series. Newly established observations of the particle size distribution in the refractory particle fraction can serve as indicator of aerosol atmospheric processing time. The spectral dependence of particle light absorption at Zeppelin indicates a contribution of absorbing components with spectral dependence due to chemical composition, e.g., brown carbon or mineral dust.

The conclusion of no obvious trends applies also to the optical aerosol properties observed at Birkenes, and Trollhaugen, and is confirmed by the trend study of Collaud Coen et al. (2020), whereas Zeppelin aerosol absorption continues to show a decreasing trend (Eleftheriadis et al., 2009). At Birkenes, the annual and inter-annual variability is governed by the same processes mentioned when discussing the particle concentrations. More specifically, the aerosol is more absorbing in winter, and hence more warming, due to emissions from wood burning for domestic heating, which come on top of a baseline of absorbing aerosol emitted from traffic. This is reflected in higher particle absorption coefficient values in winter, and even more significantly in lower winter values of the single scattering albedo (lower meaning higher average particle absorption).

The transport episodes observed in 2021 at the Birkenes station originate often in Central and South-East Europe. Air masses are being transported over land over an extended period. Occasionally, these events are superimposed by emissions from wildfires in South-Eastern Europe. Most of the investigated episodes at the Zeppelin station originate from industrial emissions in the Russian Arctic (Kola/Yamal/Kanin peninsula). The exception is the transport event in early August 2021, likely caused



by a forest fire in Sweden. At Trollhaugen, transport episodes are traces back to emissions from neighbouring stations.

### 3.6 Column optical aerosol properties measured by ground-based remote sensing

Ground-based remote sensing of the optical characteristics of aerosols in the atmospheric total column is conducted with multi-wavelength sun-photometers. A sun-photometer is oriented towards the sun to detect the solar radiation attenuated along the slant path from the top-of-atmosphere to the ground. The atmospheric aerosol load leads to a decrease in the solar radiation transmitted through the atmosphere. This decrease depends on the aerosol optical depth (AOD), which is given by the integral of the volume aerosol extinction coefficient along the vertical path of the atmosphere. The wavelength dependence of AOD, described by the Ångström exponent ( $\text{Å}$ ) is a qualitative indicator of the particle size and contains information about the aerosol type. The larger the Ångström exponent, the smaller the size of the particles measured.

Photos of instruments used for monitoring of spectral resolved AOD at Birkenes and Ny-Ålesund, their main characteristics are given in Appendix II, and detailed tables with monthly data for all years are given in Appendix I. The instrument at Trollhaugen, Antarctica, which is also reported here, is of the same type as the instrument in Ny-Ålesund, but due to the logistical and calibration challenges, also here two sensor heads are available and are exchanged during the annual maintenance visits.

#### 3.6.1 Column optical aerosol properties measured by ground-based remote sensing at Birkenes Observatory

**Key findings column-integrated optical aerosol properties Birkenes:** Most aerosol optical depth (AOD) monthly means in 2021 are very close to and slightly below the multi-year average, but the months of April, July, and September show relatively large variation due to single high-AOD events. The July event was also prolonged, thus increasing the monthly mean significantly. As in previous years, the high-AOD events are probably caused by biomass burning. The means of Ångström coefficients ( $\text{Å}$ ) are close to or above the long-term means with higher-than-normal values mainly during winter. There is no statistically significant trend, neither in AOD nor in  $\text{Å}$ , in the eleven years of AOD observations at Birkenes.

AOD measurements started at the Birkenes Observatory in spring 2009, utilizing an automatic sun and sky radiometer (CIMEL type CE-318, instrument #513). The retrieval method is that of the AERONET version 3 direct sun algorithm (for details: <http://aeronet.gsfc.nasa.gov>).

A second Cimel instrument (#1163) was purchased in summer 2018 and subsequently calibrated at the University of Valladolid in October 2018; it was for the first time installed at Birkenes in November 2018. Unfortunately, this has not completely resolved the issue of missing observations due to calibration needs, as both instruments have exhibited technical problems, especially related to tracking. Nevertheless, 2021 was the first year with an almost complete annual cycle of measurements. The older Cimel instrument (#513) was in operation until 3 March 2021, while the newer instrument (#1163) continued from March 5. Recording of usable data stopped in early December, and technical challenges with the tracking robot continued into 2022.

Cimel #1163 was again exchanged with #513 in February 2022 and sent to the University of Valladolid for calibration.

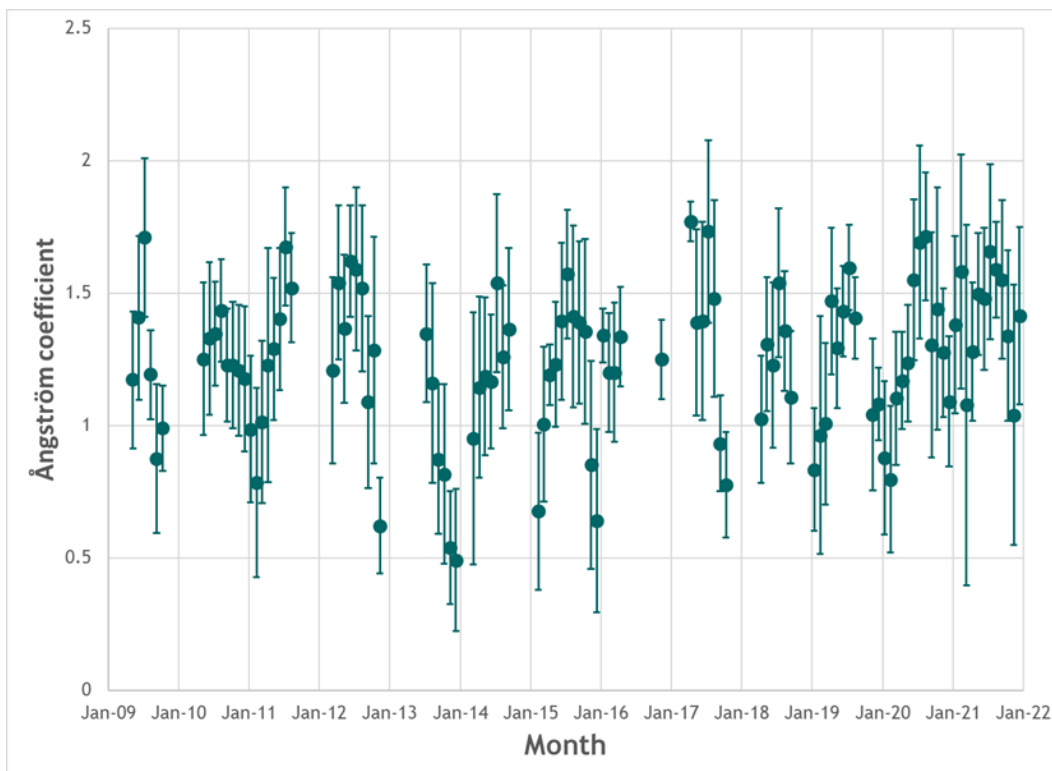
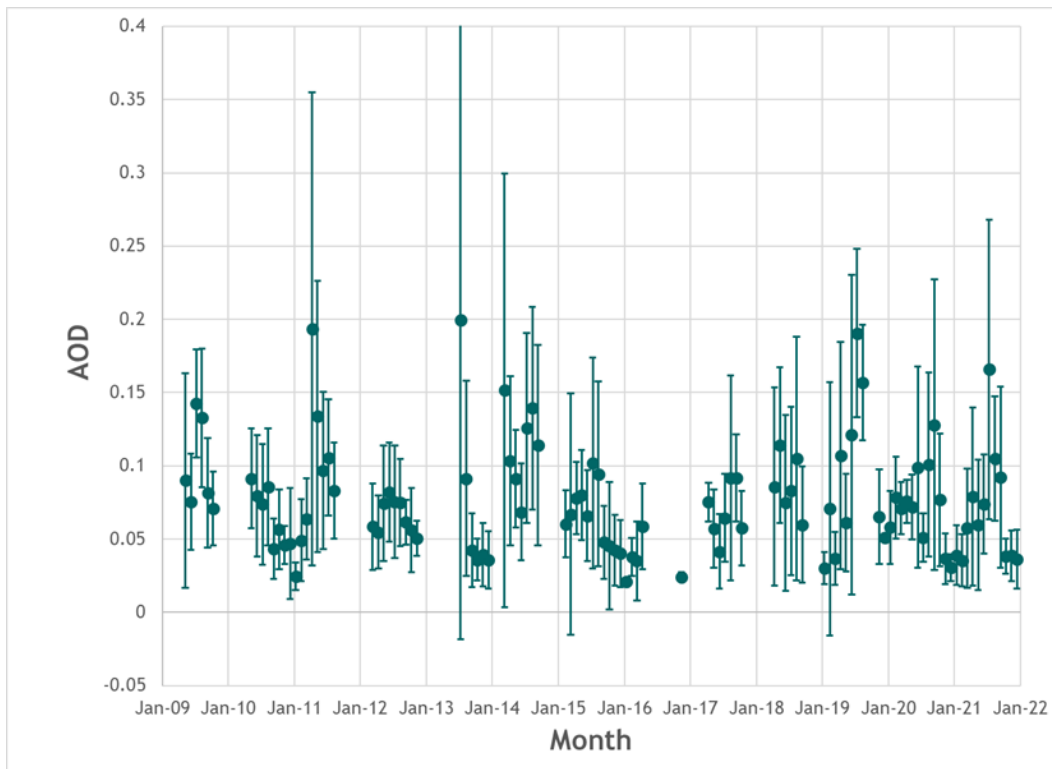


Figure 56: 2009 - 2021 time series of aerosol optical depth (AOD) at 500 nm wavelength in the atmospheric column above Birkenes (upper panel) and (470 nm, 800 nm) Ångström exponent describing the AOD wavelength dependence (lower panel). Monthly mean values and standard deviations are given.

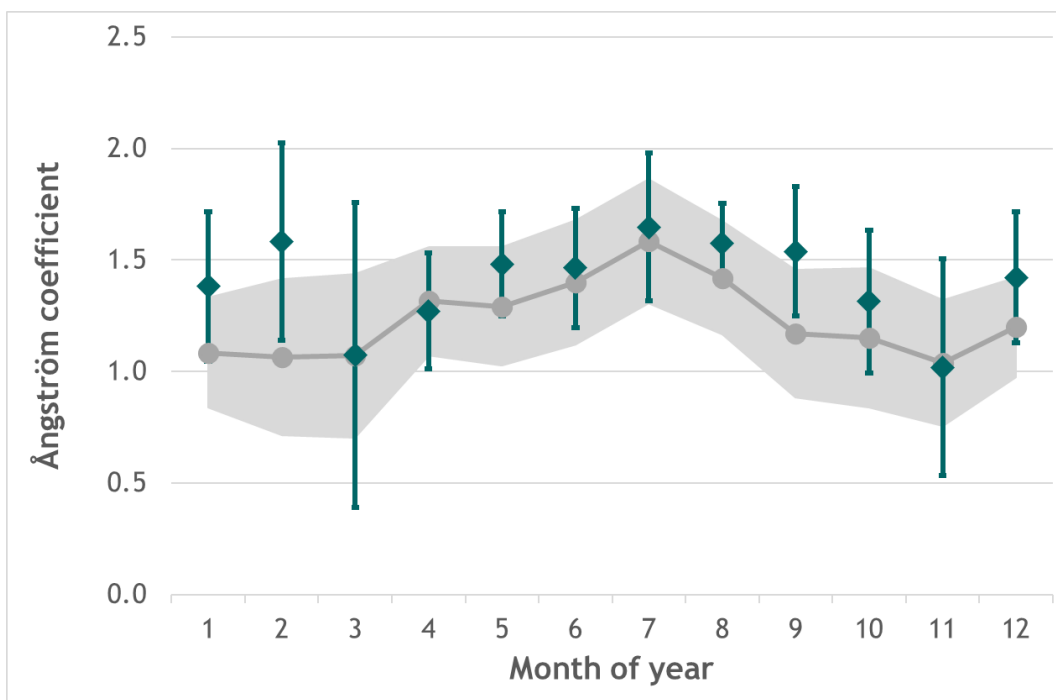
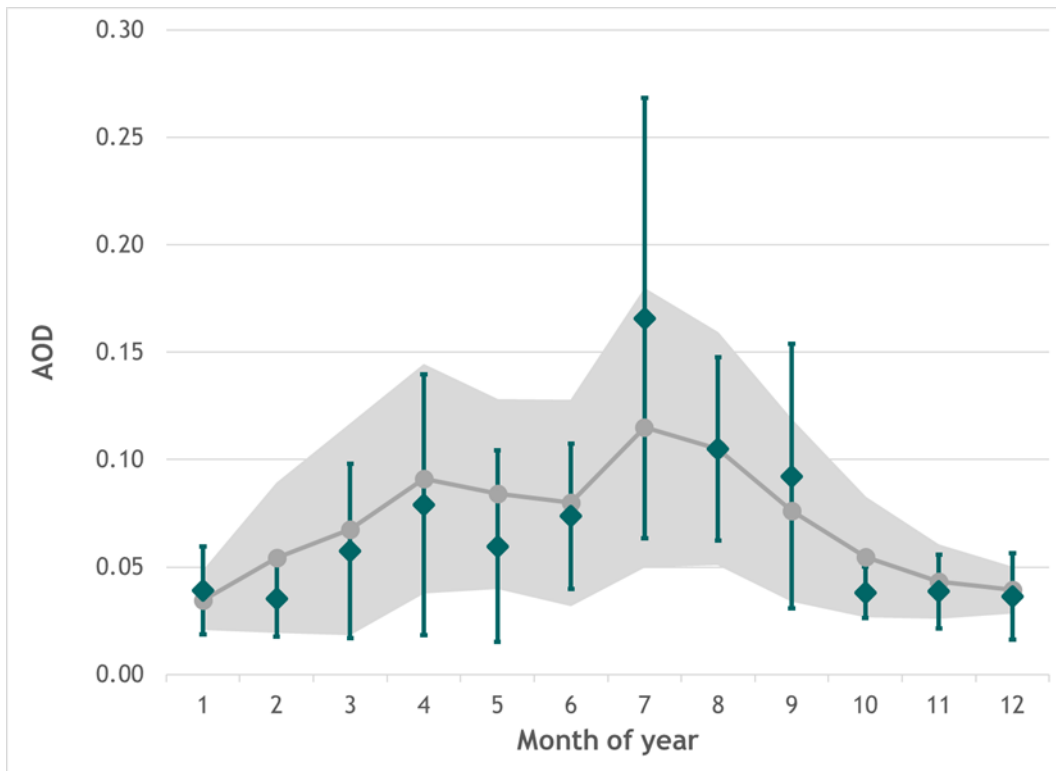


Figure 57: 2021 monthly mean aerosol optical depth (AOD) at 500 nm wavelength in the atmospheric column above Birkenes (upper panel) and (470, 800 nm) Ångström coefficient describing the AOD wavelength dependence (lower panel). Mean values and standard deviations are given. Values marked in grey are the mean and standard deviations for the 2009-2021.

The AOD and Ångström coefficient time series including 2021 and seasonal variations for 2021 are shown in Figure 56 and Figure 57, respectively. The 2021 monthly mean and mean values for all years

are given in Table 9, while data for all years can be found in Appendix I. AERONET calculates daily averages in case of more than 3 single measurements. This yielded 189 daily means. In the monthly means we include all approved single measurements from the respective month instead of daily averages weighted with the number of single measurements included in the respective daily means. There are no obvious (and statistically significant) trends visible in the 12-year series of AOD and AE monthly means.

Compared to central European observations, where AOD monthly means can reach well above 1.0 for large parts of the year, the aerosol load at Birkenes is relatively low, but episodes with advected airmasses rich in pollution/aerosol load occur. Figure 58, which shows single measurements (small dots), daily means (filled circles with the spread of observations as “error” bars) and monthly means (filled squares with “error” bars) in 2021, reveals such episodes both in spring (around DoY 110, i.e., 20 April) and, in a more extended period, in summer after July 20 (DoY 200). On the other hand, in the first three months and the last three months AOD values are consistently below 0.1. However, in the winter half-year measurements are much sparser, so that this does not exclude the possibility of short-lived high-AOD events. The elevated episodes in summer were, as in 2020, typically 10-20 days long, with single days of AOD values up to 0.4 embedded. The monthly means of July, August and September are clearly influenced by these episodes, with the highest mean and a large scattering in July. From the second half of October, values again dropped below 0.1. The highest monthly average AOD of 0.16 occurred in July, while the highest daily average of 0.45 was registered on 17 April. The lowest monthly means (between 0.035 and 0.04) were observed in the winter months at the start and the end of the year.

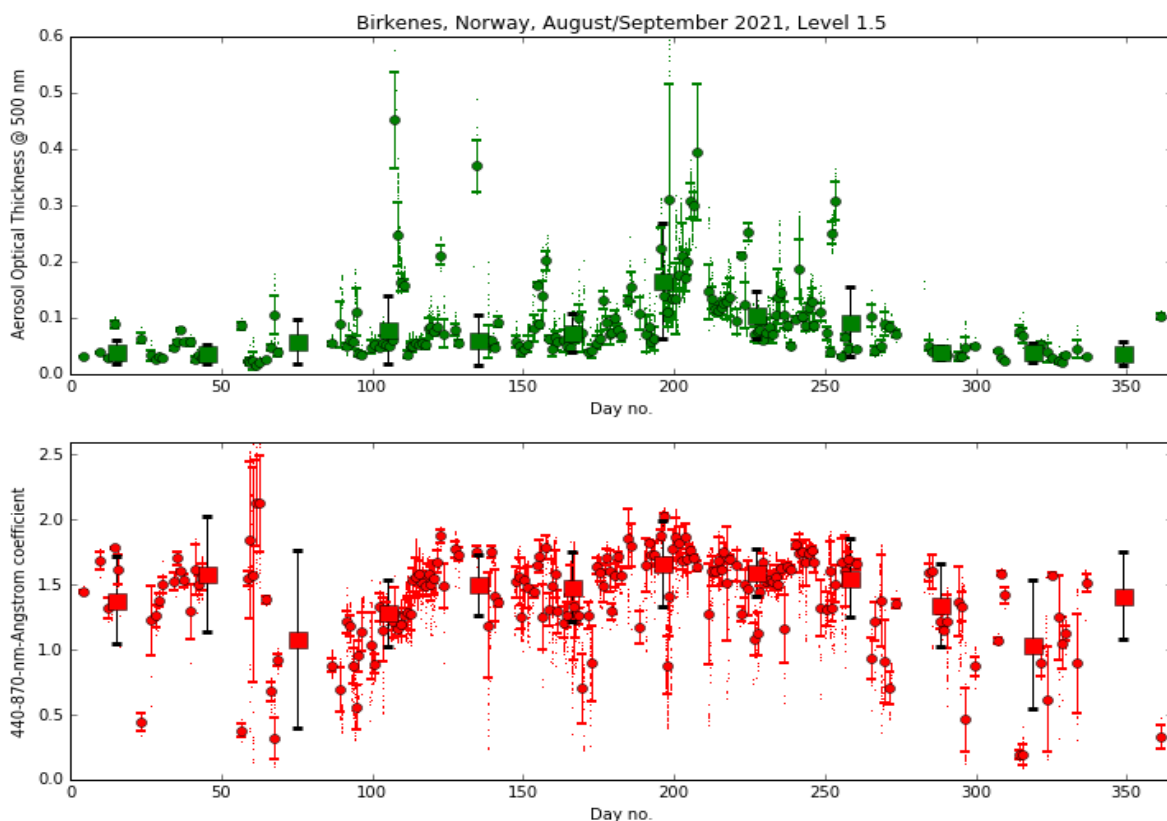


Figure 58: 2021 single (small dots), daily mean (filled circles, with “error” bars), and monthly mean (filled squares, with “error” bars) aerosol optical depth (AOD) at 500 nm wavelength in the atmospheric column above Birkenes (upper panel) and (470, 800 nm) Ångström coefficient describing the AOD wavelength dependence (lower panel). Error bars denote standard deviation of single measurements included in means.

The Ångström exponent monthly means were relatively stable around 1.5 in the period May to September, but similar values were also observed in January and February, which is significantly above the long-term means (close to 1.0). The other months follow rather closely the long-term annual variation of a winter minimum around 1.0 and a summer maximum of 1.5 varied much less than AOD means and were all within the standard deviations of the 12-year series throughout the year. The largest variation was seen in March and early April with AE values rising from around 0.8 to 1.5 within 3 weeks.

*Table 9: Monthly mean values for 2021 and mean for the time period 2009-2021, plus standard deviations, for aerosol optical depth (AOD) and Ångström exponent observed in Birkenes. In addition, the number of days with cloud free and quality assured observations are given.*

Month/Year	Jan	Feb	Mar	Apr	May	Jun	Jul	Aug	Sep	Oct	Nov	Dec
Aerosol optical depth (AOD)												
<b>2021</b>	<b>0.04</b> ±0.02	<b>0.04</b> ±0.02	<b>0.06</b> ±0.04	<b>0.08</b> ±0.06	<b>0.06</b> ±0.04	<b>0.07</b> ±0.03	<b>0.17</b> ±0.10	<b>0.10</b> ±0.04	<b>0.09</b> ±0.06	<b>0.04</b> ±0.01	<b>0.04</b> ±0.02	<b>0.03</b> ±0.02
<b>Mean</b> <b>09-21</b>	<b>0.03</b> <b>0.01</b>	<b>0.05</b> ±0.03	<b>0.07</b> ±0.05	<b>0.09</b> ±0.05	<b>0.08</b> ±0.04	<b>0.08</b> ±0.05	<b>0.11</b> ±0.06	<b>0.11</b> ±0.05	<b>0.08</b> ±0.04	<b>0.05</b> ±0.03	<b>0.04</b> ±0.02	<b>0.04</b> ±0.01
Ångström coefficient (Å)												
<b>2021</b>	<b>1.38</b> ±0.34	<b>1.58</b> ±0.44	<b>1.07</b> ±0.68	<b>1.27</b> ± 0.26	<b>1.48</b> ± 0.23	<b>1.47</b> ± 0.27	<b>1.65</b> ± 0.33	<b>1.58</b> ± 0.18	<b>1.54</b> ±0.29	<b>1.31</b> ±0.32	<b>1.02</b> ±0.49	<b>1.42</b> ±0.29
<b>Mean</b> <b>09-21</b>	<b>1.08</b> ±0.25	<b>1.06</b> ±0.35	<b>1.07</b> ±0.37	<b>1.31</b> ±0.24	<b>1.29</b> ±0.26	<b>1.40</b> ±0.28	<b>1.58</b> ±0.28	<b>1.42</b> ±0.25	<b>1.17</b> ±0.29	<b>1.15</b> ±0.31	<b>1.04</b> ±0.28	<b>1.20</b> ±0.23
Number of days with cloud-free and quality assured observations (AERONET level 2)												
<b>2021</b>	<b>10</b>	<b>11</b>	<b>9</b>	<b>27</b>	<b>15</b>	<b>26</b>	<b>23</b>	<b>27</b>	<b>18</b>	<b>9</b>	<b>12</b>	<b>1</b>
<b>Total</b> <b>09-21</b>	<b>47</b>	<b>56</b>	<b>93</b>	<b>131</b>	<b>199</b>	<b>224</b>	<b>233</b>	<b>217</b>	<b>137</b>	<b>83</b>	<b>65</b>	<b>30</b>

### 3.6.2 Column optical aerosol properties measured by ground-based remote sensing at Ny-Ålesund

**Key findings column-integrated optical aerosol properties Ny-Ålesund:** Measurements until end of September were unspectacular, with only one extended period of increased AOD values in August. Measurements with the AWIPEV Cimel instrument close to the PFR instrument indicate several events with moderately increased AOD in April, but none of the Ny-Ålesund instruments registered the only major high-AOD incident registered with the Cimel instrument in Hornsund in early May.

In 2002, Physikalisch-Meteorologisches Observatorium Davos/World Radiation Center (PMOD/WRC), in collaboration with NILU, started AOD observations in Ny-Ålesund (at the Sverdrup station, 46 m a.s.l.) as part of the global AOD network on behalf of the WMO GAW program. A precision filter radiometer (PFR) measures the extinction in four narrow spectral bands.

In Ny-Ålesund, the solar elevation is less than 5° before 4<sup>th</sup> March and after 10<sup>th</sup> October, limiting the period with suitable sun-photometer observations to the spring-summer-early autumn period. In 2021, measurements did not start until late April due to a combination of technical issues and absence of staff at the station. They continued until 13 September, followed by continuously cloudy weather until the end of the measurement season at the beginning of October. The AOD and Ångström exponent time series of monthly means and standard deviation since the start of measurements in 2002 are shown in Fig. 59, while the 2021 values on the background of the average data and their standard deviation from the whole 20-year period (including 2021) are shown in Fig. 60. The 2021 monthly mean values and standard deviations for all years are given in Table 10. Data for all years are given in Appendix I.

In order to fill the long data gap during the Arctic winter, a PFR version making use of the moonlight around full moon (Lunar PFR) has been developed and tested by PMOD/WRC since 2015. In 2018, the Lunar PFR was integrated in the Svalbard Integrated Arctic Earth Observing Network (SIOS), and data are made available also for monitoring purposes. In principle, reliable measurements are possible from rising half-moon to waxing half-moon, but in Ny-Ålesund the period is further limited by the rapidly changing maximum elevation during the lunar cycle. In 2021, lunar observations were performed in the first three months. In autumn, the instrument participated in an inter-comparison campaign and could not be sent to Ny-Ålesund before end of December.

A Svalbard Science Forum strategic grant coordinated by NILU with the aim to collect, harmonize and store all available AOD/AE measurements from Svalbard and surrounding marine areas since their start in 2002 was completed (Hansen et al., 2022). This covered observations with the sun and lunar PFR, the SP1A sun photometers at the AWIPEV station and at Zeppelin Observatory, Cimel observations at AWIPEV, all these in Ny-Ålesund, Cimel observations at the Polish Polar Station in Hornsund, and various marine observations on research vessels (Oceania, Polarstern, Oden) since 2007. In 2021, the Cimel instrument at AWIPEV station measured from mid-February until end of April and for a short period in May, thus complementing the PFR data series. The two data sets of AOD and AE are displayed in Figure 61.

As one can see in Figures 59-61, 2021 was a rather unspectacular year with respect to aerosol load. The Cimel in Ny-Ålesund registered a few moderate episodes in March and April, but all related to Ångström exponents <0.5, which are excluded from the PFR measurements. In August, the PFR measured elevated AOD values (0.1 – 0.15) during a 2-week period, which was also registered by both Cimel instruments in Ny-Ålesund and Hornsund. These enhanced AOD values were probably caused by the Siberian forest fires in August 2021. For the PFR instrument the measurement statistics in this period was too poor to allow further reaching conclusions. Lunar PFR measurements funded through the SIOS-InfraNor project were performed in the January-March period, but only in late January over a series of 7 days. One of these exhibited unusually high AODs, while on the others, the values were in agreement with low values typical in mid-winter. In autumn, no lunar measurements could be performed because the instrument was sent to an inter-comparison campaign.

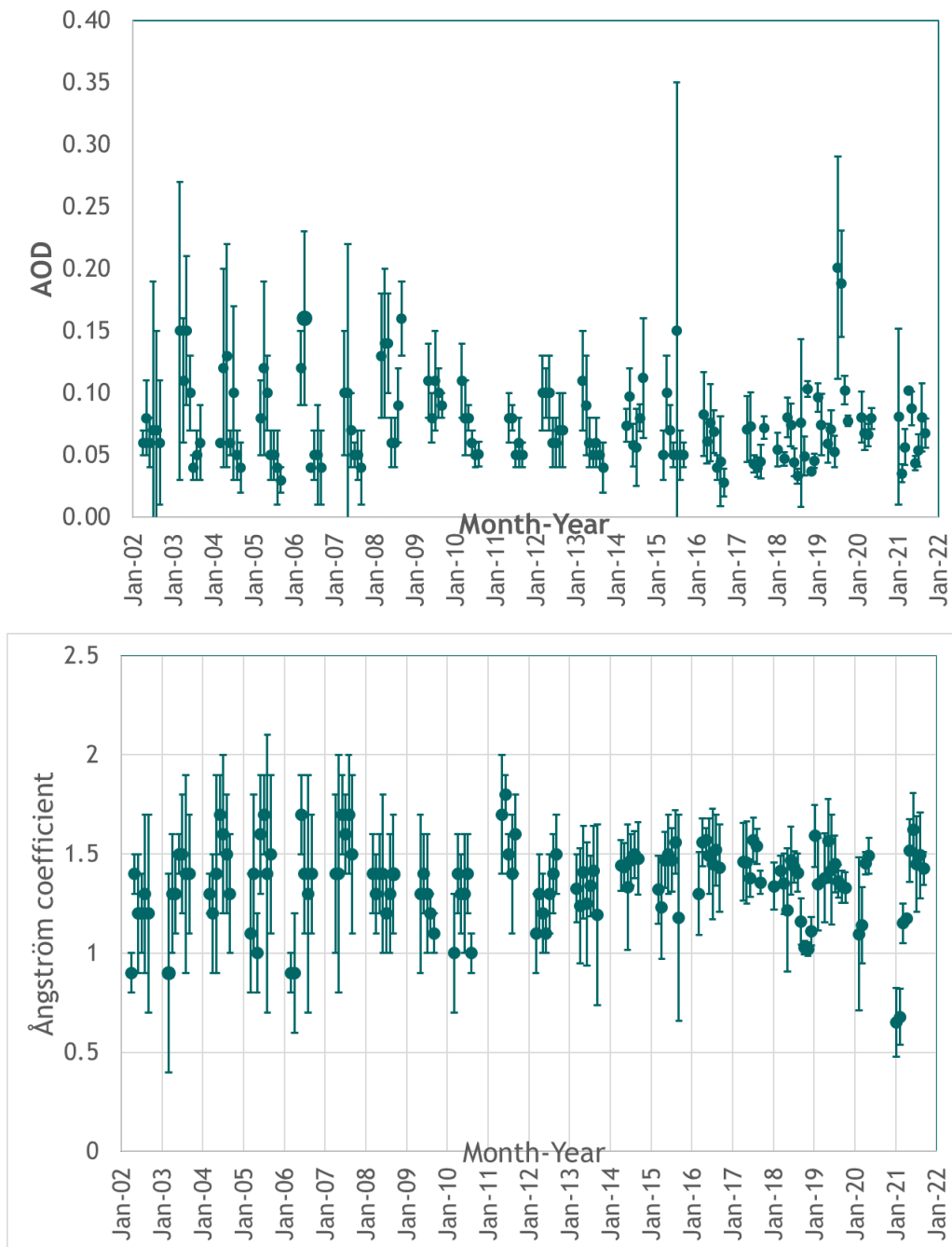


Figure 59: 2002 - 2021 time series of aerosol optical depth (AOD) at 500.5 nm wavelength in the atmospheric column above Ny-Ålesund (upper panel) and Ångström coefficient (lower panel). Monthly mean values and standard deviations are given.

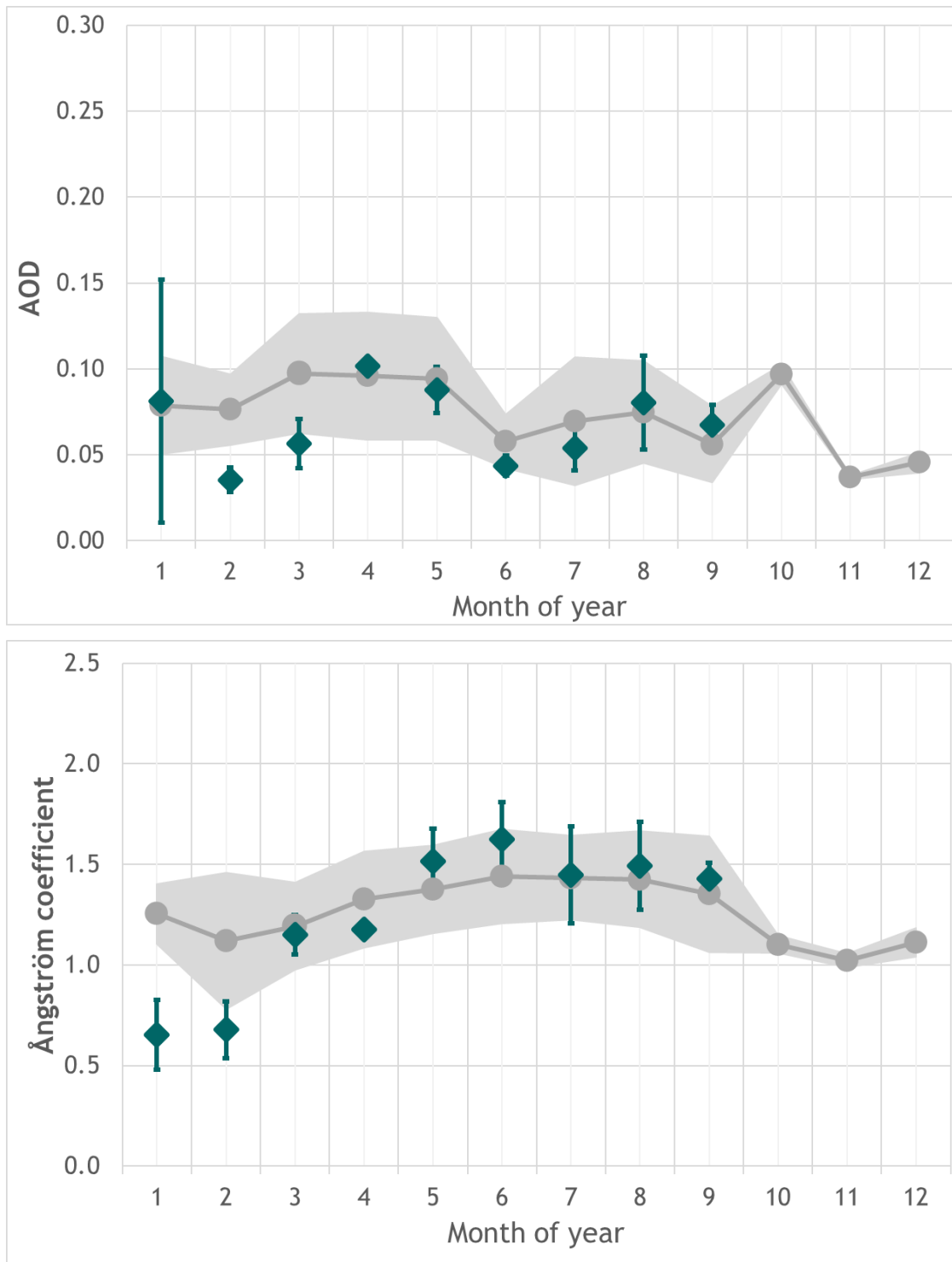


Figure 60: Seasonal variation of the aerosol optical depth (AOD) (upper panel) and Ångström coefficient (lower panel) observed in Ny-Ålesund in 2021. Values marked in grey are the mean and standard deviations for the time period 2002-2021; the 2021 monthly mean and standard deviations are shown in green.



Table 10: Monthly mean values for 2021 and mean for the time period 2002-2021, plus standard deviations, for aerosol optical depth (AOD) and Ångström coefficient observed in Ny-Ålesund. In addition, the number of days with cloud free and quality assured observations are given. Values in February and March are derived from lunar PFR observations.

	Jan	Feb	Mar	Apr	May	Jun	Jul	Aug	Sep	Oct	Nov	Dec
Aerosol optical depth (AOD)												
<b>2021</b>	<b>0.08</b> $\pm 0.07$	<b>0.04</b> $\pm 0.01$	<b>0.06</b> $\pm 0.01$	<b>0.10</b> $\pm 0.00$	<b>0.09</b> $\pm 0.01$	<b>0.04</b> $\pm 0.01$	<b>0.05</b> $\pm 0.01$	<b>0.08</b> $\pm 0.03$	<b>0.07</b> $\pm 0.01$			
<b>Mean 02-21</b>	<b>0.08</b> $\pm 0.03$	<b>0.08</b> $\pm 0.02$	<b>0.10</b> $\pm 0.03$	<b>0.10</b> $\pm 0.04$	<b>0.09</b> $\pm 0.04$	<b>0.06</b> $\pm 0.02$	<b>0.07</b> $\pm 0.04$	<b>0.07</b> $\pm 0.03$	<b>0.06</b> $\pm 0.02$	<b>0.10</b> $\pm 0.01$	<b>0.04</b> $\pm 0.00$	<b>0.05</b> $\pm 0.01$
Ångström coefficient (Å)												
<b>2021</b>	<b>0.65</b> $\pm 0.17$	<b>0.68</b> $\pm 0.14$	<b>1.15</b> $\pm 0.10$	<b>1.18</b> $\pm 0.00$	<b>1.52</b> $\pm 0.16$	<b>1.62</b> $\pm 0.19$	<b>1.45</b> $\pm 0.24$	<b>1.49</b> $\pm 0.22$	<b>1.43</b> $\pm 0.08$			
<b>Mean 02-21</b>	<b>1.25</b> $\pm 0.15$	<b>1.12</b> $\pm 0.34$	<b>1.19</b> $\pm 0.22$	<b>1.33</b> $\pm 0.24$	<b>1.38</b> $\pm 0.22$	<b>1.44</b> $\pm 0.23$	<b>1.43</b> $\pm 0.21$	<b>1.43</b> $\pm 0.24$	<b>1.35</b> $\pm 0.29$	<b>1.10</b> $\pm 0.04$	<b>1.02</b> $\pm 0.03$	<b>1.11</b> $\pm 0.07$
Number of days with cloud-free and quality assured observations (AERONET level 2)												
<b>2021</b>	<b>6</b>	<b>1</b>	<b>1</b>	<b>1</b>	<b>18</b>	<b>14</b>	<b>17</b>	<b>9</b>	<b>8</b>			
<b>Total 02-21</b>	<b>22</b>	<b>15</b>	<b>76</b>	<b>214</b>	<b>229</b>	<b>207</b>	<b>226</b>	<b>177</b>	<b>141</b>	<b>3</b>	<b>2</b>	<b>2</b>

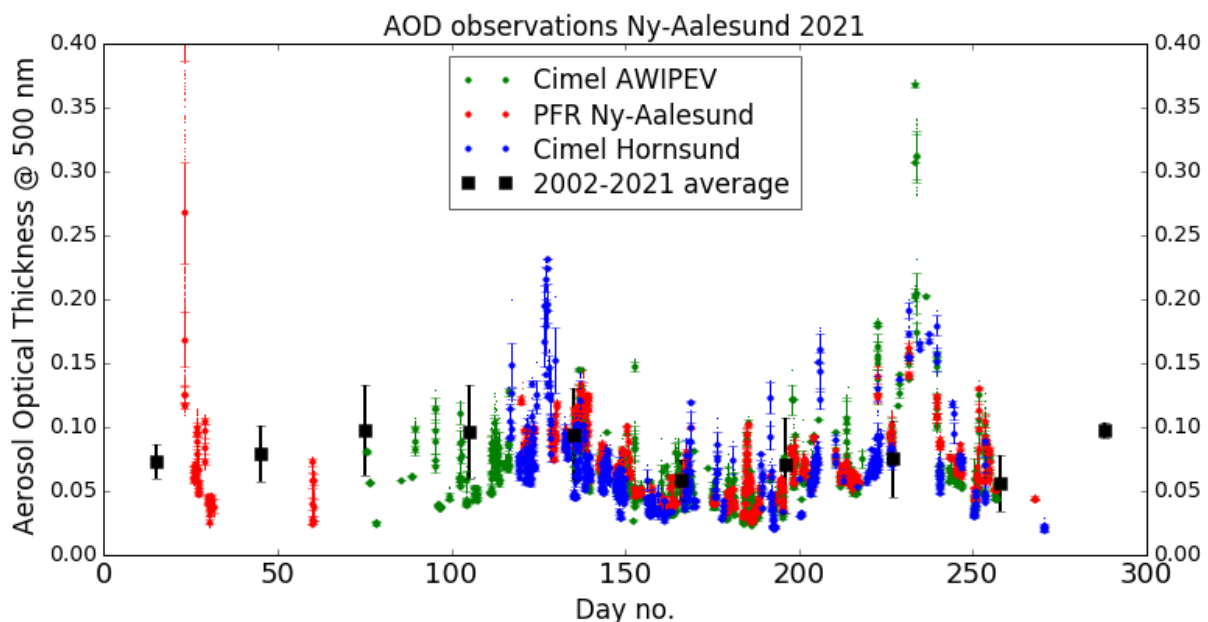


Figure 61: AOD data from Ny-Ålesund in 2021, combining PFR (red; lunar and solar) and Cimel Ny-Ålesund (green) observations. For comparison: Cimel observations in Hornsund (blue) and long-term monthly means from Ny-Ålesund (black squares).

### 3.6.3 Column optical aerosol properties measured by ground-based remote sensing at Troll Station, Antarctica

**Key findings column optical aerosol properties measured by ground-based remote sensing at Troll Station, Antarctica** Aerosol optical depth (AOD) values returned to typical monthly mean values after a deviation in 2020, including a large monthly variation which also has been recorded in previous years. Ångström exponents and their annual also follow closely the 7-year mean.

In austral summer 2006/2007, NILU established an atmospheric observatory at the Norwegian Troll Station (72°01'S, 2°32'E, 1270 m a.s.l.). During the first years of operation, the observatory was located close to the main building of Troll, which caused frequent episodes of local pollution inhibiting aerosol and pollution measurements focusing on long-range transport. For this reason, in January 2014, the atmospheric monitoring station was moved to Trollhaugen, which is more than 2 km away from the main station and at an elevation of more than 280 m above the station. The original instrumentation included a sun PFR instrument from PMOD/WRC (instrument #513); it has been operated quasi-continuously since, but with largely improved measurement statistics after the move of the atmospheric observatory to Trollhaugen.

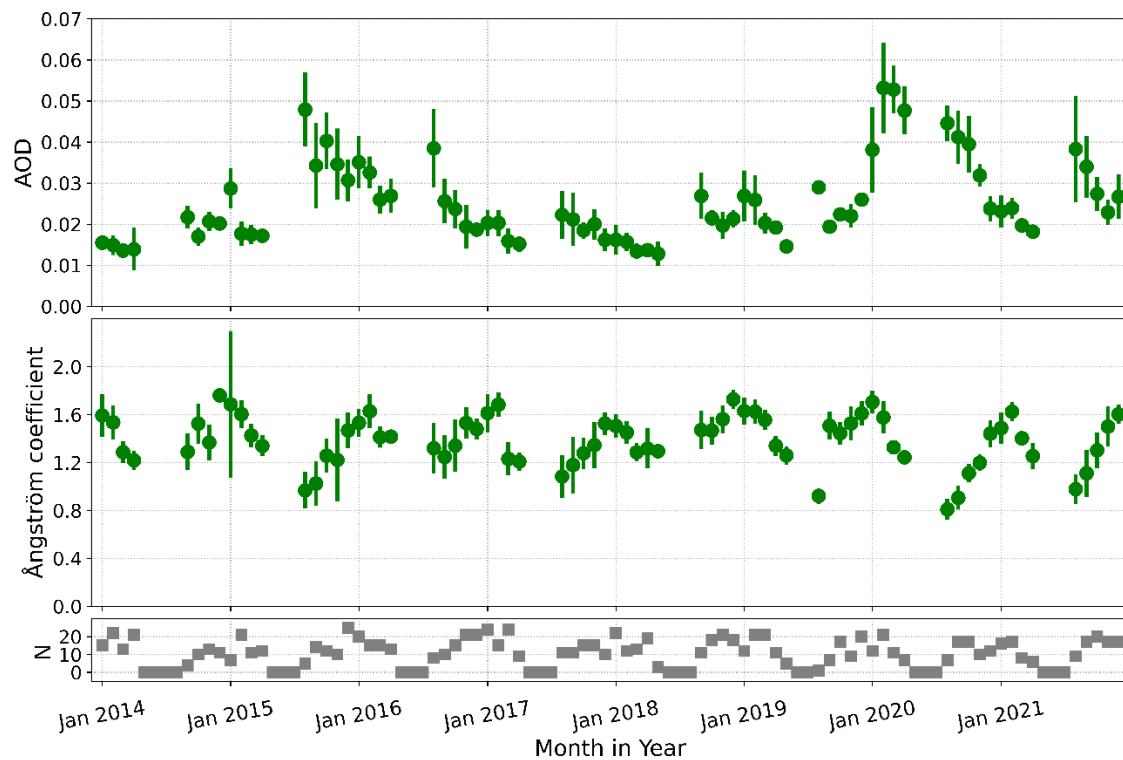


Figure 62: 2014 - 2021 time series of aerosol optical depth (AOD) at 500.5 nm wavelength in the atmospheric column above Trollhaugen Observatory, Antarctica (upper panel), Ångström coefficient (centre panel), and number of days per month with measurements. Monthly mean values and standard deviations are given

Here we present the measurements collected since the move, i.e., from the years 2014 to 2021. Figure 62 shows the series of monthly means of both AOD at 500.5 nm, the multi-wavelength Ångström exponent, and the number of days with usable observations, while Figure 63 displays the 2021 monthly means on the background of the whole 7-year average and the total variability. In contrast to 2020, the AOD values returned to typical monthly mean values (0.013 to 0.023 before the polar night, 0.025

to 0.04 after the polar night) in 2021. Also the Ångström exponents and their annual cycle with lowest values (around 1.0) in austral winter and a maximum of 1.6 in summer follow closely the 7-year mean.

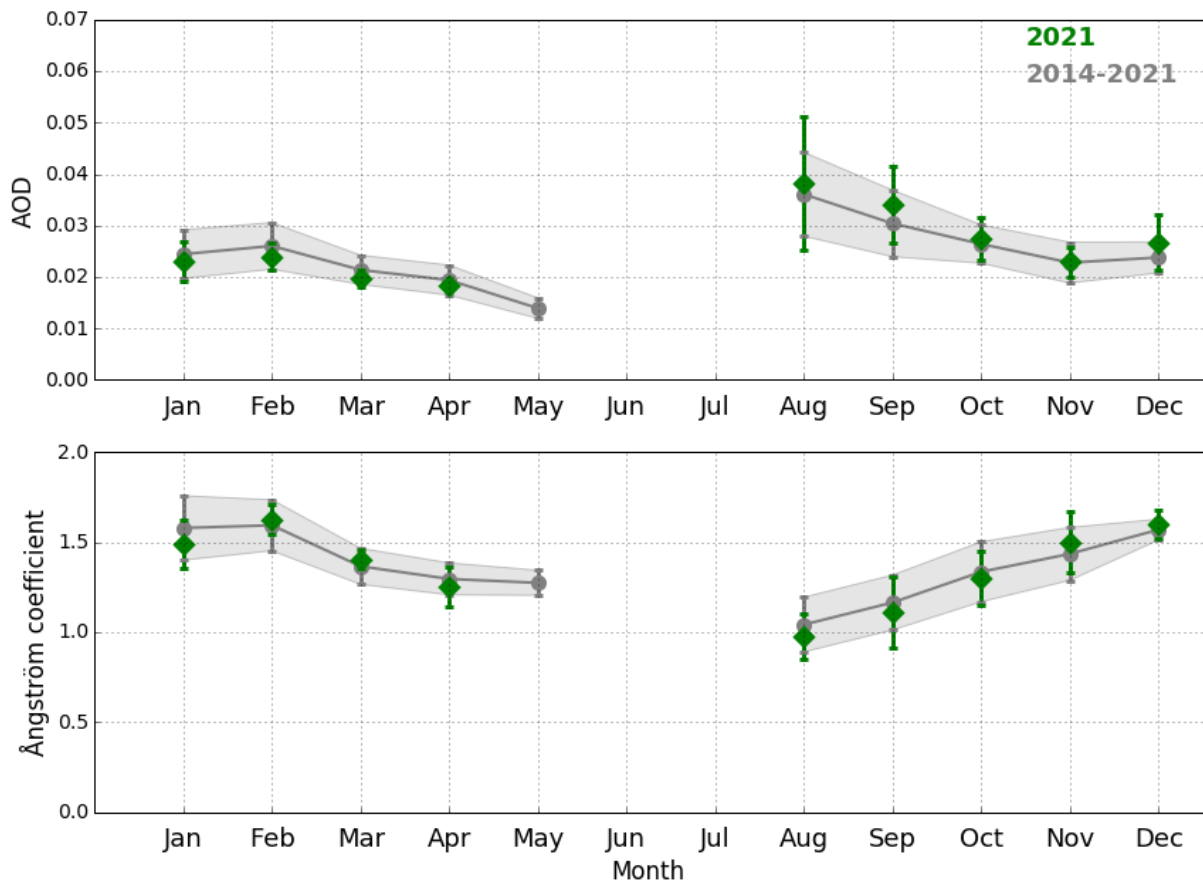


Figure 63: Seasonal variation of the aerosol optical depth (AOD) (upper panel) and Ångström coefficient (lower panel) observed at Troll Station, Antarctica. Values marked in grey are the mean and standard deviations for the time period 2009-2021; the 2021 monthly mean and standard deviations are shown in green.

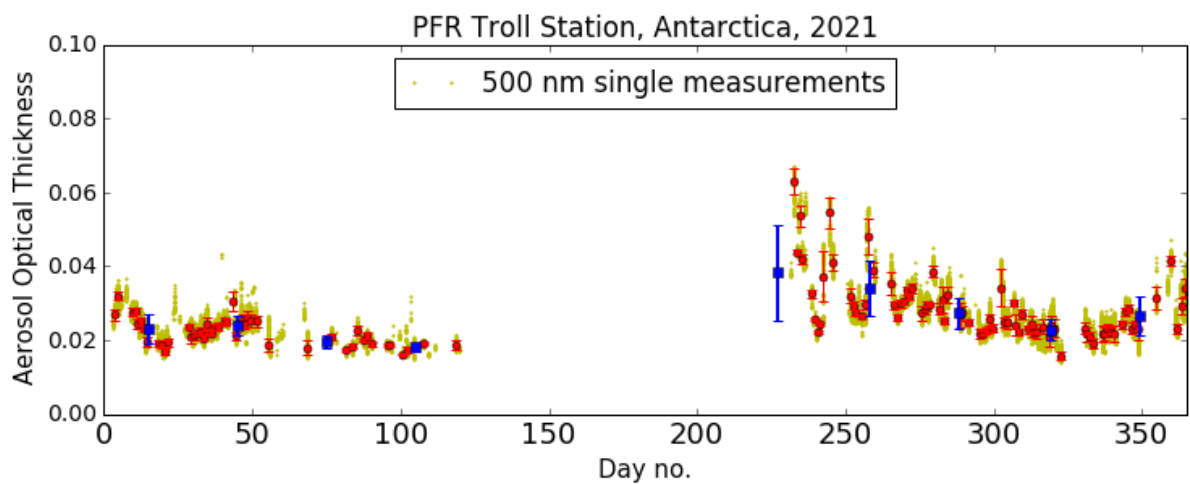


Figure 64: Aerosol optical depth (AOD) observations from Troll in 2021. The graph shows both monthly means (dark blue squares with “error bars”), daily means with variations (red dots with “error” bars) and single measurements (yellow-green marks).

Figure 64 underlines the relatively stable low-AOD conditions in early 2021, while in August and early September there was larger (though systematic/consistent) variation at a weekly time scale resulting in the marked larger monthly variation which also has been recorded in previous years.

*Table 11: Monthly mean values for 2021 and means for the time period 2014-2021 plus standard deviations, for aerosol optical depth (AOD) and Ångström coefficient observed at Trollhaugen Observatory. In addition, the number of days with cloud-free and quality-assured observations is given.*

	Jan	Feb	Mar	Apr	May	Jun	Jul	Aug	Sep	Oct	Nov	Dec
Aerosol optical depth (AOD)												
<b>2021</b>	<b>0.023</b> ±0.004	<b>0.024</b> ±0.003	<b>0.020</b> ±0.002	<b>0.018</b> ±0.001				<b>0.038</b> ±0.013	<b>0.034</b> ±0.008	<b>0.027</b> ±0.004	<b>0.023</b> ±0.003	<b>0.027</b> ±0.005
<b>Mean 14-21</b>	<b>0.024</b> ±0.005	<b>0.026</b> ±0.005	<b>0.021</b> ±0.003	<b>0.019</b> ±0.003	<b>0.014</b> ±0.002			<b>0.036</b> ±0.008	<b>0.030</b> ±0.006	<b>0.026</b> ±0.004	<b>0.023</b> ±0.004	<b>0.024</b> ±0.003
Ångström coefficient (Å)												
<b>2021</b>	<b>1.49</b> ± 0.13	<b>1.63</b> ± 0.08	<b>1.40</b> ± 0.05	<b>1.25</b> ± 0.11				<b>0.98</b> ± 0.13	<b>1.11</b> ± 0.20	<b>1.30</b> ± 0.15	<b>1.50</b> ± 0.17	<b>1.60</b> ± 0.08
<b>Mean 14-21</b>	<b>1.58</b> ±0.16	<b>1.59</b> ±0.12	<b>1.37</b> ±0.09	<b>1.30</b> ±0.09	<b>1.27</b> ±0.07			<b>1.04</b> ±0.15	<b>1.16</b> ±0.17	<b>1.34</b> ±0.13	<b>1.43</b> ±0.16	<b>1.57</b> ± 0.10
Number of days with cloud-free and quality assured observations (AERONET level 2)												
<b>2021</b>	<b>16</b>	<b>17</b>	<b>8</b>	<b>6</b>				<b>9</b>	<b>17</b>	<b>20</b>	<b>17</b>	<b>17</b>
<b>Total 14-21</b>	<b>128</b>	<b>144</b>	<b>116</b>	<b>98</b>	<b>8</b>			<b>41</b>	<b>91</b>	<b>124</b>	<b>116</b>	<b>134</b>

### 3.7 Summary of aerosol column properties

As pointed out in the introduction, these type of measurements gives information about the total load of aerosols in the radiation path between the sun or another external light source, like the moon and bright stars and the instrument. The Cimel network has introduced routine moon measurements in many of their instruments, including the one at Birkenes, but because of the additional challenge of reference lunar radiance (due to the continuously changing lunar phase), only preliminary data (level 1.5) are currently provided. As there are more reliable solar measurements throughout the year, moon measurements have not been used so far. In Ny-Ålesund, the need for moon measurements is much severe because of the almost 5 months without sufficient sunshine (the sun elevation must be larger than 5 degrees).

The mostly weak attenuation due to aerosols necessitates an extremely careful and frequent calibration of the instrument and regular updates on the respective external light source. The only solution to fulfil these criteria has been to have dual instruments at sites with continuous light (Birkenes) and very limited accessibility (Troll), and complementary instruments at sites with long periods without the main light source (the sun; Ny-Ålesund). From the end of 2018, this has been in place at all our sites.

The columnar character of the AOD measurements and the missing knowledge about the altitude of an observed aerosol layer poses a severe hinder to combine them with in-situ measurements. In a recent project (*Re-evaluation and Homogenization of Aerosol Optical Depth Observations in Svalbard, ReHearsol*), 19 years of AOD and in-situ measurements in Ny-Ålesund were analysed with respect to high-aerosol load episodes. The conclusion was that the in-situ measurements only catch about 15 – 25% of the events that are seen in the AOD data (Hansen et al., 2022). The only solution to this problem is to increase the amount of height-resolved observations, either with airborne techniques or through the inclusion of more satellite RS observations (which, however, also have large methodological and technical challenges at high latitudes).

With regard to the year 2021, the columnar observations at all three Norwegian sites showed a return to rather “normal” conditions after the unusual and in periods extreme conditions in 2019 and 2020. A noticeable detail of the measurements in Birkenes and Ny-Ålesund is that the only high-AOD episodes occurred in late summer. This continues the trend of fewer pollution events in late winter (Arctic haze) and more frequent and intense pollution events during summer due to biomass burning in the boreal forests (Xian et al., 2022; Hansen et al., 2022).

## 4 References

- Aas, W., Berglen, T. F., Eckhardt, S., Fiebig, M., Solberg, S., Yttri, K.E. (2022) Monitoring of long-range transported air pollutants in Norway. Annual Report 2021. (NILU rapport 18/2022). Kjeller: NILU.
- Asmi, A., Collaud Coen, M., Ogren, J. A., Andrews, E., Sheridan, P., Jefferson, A., Weingartner, E., Baltensperger, U., Bukowiecki, N., Lihavainen, H., Kivekäs, N., Asmi, E., Aalto, P. P., Kulmala, M., Wiedensohler, A., Birmili, W., Hamed, A., O'Dowd, C., G Jennings, S., Weller, R., Flentje, H., Fjaeraa, A. M., Fiebig, M., Myhre, C.E.L., Hallar, A. G., Swietlicki, E., Kristensson, A., Laj, P. (2013) Aerosol decadal trends - Part 2: In-situ aerosol particle number concentrations at GAW and ACTRIS stations. *Atmos. Chem. Phys.*, *13*, 895-916. <https://doi.org/10.5194/acp-13-895-2013>.
- Baasandorj, M., Hall, B. D., Burkholder, J. B. (2012) Rate coefficients for the reaction of O(<sup>1</sup>D) with the atmospherically long-lived greenhouse gases NF<sub>3</sub>, SF<sub>5</sub>CF<sub>3</sub>, CHF<sub>3</sub>, C<sub>2</sub>F<sub>6</sub>, c-C<sub>4</sub>F<sub>8</sub>, n-C<sub>5</sub>F<sub>12</sub>, and n-C<sub>6</sub>F<sub>14</sub>. *Atmos. Chem. Phys.*, *12*, 11753-11764. <https://doi.org/10.5194/acp-12-11753-2012>.
- Coen, M. Collaud., Andrews, E., Alastuey, A., Arsov, T. P., Backman, J., Brem, B. T., Bukowiecki, N., Couret, C., Eleftheriadis, K., Flentje, H., Fiebig, M., Gysel-Beer, M., Hand, J. L., Hoffer, A., Hooda, R., Hueglin, C., Joubert, W., Keywood, M., Kim, J. E., Kim, S.-W., Labuschagne, C., Lin, N.-H., Lin, Y., Lund Myhre, C., Luoma, K., Lyamani, H., Marinoni, A., Mayol-Bracero, O. L., Mihalopoulos, N., Pandolfi, M., Prats, N., Prenni, A. J., Putaud, J.-P., Ries, L., Reisen, F., Sellegri, K., Sharma, S., Sheridan, P., Sherman, J. P., Sun, J., Titos, G., Torres, E., Tuch, T., Weller, R., Wiedensohler, A., Zieger, P. and Laj, P. (2020) Multidecadal trend analysis of in situ aerosol radiative properties around the world. *Atmos. Chem. Phys.*, *20*, 8867-8908. <https://doi.org/10.5194/acp-20-8867-2020>.
- Coen, M. C., Andrews, E., Asmi, A., Baltensperger, U., Bukowiecki, N., Day, D., Fiebig, M., Fjaeraa, A. M., Flentje, H., Hyvärinen, A., Jefferson, A., Jennings, S. G., Kouvarakis, G., Lihavainen, H., Myhre, C. L., Malm, W. C., Mihalopoulos, N., Molnar, J. V., O'Dowd, C., Ogren, J. A., Schichtel, B. A., Sheridan, P., Virkkula, A., Weingartner, E., Weller, R., Laj, P. (2013) Aerosol decadal trends - Part 1: In-situ optical measurements at GAW and IMPROVE stations. *Atmos. Chem. Phys.*, *13*, 869-894. <https://doi.org/10.5194/acp-13-869-2013>.
- Coen, M.C., Weingartner, E., Apituley, A., Ceburnis, D., Fierz-Schmidhauser, R., Flentje, H., Henzing, J. S. (2010) Minimizing light absorption measurement artifacts of the Aethalometer: evaluation of five correction algorithms. *Atmos. Meas. Tech*, *3*, 457–474. <https://doi.org/10.5194/amt-3-457-2010>.
- Dalsøren, S. B., Myhre, C. L., Myhre, G., Gomez-Pelaez, A. J., Spøvde, O. A., Isaksen, I. S. A., Weiss, R. F., Harth, C. M. (2016) Atmospheric methane evolution the last 40 years. *Atmos. Chem. Phys.*, *16*, 3099-3126. <https://doi.org/10.5194/acp-16-3099-2016>.
- Dalsøren, S. D., Myhre, G., Hodnebrog, Ø., Myhre, C. L., Stohl, A., Pissò, I., Schwietzke, S., Höglund-Isaksson, L., Helmig, D., Reimann, S., Sauvage, S., Schmidbauer, N., Read, K. A., Carpenter, L. J., Lewis, A. C., Punjabi, S., Wallasch, M. (2018) Discrepancy between simulated and observed ethane and propane levels explained by underestimated fossil emissions. *Nature Geosci.*, *11*, 178-184. <https://doi.org/10.1038/s41561-018-0073-0>.
- Delene, D.J., Ogren, J.A. (2002) Variability of aerosol optical properties at four North American surface monitoring sites. *J. Atmos. Sci.*, *59*, 1135-1150.
- Dlugokencky, E.J., Hall, B. D., Montzka, S. A., Dutton, G., Mühle, J., Elkins, J. W. (2019) Long-lived greenhouse gases [in "State of the Climate in 2019"]. *Bull. Amer. Meteor. Soc.*, *101*, No 8, S48–52. <https://doi.org/10.1175/2020BAMSStateoftheClimate.1>.
- Dlugokencky, E.J., Hall, B. D., Montzka, S. A., Dutton, G., Mühle, J., Elkins, J. W. (2018) Long-lived greenhouse gases [in "State of the Climate in 2017"]. *Bull. Amer. Meteor. Soc.*, *99*, S46-49. <https://doi.org/10.1175/2018BAMSStateoftheClimate.1>.

- Drinovec, L., Močnik, G., Zotter, P., Prévôt, A. S. H., Ruckstuhl, C., Coz, E., Rupakheti, M., Sciare, J., Müller, T., Wiedensohler, A., Hansen, A. D. A. (2015) The “dual-spot” Aethalometer: an improved measurement of aerosol black carbon with real-time loading compensation. *Atmos. Meas. Tech.*, **8**, 1965-1979. <https://doi.org/10.5194/amt-8-1965-2015>.
- Etioppe, G., Ciccioli, P. (2009) Earth's Degassing: A Missing Ethane and Propane Source. *Science* **323**, 478. <https://doi.org/10.1126/science.1165904>.
- Etminan, M., Myhre, G., Highwood, E. J., Shine, K. P. (2016) Radiative forcing of carbon dioxide, methane, and nitrous oxide: A significant revision of the methane radiative forcing, *Geophys. Res. Lett.*, **43**, 12,614-12,623. <https://doi.org/10.1002/2016GL071930>.
- Fiebig, M., Hirdman, D., Lunder, C. R., Ogren, J. A., Solberg, S., Stohl, A., Thompson, R. L. (2014) Annual cycle of Antarctic baseline aerosol: controlled by photooxidation-limited aerosol formation. *Atmos. Chem. Phys.*, **14**, 3083-3093. <https://doi.org/10.5194/acp-14-3083-2014>.
- Fisher, R. E., France, J. L., Lowry, D., Lanoisellé, M., Brownlow, R., Pyle, J. A., Cain, M., Warwick, N., Skiba, U. M., Drewer, J., Dinsmore, K. J., Leeson, S. R., Bauguitte, S. J.-B., Wellpott, A., O'Shea, S. J., Allen, G., Gallagher, M. W., Pitt, J., Percival, C. J., Bower, K., George, C., Hayman, G. D., Aalto, T., Lohila, A., Aurela, M., Laurila, T., Crill, P. M., McCalley, C. K. and Nisbet, E. G. (2017) Measurement of the  $^{13}\text{C}$  isotopic signature of methane emissions from northern European wetlands. *Global Biogeochem. Cycles*, **31**, 605-623. <https://doi.org/10.1002/2016GB005504>.
- Forster, P., T. Storelvmo, K. Armour, W. Collins, J. L. Dufresne, D. Frame, D. J. Lunt, T. Mauritsen, M. D. Palmer, M. Watanabe, M. Wild, H. Zhang, 2021, The Earth's Energy Budget, Climate Feedbacks, and Climate Sensitivity. In: *Climate Change 2021: The Physical Science Basis. Contribution of Working Group I to the Sixth Assessment Report of the Intergovernmental Panel on Climate Change* [Masson-Delmotte, V., P. Zhai, A. Pirani, S. L. Connors, C. Péan, S. Berger, N. Caud, Y. Chen, L. Goldfarb, M. I. Gomis, M. Huang, K. Leitzell, E. Lonnoy, J.B.R. Matthews, T. K. Maycock, T. Waterfield, O. Yelekçi, R. Yu and B. Zhou (eds.)]. Cambridge University Press. In Press.
- France, J. L., Cain, M., Fisher, R. E., Lowry, D., Allen, G., O'Shea, S. J., Illingworth, S., Pyle, J., Warwick, N., Jones, B. T., Gallagher, M. W., Bower, K., Le Breton, M., Percival, C., Muller, J., Wellpott, A., Bauguitte, S., George, C., Hayman, G. D., Manning, A. J., Myhre, C. L., Lanoisellé, M., Nisbet, E. G. (2016) Measurements of  $\delta^{13}\text{C}$  in  $\text{CH}_4$  and using particle dispersion modeling to characterize sources of Arctic methane within an air mass. *J. Geophys. Res. Atmos.*, **121**, 14,257-14,270. <https://doi.org/10.1002/2016JD026006>.
- Gliß, J., Mortier, A., Schulz, M., Andrews, E., Balkanski, Y., Bauer, S. E., Benedictow, A. M. K., Bian, H., Checa-Garcia, R., Chin, M., Ginoux, P., Griesfeller, J. J., Heckel, A., Kipling, Z., Kirkevåg, A., Kokkola, H., Laj, P., Le Sager, P., Lund, M. T., Lund Myhre, C., Matsui, H., Myhre, G., Neubauer, D., van Noije, T., North, P., Olivie, D. J. L., Sogacheva, L., Takemura, T., Tsigaridis, K. and Tsyro, S. G. (2020) Multi-model evaluation of aerosol optical properties in the AeroCom phase III Control experiment, using ground and space based columnar observations from AERONET, MODIS, AATSR and a merged satellite product as well as surface in-situ observations from GAW sites. *Atmos. Chem. Phys.* <https://doi.org/10.5194/acp-2019-1214>.
- Groot Zwaftink, C. D., Aas, W., Eckhardt, S., Evangelidou, N., Hamer, P., Johnsrud, M., Kylling, A., Platt, S. M., Stebel, K., Uggerud, H., and Yttri, K. E. (2022) What caused a record high PM10 episode in northern Europe in October 2020? *Atmos. Chem. Phys.*, **22**, 3789-3810. <https://doi.org/10.5194/acp-22-3789-2022>.
- Gulev, S. K., P. W. Thorne, J. Ahn, F. J. Dentener, C. M. Domingues, S. Gerland, D. Gong, D. S. Kaufman, H. C. Nnamchi, J. Quaas, J. A. Rivera, S. Sathyendranath, S. L. Smith, B. Trewin, K. von Shuckmann, R. S. Vose (2021) Changing State of the Climate System. In: *Climate Change 2021: The Physical Science Basis. Contribution of Working Group I to the Sixth Assessment Report of the*

- Intergovernmental Panel on Climate Change* [Masson-Delmotte, V., P. Zhai, A. Pirani, S. L. Connors, C. Péan, S. Berger, N. Caud, Y. Chen, L. Goldfarb, M. I. Gomis, M. Huang, K. Leitzell, E. Lonnoy, J. B. R. Matthews, T. K. Maycock, T. Waterfield, O. Yelekçi, R. Yu and B. Zhou (eds.)]. Cambridge University Press. In Press.
- Hall, B. D., Montzka, S. A., Dutton, G., Mühle, J., Elkins, J. W. (2017) Long-lived greenhouse gases [in "State of the Climate in 2016"]. *Bull. Amer. Meteor. Soc.*, 98 (8), S43-S46. <https://doi.org/10.1175/2017BAMSStateoftheClimate.1>.
- Hall, B. D., Montzka, S. A., Dutton, G., Miller, B. R., Elkins, J. W. (2020) Ozone-depleting substances [in "State of the Climate in 2019"]. *Bull. Amer. Meteor. Soc.*, 101 (8), S75-S76. <https://doi.org/10.1175/BAMS-D-20-0104.1>.
- Hansen, K. M., Christensen, J. H., Geels, C., Silver, J. D., and Brandt, J. (2015) Modelling the impact of climate change on the atmospheric transport and the fate of persistent organic pollutants in the Arctic. *Atmos. Chem. Phys.*, 15, 6549–6559, <https://doi.org/10.5194/acp-15-6549-2015>.
- Hansen, G. H., Zielinski, T., Pakszys, P., Ritter, C., Gilardoni, S., Eleftheriadis, K., Kouremeti, N., Mateos, D., Herrero, S., Kazadzis, S., Mazzola, M., and Stebel, K. (2022) Re-evaluation and Homogenization of Aerosol Optical Depth Observations in Svalbard (ReHearsol). Annual report (NILU report 28/2022). Kjeller: NILU.
- Hartmann, D.L., Klein Tank, A. M. G., Rusticucci, M., Alexander, L.V., Brönnimann, S., Charabi, Y., Dentener, F. J., Dlugokencky, E. J., Easterling, D. R., Kaplan, A., Soden, B. J., Thorne, P. W., Wild, M., Zhai, P. M. (2013) Observations: atmosphere and surface. In: *Climate Change 2013: The Physical Science Basis. Contribution of Working Group I to the Fifth Assessment Report of the Intergovernmental Panel on Climate Change*. Ed. by Stocker, T. F., Qin, D., Plattner, G.-K., Tignor, M., Allen, S. K., Boschung, J., Nauels, A., Xia, Y., Bex, V., Midgley, P.M. Cambridge, Cambridge University Press. pp. 159-254.
- Heintzenberg, J. (1980) Particle size distribution and optical properties of Arctic haze. *Tellus*, 32, 251-260. <https://doi.org/10.3402/tellusa.v32i3.10580>.
- Helmig, D., Rossabi, S., Hueber, J., Tans, P., Montzka, S. A., Masarie, K., Thoning, K., Plass-Duelmer, C., Claude, A., Carpenter, L. J., Lewis, A. C., Punjabi, S., Reimann, S., Vollmer, M. K., Steinbrecher, R., Hannigan, J. W., Emmons, L. K., Mahieu, E., Franco, B., Smale, D., Pozzer, A. (2016) Reversal of global atmospheric ethane and propane trends largely due to US oil and natural gas production. *Nature Geosci.*, 9, 490-495. <https://doi.org/10.1038/ngeo2721>.
- Hewitt, C. Nicholas (ed.) (1999) *Reactive Hydrocarbons in the Atmosphere*. San Diego, CA, Academic Press. P. 313.
- Hodnebrog, Ø., Etmann, M., Fuglestad, J.S., Marston, G., Myhre, G., Nielsen, C.J., Shine, K.P., Wallington, T.J. (2013) Global warming potentials and radiative efficiencies of halocarbons and related compounds: A comprehensive review, (2013) *Reviews of Geophysics*, 51, 300-378. <https://doi.org/10.1002/rog.20013>.
- Hossaini, R., Chipperfield, M. P., Montzka, S. A., Leeson, A. A., Dhomse, S. and Pyle, J. A (2017) The increasing threat to stratospheric ozone from dichloromethane. *Nat. Commun.*, 8, 15962, <https://doi.org/10.1038/ncomms15962>.
- IPCC (2021) *Climate Change 2021: The Physical Science Basis. Contribution of Working Group I to the Sixth Assessment Report of the Intergovernmental Panel on Climate Change*[Masson-Delmotte, V., P. Zhai, A. Pirani, S.L. Connors, C. Péan, S. Berger, N. Caud, Y. Chen, L. Goldfarb, M.I. Gomis, M. Huang, K. Leitzell, E. Lonnoy, J.B.R. Matthews, T.K. Maycock, T. Waterfield, O. Yelekçi, R. Yu, and B. Zhou (eds.)]. Cambridge University Press, Cambridge, United Kingdom and New York, NY, USA, In press, <https://doi.org/10.1017/9781009157896>.



- IPCC (2021b) Summary for Policymakers. In: *Climate Change 2021: The Physical Science Basis. Contribution of Working Group I to the Sixth Assessment Report of the Intergovernmental Panel on Climate Change* [Masson-Delmotte, V., P. Zhai, A. Pirani, S.L. Connors, C. Péan, S. Berger, N. Caud, Y. Chen, L. Goldfarb, M.I. Gomis, M. Huang, K. Leitzell, E. Lonnoy, J.B.R. Matthews, T.K. Maycock, T. Waterfield, O. Yelekçi, R. Yu, and B. Zhou (eds.)]. Cambridge University Press, Cambridge, United Kingdom and New York, NY, USA, pp. 3–32, <https://doi.org/10.1017/9781009157896.001>.
- Isaksen, I. S. A., Hov, Ø. (1987) Calculation of trends in the tropospheric concentration of O<sub>3</sub>, OH, CO, CH<sub>4</sub> and NO<sub>x</sub>. *Tellus*, 39B, 271-285.
- Jackson, R.B., Saunio, M., Bousquet, P., Canadell, J.G., Poulter, B., Stavert, A.R., Bergamaschi, P., Niwa, Y., Segers, A., and Tsuruta, A. (2020) *Environ. Res. Lett.*, 15, 071002. <https://doi.org/10.1088/1748-9326/ab9ed2>.
- Laj, P., Bigi, A., Rose, C. Andrews, E. Lund Myhre, C. Collaud Coen, M. Lin, Y. Wiedensohler, A. Schulz, M. Ogren, J. A. Fiebig, M. Gliß, J. Mortier, A. Pandolfi, M. Petäjä, T. Kim, S.-W. Aas, W. Putaud, J.-P. Mayol-Bracero, O. Keywood, M., Labrador, L. Aalto, P. Ahlberg, E. Alados Arboledas, L. Alastuey, A. Andrade, M. Artíñano, B. Ausmeel, S. Arsov, T. Asmi, E. Backman, J. Baltensperger, U., Bastian, S., Bath, O., Beukes, J. P., Brem, B. T., Bukowiecki, N., Conil, S., Couret, C., Day, D., Dayantolis, W., Degorska, A., Eleftheriadis, K., Fetfatzis, P., Favez, O., Flentje, H., Gini, M. I., Gregorič, A., Gysel-Beer, M., Hallar, A. G., Hand, J., Hoffer, A., Hueglin, C., Hooda, R. K., Hyvärinen, A., Kalapov, I., Kalivitis, N., Kasper-Giebl, A., Kim, J. E., Kouvarakis, G., Kranjc, I., Krejci, R., Kulmala, M., Labuschagne, C., Lee, H.-J., Lihavainen, H., Lin, N.-H., Löschau, G., Luoma, K., Marinoni, A., Martins Dos Santos, S., Meinhardt, F., Merkel, M., Metzger, J.-M., Mihalopoulos, N., Nguyen, N. A., Ondracek, J., Pérez, N., Perrone, M. R., Petit, J.-E., Picard, D., Pichon, J.-M., Pont, V., Prats, N., Prenni, A., Reisen, F., Romano, S., Sellegri, K., Sharma, S., Schauer, G., Sheridan, P., Sherman, J. P., Schütze, M., Schwerin, A., Sohmer, R., Sorribas, M., Steinbacher, M., Sun, J., Titos, G., Toczko, B., Tuch, T., Tulet, P., Tunved, P., Vakkari, V., Velarde, F., Velasquez, P., Villani, P., Vratolis, S., Wang, S.-H., Weinhold, K., Weller, R., Yela, M., Yus-Diez, J., Zdimal, V., Zieger, P., and Zikova, N. (2020) A global analysis of climate-relevant aerosol properties retrieved from the network of Global Atmosphere Watch (GAW) near-surface observatories. *Atmos. Meas Tech.*, 13, 4353-4392. <https://doi.org/10.5194/amt-13-4353-2020>.
- Lan, X., B. D. Hall, G. Dutton, J. Mühle, J. W. Elkins, and I. J. Vimon (2022) Long-lived greenhouse gases [in "State of the Climate in 2021"]. *Bull. Amer. Meteor. Soc.*, 103 (8), S81–S84. <https://doi.org/10.1175/BAMS-D-22-0092.1>
- Lan, X., Tans, P., Hall, B. D., Dutton, G., Mühle, J., Elkins, J. W., Vimont, I. (2021) Long-lived greenhouse gases [in "State of the Climate in 2020"]. *Bull. Amer. Meteor.*, 102 (8), S53–S87. <https://doi.org/10.1175/BAMS-D-21-0098.1>.
- Montzka, S. A., Dutton, G. S., Yu, P., Ray, E., Portmann, R. W., Daniel, J. S., Kuijpers, L., Hall, B. D., Mondeel, D., Siso, Nance, J. D., Rigby, M., Manning, A. J., Hu, L., Moore, F., Miller, B. R., Elkins, J. W. (2018) An unexpected and persistent increase in global emissions of ozone-depleting CFC-11. *Nature*, 557, 413-417.
- Mortier, A., Gliss, J., Schulz, M., Aas, W., Andrews, E., Bian, H., Chin, M., Ginoux, P., Hand, J., Holben, B., Hua, Z., Kipling, Z., Kirkevåg, A., Laj, P., Lurton, T., Myhre, G., Neubauer, D., Olivié, D., von Salzen, K., Takemura, T. and Tilmes, S. (2020) Evaluation of climate model aerosol trends with ground-based observations over the last two decades -- an AeroCom and CMIP6 analysis. *Atmos. Chem. Phys.*, 20, 13355-13378. <https://doi.org/10.5194/acp-20-13355-2020>.
- Moskvitch, K. (2014) Mysterious Siberian crater attributed to methane. *Nature*. <https://doi.org/10.1038/nature.2014.15649>.
- Myhre, C. L., Hermansen, O., Fiebig, M., Lunder, C., Fjæraa, A. M., Svendby, T., Platt, M., Hansen, G., Schmidbauer, N., Krognæs, T. (2016) Monitoring of greenhouse gases and aerosols at Svalbard and

- Birkenes in 2015 - Annual report. Kjeller, NILU (Miljødirektoratet rapport, M-694/2016) (NILU report, 31/2016).
- Myhre, C. L., Ferré, B., Platt, S. M., Silyakova, A., Hermansen, O., Allen, G., Pisso, I., Schmidbauer, N., Stohl, A., Pitt, J., Jansson, P., Greinert, J., Percival, C., Fjaeraa, A. M., O'Shea, S., Gallagher, M., Le Breton, M., Bower, K., Bauguitte, S., Dalsøren, S., Vadakkepuliambatta, S., Fisher, R., Nisbet, E., Lowry, D., Myhre, G., Pyle, J., Cain, M., Mienert, J. (2016) Large methane release from the Arctic seabed west of Svalbard, but small release to the atmosphere. *Geophys. Res. Lett.*, *43*, 4624–4631. <https://doi.org/10.1002/2016GL068999>.
- Myhre, G., Myhre C. L., Forster, P. M., Shine, K. P. (2017) Halfway to doubling of CO<sub>2</sub> radiative forcing. *Nature Geosci.*, *10*, 710-711. <https://doi.org/10.1038/ngeo3036>.
- Myhre, G., Myhre, C. L., Samset, B. H., Storelvmo, T. (2013a) Aerosols and their relation to global climate and climate sensitivity. *Nature Education Knowledge*, *4*(5), 7. <http://www.nature.com/scitable/knowledge/library/aerosols-and-their-relation-to-global-climate-102215345>.
- Myhre, G., Shindell, D., Bréon, F.-M., Collins, W., Fuglestedt, J., Huang, J., Koch, D., Lamarque, J.-F., Lee, D., Mendoza, B., Nakajima, T., Robock, A., Stephens, G., Takemura, T., Zhang, H. (2013b) Anthropogenic and natural radiative forcing. In: *Climate Change 2013: The Physical Science Basis. Contribution of Working Group I to the Fifth Assessment Report of the Intergovernmental Panel on Climate Change*. Ed. by Stocker, T.F., Qin, D., Plattner, G.-K., Tignor, M., Allen, S.K., Boschung, J., Nauels, A., Xia, Y., Bex, V., Midgley, P.M. Cambridge, Cambridge University Press. pp. 659-740.
- Mühle, J., Trudinger, C. M., Western, L. M., Rigby, M., Vollmer, M. K., Park, S., Manning, A. J., Say, D., Ganesan, A., Steele, L. P., Ivy, D. J., Arnold, T., Li, S., Stohl, A., Harth, C. M., Salameh, P. K., McCulloch, A., O'Doherty, S., Park, M.-K., Jo, C. O., Young, D., Stanley, K. M., Krummel, P. B., Mitrevski, B., Hermansen, O., Lunder, C., Evangeliou, N., Yao, B., Kim, J., Hmiel, B., Buizert, C., Petrenko, V. V., Arduini, J., Maione, M., Etheridge, D. M., Michalopoulou, E., Czerniak, M., Severinghaus, J. P., Reimann, S., Simmonds, P. G., Fraser, P. J., Prinn, R. G., and Weiss, R. F. (2019) Perfluorocyclobutane (PFC-318, c-C<sub>4</sub>F<sub>8</sub>) in the global atmosphere. *Atmos. Chem. Phys.*, *19*, 10335–10359. <https://doi.org/10.5194/acp-19-10335-2019>.
- Naik, V., S. Szopa, B. Adhikary, P. Artaxo, T. Berntsen, W. D. Collins, S. Fuzzi, L. Gallardo, A. Kiendler Scharr, Z. Klimont, H. Liao, N. Unger, P. Zanis, 2021, Short-Lived Climate Forcers. In: *Climate Change 2021: The Physical Science Basis. Contribution of Working Group I to the Sixth Assessment Report of the Intergovernmental Panel on Climate Change* [Masson-Delmotte, V., P. Zhai, A. Pirani, S. L. Connors, C. Péan, S. Berger, N. Caud, Y. Chen, L. Goldfarb, M. I. Gomis, M. Huang, K. Leitzell, E. Lonnoy, J. B. R. Matthews, T. K. Maycock, T. Waterfield, O. Yelekçi, R. Yu and B. Zhou (eds.)]. Cambridge University Press. In Press.
- Ng, N. L., Kroll, J.H., Chan, A. W. H., Chhabra, P. S., Flagan, R. C., Seinfeld, J. H. (2007) Secondary organic aerosol formation from m-xylene, toluene, and benzene. *Atmos. Chem. Physics*, *7*, 3909-3922.
- Nicewonger, M. R., Verhulst, K. R., Aydin, M., Saltzman, E. S. (2016) Preindustrial atmospheric ethane levels inferred from polar ice cores: A constraint on the geologic sources of atmospheric ethane and methane. *Geophys. Res. Lett.*, *43*, 214-221. <https://doi.org/10.1002/2015GL066854>.
- Oram, D. E., Mani, F. S., Laube, J. C., Newland, M. J., Reeves, C. E., Sturges, W. T., Penkett, S. A., Brenninkmeijer, C. A. M., Röckmann, T., and Fraser, P. J. (2012) Long-term tropospheric trend of octafluorocyclobutane (c-C<sub>4</sub>F<sub>8</sub> or PFC-318), *Atmos. Chem. Phys.*, *12*, 261-269. <https://doi.org/10.5194/acp-12-261-2012>.
- Pandolfi, M. et al., 2018: A European aerosol phenomenology – 6: scattering properties of atmospheric aerosol particles from 28 ACTRIS sites. *Atmos. Chem. Phys.*, *18*, 7877-7911. <https://doi.org/10.5194/acp-18-7877-2018>.

- Park, S., Western, L. M., Saito, T., Redington, A., Henne, S., Fang, X., Prinn, R. G., Manning, A. J., Montzka, S. A., Fraser, P. J., Ganesan, A. L., Harth, C. M., Kim, J., Krummel, P. B., Liang, Q., Mühle, J., O'Doherty, S., Park, H., Park, M.-K., Reimann, S., Salameh, P. K., Weiss, R. F., Rigby, M. (2021) A decline in emissions of CFC-11 and related chemicals from eastern China. *Nature*, 590(7846), 433-437. <https://doi.org/10.1038/s41586-021-03277-w>.
- Platt, S. M., Eckhardt, S., Ferré, B., Fisher, R. E., Hermansen, O., Jansson, P., Lowry, D., Nisbet, E. G., Pisso, I., Schmidbauer, N., Silyakova, A., Stohl, A., Svendby, T. M., Vadakkepuliambatta, S., Mienert, J., and Lund Myhre, C. (2018) Methane at Svalbard and over the European Arctic Ocean. *Atmos. Chem. Phys.*, 18, 17207-17224. <https://doi.org/10.5194/acp-18-17207-2018>.
- Platt, S. M., Hov, Ø., Berg, T., Breivik, K., Eckhardt, S., Eleftheriadis, K., Evangeliou, N., Fiebig, M., Fisher, R., Hansen, G., Hansson, H.-C., Heintzenberg, J., Hermansen, O., Heslin-Rees, D., Holmén, K., Hudson, S., Kallenborn, R., Krejci, R., Krognnes, T., Larssen, S., Lowry, D., Lund Myhre, C., Lunder, C., Nisbet, E., Nizetto, P. B., Park, K.-T., Pedersen, C. A., Aspö Pfaffhuber, K., Röckmann, T., Schmidbauer, N., Solberg, S., Stohl, A., Ström, J., Svendby, T., Tunved, P., Tørnkvist, K., van der Veen, C., Vratolis, S., Yoon, Y. J., Yttri, K. E., Zieger, P., Aas, W., and Tørseth, K. (2022) Atmospheric composition in the European Arctic and 30 years of the Zeppelin Observatory, Ny-Ålesund. *Atmos. Chem. Phys.*, 22, 3321-3369. <https://doi.org/10.5194/acp-22-3321-2022>.
- Prather, M., Ehhalt, D., Dentener, F., Derwent, R. G., Dlugokencky, E., Holland, E., Isaksen, I. S. A., Katima, J., Kirchhoff, V., Matson, P., Midgley, P. M., Wang, M. (2001) Atmospheric chemistry and greenhouse gases. In: *Climate Change 2001: The Scientific Basis, Contribution of Working Group I to the Third Assessment Report of the Intergovernmental Panel on Climate Change*. Ed. by: Houghton, J. T., Ding, Y., Griggs, D. J., Noguer, M., van der Linden, P. J., Dai, X., Maskell, K., Johnson, C. A. Cambridge, Cambridge University Press. pp. 239-287.
- Pisso, I., Myhre, C. L., Platt, S. M., Eckhardt, S., Hermansen, O., Schmidbauer, N., Mienert, J., Vadakkepuliambatta, S., Bauguitte, S., Pitt, J., Allen, G., Bower, K.N., O'Shea, S., Gallagher, M. W., Percival, C.J., Pyle, J., Cain, M., Stohl, A. (2016) Constraints on oceanic methane emissions west of Svalbard from atmospheric in situ measurements and Lagrangian transport modelling. *J. Geophys. Res.*, 121, 14188-14200. <https://doi.org/10.1002/2016JD025590>.
- Putaud, J.-P. et al., 2010: A European aerosol phenomenology – 3: Physical and chemical characteristics of particulate matter from 60 rural, urban, and kerbside sites across Europe. *Atmos. Environ.*, 44(10), 1308-1320. <https://doi.org/10.1016/j.atmosenv.2009.12.011>.
- R Core Team (2018) R: A language and environment for statistical computing. Vienna, Austria, R Foundation for Statistical Computing. <https://www.R-project.org/>.
- Ramonet, M., P. Ciais, F. Apadula, J. Bartyzal, Bartyzel, A. Bastos, P. Bergamaschi, P.E. Blanc, D. Brunner, L. C. di Torchiareolo, F. Calzolari, H. Chen, L. Chmura, A. Colomb, S. Conil, P. Cristofanelli, E. Cuevas, R. Curcoll, M. Delmotte, A. di Sarra, L. Emmenegger, G. Forster, A. Frumau, C. Gerbig, F. Gheusi, S. Hammer, L. Haszpra, J. Hatakka, L. Hazan, M. Heliasz, S. Henne, A. Hensen, O. Hermansen, P. Keronen, R. Kivi, K. Komínková, D. Kubistin, O. Laurent, T. Laurila, J.V. Lavric, I. Lehner, K.E.J. Lehtinen, A. Leskinen, M. Leuenberger, I. Levin, M. Lindauer, M. Lopez, C. LundMyhre, I. Mammarella, G. Manca, A. Manning, M.V. Marek, P. Marklund, D. Martin, F. Meinhardt, N. Mihalopoulos, M. Mölder, J.A. Morgui, J. Necki, S. O'Doherty, C. O'Dowd, M. Ottosson, C. Philippon, S. Piacentino, J.M. Pichon, C. Plass-Duelmer, A. Resovsky, L. Rivier, X. Rodó, M.K. Sha, H.A. Scheeren, D. Sferlazzo, T.G. Spain, K.M. Stanley, M. Steinbacher, P. Trisolino, A. Vermeulen, G. Vítková, D. Weyrauch, I. Xueref-Remy, K. Yala, C. Yver Kwok. The fingerprint of the summer 2018 drought in Europe on ground-based atmospheric CO<sub>2</sub> measurements. *Phil. Trans. R. Soc. B*, 375, 20190513. <https://doi.org/10.1098/rstb.2019.0513>
- Repo, M. E., Susiluoto, S., Lind, S. E., Jokinen, S., Elsakov, V., Biasi, C., Virtanen, T., Pertti, J., Martikainen, P. J. (2009) Large N<sub>2</sub>O emissions from cryoturbated peat soil in tundra. *Nature Geosci.*, 2, 189-192. <https://doi.org/10.1038/ngeo434>.

- Rigby, M., Park, S., Saito, T., Western, L. M., Redington, A. L., Fang, X., Henne, S., Manning, A. J., Prinn, R. G., Dutton, G. S., Fraser, P. J., Ganesan, A. L., Hall, B. D., Harth, C. M., Kim, J., Kim, K.-R., Krummel, P. B., Lee, T., Li, S., Liang, Q., Lunt, M. F., Montzka, S. A., Mühle, J., O'Doherty, S., Park, M.-K., Reimann, S., Salameh, P. K., Simmonds, P., Tunnicliffe, R. L., Weiss, R. F., Yokouchi, Y., Young, D. (2019) Increase in CFC-11 emissions from eastern China based on atmospheric observations. *Nature*, 569, 546-550. <https://doi.org/10.1038/s41586-019-1193-4>.
- Saunio, M., Stavert, A. R., Poulter, B., Bousquet, P., Canadell, J. G., Jackson, R. B., Raymond, P. A., Dlugokencky, E. J., Houweling, S., Patra, P. K., Ciais, P., Arora, V. K., Bastviken, D., Bergamaschi, P., Blake, D. R., Brailsford, G., Bruhwiler, L., Carlson, K. M., Carrol, M., Castaldi, S., Chandra, N., Crevoisier, C., Crill, P. M., Covey, K., Curry, C. L., Etiope, G., Frankenberg, C., Gedney, N., Hegglin, M. I., Höglund-Isaksson, L., Hugelius, G., Ishizawa, M., Ito, A., Janssens-Maenhout, G., Jensen, K. M., Joos, F., Kleinen, T., Krummel, P. B., Langenfelds, R. L., Laruelle, G. G., Liu, L., Machida, T., Maksyutov, S., McDonald, K. C., McNorton, J., Miller, P. A., Melton, J. R., Morino, I., Müller, J., Murguía-Flores, F., Naik, V., Niwa, Y., Noce, S., O'Doherty, S., Parker, R. J., Peng, C., Peng, S., Peters, G. P., Prigent, C., Prinn, R., Ramonet, M., Regnier, P., Riley, W. J., Rosentreter, J. A., Segers, A., Simpson, I. J., Shi, H., Smith, S. J., Steele, L. P., Thornton, B. F., Tian, H., Tohjima, Y., Tubiello, F. N., Tsuruta, A., Viovy, N., Voulgarakis, A., Weber, T. S., van Weele, M., van der Werf, G. R., Weiss, R. F., Worthy, D., Wunch, D., Yin, Y., Yoshida, Y., Zhang, W., Zhang, Z., Zhao, Y., Zheng, B., Zhu, Q., Zhu, Q., and Zhuang, Q. (2020) The Global Methane Budget 2000–2017. *Earth Syst. Sci. Data*, 12, 1561-1623. <https://doi.org/10.5194/essd-12-1561-2020>.
- Simmonds, P. G., Manning, A. J., Cunnold, D. M., Fraser, P. J., McCulloch, A., O'Doherty, S., Krummel, P. B., Wang, R. H. J., Porter, L. W., Derwent, R. G., Grealley, B., Salameh, P., Miller, B. R., Prinn, R. G., Weiss, R. F. (2006) Observations of dichloromethane, trichloroethene and tetrachloroethene from the AGAGE stations at Cape Grim, Tasmania, and Mace Head, Ireland. *J. Geophys. Res.*, 111, D18304. <https://doi.org/10.1029/2006JD007082>.
- Stohl, A., Klimont, Z., Eckhardt, S., Kupiainen, K., Shevchenko, V. P., Kopeikin, V. M., and Novigatsky, A. N. (2013) Black carbon in the Arctic: the underestimated role of gas flaring and residential combustion emissions. *Atmos. Chem. Phys.*, 13, 8833–8855, <https://doi.org/10.5194/acp-13-8833-2013>.
- Svendby, T.M., Hansen, G.H., Bäcklund, A., Bernet, L., Nilsen, A.C., Schulze, D., Johnsen, B. (2022) Monitoring of the atmospheric ozone layer and natural ultraviolet radiation. Annual Report 2021. (NILU report 25/2022; Norwegian Environment Agency, M-2335 | 2022). Kjeller: NILU.
- Thompson R.L. G. Broquet, C. Gerbig, T. Koch, M. Lang, G. Monteil, S. Munassar, A. Nickless, M. Scholze, M. Ramonet, U. Karstens, E. van Schaik, Z. Wu and C. Rödenbeck, (2020) Changes in net ecosystem exchange over Europe during the 2018 drought based on atmospheric observations. *Phil. Trans. R. Soc. B*, 375, 20190512. <https://doi.org/10.1098/rstb.2019.0512>
- Thompson, R. L., Sasakawa, M., Machida, T., Aalto, T., Worthy, D., Lavric, J. V., Myhre, C. L., Stohl, A. (2017) Methane fluxes in the high northern latitudes for 2005–2013 estimated using a Bayesian atmospheric inversion. *Atmos. Chem. Phys.*, 17, 3553-3572. <https://doi.org/10.5194/acp-2016-660>.
- Thompson, R. L., Dlugokencky, E., Chevallier, F., Ciais, P., Dutton, G., Elkins, J. W., Langenfelds, R. L., Prinn, R. G., Weiss, R. F., Tohjima, Y., Krummel, P. B., Fraser, P., Steele, L. P. (2013) Interannual variability in tropospheric nitrous oxide. *Geophys. Res. Lett.*, 40, 4426-4431. <https://doi.org/10.1002/grl.50721>.
- Tørseth, K., Aas, W., Breivik, K., Fjæraa, A. M., Fiebig, M., Hjellbrekke, A. G., Myhre, C. L., Solberg, S., Yttri, K. E. (2012) Introduction to the European Monitoring and Evaluation Programme (EMEP) and observed atmospheric composition change during 1972–200. *Atmos. Chem. Phys.*, 12, 5447-5481. <https://doi.org/10.5194/acp-12-5447-2012>.

- Umezawa, T., Baker, A. K., Oram, D., Sauvage, C., O'Sullivan, D., Rauthe-Schöch, A., Montzka, S. A., Zahn, A., Brenninkmeijer, C. A. M. (2014) Chloromethane in the upper troposphere observed by the CARIBIC passenger aircraft observatory: Large-scale distributions and Asian summer monsoon outflow. *J. Geophys. Res. Atmos.*, *119*, 5542-5558. <https://doi.org/10.1002/2013JD021396>.
- Vollmer, M. K., Young, D., Trudinger, C. M., Muhle, J., Henne, S., Rigby, M., Park, S., Li, S., Guillevic, M., Mitrevski, B., Harth, C. M., Miller, B. R., Reimann, S., Yao, B., Steele, L. P., Wyss, S. A., Lunder, C. R., Arduini, J., McCulloch, A., Wu, S., Rhee, T. S., Wang, R. H. J., Salameh, P. K., Hermansen, O., Hill, M., Langenfelds, R. L., Ivy, D., O'Doherty, S., Krummel, P. B., Maione, M., Etheridge, D. M., Zhou, L., Fraser, P. J., Prinn, R. G.; Weiss, R. F., Simmonds, P. G. (2018) Atmospheric histories and emissions of chlorofluorocarbons CFC-13 (CClF<sub>3</sub>),  $\Sigma$ CFC-114 (C<sub>2</sub>Cl<sub>2</sub>F<sub>4</sub>), and CFC-115 (C<sub>2</sub>ClF<sub>5</sub>). *Atmos. Chem. Phys.*, *18*, 979-1002. <https://doi.org/10.5194/acp-18-979-2018>.
- Wiedensohler, A., Birmili, W., Nowak, A., Sonntag, A., Weinhold, K., Merkel, M., Wehner, B., Tuch, T., Pfeifer, S., Fiebig, M., Fjåraa, A. M., Asmi, E., Sellegri, K., Depuy, R., Venzac, H., Villani, P., Laj, P., Aalto, P., Ogren, J. A., Swietlicki, E., Williams, P., Roldin, P., Quincey, P., Hüglin, C., Fierz-Schmidhauser, R., Gysel, M., Weingartner, E., Riccobono, F., Santos, S., Gröning, C., Faloon, F., Beddows, D., Harrison, R., Monahan, C., Jennings, S. G., O'Dowd, C. D., Marinoni, A., Horn, H.-G., Keck, L., Jiang, J., Scheckman, J., McMurry, P.H., Deng, Z., Zhao, C. S., Moerman, M., Henzing, B., de Leeuw, G., Löschau, G., Bastian, S. (2012) Mobility particle size spectrometers: harmonization of technical standards and data structure to facilitate high quality long-term observations of atmospheric particle number size distributions. *Atmos. Meas. Tech.*, *5*, 657-685. <https://doi.org/10.5194/amt-5-657-2012>.
- Wilkinson, M. D., Dumontier, M., Aalbersberg, I. J., Appleton, G., Axton, M., Baak, A., Blomberg, N., Boiten, J. W., Santos, L. B. D., Bourne, P. E., Bouwman, J., Brookes, A. J., Clark, T., Crosas, M., Dillo, I., Dumon, O., Edmunds, S., Evelo, C. T., Finkers, R., Gonzalez-Beltran, A., Gray, A. J. G., Groth, P., Goble, C., Grethe, J. S., Heringa, J., Hoen, P. A. C., Hooft, R., Kuhn, T., Kok, R., Kok, J., Lusher, S. J., Martone, M. E., Mons, A., Packer, A. L., Persson, B., Rocca-Serra, P., Roos, M., van Schaik, R., Sansone, S. A., Schultes, E., Sengstag, T., Slater, T., Strawn, G., Swertz, M. A., Thompson, M., van der Lei, J., van Mulligen, E., Velterop, J., Waagmeester, A., Wittenburg, P., Wolstencroft, K., Zhao, J., and Mons, B. (2016) The FAIR Guiding Principles for scientific data management and stewardship. *Sci. Data*, *3*, 160018. <https://doi.org/https://doi.org/10.1038/sdata.2016.18>.
- WMO (2022) Greenhouse Gas Bulletin. The State of Greenhouse Gases in the Atmosphere Based on Global Observations through 2021. Geneva, World Meteorological Organization (GHG Bulletin No. 18, 26 October 2022).
- WMO (2021) Greenhouse Gas Bulletin. The State of Greenhouse Gases in the Atmosphere Based on Global Observations through 2020. Geneva, World Meteorological Organization (GHG Bulletin No. 17, 25 October 2021).
- WMO (2020) Greenhouse Gas Bulletin. The state of greenhouse gases in the atmosphere using global observations through 2019. Geneva, World Meteorological Organization (GHG Bulletin No. 16, 23 November 2020). [https://library.wmo.int/doc\\_num.php?explnum\\_id=10437](https://library.wmo.int/doc_num.php?explnum_id=10437).
- WMO (2019) Greenhouse Gas Bulletin. The state of greenhouse gases in the atmosphere using global observations through 2018. Geneva, World Meteorological Organization (GHG Bulletin No. 15, 25 November 2019). [https://library.wmo.int/index.php?lvl=notice\\_display&id=21620#.X1i3NN7VI2w](https://library.wmo.int/index.php?lvl=notice_display&id=21620#.X1i3NN7VI2w)
- WMO (2018) Scientific assessment of ozone depletion: 2018. Geneva, World Meteorological Organization (Global Ozone Research and Monitoring Project-Report No. 58). <https://www.esrl.noaa.gov/csd/assessments/ozone/2018/>.
- WMO (2017) Greenhouse Gas Bulletin. The state of greenhouse gases in the atmosphere using global observations through 2016. Geneva, World Meteorological Organization (GHG Bulletin No. 13, 30 October 2017). [https://library.wmo.int/opac/doc\\_num.php?explnum\\_id=4022](https://library.wmo.int/opac/doc_num.php?explnum_id=4022).

- WMO (2016) Greenhouse Gas Bulletin. The state of greenhouse gases in the atmosphere using global observations through 2015. Geneva, World Meteorological Organization (GHG Bulletin No. 12, 24 October 2016). [http://library.wmo.int/pmb\\_ged/ghg-bulletin\\_12\\_en.pdf](http://library.wmo.int/pmb_ged/ghg-bulletin_12_en.pdf).
- WMO (2015) Greenhouse Gas Bulletin. The state of greenhouse gases in the atmosphere using global observations through 2014. Geneva, World Meteorological Organization (GHG Bulletin No. 11, 9 November 2015). [http://library.wmo.int/pmb\\_ged/ghg-bulletin\\_11\\_en.pdf](http://library.wmo.int/pmb_ged/ghg-bulletin_11_en.pdf).
- WMO (2014) Greenhouse Gas Bulletin. The state of greenhouse gases in the atmosphere using global observations through 2013. Geneva, World Meteorological Organization (GHG Bulletin No. 10, 9<sup>th</sup> September 2014).  
[http://library.wmo.int/opac/index.php?lvl=notice\\_display&id=16396#.VGHPz5-gQtK](http://library.wmo.int/opac/index.php?lvl=notice_display&id=16396#.VGHPz5-gQtK).
- WMO (2014b) Scientific assessment of ozone depletion: 2014. Geneva, World Meteorological Organization (Global ozone research and monitoring project, Report No. 55).  
<https://www.esrl.noaa.gov/csd/assessments/ozone/2014/chapters/2014OzoneAssessment.pdf>.
- WMO (2013) Greenhouse Gas Bulletin. The state of greenhouse gases in the atmosphere using global observations through 2012. Geneva, World Meteorological Organization (GHG Bulletin No. 9, 6 November 2013).  
[http://www.wmo.int/pages/prog/arep/gaw/ghg/documents/GHG\\_Bulletin\\_No.9\\_en.pdf](http://www.wmo.int/pages/prog/arep/gaw/ghg/documents/GHG_Bulletin_No.9_en.pdf).
- WMO (2012) Greenhouse Gas Bulletin. The state of greenhouse gases in the atmosphere using global observations through 2011. Geneva, World Meteorological Organization (GHG Bulletin No. 8, 19 November 2012).  
[http://www.wmo.int/pages/prog/arep/gaw/ghg/documents/GHG\\_Bulletin\\_No.8\\_en.pdf](http://www.wmo.int/pages/prog/arep/gaw/ghg/documents/GHG_Bulletin_No.8_en.pdf).
- WMO (2011) Scientific assessment of ozone depletion: 2010. Geneva, World Meteorological Organization (Global ozone research and monitoring project, Report No. 52).
- Xian, P., Zhang, J., O'Neill, N.T., Reid, J.S., Toth, T.D., Sorenson, B., Hyer, E.J., Campbell, J.R., and K. Ranjbar (2022) Arctic spring and summertime aerosol optical depth baseline from long-term observations and model reanalyses – Part 2: Statistics of extreme AOD events, and implications for the impact of regional biomass burning processes. *Atmos. Chem. Phys.*, 22, 9949-9967, <https://doi.org/10.5194/acp-22-9949-2022>.
- Xu, Y., Zaelke, D., Velders, G.J.M., Ramanathan, V. (2013) The role of HFCs in mitigating 21st century climate change. *Atmos. Chem. Phys.*, 13, 6083-6089. <https://doi.org/10.5194/acp-13-6083-2013>.
- Zanatta, M. et al., 2016: A European aerosol phenomenology-5: Climatology of black carbon optical properties at 9 regional background sites across Europe. *Atmos. Environ.*, 145, 346-364. <https://doi.org/10.1016/j.atmosenv.2016.09.035>.
- Zeileis A. (2004) Econometric Computing with HC and HAC Covariance Matrix Estimators. *J. Stat. Software*, 11, 1-17. <https://doi.org/https://doi.org/10.18637/jss.v011.i10>.
- Zeileis, A. (2006) Object-oriented computation of sandwich estimators. *J. Stat. Software*, 16, 1-16. <https://doi.org/10.18637/jss.v016.i09>.

# Appendix I

## Data Tables

Table A 1: Annual mean concentration for all greenhouse gases included in the programme at Zeppelin and Birkenes. All concentrations are mixing ratios in ppt, except for methane and carbon monoxide (ppb) and carbon dioxide (ppm). The annual means are based on a combination of the measurements and the fitted values; during periods with lacking observations we have used the fitted mixing ratios in the calculation of the annual mean. All underlying measurement data are open and accessible and can be downloaded directly from the database: <http://ebas.nilu.no/>

Component	2001	2002	2003	2004	2005	2006	2007	2008	2009	2010	2011	2012	2013	2014	2015	2016	2017	2018	2019	2020	2021		
Carbon dioxide - Zeppelin												394.8	397.4	399.6	401.4	404.4	408.0	409.3	411.9	414.2	417.4		
Carbon dioxide - Birkenes									391.4	394.0	396.6	397.9	400.7	402.8	405.2	409.8	411.2	415.2	416.1	418.8	421.3		
Methane - Zeppelin	1844.4	1843.0	1855.5	1852.9	1852.1	1853.3	1863.4	1873.3	1888.6	1881.2	1879.9	1891.9	1898.1	1910.0	1920.2	1931.8	1938.9	1938.5	1953.0	1968.7	1981.4		
Methane - Birkenes									1880.9	1887.1	1895.6	1900.5	1902.5	1917.3	1926.1	1941.9	1945.3	1953.0	1961.2	1975.3	1991.7		
Carbon monoxide	130.9	126.1	140.3	130.4	128.6	126.1	120.2	119.9	117.9	128.7	115.5	120.7	113.1	113.4	112.9	112.4	114.3	113.6	115.6	117.7	128.0		
Nitrous oxide												323.6	324.2	325.1	326.1	327.2	328.0	329.0	330.0	331.3	332.1	333.4	334.5
<b>Chlorofluorocarbons</b>																							
CFC-11	259.3	257.2	254.9	253.3	251.0	249.2	246.5	244.6	242.7	240.8	238.6	237.3	235.8	234.2	232.9	231.4	230.1	229.1	227.4	225.0	222.6		
CFC-12	547.4	547.6	547.6	545.6	546.8	546.2	542.3	541.5	537.7	534.5	531.6	528.9	526.1	522.7	519.2	516.1	512.4	509.1	505.5	501.7	498.0		
CFC-113	81.4	80.8	80.0	79.4	78.8	77.9	77.5	76.8	76.2	75.5	74.7	74.1	73.5	73.0	72.3	71.7	71.1	70.6	70.0	69.5	69.1		
CFC-115	8.22	8.18	8.22	8.28	8.41	8.39	8.37	8.40	8.43	8.42	8.42	8.44	8.43	8.46	8.51	8.53	8.59	8.66	8.73	8.76	8.81		
<b>Hydrochlorofluorocarbons</b>																							
HCFC-22	158.5	164.1	170.7	175.8	181.5	189.2	196.3	204.6	212.4	219.7	225.8	231.0	236.4	241.2	245.4	248.8	252.2	255.1	257.2	257.5	258.6		
HCFC-141b	16.8	17.9	18.7	19.3	19.5	20.0	20.5	21.2	21.6	22.2	23.1	24.0	24.6	25.3	25.6	25.9	25.8	25.6	25.8	26.1	26.2		
HCFC-142b	14.3	15.0	15.9	16.6	17.3	18.2	19.3	20.3	21.3	22.0	22.7	22.9	23.2	23.3	23.5	23.5	23.5	23.3	23.2	22.9	22.6		
<b>Hydrofluorocarbons</b>																							
HFC-125	2.2	2.6	2.9	3.3	4.0	4.9	5.8	6.9	8.0	9.6	11.8	13.5	15.6	17.9	20.3	22.9	25.8	28.9	32.3	35.6	39.4		
HFC-134a	21.1	26.0	30.7	35.4	39.8	44.1	48.5	53.4	57.8	63.6	68.6	73.7	78.9	84.5	90.2	96.5	103.1	108.4	114.7	120.1	126.0		
HFC-152a	2.6	3.4	4.3	5.1	5.8	6.8	7.8	8.6	9.0	9.5	10.0	10.2	10.2	10.1	10.1	10.2	10.3	10.3	10.6	10.5	10.6		
HFC-23												23.7	24.7	25.6	26.7	27.7	28.7	29.6	30.7	31.9	33.2	34.5	35.6
HFC-365mfc												0.73	0.79	0.87	0.92	1.02	1.10	1.19	1.24	1.29	1.32	1.33	1.34



Component	2001	2002	2003	2004	2005	2006	2007	2008	2009	2010	2011	2012	2013	2014	2015	2016	2017	2018	2019	2020	2021	
HFC-227ea										0.70	0.79	0.88	0.99	1.10	1.21	1.34	1.47	1.59	1.75	1.90	2.07	
HFC-236fa										0.09	0.10	0.11	0.13	0.14	0.15	0.16	0.17	0.19	0.21	0.22	0.22	
HFC-245fa										1.63	1.80	1.98	2.19	2.39	2.58	2.80	3.04	3.26	3.53	3.71	3.83	
HFC-32										5.75	6.57	7.65	9.28	10.92	12.89	15.24	18.26	21.55	25.22	28.70	32.74	
HFC-4310mee										0.21	0.22	0.24	0.25	0.26	0.27	0.28	0.29	0.29	0.30	0.31	0.32	
HFC-143a										11.89	13.18	14.57	16.03	17.63	19.09	20.73	22.51	23.93	25.57	27.10	28.79	
<b>Perfluorinated compounds</b>																						
PFC-14																82.43	83.32	84.27	85.25	86.11	86.94	87.98
PFC-116										4.11	4.20	4.27	4.37	4.45	4.55	4.64	4.74	4.82	4.91	5.00	5.10	
PFC-218										0.56	0.57	0.59	0.60	0.61	0.63	0.64	0.66	0.67	0.69	0.71	0.73	
PFC-318										1.28	1.33	1.38	1.43	1.47	1.53	1.59	1.66	1.73	1.80	1.87	1.95	
Sulphurhexafluoride	4.95	5.14	5.37	5.61	5.82	6.09	6.31	6.64	6.93	7.19	7.50	7.79	8.11	8.43	8.75	9.09	9.46	9.80	10.14	10.45	10.84	
Nitrogen trifluoride																1.61	1.76	1.98	2.21	2.48	2.78	
Sulfuryl fluoride										1.71	1.81	1.91	2.03	2.12	2.22	2.33	2.45	2.53	2.63	2.74	2.87	
<b>Halons</b>																						
H-1211	4.39	4.43	4.48	4.53	4.52	4.48	4.43	4.39	4.33	4.26	4.18	4.09	3.97	3.87	3.77	3.65	3.55	3.45	3.37	3.27	3.18	
H-1301	2.99	3.07	3.13	3.17	3.21	3.22	3.24	3.28	3.29	3.32	3.33	3.35	3.36	3.37	3.39	3.38	3.39	3.38	3.39	3.39	3.39	
H-2402										0.47	0.46	0.45	0.44	0.44	0.43	0.42	0.41	0.41	0.41	0.40	0.40	
<b>Other halocarbons</b>																						
Chloromethane	506.7	521.1	526.5	522.6	519.1	520.7	523.2	525.2	526.3	520.7	509.6	515.5	519.2	514.4	512.7	521.5	516.7	514.2	507.7	508.5	511.0	
Bromomethane	9.13	9.13	8.88	8.86	8.53	8.57	8.32	7.77	7.37	7.29	7.20	7.06	6.99	6.87	6.68	6.73	6.55	6.54	6.72	6.69	6.76	
Dichloromethane	31.33	31.46	32.47	32.41	32.15	33.47	35.52	37.59	38.59	42.16	42.07	44.97	53.61	54.29	53.85	56.52	61.24	60.73	59.09	63.02	68.77	
Trichloromethane	11.14	10.69	10.69	10.33	10.36	10.42	10.60	10.43	10.87	11.52	11.99	12.21	12.76	13.49	13.68	14.24	15.32	14.80	12.30	13.10	12.71	
Carbon tetrachloride										86.68	85.27	84.44	83.49	82.54	81.74	80.63	79.46	78.83	78.02	77.17	76.16	
Trichloroethane	37.75	31.96	27.29	22.91	19.22	15.97	13.37	11.11	9.23	7.74	6.47	5.34	4.48	3.77	3.29	2.80	2.34	2.01	1.72	1.53	1.36	

Component	2001	2002	2003	2004	2005	2006	2007	2008	2009	2010	2011	2012	2013	2014	2015	2016	2017	2018	2019	2020	2021
Trichloroethene*	0.71	0.66	0.57	0.53	0.51	0.49	0.34	0.38	0.53	0.53	0.55	0.49	0.55	0.49	0.45	0.42	0.41	0.42	0.37	0.30	0.31
Tetrachloroethene**	4.65	4.21	4.07	3.88	3.38	2.91	3.14	2.72	2.97	3.13	2.82	2.67	2.55	2.57	2.58	2.55	2.48	2.31	2.29	2.11	2.14
<b>Volatile Organic Compounds (VOC)</b>																					
Ethane										1486.4	1471.7	1584.4	1568.1	1644.4	1634.4	1571.5	1576.9	1525.7	1603.9	1522.4	1541.4
Propane										499.7	526.8	572.0	579.7	571.0	540.6	555.5	583.7	497.1	454.7	340.2	352.1
Butane										184.9	186.7	200.8	204.3	192.8	179.6	163.9	193.3	143.3	140.2	119.5	115.9
Pentane										63.9	61.5	63.4	67.6	64.0	60.4	56.5	60.9	39.2	43.9	41.5	41.9
Benzene										85.7	72.8	74.4	69.5	71.3	68.0	67.3	62.9	64.9	64.3	66.8	69.3
Toluene										35.4	29.3	28.5	26.6	28.6	25.8	25.5	18.2	21.2	19.4	20.0	20.5

\*Trichloroethene: Larger uncertainties in the numbers due to low concentrations, memory effects and blanks in the instrument. The reference numbers (scale UB-98) have also larger uncertainties for the same reasons.

\*\*Tetrachloroethene: Larger uncertainties in the 2001-2010 numbers due to larger variability in the measurements with the ADS-GCMS instrument.

Table A 2: All calculated trends per year, error and regression coefficient for the fit. The trends are all in ppt per year, except for CH<sub>4</sub>, N<sub>2</sub>O, and CO which are in ppb and CO<sub>2</sub> is in ppm. The negative trends are in blue, and the positive trends are shown in red. Generally, the period is from 2001 to 2021, but for some compounds the measurements started after September 2010. For these compounds the trends are in general more uncertain.

Component	Formula	Trend/yr	Error	R <sup>2</sup>
Carbon dioxide - Zeppelin	CO <sub>2</sub>	2.48	0.03	0.97
Carbon dioxide - Birkenes		2.53	0.04	0.80
Methane - Zeppelin	CH <sub>4</sub>	6.71	0.10	0.92
Methane - Birkenes		8.98	0.20	0.73
Carbon monoxide	CO	-0.83	0.25	0.76
Nitrous oxide	N <sub>2</sub> O	1.01	0.01	0.99
<b>Chlorofluorocarbons</b>				
CFC-11	CCl <sub>3</sub> F	-1.77	0.013	0.99
CFC-12	CF <sub>2</sub> Cl <sub>2</sub>	-2.64	0.020	0.99
CFC-113	CF <sub>2</sub> ClCFCl <sub>2</sub>	-0.63	0.002	1.00
CFC-115	CF <sub>3</sub> CF <sub>2</sub> Cl	0.03	0.001	0.80
<b>Hydrochlorofluorocarbons</b>				
HCFC-22	CHClF <sub>2</sub>	5.42	0.033	0.997
HCFC-141b	C <sub>2</sub> H <sub>3</sub> FCl <sub>2</sub>	0.49	0.016	0.972
HCFC-142b	CH <sub>3</sub> CF <sub>2</sub> Cl	0.46	0.012	0.983
<b>Hydrofluorocarbons</b>				
HFC-125	CHF <sub>2</sub> CF <sub>3</sub>	1.83	0.006	0.999
HFC-134a	CH <sub>2</sub> FCF <sub>3</sub>	5.24	0.012	0.999
HFC-152a	CH <sub>3</sub> CHF <sub>2</sub>	0.38	0.010	0.964
HFC-23	CHF <sub>3</sub>	1.08	0.004	0.998
HFC-365mfc	CH <sub>3</sub> CF <sub>2</sub> CH <sub>2</sub> CF <sub>3</sub>	0.06	0.000	0.982
HFC-227ea	CF <sub>3</sub> CHFCF <sub>3</sub>	0.12	0.000	0.999
HFC-236fa	CF <sub>3</sub> CH <sub>2</sub> CF <sub>3</sub>	0.01	0.000	0.987
HFC-245fa	CHF <sub>2</sub> CH <sub>2</sub> CF <sub>3</sub>	0.21	0.001	0.996
HFC-32	CH <sub>2</sub> F <sub>2</sub>	2.46	0.012	0.999
HFC-4310mee	C <sub>5</sub> H <sub>2</sub> F <sub>10</sub>	0.01	0.000	0.957
HFC-143a	CH <sub>3</sub> CF <sub>3</sub>	1.55	0.003	0.998
<b>Perfluorinated compounds</b>				
PFC-14	CF <sub>4</sub>	0.919	0.0463	0.996
PFC-116	C <sub>2</sub> F <sub>6</sub>	0.090	0.0003	0.997
PFC-218	C <sub>3</sub> F <sub>8</sub>	0.016	0.0001	0.985
PFC-318	c-C <sub>4</sub> F <sub>8</sub>	0.060	0.0002	0.996
Sulphurhexafluoride	SF <sub>6</sub>	0.297	0.0004	0.999
Nitrogen trifluoride	NF <sub>3</sub>	0.234	0.0262	0.997
Sulfuryl fluoride	SO <sub>2</sub> F <sub>2</sub>	0.104	0.0008	0.994

Component	Formula	Trend/yr	Error	R <sup>2</sup>
<b>Halons</b>				
H-1211	CBrClF <sub>2</sub>	-0.070	0.0003	0.997
H-1301	CBrF <sub>3</sub>	0.017	0.0003	0.786
H-2402	CBrF <sub>2</sub> CBrF <sub>2</sub>	-0.007	0.0000	0.968
<b>Halogenated compounds</b>				
Chloromethane	CH <sub>3</sub> Cl	-0.482	0.1819	0.869
Bromomethane	CH <sub>3</sub> Br	-0.144	0.0053	0.884
Dichloromethane	CH <sub>2</sub> Cl <sub>2</sub>	1.971	0.0616	0.936
Trichloromethane	CHCl <sub>3</sub>	0.203	0.0154	0.687
Carbon tetrachloride	CCl <sub>4</sub>	-0.933	0.0110	0.964
Trichloroethane	CH <sub>3</sub> CCl <sub>3</sub>	-1.598	0.0090	0.999
Trichloroethene*	CHClCCl <sub>2</sub>	-0.013	0.0031	0.406
Tetrachloroethene**	CCl <sub>2</sub> CCl <sub>2</sub>	-0.104	0.0068	0.540
<b>Volatile Organic Compounds (VOC)</b>				
Ethane***	C <sub>2</sub> H <sub>6</sub>	2.77	3.78	0.87
Propane***	C <sub>3</sub> H <sub>8</sub>	-15.72	3.23	0.80
Butane***	C <sub>4</sub> H <sub>10</sub>	-7.42	1.43	0.72
Pentane***	C <sub>5</sub> H <sub>12</sub>	-2.49	0.47	0.67
Benzene***	C <sub>6</sub> H <sub>6</sub>	-1.23	0.41	0.86
Toluene***	C <sub>6</sub> H <sub>5</sub> CH <sub>3</sub>	-1.32	0.25	0.70

\*Trichloroethene: Larger uncertainties in the numbers due to low concentrations, memory effects and blanks in the instrument. The reference numbers (scale UB-98) have also larger uncertainties for the same reasons.

\*\*Tetrachloroethene: Larger uncertainties in the 2001-2010 numbers due to larger variability in the measurements with the ADS-GCMS instrument.

\*\*\* Larger uncertainty for VOC due to shorter timeseries

Table A 3: 2010 - 2021 seasonal and annual means of integral particle concentrations in the ultrafine, fine and coarse particle size range for Birkenes, Trollhaugen, and Zeppelin stations

Year	Season	Birkenes				Trollhaugen <sup>1</sup>		Zeppelin	
		N <sub>ait</sub> /cm <sup>-3</sup>	N <sub>acc</sub> /cm <sup>-3</sup>	N <sub>coa</sub> /cm <sup>-3</sup>	N <sub>tot</sub> /cm <sup>-3</sup>	N <sub>ait</sub> /cm <sup>-3</sup>	<sup>2</sup> N <sub>acc</sub> /cm <sup>-3</sup>	N <sub>ait</sub> /cm <sup>-3</sup>	<sup>2</sup> N <sub>acc</sub> /cm <sup>-3</sup>
2009/10	Winter	467	433	0.296	967				
2010	Spring	1249	372	0.704	1633				
2010	Summer	1807	555	0.643	2381				
2010	Autumn	912	343	0.562	1358				
2010	Whole Year	1101	412	0.575	1593				
2010/11	Winter	544	320	0.974	863				
2011	Spring	1341	422	1.620	1765				
2011	Summer	1661	497	1.250	2161				
2011	Autumn	1908	560	1.844	2470				
2011	Whole Year	1215	417	1.427	1644				
2011/12	Winter	433	217	0.927	664				
2012	Spring	1179	303	0.982	1523				
2012	Summer	1447	435	1.041	1892				
2012	Autumn	722	169	0.918	898				
2012	Whole Year	951	288	0.912	1258				
2012/13	Winter	421	203	0.550	626				
2013	Spring	1314	392	1.012	1711				
2013	Summer	1680	497	0.951	2182				
2013	Autumn	785	183	0.952	968				
2013	Whole Year	1107	335	0.951	1454				
2013/14	Winter	737	342	1.246	1079				
2014	Spring	1569	429	0.823	1998	183	32		
2014	Summer	1717	642	0.757	2358	43	19		
2014	Autumn	1286	532	0.950	1818	207	28		
2014	Whole Year	1333	488	0.859	1821	183	34		
2014/15	Winter	567	203	1.038	770	368	67		
2015	Spring	1571	360	1.030	1931	134	25		
2015	Summer	2198	614	0.866	2812	38	23		
2015	Autumn	1081	378	0.766	1459	221	28		
2015	Whole Year	1363	395	0.963	1758	171	32		
2015/16	Winter	594	245	0.867	839				
2016	Spring	1471	483	0.848	1954	170	26		
2016	Summer	1608	535	0.876	2143	47	18	156	64
2016	Autumn	983	319	0.707	1302	262	35	47	31
2016	Whole Year	1167	391	0.804	1558	231	37	---	---
2016/17	Winter	585	219	0.717	804	473	74	---	---
2017	Spring	1474	476	0.564	1950	157	31	96	126
2017	Summer	1599	537	1.013	2136	51	20	282	70
2017	Autumn	1291	440	0.734	1731	265	27	56	63
2017	Whole Year	1256	424	0.721	1679	238	38	---	---
2017/18	Winter	517	275	0.399	792	482	78	27	44
2018	Spring	1511	649	---	2159	170	24	107	85
2018	Summer	1948	617	---	2565	45	18	225	66
2018	Autumn	986	300	---	1286	273	28	30	25
2018	Whole Year	1255	460	---	1715	233	35	92	55
2018/19	Winter	578	229	---	806	427	64	18	60
2019	Spring	1406	500	---	1906	183	25	78	95
2019	Summer	1867	509	---	2376	34	14	224	68
2019	Autumn	805	185	---	990	233	29	29	28

Year	Season	Birkenes				Trollhaugen <sup>1</sup>		Zeppelin	
		N <sub>ait</sub> /cm <sup>-3</sup>	N <sub>acc</sub> /cm <sup>-3</sup>	N <sub>coa</sub> /cm <sup>-3</sup>	N <sub>tot</sub> /cm <sup>-3</sup>	N <sub>ait</sub> /cm <sup>-3</sup>	<sup>2</sup> N <sub>acc</sub> /cm <sup>-3</sup>	N <sub>ait</sub> /cm <sup>-3</sup>	<sup>2</sup> N <sub>acc</sub> /cm <sup>-3</sup>
2019	Whole Year	1163	356	---	1519	202	31	87	64
2019/20	Winter	567	133	---	700	398	78	25	78
2020	Spring	1480	291	---	1770	187	27	90	88
2020	Summer	1570	554	---	2125	36	13	148	96
2020	Autumn	907	251	---	1158	237	28	34	38
2020	Whole Year	1133	306	---	1439	219	37	77	75
2020/2021	Winter	503	160	---	721	395	72	16	23
2021	Spring	1107	255	---	1490	213	29	38	54
2021	Summer	1560	548	0.608	2217	46	11	127	39
2021	Autumn	977	195	0.703	1236	429	33	35	23
2021	Whole Year	1062	294	---	1445	289	38	61	34

<sup>1</sup> Cells shaded in grey mark values obtained with an older instrument version that can't be compared directly with later values. Numbers

given for the time when the respective season is present in the Northern hemisphere. Actual seasons in Southern hemisphere are shifted by 6 months. In 2020, numbers for Birkenes have been reprocessed for all years since 2010 taking into account recent intercalibrations.

<sup>2</sup>The accumulation mode integral particle concentration N<sub>acc</sub> at Trollhaugen and Zeppelin extends only up to 0.8 µm particle diameter due to lack of an instrument covering larger particles. For Birkenes, N<sub>acc</sub> includes particles up to 1 µm diameter

Table A 4: 2010 - 2021 seasonal and annual means of optical aerosol properties scattering coefficient, absorption coefficient, and single scattering albedo (all at 550 nm) for Birkenes, Trollhaugen, and Zeppelin stations, as far as available.

Year	Season	Birkenes			Trollhaugen <sup>1</sup>			Zeppelin		
		$\sigma_{sp}$ Mm <sup>-1</sup>	$\sigma_{ap}$ Mm <sup>-1</sup>	$V_0$	$\sigma_{sp}$ Mm <sup>-1</sup>	$\sigma_{ap}$ Mm <sup>-1</sup>	$V_0$	$\sigma_{sp}$ Mm <sup>-1</sup>	$\sigma_{ap}$ Mm <sup>-1</sup>	$V_0$
2009/10	Winter	16.82	3.09	0.88						
2010	Spring	12.33	0.78	0.93						
2010	Summer	11.30	0.70	0.94						
2010	Autumn	7.26	0.71	0.90						
2010	Whole Year	11.52	1.24	0.91						
2010/11	Winter	16.96	2.18	0.89						
2011	Spring	18.67	1.26	0.93						
2011	Summer	15.43	0.74	0.95						
2011	Autumn	29.74	2.87	0.92						
2011	Whole Year	20.26	1.69	0.93						
2011/12	Winter	11.29	1.00	0.91						
2012	Spring	15.10	0.86	0.93						
2012	Summer	12.62	0.67	0.95						
2012	Autumn	9.80	0.65	0.92						
2012	Whole Year	12.22	0.83	0.92						
2012/13	Winter	12.48	1.84	0.84						
2013	Spring	17.03	1.48	0.90						
2013	Summer	13.81	1.15	0.92						
2013	Autumn	8.89	1.25	0.85						
2013	Whole Year	13.73	1.40	0.88						
2013/14	Winter	22.89	2.64	0.87						
2014	Spring	12.95	2.09	0.87	0.74	-0.05	0.95			
2014	Summer	15.85	1.26	0.92	1.39	0.04	0.98			
2014	Autumn	18.76	3.41	0.82	1.02	0.15	0.93			
2014	Whole Year	16.99	2.30	0.87	1.01	0.09	0.95			
2014/15	Winter	13.98	1.30	0.89	0.74	0.04	0.94			
2015	Spring	12.72	1.48	0.89	0.65	0.02	0.97			
2015	Summer	12.45	1.46	0.90	2.44	0.02	0.98		0.30	
2015	Autumn	15.69	2.45	0.95	1.32	0.07	0.94		0.14	
2015	Whole Year	14.36	1.56	0.90	1.32	0.04	0.96			
2015/16	Winter	13.59	1.24	0.88	0.87	0.05	0.94		0.38	
2016	Spring	14.86	1.10	0.91	0.78	0.17	0.97		0.39	
2016	Summer	11.93	0.77	0.94	2.01	0.00	0.99		0.09	
2016	Autumn	11.47	1.46	0.85	1.54	0.04	0.95		0.12	
2016	Whole Year	12.26	1.12	0.89	1.31	0.06	0.97		0.24	
2016/17	Winter	12.27	2.24	0.81	0.82	0.05	0.94		0.40	
2017	Spring	8.71			0.76	0.02	0.97		0.48	
2017	Summer	8.58			1.57	0.01	0.99		0.10	
2017	Autumn	8.09	1.21	0.85	1.22	0.05	0.94		0.29	
2017	Whole Year	9.07			1.10	0.03	0.96		0.33	
2017/18	Winter	13.56	1.66	0.83	0.72	0.04	0.95		0.34	
2018	Spring	17.10	2.45	0.87	0.60	0.03	0.97		0.32	
2018	Summer	13.62	1.23	0.91	1.78	0.06	0.98		0.12	
2018	Autumn	14.08	2.04	0.86	1.31	0.04	0.95		0.10	
2018	Whole Year	14.54	1.90	0.86	1.10	0.04	0.96		0.21	
2018/19	Winter	---	---	---	0.73	0.04	0.94		0.45	
2019	Spring	---	---	---	0.81	0.03	0.97		0.46	
2019	Summer	---	---	---	1.81	0.01	0.99		0.19	
2019	Autumn	6.26	0.93	0.85	1.61	0.04	0.96		0.13	
2019	Whole Year	---	---	---	1.26	0.03	0.97		0.33	
2019/20	Winter	10.15	0.96	0.87	0.88	0.04	0.95		0.73	
2020	Spring	10.84	1.03	0.90	0.89	0.02	0.98		0.36	
2020	Summer	11.28	1.07	0.91	1.43	0.01	0.99		0.24	
2020	Autumn	12.63	1.53	0.88	1.60	0.04	0.97		0.13	
2020	Whole Year	11.62	1.21	0.89	1.19	0.03	0.97		0.36	
2020/21	Winter	9.81	1.76	0.80	0.80	0.11	0.95		0.17	
2021	Spring	8.38	0.76	0.87	0.66	0.02	0.98		0.50	
2021	Summer	17.36	1.08	0.93	1.88	0.02	0.99		0.08	
2021	Autumn	12.23	1.21	0.86	1.27	0.14	0.95		0.20	
2021	Whole Year	11.42	1.14	0.86	1.23	0.07	0.97		0.25	

Table A 5: Monthly means and standard deviation of aerosol optical depth (AOD) at 500 nm at Ny-Ålesund.

Month/ Year	Jan	Feb	Mar	Apr	May	Jun	Jul	Aug	Sep	Oct	Nov	Dec
Aerosol optical depth (AOD)												
2002				0.06 ±0.01	0.08 ±0.03	0.06 ±0.02	0.07 ±0.12	0.07 ±0.08	0.06 ±0.05			
2003			0.15 ±0.12	0.11 ±0.05	0.15 ±0.06	0.10 ±0.03	0.04 ±0.01	0.05 ±0.02	0.06 ±0.03			
2004			0.06 ±0.00	0.12 ±0.08	0.13 ±0.09	0.06 ±0.01	0.10 ±0.07	0.05 ±0.02	0.04 ±0.02			
2005			0.08 ±0.03	0.12 ±0.07	0.10 ±0.03	0.05 ±0.02	0.05 ±0.02	0.04 ±0.03	0.03 ±0.01			
2006			0.12 ±0.03	0.16 ±0.07		0.04 ±0.00	0.05 ±0.02	0.05 ±0.04	0.04 ±0.03			
2007				0.10 ±0.05	0.10 ±0.12	0.07 ±0.03	0.05 ±0.01	0.05 ±0.02	0.04 ±0.03			
2008			0.13 ±0.05	0.14 ±0.06	0.14 ±0.04	0.06 ±0.02	0.06 ±0.02	0.09 ±0.03	0.16 ±0.03			
2009					0.11 ±0.03	0.08 ±0.02	0.11 ±0.04	0.10 ±0.02	0.09 ±0.01			
2010			0.11±0.03	0.08 ±0.03	0.08 ±0.01	0.06 ±0.01	0.05 ±0.01	0.05 ±0.01				
2011					0.08 ±0.02	0.08 ±0.01	0.05 ±0.01	0.06 ±0.02	0.05 ±0.01			
2012			0.10 ±0.03	0.10 ±0.02	0.10 ±0.03	0.06 ±0.02	0.06 ±0.02	0.07 ±0.03	0.07 ±0.03			
2013			0.11 ±0.04	0.09 ±0.04	0.06 ±0.02	0.05 ±0.01	0.06 ±0.02	0.05 ±0.01	0.04 ±0.02			
2014				0.07 ±0.01	0.10 ±0.02	0.06 ±0.02	0.06 ±0.03	0.08 ±0.01	0.11 ±0.05			
2015			0.05 ±0.02	0.10 ±0.03	0.07 ±0.02	0.05 ±0.01	0.15 ±0.20	0.05 ±0.02	0.05 ±0.01			
2016			0.08 ±0.03	0.06 ±0.02	0.08 ±0.03	0.07 ±0.02	0.04 ±0.01	0.05 ±0.04	0.03 ±0.01			
2017				0.07 ±0.03	0.07 ±0.03	0.04 ±0.01	0.04 ±0.01	0.05 ±0.01	0.07 ±0.01			
2018	0.05 ±0.01		0.05 ±0.01	0.08 ±0.02	0.07 ±0.02	0.04 ±0.01	0.03 ±0.01	0.08 ±0.07	0.05 ±0.02	0.10 ±0.01	0.04 ±0.00	0.05 ±0.01
2019	0.10 ±0.01	0.07 ±0.02		0.06 ±0.02	0.07 ±0.02	0.05 ±0.01	0.20 ±0.09	0.19 ±0.04	0.10 ±0.01	0.08 ±0.00		
2020		0.08 ±0.02	0.07 ±0.04	0.07 ±0.01	0.08 ±0.01							
2021	0.08 ±0.07	0.04 ±0.01	0.06 ±0.01	0.10 ±0.00	0.09 ±0.01	0.04 ±0.01	0.05 ±0.01	0.08 ±0.03	0.07 ±0.01			
Mean (2002- 2021)	0.08 ±0.03	0.08 ±0.02	0.10 ±0.03	0.10 ±0.04	0.09 ±0.04	0.06 ±0.02	0.07 ±0.04	0.07 ±0.03	0.06 ±0.02	0.10 ±0.01	0.04 ±0.00	0.05 ±0.01

<sup>1</sup>Numbers given for the time when the respective season is present in the Northern hemisphere. Actual seasons in Southern hemisphere are shifted by 6 months.



Table A 6: Monthly means and standard deviation of the Ångström coefficient ( $\text{\AA}$ ) at Ny-Ålesund. There are no observations of this parameter during the winter months due to polar night.

Month/ Year	Jan	Feb	Mar	Apr	May	Jun	Jul	Aug	Sep	Oct	Nov	Dec
Ångström Exponent												
2002				0.9 ±0.1	1.4 ±0.1	1.2 ±0.3	1.2 ±0.2	1.3 ±0.4	1.2 ±0.5			
2003			0.9 ±0.5	1.3 ±0.3	1.3 ±0.2	1.5 ±0.1	1.5 ±0.3	1.4 ±0.5	1.4 ±0.3			
2004			1.3 ±0.1	1.2 ±0.3	1.4 ±0.5	1.7 ±0.2	1.6 ±0.4	1.5 ±0.3	1.3 ±0.3			
2005			1.1 ±0.3	1.4 ±0.4	1.0 ±0.2	1.6 ±0.3	1.7 ±0.2	1.4 ±0.7	1.5 ±0.4			
2006			0.9 ±0.1	0.9 ±0.3		1.7 ±0.2	1.4 ±0.3	1.3 ±0.6	1.4 ±0.3			
2007				1.4 ±0.4	1.4 ±0.6	1.7 ±0.2	1.6 ±0.2	1.7 ±0.3	1.5 ±0.4			
2008			1.4 ±0.2	1.3 ±0.2	1.4 ±0.2	1.4 ±0.4	1.2 ±0.2	1.3 ±0.3	1.4 ±0.3			
2009					1.3 ±0.4	1.4 ±0.2	1.3 ±0.3	1.2 ±0.1	1.1 ±0.1			
2010			1.0 ±0.3	1.4 ±0.2	1.3 ±0.2	1.3 ±0.3	1.4 ±0.2	1.0 ±0.1				
2011					1.7 ±0.3	1.8 ±0.1	1.5 ±0.1	1.4 ±0.3	1.6 ±0.2			
2012			1.1 ±0.2	1.3 ±0.2	1.2 ±0.2	1.1 ±0.1	1.3 ±0.2	1.4 ±0.2	1.5 ±0.2			
2013			1.3 ±0.2	1.2 ±0.3	1.4 ±0.2	1.6 ±0.3	1.3 ±0.2	1.4 ±0.2	1.2 ±0.5			
2014				1.4 ±0.1	1.4 ±0.1	1.3 ±0.3	1.5 ±0.1	1.5 ±0.1	1.5 ±0.2			
2015			1.32 ±0.17	1.23 ±0.26	1.47 ±0.14	1.50 ±0.20	1.47 ±0.16	1.56 ±0.16	1.18 ±0.52			
2016			1.30 ±0.21	1.56 ±0.12	1.57 ±0.06	1.49 ±0.19	1.45 ±0.28	1.52 ±0.18	1.43 ±0.22			
2017				1.46 ±0.20	1.46 ±0.21	1.38 ±0.09	1.57 ±0.11	1.54 ±0.09	1.36 ±0.06			
2018	1.34 ±0.12		1.41 ±0.08	1.35 ±0.15	1.22 ±0.31	1.47 ±0.17	1.43 ±0.08	1.41 ±0.10	1.16 ±0.12	1.03 ±0.03	1.02 ±0.03	1.11 ±0.07
2019	1.59 ± 0.16	1.35 ± 0.23		1.25 ± 0.27	1.47 ± 0.23	1.35 ± 0.23	1.38± 0.18	1.30 ± 0.10	1.28 ± 0.06	1.19 ± 0.12		
2020		1.10 ± 0.39	1.14 ±0.19	1.45 ± 0.06	1.49 ± 0.09							
<b>2021</b>	<b>0.65 ± 0.17</b>	<b>0.68 ± 0.14</b>	<b>1.15 ± 0.10</b>	<b>1.18 ± 0.00</b>	<b>1.52 ± 0.16</b>	<b>1.62 ± 0.19</b>	<b>1.45 ± 0.24</b>	<b>1.49 ± 0.22</b>	<b>1.43 ± 0.08</b>			
<b>Mean (2002- 2021)</b>	<b>1.25 ±0.15</b>	<b>1.12 ±0.34</b>	<b>1.19 ±0.22</b>	<b>1.33 ±0.24</b>	<b>1.38 ±0.22</b>	<b>1.44 ±0.23</b>	<b>1.43 ±0.21</b>	<b>1.43 ±0.24</b>	<b>1.35 ±0.29</b>	<b>1.10 ±0.04</b>	<b>1.02 ±0.03</b>	<b>1.11 ± 0.07</b>

Table A 7: Number of days with AOD observations at Ny-Ålesund made within the months.

Month/Year	Jan	Feb	Mar	Apr	May	Jun	Jul	Aug	Sep	Oct	Nov	Dec
Number of days with cloud-free and quality assured observations												
2002				4	15	11	6	9	14			
2003			3	12	16	8	15	17	12			
2004			2	8	13	9	5	12	12			
2005			12	17	24	15	10		11			
2006			6	12		5	12	4	13			
2007				16	9	12	17	10	9			
2008			15	12	14	20	16	13	2			
2009					7	10	17	8	8			
2010			7	18	7	10	12	3	1			
2011					2	2	7	4	6			
2012			6	18	12	15	16	11	4			
2013			5	13	10	10	8	7	9			
2014				13	9	9	9	14	4			
2015			5	17	15	9	17	13	6			
2016			6	14	8	7	12	10	7			
2017				13	19	11	12	6	3			
2018	7		3	10	5	12	9	11	5	2	2	2
2019	9	3		10	19	18	9	16	7	1		
2020		11	5	6	7							
<b>2021</b>	<b>6</b>	<b>1</b>	<b>1</b>	<b>1</b>	<b>18</b>	<b>14</b>	<b>17</b>	<b>9</b>	<b>8</b>			
<b>Total (2002-2021)</b>	<b>22</b>	<b>15</b>	<b>76</b>	<b>214</b>	<b>229</b>	<b>207</b>	<b>226</b>	<b>177</b>	<b>141</b>	<b>3</b>	<b>2</b>	<b>2</b>

*Table A 8: Monthly means and standard deviation of aerosol optical depth (AOD) at 500 nm at Birkenes.*

Month/Year	Jan	Feb	Mar	Apr	May	Jun	Jul	Aug	Sep	Oct	Nov	Dec
Aerosol optical depth (AOD)												
2009				0.29 ±0.00	0.09 ±0.05	0.09 ±0.05	0.18 ±0.06	0.17 ±0.07	0.10 ±0.04	0.08 ±0.03		
2010					0.10 ±0.04	0.09 ±0.04	0.10 ±0.07	0.10 ±0.05	0.05 ±0.02	0.07 ±0.03	0.04 ±0.01	
2011	0.02 ±0.01	0.03 ±0.01	0.07 ±0.02	0.21 ±0.19	0.13 ±0.07	0.10 ±0.04	0.13 ±0.06	0.09 ±0.05				
2012			0.07 ±0.05	0.05 ±0.02	0.08 ±0.04	0.09 ±0.04	0.07 ±0.03	0.08 ±0.03	0.07 ±0.01	0.06 ±0.03	0.04 ±0.00	
2013							0.17 ±0.17	0.12 ±0.09	0.05 ±0.03	0.05 ±0.03		
2014			0.15 ±0.14	0.11 ±0.06	0.10 ±0.03	0.08 ±0.03	0.13 ±0.06	0.15 ±0.07	0.14 ±0.06			
2015			0.04 ±0.02	0.07 ±0.02	0.07 ±0.03	0.06 ±0.02	0.10 ±0.07	0.09 ±0.06	0.04 ±0.02	0.03 ±0.03	0.04 ±0.01	
2016	0.01 ±0.00	0.03 ±0.01	0.03 ±0.02	0.05 ±0.03							0.02 ±0.00	
2017*				0.08 ±0.01	0.06 ±0.03	0.04 ±0.03	0.06 ±0.03	0.09 ±0.07	0.09 ±0.03	0.06 ±0.03		
2018*				0.09 ±0.07	0.11 ±0.05	0.07 ±0.06	0.08 ±0.06	0.10 ±0.08	0.06 ±0.04			
2019	0.03 ±0.01	0.07 ±0.09	0.04 ±0.02	0.11 ±0.08	0.06 ±0.03	0.12 ±0.11	0.19 ±0.06	0.16 ±0.04			0.07 ±0.03	0.05 ±0.00
2020	0.06 ±0.02	0.08 ±0.07	0.07 ±0.02	0.08 ±0.01	0.07 ±0.02	0.10 ±0.07	0.06 ±0.02	0.11 ±0.06	0.14 ±0.10	0.08 ±0.04	0.04 ±0.02	0.03 ±0.01
2021	<b>0.04</b> ±0.02	<b>0.04</b> ±0.02	<b>0.06</b> ±0.04	<b>0.08</b> ±0.06	<b>0.06</b> ±0.04	<b>0.07</b> ±0.03	<b>0.17</b> ±0.10	<b>0.10</b> ±0.06	<b>0.09</b> ±0.06	<b>0.04</b> ±0.01	<b>0.04</b> ±0.02	<b>0.03</b> ±0.02
<b>Mean 2009 -2021</b>	<b>0.03</b> <b>0.01</b>	<b>0.05</b> <b>±0.03</b>	<b>0.07</b> <b>±0.05</b>	<b>0.09</b> <b>±0.05</b>	<b>0.08</b> <b>±0.04</b>	<b>0.08</b> <b>±0.05</b>	<b>0.11</b> <b>±0.06</b>	<b>0.11</b> <b>±0.05</b>	<b>0.08</b> <b>±0.04</b>	<b>0.05</b> <b>±0.03</b>	<b>0.04</b> <b>±0.02</b>	<b>0.04</b> <b>±0.01</b>

\* version 3 data analysis (Aeronet)

Table A 9: Monthly means and standard deviation of the Ångström coefficient (Å) at Birkenes

Month/Year	Jan	Feb	Mar	Apr	May	Jun	Jul	Aug	Sep	Oct	Nov	Dec
Ångström coefficient (Å)												
2009				1.5 ±0.0	1.2 ±0.3	1.4 ±0.3	1.4 ±0.4	1.1 ±0.2	1.0 ±0.2	1.1 ±0.2		
2010					1.3 ±0.3	1.4 ±0.3	1.4 ±0.2	1.4 ±0.2	1.3 ±0.3	1.3 ±0.3	1.3 ±0.23	
2011	1.0 ±0.2	1.0 ±0.1	1.0 ±0.3	1.2 ±0.5	1.3 ±0.3	1.5 ±0.3	1.6 ±0.3	1.6 ±0.1				
2012			1.1 ±0.4	1.6 ±0.3	1.4 ±0.4	1.7 ±0.1	1.6 ±0.3	1.5 ±0.3	1.1 ±0.3	1.4 ±0.4	0.8 ±0.3	
2013							1.3 ±0.2	1.2 ±0.3	0.8 ±0.2	0.8 ±0.3		
2014			0.87 ±0.48	1.04 ±0.33	1.07 ±0.27	1.02 ±0.24	1.38 ±0.33	1.14 ±0.25	1.19 ±0.16			
2015			0.93 ±0.16	1.06 ±0.13	1.11 ±0.20	1.30 ±0.20	1.49 ±0.20	1.37 ±0.26	1.30 ±0.23	1.23 ±0.25	0.84 ±0.33	
2016	0.68 ±0.07	1.00 ±0.2	0.90 ±0.3	1.13 ±0.2							1.11 ±0.08	
2017*				1.77 ±0.07	1.39 ±0.35	1.39 ±0.37	1.73 ±0.34	1.48 ±0.37	0.93 ±0.18	0.78 ±0.20		
2018				1.02 ±0.24	1.31 ±0.25	1.23 ±0.31	1.54 ±0.28	1.36 ±0.23	1.11 ±0.25			
2019	0.83 ±0.23	0.96 ±0.45	1.01 ±0.31	1.47 ±0.28	1.29 ±0.23	1.43 ±0.17	1.60 ±0.16	1.41 ±0.15			1.04 ±0.29	1.08 ±0.14
2020	0.88 ±0.29	0.80 ±0.28	1.10 ±0.25	1.17 ±0.18	1.18 ±0.24	1.39 ±0.28	1.41 ±0.21	1.51 ±0.21	1.16 ±0.35	1.24 ±0.38	1.05 ±0.18	0.94 ±0.22
2021	1.38 ±0.34	1.58 ±0.44	1.07 ±0.68	1.27 ±0.26	1.48 ±0.23	1.47 ±0.27	1.65 ±0.33	1.58 ±0.18	1.54 ±0.29	1.31 ±0.32	1.02 ±0.49	1.42 ±0.29
Mean 2009-2021	1.08 ±0.25	1.06 ±0.35	1.07 ±0.37	1.32 ±0.24	1.29 ±0.26	1.40 ±0.28	1.58 ±0.28	1.42 ±0.25	1.17 ±0.29	1.15 ±0.31	1.04 ±0.28	1.20 ±0.24

\* version 3 data analysis (Aeronet)

Table A 10: Number of days with AOD observations at Birkenes made within the months.

Month/Year	Jan	Feb	Mar	Apr	May	Jun	Jul	Aug	Sep	Oct	Nov	Dec
Number of days with cloud-free and quality assured observations (lev 2; lev 1.5 for 2013)												
2009*					20	23	10	12	13	13		
2010*					13	16	17	19	16	10	11	13
2011*	13	4	19	22	19	23	15	15				
2012*			11	14	11	8	17	23	10	13	3	
2013*							27	21	14	7	14	6
2014*			12	19	17	26	22	14	19			
2015*		7	10	3	21	25	27	19	12	11	10	4
2016*	5	13	11	10							2	
2017*				2	19	17	21	16	6	9		
2018*				8	29	24	27	18	12			
2019	6	9	14	23	24	15	5	11			4	3
2020*	13	12	7	3	11	21	22	22	17	11	9	3
<b>2021*</b>	<b>10</b>	<b>11</b>	<b>9</b>	<b>27</b>	<b>15</b>	<b>26</b>	<b>23</b>	<b>27</b>	<b>18</b>	<b>9</b>	<b>12</b>	<b>1</b>
<b>Total</b>	<b>47</b>	<b>56</b>	<b>93</b>	<b>131</b>	<b>199</b>	<b>224</b>	<b>233</b>	<b>217</b>	<b>137</b>	<b>83</b>	<b>65</b>	<b>30</b>

*Table A 11: Monthly means and standard deviation of aerosol optical depth (AOD) at 500 nm at Trollhaugen Observatory*

Month/ Year	Jan	Feb	Mar	Apr	May	Jun	Jul	Aug	Sep	Oct	Nov	Dec
Aerosol optical depth (AOD)												
2014	0.016 ±0.002	0.015 ±0.002	0.014 ±0.002	0.014 ±0.005					0.022 ±0.003	0.017 ±0.002	0.021 1±0.002	0.020 ±0.002
2015	0.029 ±0.003	0.018 ±0.003	0.018 ±0.002	0.017 ±0.001				0.048 ±0.009	0.034 ±0.010	0.040 ±0.007	0.035 ±0.009	0.031 ±0.005
2016	0.035 ±0.006	0.033 ±0.004	0.026 ±0.003	0.027 ±0.004				0.039 ±0.010	0.026 ±0.005	0.024 ±0.005	0.019 ±0.005	0.019 ±0.001
2017	0.020 ±0.003	0.020 ±0.003	0.016 ±0.003	0.015 ±0.002				0.022 ±0.006	0.021 ±0.006	0.019 ±0.002	0.020 ±0.004	0.016 ±0.003
2018	0.016 ±0.004	0.016 ±0.002	0.013 ±0.002	0.014 ±0.001	0.013 ±0.003				0.027 ±0.006	0.022 ±0.002	0.020 ±0.003	0.021 ±0.002
2019	0.027 ±0.006	0.026 ±0.006	0.020 ±0.003	0.019 ±0.002	0.015 ±0.001			0.029 ±0.002	0.019 ±0.001	0.022 ±0.001	0.022 ±0.003	0.026 ±0.002
2020	0.038 ±0.01	0.053 ±0.01	0.053 ±0.01	0.048 ±0.01				0.045 ±0.004	0.041 ±0.007	0.040 ±0.007	0.032 ±0.003	0.024 ±0.003
2021	0.023 ±0.004	0.024 ±0.003	0.020 ±0.002	0.018 ±0.001				0.038 ±0.013	0.034 ±0.008	0.027 ±0.004	0.023 ±0.003	0.027 ±0.003
<b>Mean 2014-2021</b>	<b>0.024 ±0.005</b>	<b>0.026 ±0.005</b>	<b>0.021 ±0.003</b>	<b>0.019 ±0.003</b>	<b>0.014 ±0.002</b>			<b>0.036 ±0.008</b>	<b>0.030 ±0.006</b>	<b>0.026 ±0.004</b>	<b>0.023 ±0.004</b>	<b>0.023 ±0.003</b>

\* version 3 data analysis (Aeronet) – all data have been re-analyzed

Table A 12: Monthly means and standard deviation of the Ångström coefficient (Å) at Trollhaugen.

Month/Year	Jan	Feb	Mar	Apr	May	Jun	Jul	Aug	Sep	Oct	Nov	Dec
Ångström coefficient (Å)												
2014	1.59 ±0.18	1.54 ±0.14	1.29 ±0.09	1.22 ±0.08					1.29 ±0.15	1.52 ±0.17	1.37 ±0.15	1.76 ±0.06
2015	1.69 ±0.61	1.60 ±0.12	1.43 ±0.10	1.34 ±0.09				0.97 ±0.15	1.03 ±0.18	1.26 ±0.14	1.22 ±0.34	1.47 ±0.15
2016	1.53 ±0.12	1.63 ±0.14	1.41 ±0.09	1.42 ±0.05				1.32 ±0.21	1.25 ±0.18	1.34 ±0.22	1.53 ±0.13	1.48 ±0.09
2017	1.61 ±0.16	1.68 ±0.10	1.23 ±0.14	1.21 ±0.08				1.08 ±0.18	1.18 ±0.24	1.28 ±0.13	1.35 ±0.19	1.53 ±0.10
2018	1.51 ±0.10	1.45 ±0.09	1.29 ±0.08	1.32 ±0.17	1.30 ±0.06				1.47 ±0.16	1.47 ±0.11	1.56 ±0.12	1.73 ±0.08
2019	1.63 ±0.11	1.63 ±0.10	1.56 ±0.08	1.34 ±0.08	1.26 ±0.08			0.92 ±0.07	1.51 ±0.12	1.44 ±0.09	1.53 ±0.14	1.61 ±0.10
2020	1.71 ±0.10	1.58 ±0.14	1.33 ±0.04	1.24 ±0.03				0.81 ±0.09	0.91 ±0.10	1.11 ±0.08	1.20 ±0.07	1.44 ±0.11
2021	1.49 ±0.10	1.63 ±0.08	1.40 ±0.05	1.25 ±0.11				0.98 ±0.13	1.11 ±0.20	1.30 ±0.15	1.50 ±0.17	1.60 ±0.08
Mean 2014-2021	1.58 ±0.16	1.59 ±0.12	1.37 ±0.09	1.30 ±0.09	1.27 ±0.07			1.04 ±0.15	1.16 ±0.17	1.34 ±0.13	1.43 ±0.16	1.57 ±0.10

Table A 13: Number of days with AOD observations at Trollhaugen made per month

Month/Year	Jan	Feb	Mar	Apr	May	Jun	Jul	Aug	Sep	Oct	Nov	Dec
Number of days with cloud-free and quality assured observations (lev 2; lev 1.5 for 2013)												
2014	15	22	13	21					4	10	13	11
2015	7	21	11	12				5	14	12	10	25
2016	20	15	15	13				8	10	15	21	21
2017	24	15	24	9				11	11	15	15	10
2018	22	12	13	19	3				11	18	21	18
2019	12	21	21	11	5			1	7	17	9	20
2020	12	21	11	7				7	17	17	10	12
<b>2021</b>	<b>16</b>	<b>17</b>	<b>8</b>	<b>6</b>				<b>9</b>	<b>17</b>	<b>20</b>	<b>17</b>	<b>17</b>
<b>Total</b>	<b>112</b>	<b>129</b>	<b>109</b>	<b>95</b>	<b>8</b>			<b>32</b>	<b>75</b>	<b>106</b>	<b>99</b>	<b>125</b>



## **Appendix II**

### **Description of instruments and methodologies**

**ON THE INSTRUMENTAL METHODS USED FOR THE MEASUREMENTS OF THE VARIOUS GREENHOUSE GASES AT BIRKENES AND ZEPPELIN OBSERVATORIES**

In this section of the appendix, the instrumental methods used for the measurements of the various greenhouse gases are presented, see also Platt et al., 2022 for more details and historical development of Zeppelin. Additionally, we explain the theoretical methods used in calculation of the trends.

The next table provides details about greenhouse gas measurements and recent improvement and extensions.

Table A 14: Instrumental details for greenhouse gas measurements at Zeppelin and Birkenes.

Component		Instrument and method	Time res.	Calibration procedures	Start - End	Comment
<b>Methane (Birkenes)</b>	CH <sub>4</sub>	Picarro CRDS G1301 CO <sub>2</sub> /CH <sub>4</sub> /H <sub>2</sub> O	1 h 5 s	Working std. calibrated against GAW stds at EMPA	19 <sup>th</sup> May 2009 – Jan 2018	
<b>Methane (Birkenes)</b>	CH <sub>4</sub>	Picarro CRDS G2401 CO <sub>2</sub> /CH <sub>4</sub> /CO	1 h 5 s	ICOS reference standards	1 <sup>st</sup> Jan 2018 ->	Data coverage in 2021: 92%
<b>Methane (Zeppelin)</b>	CH <sub>4</sub>	GC-FID	1h	NOAA reference standards	Aug 2001- Apr 2012	
<b>Methane (Zeppelin)</b>	CH <sub>4</sub>	Picarro CRDS	1 h 5 sec	ICOS reference standards	20 <sup>th</sup> Apr. 2012 ->	Data coverage 2021: 81%
<b>Nitrous oxide (Zeppelin)</b>	N <sub>2</sub> O	GC-ECD	30 min	NOAA reference standards	27 <sup>th</sup> Mar 2010 – 31 <sup>st</sup> Dec 2017	
<b>Nitrous oxide (Zeppelin)</b>	N <sub>2</sub> O	Picarro CRDS	1 h 5 sec	ICOS reference standards	1 <sup>st</sup> Jan 2018 ->	Data coverage 2020 88%
<b>Carbon monoxide (Zeppelin)</b>	CO	GC-HgO/UV	20 min	Every 20 min, working std. calibrated vs. GAW std.	Sep. 2001 - 2012	
<b>Carbon monoxide (Zeppelin)</b>	CO	Picarro CRDS	1 h 5 sec	ICOS reference standards.	20 <sup>th</sup> Apr 2012 ->	Data coverage 2021: 97%
<b>Carbon monoxide (Birkenes)</b>	CO	Picarro CRDS G2401 CO <sub>2</sub> /CH <sub>4</sub> /CO	1 h 5 sec	ICOS reference standards.	1 <sup>st</sup> Jan 2018 ->	Data coverage in 2021: 92%
<b>Carbon dioxide (Zeppelin)</b>	CO <sub>2</sub>	Li-Cor	1 h	NOAA reference standards	1989 - 2012	CO <sub>2</sub> measured by ITM Stockholm University (SU) until 2012
<b>Carbon dioxide (Zeppelin)</b>	CO <sub>2</sub>	Picarro CRDS	1 h 5 sec	ICOS reference standards	20 <sup>th</sup> Apr. 2012 ->	Data coverage 2021: 81%
<b>Carbon dioxide (Birkenes)</b>	CO <sub>2</sub>	Picarro CRDS G1301 CO <sub>2</sub> /CH <sub>4</sub> /H <sub>2</sub> O	1 h 5 s	Working std. calibrated against GAW stds at EMPA	19 <sup>th</sup> May 2009 — Jan 2018>	Data coverage in 2019: 95%
<b>Carbon dioxide (Birkenes)</b>	CO <sub>2</sub>	Picarro CRDS G2401 CO <sub>2</sub> /CH <sub>4</sub> /CO	1 h 5 s	ICOS reference standards	1 <sup>st</sup> Jan 2018 ->	Data coverage in 2021: 92%
CFC-11 CFC-12 CFC-113 CFC-115 HFC-125 HFC-134a HFC-152a HFC-365mfc HCFC-22 HCFC-141b HCFC-142b H-1301 H-1211 H-2402	CFCl <sub>3</sub> CF <sub>2</sub> Cl <sub>2</sub> CF <sub>2</sub> ClCFCl <sub>2</sub> CF <sub>3</sub> CF <sub>2</sub> Cl CHF <sub>2</sub> CF <sub>3</sub> CH <sub>2</sub> FCF <sub>3</sub> CH <sub>3</sub> CHF <sub>2</sub> CF <sub>3</sub> CH <sub>2</sub> CHF <sub>2</sub> CH <sub>3</sub> CHF <sub>2</sub> Cl CH <sub>3</sub> CFCl <sub>2</sub> CH <sub>3</sub> CF <sub>2</sub> Cl CF <sub>3</sub> Br CF <sub>2</sub> ClBr	ADS-GCMS	4 h	Every 4 hours, working std. calibrated vs. AGAGE std.	4 <sup>th</sup> Jan 2001- 2010	The measurements of the CFCs, TCE and PCE have higher uncertainty and are not within the required precision of AGAGE. See next section for details.

TComponent		Instrument and method	Time res.	Calibration procedures	Start - End	Comment
Chloromethane Bromomethane Dichloromethane Trichloromethane Trichloroethane Trichloroethene Tetrachloroethene Sulphurhexafluoride	CH <sub>3</sub> Cl CH <sub>3</sub> Br CH <sub>2</sub> Cl <sub>2</sub> CHCl <sub>3</sub> CH <sub>3</sub> CCl <sub>3</sub> CHClCCl <sub>2</sub> CCl <sub>2</sub> CCl <sub>2</sub> SF <sub>6</sub>	ADS-GCMS	4h	Every 4 hours, working std. calibrated vs. AGAGE std.	4 <sup>th</sup> Jan 2001-2010	
Nitrogen trifluoride PFC-14 PFC-116 PFC-218 PFC-318 Sulphurhexafluoride Sulfuryl fluoride HFC-23 HFC-32 HFC-125 HFC-134a HFC-143a HFC-152a HFC-227ea HFC-236fa HFC-245fa HFC-365mfc HFC-43-10mee HCFC-22 HCFC-141b HCFC-142b CFC-11 CFC-12 CFC-113 CFC-115 H-1211 H-1301 H-2402 Chloromethane Bromomethane Dichloromethane Trichloromethane Trichloroethane Dibromomethane Trichloroethene Tetrachloroethene Carbon tetrachloride Ethane Propane Butane Pentane Benzene Toluene Ozone	NF <sub>3</sub> CF <sub>4</sub> C <sub>2</sub> F <sub>6</sub> C <sub>3</sub> F <sub>8</sub> c-C <sub>4</sub> F <sub>8</sub> SF <sub>6</sub> SO <sub>2</sub> F <sub>2</sub> CHF <sub>3</sub> CH <sub>2</sub> F <sub>2</sub> CHF <sub>2</sub> CF <sub>3</sub> CH <sub>2</sub> FCF <sub>3</sub> CH <sub>3</sub> CF <sub>3</sub> CH <sub>3</sub> CHF <sub>2</sub> CF <sub>3</sub> CHFCF <sub>3</sub> CF <sub>3</sub> CH <sub>2</sub> CF <sub>3</sub> CF <sub>3</sub> CH <sub>2</sub> CHF <sub>2</sub> CH <sub>3</sub> CF <sub>2</sub> CH <sub>2</sub> CF <sub>3</sub> CF <sub>3</sub> (CHF) <sub>2</sub> CF <sub>2</sub> CF <sub>3</sub> CHClF <sub>2</sub> CH <sub>3</sub> CCl <sub>2</sub> F CH <sub>3</sub> CClF <sub>2</sub> CCl <sub>3</sub> F CCl <sub>2</sub> F <sub>2</sub> CCl <sub>2</sub> FCClF <sub>2</sub> CClF <sub>2</sub> CF <sub>3</sub> CBrClF <sub>2</sub> CBrF <sub>3</sub> C <sub>2</sub> Br <sub>2</sub> F <sub>4</sub> CH <sub>3</sub> Cl CH <sub>3</sub> Br CH <sub>2</sub> Cl <sub>2</sub> CHCl <sub>3</sub> CH <sub>3</sub> CCl <sub>3</sub> CH <sub>2</sub> Br <sub>2</sub> CHClCCl <sub>2</sub> CCl <sub>2</sub> CCl <sub>2</sub> CCl <sub>4</sub> C <sub>2</sub> H <sub>6</sub> C <sub>3</sub> H <sub>8</sub> C <sub>4</sub> H <sub>10</sub> C <sub>5</sub> H <sub>12</sub> C <sub>6</sub> H <sub>6</sub> C <sub>6</sub> H <sub>5</sub> CH <sub>3</sub> O <sub>3</sub>	Medusa-GCMS No. 19	2 h	Every 2 hours, working std. calibrated vs. AGAGE std	1 <sup>st</sup> September 2010	Data coverage 2021: 94% (except for Propane, Benzene, Toluene (78 %))

The overall data coverage for 2021 was 94%. A new sample pump was installed in March 2021 and solved the last years issues for Benzene and Toluene.

## DATA QUALITY AND UNCERTAINTIES

### HALOCARBONS

In 2001 – 2010 measurements of a wide range of hydrochlorofluorocarbons, hydrofluorocarbons (HCFC-141b, HCFC-142b, HFC-134a etc.), methyl halides (CH<sub>3</sub>Cl, CH<sub>3</sub>Br, CH<sub>3</sub>I) and the halons (e.g. H-1211, H-1301) were measured with good scientific quality by using ADS-GCMS. The system also measured other compounds like the chlorofluorocarbons (CFCs), but the quality and the precision of these measurements were not at the same level. Table A 15 shows a list over those species measured with the ADS-GCMS at Zeppelin Observatory from 2001 - 2010. The species that are in blue are of acceptable scientific quality and in accordance with recommendations and criteria of the AGAGE network for measurements of halogenated greenhouse gases in the atmosphere. Those listed in red have higher uncertainties and are not within the required precision of AGAGE. There are various reasons for these increased uncertainties; unsolved instrumental problems e.g. possible electron overload in detector (for the CFC's), influence from other species, detection limits (CH<sub>3</sub>I, CHClCCl<sub>2</sub>) and unsolved calibration problems (CHBr<sub>3</sub>) or instrumental issues (CCl<sub>2</sub>CCl<sub>2</sub>). On 1<sup>st</sup> September 2010, the ADS-GCMS was replaced by a Medusa-GCMS system. The uncertainties improved for almost all species (Table A 11 for details), but there are periods where measurements of the CFC's were still not satisfactory due to a failure in the detector and still high blank values and memory effects in the instruments leads to higher uncertainties in the CHClCCl<sub>2</sub> (TCE) measurements.

Table A 15: ADS-GCMS measured species at Zeppelin from 4<sup>th</sup> January 2001 to 1<sup>st</sup> September 2010. Good scientific quality data in Blue; Data with reduced quality data in Red. The data are available through <http://ebas.nilu.no>. Please read and follow the stated data policy upon use.

Compound	Typical precision (%)	Compound	Typical precision (%)
SF <sub>6</sub>	1.5	H1301	1.5
HFC134a	0.4	H1211	0.4
HFC152a	0.6	CH <sub>3</sub> Cl	0.6
HFC125	0.8	CH <sub>3</sub> Br	0.8
HFC365mfc	1.7	CH <sub>3</sub> I	5.1
HCFC22	0.2	CH <sub>2</sub> Cl <sub>2</sub>	0.4
HCFC141b	0.5	CHCl <sub>3</sub>	0.3
HCFC142b	0.5	CHBr <sub>3</sub>	15
HCFC124	2.3	CCl <sub>4</sub>	0.5
CFC11	0.3	CH <sub>3</sub> CCl <sub>3</sub>	0.6
CFC12	0.3	CHClCCl <sub>2</sub>	1.2
CFC113	0.2	CCl <sub>2</sub> CCl <sub>2</sub>	0.7
CFC115	0.8		

Table below gives an overview over the species measured with the Medusa-GCMS systems at the AGAGE stations and the typical precision with the different instruments. The Medusa-GCMS instrument at the Zeppelin Observatory has the same precision as shown in the Table A 16.

Table A 16: AGAGE measured species.

Compound	Typical precision (%)	Compound	Typical precision (%)
NF <sub>3</sub>	1	CFC-11	0.15
CF <sub>4</sub>	0.15	CFC-12	0.05
C <sub>2</sub> F <sub>6</sub>	1	CFC-113	0.2
C <sub>3</sub> F <sub>8</sub>	3	CFC-115	0.8
c-C <sub>4</sub> F <sub>8</sub>	1.5	H-1301	1.7
SF <sub>6</sub>	0.6	H-1211	0.4
SO <sub>2</sub> F <sub>2</sub>	2	H-2402	2
HFC-23	0.7	CH <sub>3</sub> Cl	0.2
HFC-32	3	CH <sub>3</sub> Br	0.6
HFC-134a	0.5	CH <sub>2</sub> Cl <sub>2</sub>	0.5
HFC-152a	1.4	CH <sub>2</sub> Br <sub>2</sub>	1.5
HFC-125	0.7	CCl <sub>4</sub>	1
HFC-143a	1	CH <sub>3</sub> CCl <sub>3</sub>	0.7
HFC-227ea	2.2	CHClCCl <sub>2</sub>	3
HFC-236fa	10	CCl <sub>2</sub> CCl <sub>2</sub>	0.5
HFC-245fa	3	C <sub>2</sub> H <sub>6</sub>	0.3
HFC-365mfc	5	C <sub>3</sub> H <sub>8</sub>	0.6
HFC-43-10mee	3	C <sub>4</sub> H <sub>10</sub>	0.6
HCFC-22	0.3	C <sub>6</sub> H <sub>6</sub>	0.3
HCFC-141b	0.5	C <sub>7</sub> H <sub>8</sub>	0.6
HCFC-142b	0.4		

## METHANE

Methane is measured at both Birkenes and Zeppelin using a Picarro CRDS (Cavity Ring-Down Spectrometer) monitor which is calibrated against ICOS reference standards (NOAA scale). The instrument participates in ring tests and applies to the ICOS system for calibration and measurement control. The continuous data are also compared to weekly flask samples sent to NOAA CMDL, Boulder Colorado. All data are available for download from EBAS database <http://ebas.nilu.no>.

## $\delta^{13}\text{C}_{\text{CH}_4}$

Air samples from Zeppelin are collected in 1 L steel or aluminium canisters at the same air inlet as CH<sub>4</sub>. Two samples per week are sent to the Greenhouse Gas Laboratory at Royal Holloway University of London. Methane mole fraction was measured using a Picarro 1301 cavity ring down spectrometer (CRDS).  $\delta^{13}\text{C}$  analysis is carried out using a modified gas chromatography isotope ratio mass spectrometry system for all samples (Trace Gas and Isoprime mass spectrometer, Isoprime Ltd.) with 0.05‰ repeatability. All measurements for the canisters are made in triplicate. See Fischer et al., 2017 and Myhre et al., 2016 for more details.

## N<sub>2</sub>O MEASUREMENTS

N<sub>2</sub>O at Zeppelin is measured using a mid-IR Cavity Ring Down instrument (since December 2017) which is calibrated against ICOS reference standards (NOAA scale). The instrument participates in ring tests and applies to the ICOS system for calibration and measurement control. The continuous data are also compared to weekly flask samples sent to NOAA CMDL, Boulder Colorado. This instrument is doing continuous measurements with improved precision and higher measurement frequency (< 1 min).

**CO<sub>2</sub> MEASUREMENTS** Carbon dioxide (CO<sub>2</sub>) at Birkenes and Zeppelin is monitored using a Picarro Cavity Ring-Down Spectrometer for continuous measurements, calibrated against a set of ICOS reference standards (NOAA scale). The instrument participates in ring tests and applies to the ICOS system for calibration and measurement control. The continuous data are also compared to weekly flask samples sent to NOAA CMDL, Boulder Colorado. All data will be available for download from the EBAS database <http://ebas.nilu.no>.

### **CO MEASUREMENTS**

Carbon monoxide (CO) at Birkenes and Zeppelin is monitored using a Picarro Cavity Ring-Down Spectrometer for continuous measurements, calibrated against a set of ICOS reference standards (NOAA scale). The instrument participates in yearly ring tests and applies to the ICOS system for calibration and measurement control. The continuous data are also compared to weekly flask samples sent to NOAA CMDL, Boulder Colorado. All data will be available for download from the EBAS database <http://ebas.nilu.no>.

### **<sup>14</sup>C IN CO<sub>2</sub> MEASUREMENTS**

As part of the ICOS program, isotope <sup>14</sup>C in CO<sub>2</sub> is sampled every 2-weeks. CO<sub>2</sub> is absorbed by sodium hydroxide solution (NaOH 4mol/l) in a rotating Raschig-tube. The liquid sodium hydroxide samples are transferred into glass bottles and sent to the ICOS Central Radiocarbon Laboratory for analysis of the <sup>14</sup>C/C ratio in the absorbed CO<sub>2</sub>. Sampling started in 2017.

### **IMPLEMENTATION OF MEASUREMENTS FROM BIRKENES AND ZEPPELIN INTO ICOS RESEARCH INFRASTRUCTURE**

The Integrated Carbon Observation System (ICOS) is a European research infrastructure forming an observation system that will measure and assess the global carbon budget, including atmospheric CO<sub>2</sub>, CH<sub>4</sub> and CO concentrations, while ensuring independent and reliable measurements. ICOS-Norway (<https://no.icos-cp.eu>) contributes to the network of atmospheric measurements with two observatories, Birkenes and Zeppelin.

ICOS has divided their sites into two labels Class 1 and Class 2, dependent on instrumental setup. At Class 1 sites a wider range of measurements of different species are required. Whilst for Class 2 fewer parameters are mandatory. The labelling process evaluates the site set up, the instrumentation with its calibration set-up and data handling, as a quality certificate of the data output from the ICOS site (Figure 58). The labelling process is time consuming as the instrument (Picarro) needs to be evaluated for minimum 1 month at the central ICOS lab, ICOS Atmospheric Thematic Centre (ATC) in France. Another central ICOS lab, ICOS Central Analytical Laboratories (CAL) in Germany, provides calibration cylinders and it takes 4 months to produce them. The same lab provides calibration cylinders and it takes 4 months to produce them. After having the instrument and calibration routines established at the site, the measurements will have to go through a 6 months evaluation period before approval as an ICOS site. In total it typically takes about 1.5 years to get an ICOS certificate.

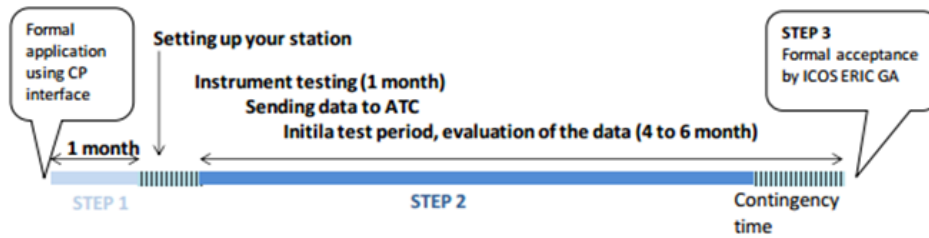
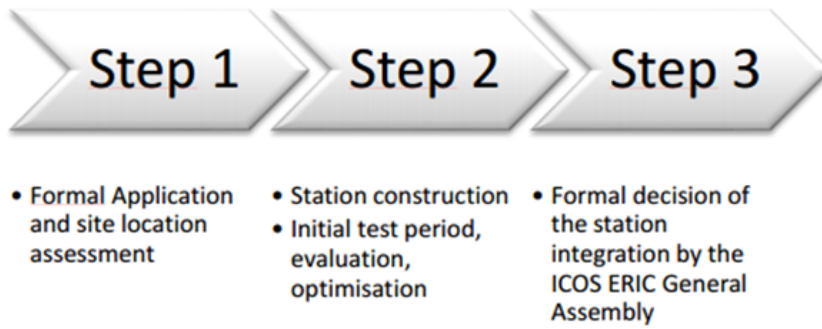


Figure 58: Outline of the labelling process for ICOS stations according to the atmosphere thematic centre (ATC).



The ATC has established the following recommended parameters for ICOS Class 1 and Class 2 sites:

Category	Gases, continuous	Gases, periodical	Meteorology, continuous	Eddy Fluxes
<b>Class 1</b> Mandatory parameters	<ul style="list-style-type: none"> <li>• CO<sub>2</sub>, CH<sub>4</sub>, CO : at each sampling height</li> </ul>	<ul style="list-style-type: none"> <li>• CO<sub>2</sub>, CH<sub>4</sub>, N<sub>2</sub>O, SF<sub>6</sub>, CO, H<sub>2</sub>, <sup>13</sup>C and <sup>18</sup>O in CO<sub>2</sub>: weekly sampled at highest sampling height†</li> <li>• <sup>14</sup>C (radiocarbon integrated samples): at highest sampling height</li> </ul>	<ul style="list-style-type: none"> <li>• Air temperature, relative humidity, wind direction, wind speed: at highest and lowest sampling height*</li> <li>• Atmospheric Pressure</li> <li>• Planetary Boundary Layer Height** †</li> </ul>	
<b>Class 2</b> Mandatory parameters	<ul style="list-style-type: none"> <li>• CO<sub>2</sub>, CH<sub>4</sub> : at each sampling height</li> </ul>		<ul style="list-style-type: none"> <li>• Air temperature, relative humidity, wind direction, wind speed: at highest and lowest sampling height*</li> <li>• Atmospheric Pressure</li> </ul>	
Recommended parameters***	<ul style="list-style-type: none"> <li>• <sup>222</sup>Rn, N<sub>2</sub>O, O<sub>2</sub>/N<sub>2</sub> ratio</li> <li>• CO for Class 2 stations</li> </ul>	<ul style="list-style-type: none"> <li>• CH<sub>4</sub> stable isotopes, O<sub>2</sub>/N<sub>2</sub> ratio for Class 1 stations: weekly sampled at highest sampling height</li> </ul>		<ul style="list-style-type: none"> <li>• CO<sub>2</sub> : at one sampling height</li> </ul>

\* Atmospheric temperature and relative humidity recommended at all sampling heights

\*\* Only required for continental stations.

\*\*\* Recommended for its scientific value but support from ATC in terms of protocols, data base, spare analyzer will not be ensured as long as the parameters are not mandatory.

The Zeppelin Observatory was labelled as an ICOS Class 1 site in 2018. Meanwhile, for sites such as Birkenes, classed as a ‘continental site’ by ICOS, the ATC requires that measurements are from air sampled at 100 m above ground or higher, typically using sampling inlets installed on a mast, with additional sampling at 10 m, and between 40-70 m. The purpose of this is to minimise the influence of vegetation (i.e. photosynthesis) on CO<sub>2</sub> measurements. For Zeppelin, a mountain top site, the only requirement was that sampling is ‘sufficiently high to avoid contamination e.g. by local sources’.

Due to the location of the Birkenes Observatory on a small hill at 40 m, construction of foundations for a 100 m would be challenging and expensive. Thus, NILU initiated negotiations with ATC to lower the required sampling height on the basis that the Observatory is already elevated by 40 m. The ATC agreed to lower the required sampling height to 75 m, a more feasible mast height requiring less extensive foundations, stating in writing: “The Birkenes Observatory location and site infrastructure fulfil the ICOS requirements and recommendations specified in the latest ICOS Atmospheric Station Specifications document (version 1.3, November 2017) when the tower will be installed.”

As of 28<sup>th</sup> August 2020 construction of the 75 m mast was complete (Figure 3 and Figure 59) and the installation of equipment on the mast (meteorological equipment, sample inlets etc.) were mostly done by the second week of September. The very first measurements from the 75-meter mast were performed on 14<sup>th</sup> September. The finalization of the installation is scheduled to the beginning of October. Note that the new mast has also required changes to the station infrastructure i.e. changing the location of the station entrance, upgraded protection from lightning strikes and falling ice, as well as changes in health and safety procedures (the station may no longer be accessed if there is a risk of thunder storms).



*Figure 59: Birkenes Observatory with the new 75 m mast installed August-September 2020 to comply with the ICOS requirements.*

**Status of the labelling process for Birkenes and Zeppelin Observatories:**

- The Zeppelin Observatory has achieved Class 1 status and is fully integrated in the network
- The Birkenes Observatory has achieved class 2 status as of May 2021

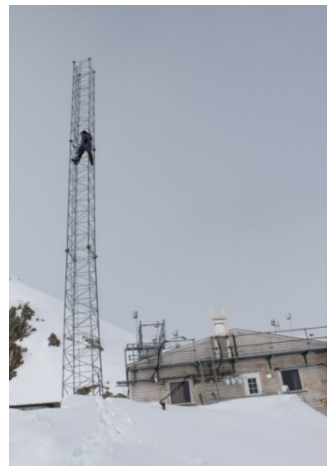
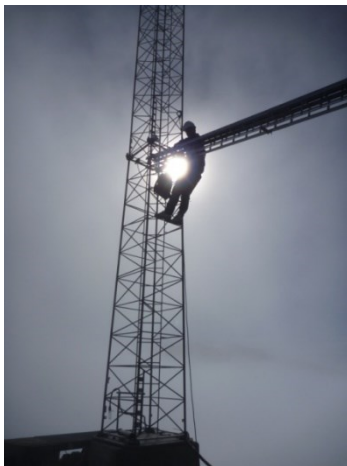
At class 1 sites an automatic flask sampler is mandatory and has been installed at the Zeppelin station. The flask sampling program is developed by ICOS but there are some issues with the automatic flask sampler. Work in progress for fixing this.

On 25<sup>th</sup> May 2021, The ICOS General Assembly unanimously accepted labelling of Birkenes Observatory as a Class 2 Atmosphere Station.

**AIR INLET AT ZEPPELIN**

In 2011 the air inlet for the GHG measurements at Zeppelin were improved to reduce possible influence from the station and visitors at the station. The inlet was moved away from the station and installed in a 15 m tower nearby for the following components:

- N<sub>2</sub>O
- CH<sub>4</sub>
- CO<sub>2</sub>
- CO
- Halogenated compounds
- NOAA flasks sampling program
- Isotope flask sampling of CO<sub>2</sub> and CH<sub>4</sub>



## DETERMINATION OF BACKGROUND DATA

Based on the daily mean concentrations an algorithm is selected to find the values assumed as clean background air. If at least 75% of the trajectories within +/- 12 hours of the sampling day are arriving from a so-called clean sector, defined below, one can assume the air for that specific day to be non-polluted. The remaining 25% of the trajectories from European, Russian or North American sector are removed before calculating the background.

## CALCULATION OF TRENDS FOR GREENHOUSE GASES AND VOCs

To calculate the annual trends the observations have been fitted as described in Simmonds et al. (2006) by an empirical equation of Legendre polynomials and harmonic functions with linear, quadratic, and annual and semi-annual harmonic terms:

$$f(t) = a + b \left( \frac{N}{12} \right) \cdot P_1 \left( \frac{t}{N} - 1 \right) + \frac{1}{3} \cdot d \left( \frac{N}{12} \right)^2 \cdot P_2 \left( \frac{t}{N} - 1 \right) + c_1 \cdot \cos \left( \frac{2\pi t}{12} \right) + s_1 \sin \left( \frac{2\pi t}{12} \right) + c_2 \cos \left( \frac{4\pi t}{12} \right) + s_2 \sin \left( \frac{4\pi t}{12} \right)$$

The observed  $f$  can be expressed as functions of time measures from the 2N-months interval of interest. The coefficient  $a$  defines the average mole fraction,  $b$  defines the trend in the mole fraction and  $d$  defines the acceleration in the trend. The  $c$  and  $s$  define the annual and inter-annual cycles in mole fraction.  $N$  is the mid-point of the period of investigation.  $P_i$  are the Legendre polynomials of order  $i$ .

This equation is used for all GHGs except for the halocarbons, where the fit between the empirical equation and observations improves if the semi-annual harmonic terms are replaced by an additional Legendre polynomial.

We are applying a new and improved method for estimating the *uncertainties* in the estimated annual trends from the time series regression modelling. In previous years, these uncertainties were estimated using a standard method from ordinary linear regression, where it was implicitly assumed that the residuals of the fitted regression models were uncorrelated. However, the use of such standard methods is known to often underestimate the true uncertainties in the estimated parameters if these assumptions are not true, i.e. if the residuals are autocorrelated, which to a large extent is the case for the regression models being fitted here.

In the current report we have replaced the standard method with a new method for estimation of uncertainties in the estimated annual trend that takes into account the presence of autocorrelated errors in the fitted model residuals. The new method also takes into account possible presence of heteroscedasticity, which means that the variances of the residuals might vary with the level of the time series, which also affects the uncertainties of the estimated trend. To this end we use the routine `vcovHAC` in the `sandwich` package in R (R Core Team, 2018) as described in Zeileis (2006; 2004), to estimate standard deviation of all estimated parameters of the time series regression models. Here HAC is short for Heteroscedastic and Autocorrelation Consistent.

It is important to emphasize that the new method only alters the estimated *uncertainties* of the annual trend estimates. The annual trend estimates themselves are not influenced by this update and have been correctly estimated using standard linear regression also in previous year's reports.

## ON THE SURFACE IN SITU OBSERVATIONS OF AEROSOL MICROPHYSICAL AND OPTICAL PROPERTIES AT BIRKENES, ZEPPELIN AND TROLLHAUGEN OBSERVATORY

*Table A 17: Overview of atmospheric aerosol parameters measured by surface in situ observations operated at which station*

	Birkenes	Trollhaugen	Zeppelin
Particle Number Size Distribution (fine size range $D_p < 0.8 \mu\text{m}$ )	X	X	X
Particle Number Size Distribution (coarse size range $D_p > 0.8 \mu\text{m}$ )	X (OPS)		X (APS)
Particle Number Size Distribution, refractory particle fraction (fine size range $D_p < 0.8 \mu\text{m}$ )			X
Aerosol Scattering Coefficient (spectral)	X	X	
Aerosol Absorption Coefficient (spectral)	X	X	X

Concerning surface in situ observations of microphysical and optical properties of atmospheric aerosol, the table on the left gives an overview over the parameters observed at Birkenes, Trollhaugen, and Zeppelin stations and operated by NILU.

To achieve high quality data with appropriate uncertainty and precision, this requires networked instruments to participate in inter-comparisons at ACTRIS aerosol calibration centre in Leipzig, Germany, in regular intervals. This activity has proven to be necessary in order to ensure comparable measure-

ments within the distributed infrastructure. The frequency of these inter-comparisons, once every 2-3 years, is balanced with minimising the downtime associated with these quality assurance measures. In 2016, instruments targeting the direct aerosol climate effect were in the focus of inter-comparisons. Both the integrating nephelometer and the newer filter absorption photometer, measuring the spectral aerosol particle scattering and absorption coefficients respectively, were scheduled for being inter-compared, with satisfactory outcome in both cases. Between inter-comparisons, instruments are field calibrated regularly to ensure internal consistency of the time series.

With respect to microphysical aerosol properties, the particle number size distribution (PNSD) at surface-level is observed at all 3 stations covered in this report, at least over parts of the relevant range in particle size. The relevant particle sizes cover a range of  $0.01 \mu\text{m} - 10 \mu\text{m}$  in particle diameter. The diameter range of  $1.0 \mu\text{m} - 10 \mu\text{m}$  is commonly referred to as coarse mode, the range  $D_p < 1.0 \mu\text{m}$  as fine mode. The fine mode is separated further into Aitken-mode ( $0.01 \mu\text{m} < D_p < 0.1 \mu\text{m}$ ) and accumulation mode ( $0.1 \mu\text{m} < D_p < 1 \mu\text{m}$ ). The distinction of these modes is justified by different predominant physical processes as function of particle size. In the Aitken-mode, particles grow by condensation of precursor gases from the gas-phase and coagulate among themselves or with accumulation mode particles. Accumulation mode particles grow by taking up Aitken-mode particles or by mass uptake while being activated as cloud droplets, and they are removed by precipitation. Coarse mode particles in turn are formed by break-up of biological or crustal material, including pollen, bacteria, and fungus spores, and removed by gravitational settling and wet removal. The PNSD of an aerosol is needed for quantifying any interaction or effect of the aerosol since all of them depend strongly on particle size.

To measure the PNSD over the full relevant size range, several measurement principles need to be combined. A Differential Mobility Particle Spectrometer (DMPS) measures the particle number size distribution, now in the range of  $0.01 - 0.8 \mu\text{m}$  particle diameter after several improvements of the instruments at all three stations, i.e. almost the full fine mode. In a DMPS, the particles in the sample air stream are put into a defined state of charge by exposing them to an ionised atmosphere in thermal equilibrium. The DMPS uses a cylindrical capacitor to select a narrow size fraction of the particle phase. The particle size of the selected size fraction is determined by the voltage applied to the capacitor. The particle number concentration in the selected size fraction is then counted by a Condensation Particle Counter (CPC). A mathematical inversion that considers charge probability, diffusional losses of

particles in the system, transfer function of the capacitor, and counting efficiency of the CPC is then used to calculate the particle number size distribution.

The PNSD of particles with diameters  $0.25 \mu\text{m} < D_p < 30 \mu\text{m}$  can be measured with 2 device types: 1) an Optical Particle Spectrometer (OPS); 2) an Aerodynamic Particle Spectrometer (APS). In the OPS, the particles in the sample stream are focussed through a laser beam. The instrument registers number and amplitude of the pulses of light scattered by the particles. The particle pulses are sorted into a histogram by their amplitude, where the pulse amplitude yields the particle diameter and the pulse number the particle concentration, i.e. together the PNSD. Particle sizing in an OPS depends on the particle refractive index, particularly its imaginary part which determines particle absorption. In an APS, particles are exposed to an air flow passage where the particles are accelerated. The time needed for the particle to pass the passage depends on the amount of acceleration, and thus its aerodynamic diameter. The time needed to pass the passage is measured by laser beams at start and end of the passage. Together with counting the number of particles per time, this yields the particle number size distribution.

Both, the DMPS, the OPS, and the APS, yield method specific measures of the particle diameter, the electrical mobility, the optical, and the aerodynamic particle diameter, respectively. When related to the spherical equivalent geometric particle diameter commonly referred to, all particle size measures depend on particle shape (causing a 5% systematic uncertainty in particle diameter), the optical particle diameter in addition on particle refractive index (causing a 20% systematic uncertainty in particle diameter), and the aerodynamic particle diameter on particle density (causing a 15% systematic uncertainty in particle diameter). Where possible, the PNSDs provided by DMPS and OPS/APS are joined into a common PNSD, in this report. To quality assure this process, PNSDs are accepted only if DMPS and OPS/APS PNSD agree within 25% in particle diameter in their overlap size range. Together, both instruments provide a PNSD that spans over 3 orders of magnitude in particle diameter, and over 6 orders of magnitude in particle concentration.

Optical aerosol parameters quantify the direct aerosol climate effect. The observation programme at Birkenes includes the spectral particle scattering coefficient  $\sigma_{sp}(\lambda)$  and the spectral particle absorption coefficient  $\sigma_{ap}(\lambda)$ . The scattering coefficient quantifies the amount of light scattered by the aerosol particle population in a sample per distance a light beam travels through the sample. The absorption coefficient is the corresponding property quantifying the amount of light absorbed by the particle population in the sample. An integrating nephelometer is used for measuring  $\sigma_{sp}(\lambda)$  at 450, 550, and 700 nm wavelength. In this instrument, the optical sensors look down a blackened tube that is filled with aerosol sample. The tube is illuminated by a light source with a perfect cosine intensity characteristic perpendicularly to the viewing direction. It can be shown mathematically that this setup integrates the scattered light seen by the optical sensors over all scattering angles. The nephelometer at Birkenes has successfully undergone quality assurance by intercomparison within the EU research infrastructure ACTRIS in 2015. In 2017 we detected drift in the older filter absorption photometer operated at Birkenes since 2009 through carefully implemented quality control within ACTRIS. The drift was detected by operating the older filter absorption photometer in parallel with a newer, more stable make and model in order to ensure a continuous, rupture-free aerosol absorption time series at Birkenes. In addition, the newer instrument was sent to an inter-comparison within the European research infrastructure for short-lived climate forcers ACTRIS. These exercises connect individual instruments to a network-wide primary standard, ensuring traceability and comparability of observations at stations in the network. The old instrument exhibiting the drift has since been decommissioned.

For the nephelometer at Trollhaugen, such intercomparisons are impossible because of the remote Antarctic location and associated logistical challenges. However, the Trollhaugen instrument undergoes the same regular on-site quality assurance as the Birkenes instrument, including regular calibration verification traceable to physical first principles (calibration with high-purity carbon dioxide,

where scattering coefficient of carbon dioxide can be calculated from fundamental quantum mechanics).

The spectral particle absorption coefficient  $\sigma_{ap}(\lambda)$  is measured by filter absorption photometers. A filter absorption photometer infers  $\sigma_{ap}(\lambda)$  by measuring the decrease in optical transmissivity of a filter while the filter is loaded with the aerosol sample. The transmissivity time series is subsequently translated into an absorption coefficient time series by using Lambert-Beer's law, the same law also used in optical spectroscopy. The filter absorption photometers deployed at Birkenes have been a custom-built 1 wavelength Particle Soot Absorption Photometer (PSAP), a commercial 3-wavelength PSAP, and a modern AE33 aethalometer. The 1-wavelength PSAP received quality assurance by intercomparison within ACTRIS in 2013 discovering calibration stability issues. The 3-wavelength PSAP has undergone ACTRIS intercalibration successfully in 2015, i.e. without discovering any issues. Thus, both instruments are interpreted in combination to benefit from both, quality assurance in a research network and spectral capabilities. For 2013 and later, the data of the 3-wavelength PSAP are used, for 2010-2012, the data of the older 1-wavelength are used after being corrected by comparison with the newer instrument during the overlap period. For comparison with the nephelometer, the PSAP data has been transferred to a wavelength of 550 nm using the measured spectral dependence (3-wavelength PSAP), or by assuming an absorption Ångström coefficient  $\alpha_{ap}$  of -1 (1-wavelength PSAP, adding 2% systematic uncertainty to the data). The AE33 aethalometer has been deployed at Birkenes in late 2017. It extends the spectral range of the  $\sigma_{ap}(\lambda)$  measurements to 370 – 950 nm (UV to near IR) with a resolution of 7 wavelengths. Previous aethalometer models suffered from high systematic uncertainties due to uncorrected dependencies on filter loading (e.g. Collaud Coen et al., 2010). Comparisons and calibrations within ACTRIS have shown that this systematic uncertainty has been reduced significantly in the AE33 model by an internal loading compensation (Drinovec et al., 2015).

The same AE33 aethalometer instrument type has been operated at Zeppelin since 2015.

Figure 60 compares the particle absorption coefficient between the Particle Absorption Photometer (PSAP) deployed at Birkenes in 2012, and the AE33 aethalometer deployed there in 2017 with a scatter plot including regression line. The analysis shows a correlation coefficient  $R^2$  of 0.97 for the whole range of values, i.e. 97% of the variation in the data of one instrument is explained by the respective variation of the other instrument. This result ensures that the new instrument will continue the time series consistently. The slope of the regression line deviates from 1. Corresponding calibration factors are currently being established by the ACTRIS Research Infrastructure.

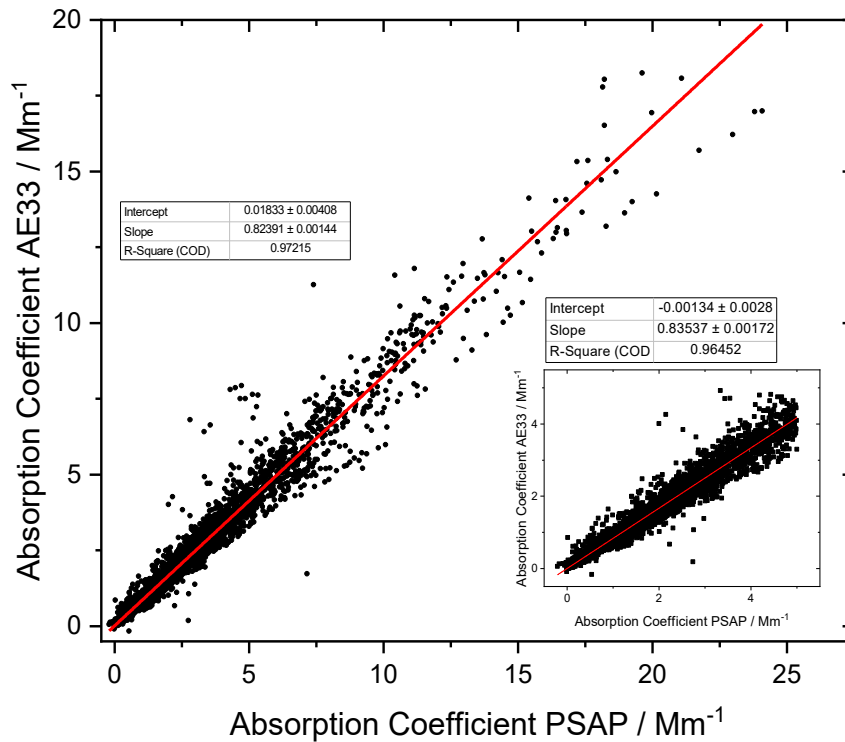


Figure 60: Comparison of particle absorption coefficient data measured the Particle Absorption Photometer (PSAP) deployed at Birkenes in 2012, and the AE33 aethalometer deployed there in 2017. The wavelength of the absorption coefficient has been interpolated to 550 nm for both instruments. The data are compared as scatter plot with regression line (red), large panel for the total range of values, small panel for values  $\leq 5 \text{ Mm}^{-1}$ .

Even though the oldest filter absorption photometer in operation at Birkenes underwent quality assurance by off-site intercomparison within ACTRIS in 2013, a drift of the reading of the older compared to the newer instrument can be observed between 2013 – 2015. These stability issues of the older filter absorption photometer were discovered already during the 2013 intercomparison. Consequently, also the newer filter absorption photometer was subjected to an ACTRIS intercomparison in 2015. The intercomparison discovered no issues with the newer instrument and confirmed stability of calibration. As a result, the whole  $\sigma_{ap}$  time series obtained with the old filter absorption photometer has been corrected with the 2012 instrument as reference, yielding a consistent aerosol absorption time series for Birkenes for the years since 2010. In 2017, the 2012 absorption photometer experienced problems related to an unstable measurement of the sample flow, leading to low data coverage in summer 2017. Due to the importance of the aerosol absorption measurement in relation to emissions from biomass combustion for domestic heating, it was decided to install the new 7-wavelength version in parallel, and keep both instruments running as mutual backup.

All in situ observations of aerosol properties representing the ground-level are conducted for the aerosol at dry-state ( $\text{RH} < 40\%$ ) for obtaining inter-comparability across the network.

#### DETAILS ABOUT AEROSOL OPTICAL DEPTH MEASUREMENTS

The amount of particles in the air during sunlit conditions is continuously monitored by means of Precision-Filter-Radiometer (PFR) sun photometers, located at the Sverdrup station in Ny-Ålesund and



at Trollhaugen Atmospheric Observatory, Troll Station, Antarctica, and a Cimel instrument at Birkenes. The observations in Ny-Ålesund and at Troll Station are performed in collaboration with PMOD/WRC (N. Kouremeti, S. Kazadzis), Davos, Switzerland. The main instrument characteristics are given below.



#### **AERONET - Cimel C-318**

- Sun (9 channels) and sky radiances
- Wavelength range: 340-1640 nm
- 15 min sampling
- No temperature stabilization
- AOD uncertainty: 0.01-0.02



#### **PFR-GAW- Precision Filter Radiometer**

- Direct sun measurements (4 channels)
- Wavelength range: 368 - 862 nm
- 1 min averages
- Temperature stabilized
- AOD uncertainty: 0.01

*Figure 61: Photos and typical features of the standard instrument of the AERONET (left panel) and GAW PFR network instruments (right panel)*

In 2002, Physikalisch-Meteorologisches Observatorium Davos/World Radiation Center (PMOD/WRC), in collaboration with NILU, started AOD observations in Ny-Ålesund (at the Sverdrup station, 46 m a.s.l.) as part of the global AOD network on behalf of the WMO GAW program. A precision filter radiometer (PFR) measures the extinction in four narrow spectral bands at 368 nm, 415 nm, 500 nm and 862 nm. Data quality control includes instrumental control like detector temperature and solar pointing control as well as objective cloud screening. Ångström coefficients are derived for each set of measurements using all four PFR channels. Calibration is performed annually at PMOD/WRC. Quality assured data are available at the World Data Centre of Aerosols (WDCA), hosted at NILU (see <https://ebas.nilu.no>). In order to calculate a daily average, at least 50 single measurements are required.

The sun-photometer measurements in Ny-Ålesund are part of the global network of aerosol optical depth (AOD) observations, which started in 1999 on behalf of the WMO GAW program. The instrument is located on the roof of the Sverdrup station, Ny-Ålesund, close to the EMEP station on the Zeppelin Mountain (78.9°N, 11.9°E, 474 m a.s.l.). The Precision Filter Radiometer (PFR) has been in operation since May 2002. In Ny-Ålesund, the sun is below 5° of elevation from 10<sup>th</sup> October to 4<sup>th</sup> March, limiting the period with sufficient sunlight to the spring-early autumn season. However, during the summer months it is possible to measure day and night if the weather conditions are satisfactory. The instrument measures direct solar radiation in four narrow spectral bands centred at 862 nm, 501 nm, 411 nm, and 368 nm. Data quality control includes instrumental control like detector temperature and solar pointing control as well as objective cloud screening. Measurements made at full minutes are averages of 10 samples for each channel made over a total duration of 1.25 seconds. SCIAMACHY

TOMSOMI and OMI ozone columns as well as meteorological data from Ny-Ålesund are used for the retrieval of aerosol optical depth (AOD).

At Birkenes Observatory, aerosol optical depth measurements started in spring 2009, utilizing an automatic sun and sky radiometer (CIMEL type CE-318) of the global Aerosol Robotic Network (AERONET) at NASA-GSFC, with spectral interference filters centred at selected wavelengths: 340 nm, 380 nm, 440 nm, 500 nm, 675 nm, 870 nm, 1020 nm, and 1640 nm. The measurement frequency is approximately 15 minutes (this depends on the air-mass and time of day). Calibration is performed about once per year, at the Atmospheric Optics Group at the University of Valladolid (GOA-UVa), Spain. GOA manages the calibration for the AERONET sun photometers of the European sub-network of AERONET. Raw data are processed and quality assured centrally by AERONET. Data reported for 2009 - 2017 are quality-assured AERONET level 2.0 data, which means they have been pre- and post-field-calibrated, automatically cloud cleared and have been manually inspected by AERONET.

From 2017, only the new analysis algorithm (version 3) is used at the central AERONET analysis unit at NASA GSFC. In this version, the data quality control, including cloud screening, has been improved and a temperature correction has been applied to all wavelength channels. A comparison between the data from all years of operations at Birkenes (2019 – 2016) analysed with version 3 and version 2 revealed an increase of 25% in number of usable data, especially in the winter half-year. While during the summer months, the agreement between the two versions is better than 2% for both AOD and (470, 870nm) Ångström coefficient, there are significant deviations (>10%) in the months with less than 1000 observations over the whole period (November – February). A comprehensive analysis of the differences between the two versions and possible effects on trend studies is in progress; a paper by the NASA GSFC team will be published in the near future.

Due to the large gaps in data acquisition caused by the obligatory annual calibrations at the University of Valladolid combined with technical problems and occasionally unfavourable weather conditions at Birkenes, NILU decided to purchase a second Cimel instrument which will be operated alternately with the current instrument. It will be taken into operation in fall 2018.

### OUTLOOK ON OBSERVATIONS OF AEROSOL OPTICAL DEPTH IN NY-ÅLESUND BEYOND 2019

A major obstacle to obtaining a year-round AOD climatology in the Arctic arises from the long polar night. To fill gaps in the aerosol climatology at Ny-Ålesund, a lunar photometer will be operated on a quasi-permanent basis in the frame of the SIOS infrastructure project. This is a collaborative initiative between NILU, PMOD/WRC and ISAC-CNR. Seasonal deployments of a lunar photometer owned by PMOD/WRC were already made in the winters of 2014/15 and 2016/17. The multiple-season deployment started in autumn 2018.

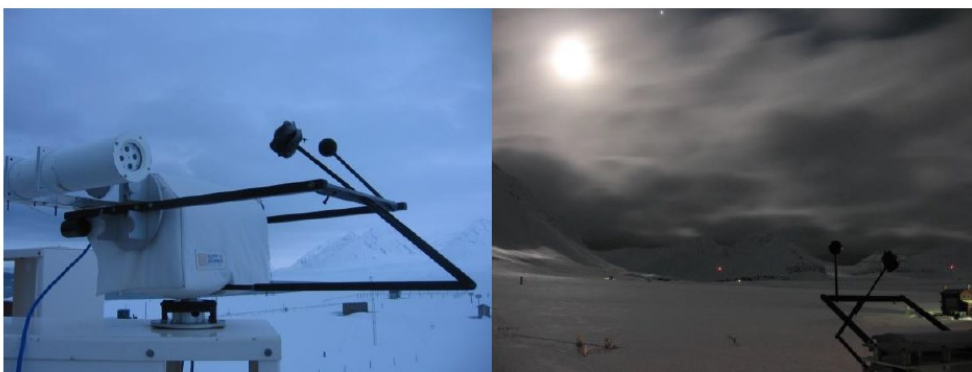


Figure 62: Moon PFR on the Kipp & Zonen tracker during the day (left, parking position) and during night-time measurements (right).

The PFR instrument modified by PMOD-WRC was installed on a tracker model Kipp & Zonen provided usually hosting a sun photometer. Figure 62 shows the instrument on the tracker during daytime and night-time. Six lunar cycles were monitored: the first during February 2014, while the other 5 during winter 2014-2015. We collected data on 66 measurement periods, from Moon-rise to Moon-set or from minimum-to-minimum elevation as in Polar Regions no set-rise events are possible. Among these, we obtained 17 distinct good measurement periods, due to the frequent occurrence of clouds. For further details see, e.g., Mazzola et al., 2015.



# **Appendix III**

## **Abbreviations**

Abbreviation	Full name
ACSM-ToF	Aerosol Chemical Speciation Monitor
ACTRIS	Aerosols, Clouds, and Trace gases Research InfraStructure Network
ADS-GCMS	Adsorption-Desorption System – Gas Chromatograph Mass Spectrometer
AeroCom	Aerosol Comparisons between Observations and Models
AERONET	<a href="#">Aerosol Robotic Network</a>
AGAGE	Advanced Global Atmospheric Gases Experiment
AIRS	Atmospheric Infrared Sounder
AMAP	Arctic Monitoring and Assessment
AOD	Aerosol optical depth
AWI	Alfred Wegener Institute
BC	Black carbon
CAMP	Comprehensive Atmospheric Monitoring Programme
CCN	Cloud Condensation Nuclei
CCNC	Cloud Condensation Nucleus Counter
CFC	Chlorofluorocarbons
CICERO	Center for International Climate and Environmental Research – Oslo
CIENS	Oslo Centre for Interdisciplinary Environmental and Social Research
CLTRAP	Convention on Long-range Transboundary Air Pollution
CO	Carbon monoxide
CPC	Condensation Particle Counter
DMPS	Differential Mobility Particle
EMEP	European Monitoring and Evaluation Programme
ENVRI <sup>plus</sup>	Environmental Research Infrastructures Providing Shared Solutions for Science and Society
EOS	Earth Observing System
ERF	Effective radiative forcing ERF
ERFaci	ERF due to aerosol–cloud interaction
EU	European Union
EUSAAR	European Supersites for Atmospheric Aerosol Research
FLEXPART	FLEXible PARTicle dispersion model
GAW	Global Atmosphere Watch
GB	Ground based
GHG	Greenhouse gas
GOA-UVA	Atmospheric Optics Group of Valladolid University

Abbreviation	Full name
GOSAT	Greenhouse Gases Observing Satellite
GOSAT-IBUKI	Greenhouse Gases Observing Satellite "IBUKI"
GWP	Global Warming Potential
HCFC	Hydrochlorofluorocarbons
HFC	Hydrofluorocarbons
ICOS	<i>Integrated Carbon Observation System</i>
InGOS	Integrated non-CO2 Greenhouse gas Observing System
IPCC	Intergovernmental Panel on Climate Change
ISAC-CNR	Institute of Atmospheric Sciences and Climate (ISAC) of the Italian National Research Council
ITM	Stockholm University - Department of Applied Environmental Science
JAXA	Japan Aerospace Exploration Agency
LLGHG	Well-mixed greenhouse gases
MOCA	Methane Emissions from the Arctic Ocean to the Atmosphere: Present and Future Climate Effects
MOE	Ministry of the Environment
NARE	Norwegian Antarctic Research Expeditions
NASA	National Aeronautics and Space Administration
NEOS-ACCM	Norwegian Earth Observation Support for Atmospheric Composition and Climate Monitoring
NIES	National Institute for Environmental Studies
NOAA	<a href="#">National Oceanic and Atmospheric Administration</a>
NRS	Norsk Romsenter
OC	Organic Carbon
ODS	Ozone-depleting substances
OH	Hydroxyl radical
OPS	Optical Particle Spectrometer
OSPAR	Convention for the Protection of the marine Environment of the North-East Atlantic
PFR	Precision filter radiometer
PMOD/WRC	Physikalisch-Meteorologisches Observatorium Davos/World Radiation Center
PNSD	Particle number size distribution
ppb	Parts per billion
ppm	Parts per million
ppt	Parts per trillion
PSAP	Particle Soot Absorption Photometers

Abbreviation	Full name
RF	Radiative forcing
RI	Research Infrastructure
RIMA	Red Ibérica de Medida fotométrica de Aerosoles
SACC	Strategic Aerosol Observation and Modelling Capacities for Northern and Polar Climate and Pollution
SCIAMACHY	SCanning Imaging Absorption spectroMeter for Atmospheric CHartography
SIS	Strategisk instituttsatsing
SMPS	Scanning Mobility Particle
TES	Tropospheric Emission Spectrometer
TOA	Top Of Atmosphere
TOMS OMI	Total Ozone Mapping Spectrometer Ozone Monitoring instrument
UN	United Nations
UNFCCC	United Nations Framework Convention on Climate Change
VOC	Volatile organic compounds
WDCA	World Data Centre for Aerosol
WDCS	World Data Centre of Aerosols
WMGHG	Well-mixed greenhouse gases
WMO	World Meteorological Organization





## **NILU – Norwegian Institute for Air Research**

NILU – Norwegian Institute for Air Research is an independent, non-profit institution established in 1969. Through its research NILU increases the understanding of climate change, of the composition of the atmosphere, of air quality and of hazardous substances. Based on its research, NILU markets integrated services and products within analysing, monitoring and consulting. NILU is concerned with increasing public awareness about climate change and environmental pollution.

*NILU's values: Integrity - Competence - Benefit to society*

*NILU's vision: Research for a clean atmosphere*

NILU – Norwegian Institute for Air Research  
P.O. Box 100, NO-2027 KJELLER, Norway

E-mail: [nilu@nilu.no](mailto:nilu@nilu.no)

<http://www.nilu.no>

ISBN: 978-82-425-3101-8

ISSN: 2464-3327